GL-TR-89-0117

AD-A223 544

# Optical Emissions From Bombarding Atmospheric Gases With Heavy Ions

Stanley Bashkin

University of Arizona
Tucson, Arizona 85721

30 October 1989

Final Report
3 August 1987-31 December 1988



GEOPHYSICS LABORATORY
AIR FORCE SYSTEMS COMMAND
UNITED STATES AIR FORCE
HANSCOM AIR FORCE BASE, MASSACHUSETTS 01731-5000

Unclassified
SECURITY CLASSIFICATION OF THIS PAGE

# REPORT DOCUMENTATION PAGE

| | |
|---|---|
| 1a. REPORT SECURITY CLASSIFICATION: Unclassified | 1b. RESTRICTIVE MARKINGS |
| 2a. SECURITY CLASSIFICATION AUTHORITY | 3. DISTRIBUTION / AVAILABILITY OF REPORT: Approved for public release; Distribution unlimited |
| 2b. DECLASSIFICATION / DOWNGRADING SCHEDULE | |
| 4. PERFORMING ORGANIZATION REPORT NUMBER(S) | 5. MONITORING ORGANIZATION REPORT NUMBER(S): GL-TR-89-0117 |
| 6a. NAME OF PERFORMING ORGANIZATION: University of Arizona; 6b. OFFICE SYMBOL (If applicable) | 7a. NAME OF MONITORING ORGANIZATION: Geophysics Laboratory |
| 6c. ADDRESS (City, State, and ZIP Code): Tucson, AZ 85721 | 7b. ADDRESS (City, State, and ZIP Code): Hanscom AFB, Massachusetts 01731-5000 |
| 8a. NAME OF FUNDING / SPONSORING ORGANIZATION; 8b. OFFICE SYMBOL (If applicable) | 9. PROCUREMENT INSTRUMENT IDENTIFICATION NUMBER: F19628-87-K-0052 |
| 8c. ADDRESS (City, State, and ZIP Code) | 10. SOURCE OF FUNDING NUMBERS |

| PROGRAM ELEMENT NO. | PROJECT NO. | TASK NO. | WORK UNIT ACCESSION NO. |
|---|---|---|---|
| 61102F | 2310 | G4 | BO |

11. TITLE (Include Security Classification): Optical Emissions from Bombarding Atmospheric Gases with Heavy Ions (Unclassified)

12. PERSONAL AUTHOR(S): Stanley Bashkin

| 13a. TYPE OF REPORT | 13b. TIME COVERED | 14. DATE OF REPORT (Year, Month, Day) | 15. PAGE COUNT |
|---|---|---|---|
| Final | FROM 8/3/87 TO 12/31/88 | 89/10/30 | 172 |

16. SUPPLEMENTARY NOTATION

| 17 COSATI CODES | | |
|---|---|---|
| FIELD | GROUP | SUB-GROUP |
| | | |
| | | |

18. SUBJECT TERMS (Continue on reverse if necessary and identify by block number): Irradiation; Optical emissions; $H_3^+$; $N_2$; $O_2$

19. ABSTRACT (Continue on reverse if necessary and identify by block number)


We have studied the optical emissions from both nitrogen and oxygen targets contained in a differentially pumped cell and bombarded by particles of $H_3^+$ with an energy of 1 MeV. The radiation was analyzed with a 1-meter air Czerny-Turner spectrometer capable of providing an instrumental line width of 0.01 nm. We covered the range from 320 to 850 nm. Most of the work was done with a line width of 0.1 nm, and some with a smaller value. Numerous lines from excited states in monatomic emitters and bands from states in molecular systems were observed.

Relative intensities of the lines were measured and compared with values in the experimental literature and also with calculated transition probabilities. We found that there was poor agreement with the experimental data provided by others, but excellent agreement with the theory. Our light source is clearly superior to most others for the measurement of relative line intensities.


| 20. DISTRIBUTION / AVAILABILITY OF ABSTRACT | 21. ABSTRACT SECURITY CLASSIFICATION |
|---|---|
| ☒ UNCLASSIFIED/UNLIMITED ☐ SAME AS RPT ☐ DTIC USERS | Unclassified |

| 22a. NAME OF RESPONSIBLE INDIVIDUAL | 22b. TELEPHONE (Include Area Code) | 22c. OFFICE SYMBOL |
|---|---|---|
| William Blumberg | (617) 377-2810 | GL/OPI |

DD FORM 1473, 84 MAR — 83 APR edition may be used until exhausted. All other editions are obsolete.

SECURITY CLASSIFICATION OF THIS PAGE

Block #19 continued

The nitrogen data failed to show any lines from neutral atoms, although such lines are seen when electrons are the initiating particles. On the other hand, oxygen shows very strong lines from the neutral atom; both nitrogen and oxygen show lines from the singly ionized atom. While the nitrogen data reveal contributions from both the neutral and singly ionized molecules, the oxygen shows bands only from the molecular ion. The absence of bands from neutral oxygen molecules is easily understood in terms of the potential curves for that structure, but the absence of lines from the neutral nitrogen atom remains obscure.

The pressure dependence for aspects of the nitrogen spectrum showed that the emissions from the ions, both monatomic and molecular, have a somewhat similar behavior. The 1P and 2P bands from the neutral molecule are similar to one another, but different from that of the ionized species. This is interpreted (in a paper prepared subsequent to the completion of this document) in terms of a two-component energy spectrum of the electrons in the source.

High-resolution scans were taken of various features, partly to let us examine the line widths, which, for monatomic lines, were obviously greater than instrumental. The line-width data were taken both with the spectrometer and with a high-resolution echelle spectrograph. The results clearly show that the monatomic ions originate in predissociative or repulsive states of the molecular ion, so that a kinetic energy of the order of 10 eV is available; that energy gives rise to Doppler broadening. That broadening is not detected in the rotational lines of the 1N(0,0) band, which was also studied with high resolution. This finding emphasizes the importance of using high spectroscopic resolution, which was missing from the predecessor experiments reported in the literature.

Our high-resolution examination of the 1N(0,0) band was also used to determine the electron temperature of our source to be 350K.

A critical examination is presented of the way in which cross sections are measured, and various factors, hitherto neglected in the literature, are clarified.

Four presentations of our results were made at international meetings. One paper has now been accepted for publication by Chemical Physics Letters. Two major papers are in preparation for submission in standard research journals.

Table of Contents

# Introduction

The ultimate purpose of this contract was to measure the absolute cross sections for the excitation of various states in atmospheric gases, principally nitrogen and oxygen, under the impact of positive ions. The two main reasons for being interested in this problem are:

1. cross sections are essential to a proper modelling of the aurora.

Although the protons which are found in the auroral zone have energies mostly of the order of a keV, there are others whose energies extend upwards to as much as 100 MeV. Furthermore, while protons are the most prominent of the energetic positive ions in the auroral zone, other species also contribute to the ionization/excitation processes that occur in nature. Thus it is also desirable to study the effects for many different particle types and energies.

2. the theory of the interactions is presently poorly developed, so that further data ought to assist in clarifying what events take place. Our experiments well illustrate the complexity of producing a theoretical analysis of the interaction between incident particles and target molecules of nitrogen and oxygen.

In the course of our extensive series of experiments, we had to be aware of the possibility that unexpected facts might emerge, and, if so, be prepared to exploit them. That proved to be our situation,

and we will discuss two special findings that were unearthed by our work. The effects may have experimental and theoretical significance.

Finally, we have been able to make some interesting comparisons of our data with those obtained by others who have studied the excitation of nitrogen and oxygen by electron impact. Among other things, we have obtained information about the states which are precursors to those whose optical emissions we observe.

The following report includes our analysis of our data.

## Preliminary Work

Although the 2 MV Van de Graaff accelerator we used for generating the energetic particles was in good operating condition from the outset, other necessary components of the experimental arrangement were not. For one thing, we had to design and construct a suitable target chamber. This went through several phases before we finally produced a satisfactory system, which is shown in Fig. 1.

This target chamber consists of a differentially-pumped gas cell, into which gas is fed via an automatic control valve so as to maintain a constant target pressure. The pressure, which could be maintained to ± 0.1 mTorr, is measured with a capacitance manometer. High-speed diffusion pumps exhaust the gas from the cell through two small-diameter cylindrical passages. With a pressure of 200 mTorr in the target cell, the pressure in the volume

adjacent to the Faraday cup, in which the incident particles were collected, is of the order of 0.4 mTorr. The incident beam must also go through the passages in order first to interact with the target molecules and then to enter the Faraday cup, where the particle current is measured and integrated.

Coincident with the construction of this chamber, the entire experimental apparatus was moved along the accelerator's target arm so as to increase the beam which could be delivered to the target. In fact, the gain was a full order of magnitude. It is the interaction of the beam with the target gas that produces the light of which we make a spectral analysis. As shown in Fig. 1, the light emerges from the cell through a vertical quartz window; it is then focussed by a quartz lens onto the entrance slit of a one-meter, air, Czerny-Turner, scanning monochromator. It must be mentioned that there was a drawback to this system, in that the index of refraction of quartz is not constant as a function of wavelength. Thus we did not always have the best focus, since an adjustment was made on one spectral feature and the lens left undisturbed for all the data. This means that we did not collect all the light that should have been delivered to the detector photomultiplier. Unfortunately there was nothing we could do to correct this situation, since we had only the crudest mechanical mount for the lens. We never had enough money to buy good screw-driven supports, and all adjustments were laboriously made by hand. This had an inevitable and deleterious effect on the relative intensities of the observations. Nonetheless,

the data we took are quite impressive. An achromatic lens would have been helpful, but we didn't have one in the laboratory.

Another important modification of the original equipment had to do with how the spectrometer received the light from the target cell. At the outset, we dealt with an optical arrangement inherited from a predecessor group. It proved to be awkward in the extreme, particularly as regards the alignment of the spectrometer along the light path. Ultimately, we altered the arrangement completely, and obtained a simplified optical coupling which was relatively easy to put into alignment and which took full advantage of the signal.

The light detector is an EMI 9659 QB photomultiplier tube, the output of which is sent to a Tracor-Northern multiscaler. In order for the data to be physically significant, they have to be normalized to the number of incident particles. This is customarily done by integrating the current received by the Faraday cup, and stepping both the spectrometer wavelength and the multiscaler channel by a fixed amount when a given amount of charge has been collected. However, one must also reckon with the noise. Specifically, if it takes a long time to collect the aliquot of charge, the noise contribution is correspondingly large. In our initial efforts, this caused considerable trouble, because occasionally the particle beam would wander from the target, and, in the several minutes that it sometimes took to restore the proper operation of the accelerator, the noise counts accumulated and badly distorted the measurements. This difficulty was eliminated by building a circuit which cut off

the recording apparatus whenever the beam current to the target fell by more than 25%. This led to a marked improvement in the quality of the results.

The incident beam we selected was ions of $H_3^+$, with an energy of 1 MeV. This particle was selected for several reasons: it had been used only rarely in experiments carried out by others, it carried electrons with it so that electron interactions could be initiated along with nuclear interactions, and the ion source in the Van de Graaff produced this particle in large numbers.

Currents up to 10 microamp were delivered to our Faraday cup, in the absence of any gas in the target cell. The measured apparent current, however, was pressure dependent, and had an effect which is detailed below in the section on pressure effects.

## Observed Spectrum of Nitrogen

Spectra were taken for a nitrogen target, over the range from approximately 320 to 850 nm, using a line width of 0.1 nm. (We might mention in passing that this is far superior in both spectral range and line width to any other similar data reported in the literature. As will be shown shortly, some of our data were taken with an even narrower line.) We exhibit the results in Figs. 2-23; Table 1 lists the identified features.

While the data of Figs. 2-23 show what was seen for a target pressure of 200 mTorr, similar curves were obtained for a number

of different target pressures. There were no significant differences from curve to curve, except, of course, that the intensities declined with the pressure. The specific pressure effects are described in a later section of this report.

It is seen from Figs. 2-23 that there are three, separate, characteristic shapes. One, a simple structure, is that of a transition from the singly-ionized nitrogen atom. A detailed view of that structure is shown in Fig 24, where we display some components of the 3p $^3D$ - 3d $^3F^o$ multiplet in N II. The feature near 500.1 nm is broadened, because there are two contributors with a separation of only 0.03 nm. The feature near 500.5 nm is isolated, but still shows a line width of the order of 0.03 nm. These results indicate the quality of the spectroscopic work; the line broadening will be discussed later in this report.

The second characteristic shape is that of the first negative (1 N) bands of $N_2^+$, a good example of which is found in Fig. 4, where the 1N(0,0) band is shown. The third shape arises from the second positive (2 P) bands of $N_2$, some examples of which are shown in Fig. 5. It is from the shape, as well as from the wavelength of the spectral feature, that the transition identification is made.

We might mention that, for wavelengths above 650 nm, there is the possibility that second-order features are being detected. This actually occurs. Indeed, the response of the spectrometer is considerably higher in second order than in first. In order to clarify the data, we took some spectra with a filter in place. The filter

eliminated all lines with wavelengths below 600 nm, which effectively cut out all second-order contributions.

## Relative Intensities in Nitrogen

We referred earlier to two unexpected pieces of data. One is that, with a single, weak exception (N I, 3s $^2P_{3/2}$ - 4p $^2S^o_{3/2}$ at 493.5 nm), we did not see any sign that neutral nitrogen atoms were excited. At least, there weren't any such states that radiated in our wavelength range. Table 2 summarizes our results.

A study of such matters as the available excitation energies, transition probabilities, and branching ratios indicates that none of those factors could likely account for the absence of excited, neutral nitrogen atoms. Even if the transitions we expected to see are actually present, one cannot overlook the fact that they are very weak. It would seem that a detailed explanation of the collision mechanism, coupled to the various decay modes, is needed to acount for the failure to see such systems; at this time, no such explanation has been developed, although it is known from the electron bobmardment of $N_2$ that the cross sections for the excitation of monatomic neutral nitrogen states is quite low, of the order of $10^{-20}$ cm$^2$. What is especially deserving of comment is that Rall *et al.* , J. Chem. Phys. 87, 2466 (1987), show a spectrum from the electron excitation of nitrogen in which three components of the N I multiplet 5p $^4D^o$ - 2p$^4$ $^4P$ near 431 nm are clearly seen,

with intensities roughly half that of the band head of the 2P(0,4) band head in $N_2$. We also see that band, but there is no sign whatsoever for the lines from the neutral atom. It certainly seems that the excitation mechanism operative in our experiment is substantially different from that in the electron bombardments. It would obviously be helpful to extend the observations into the XUV region, to see if the prominent resonance transitions at 120 nm are present in the collisions. Those transitions are very strong in the electron bombardment of nitrogen.

The second point is that the relative intensities of the components of some of the transition arrays (in singly-ionized nitrogen atoms, N II) differ considerably from those catalogued by Striganov and Sventitskii (SS). However, they agree well with the absolute transition probabilities given by Wiese, Smith, and Glennon (WSG). Figure 25 illustrates our data for the transition array N II 3s $^3P^o$ - 3p $^3D$. In Table 3, we give a comparison of our observed peak yields and the relative transition probabilities given by WSG. We have omitted any comparison with the values listed by SS. There are two reasons for this decision. One is that, as SS comment, the data taken from the literature are highly suspect and of little real significance. The second is that SS are themselves unclear as to how they indicated relative intensities. They based some on a logarithmic scale and others on a linear scale, with no identification as to what applied to any given number. In our Table 3, the numbers in both columns have been normalized to the J = 2 to

J = 3 component, that being the strongest of our observed features in this array.

The agreement between our measured relative intensities and the transition probabilities is indicative of the fact that our light source does yield statistically representative and quantitatively accurate data on transitions. Thus it seems noteworthy that this kind of source can be used to assess the quality of other experiments which give relative line intensities, and also to validate the calculations of transition probabilities.

It will be observed that we have not listed any relative intensities for the molecular bands from $N_2$ or $N_2^+$. The reason for this is that there is no single spectral feature which is proportional to the total yield of light within a given band. Furthermore, one cannot integrate the area under the spectral curves because many features overlap others, so they cannot be separated, even with infinite resolution. What this means is that the only way to find that yield is to use a theoretical model, which is so calculated as to match the experimental data, and to take the total yield from it. This is especially important because, given the variable wavelength extents of the different bands, the overlaps occur in non-uniform fashion.

The requisite model calculations can be made for the first negative (1N) bands of $N_2^+$, but not for the positive bands (1P and 2P) from $N_2$. This is because the 1N bands connect $\Sigma$ states, for which there is no fine-structure coupling. On the other hand, the

positive bands involve $\Pi$ states, for which fine-structure components are many and difficult to include in the calculations. Indeed, hyperfine contributions must also be included for constructing a proper model. Thus there is no way at present to determine the yields of the bands, other than for the 1N bands.

Work on the 1N bands is in progress. In fact, a model calculation has already been made for the purpose of obtaining the rotational temperature of the source plasma. In this calculation, an assumption was needed as to the nature of the interaction. It was assumed that the excitation of the upper state ($B\ ^2\Sigma^+_u$) came about from the electron bombardment of the $N_2$ ground state. Given this assumption, the parameters introduced into the calculation included the line width, the spectrometer step size, and the rotational temperature. The results appear in Figs. 26-30. Data were actually taken for a number of pressures, but we show only two representative spectra, for pressures of 150 and 200 mTorr, respectively; there was no discernible difference in the spectra from pressure to pressure. The uncertainty in the rotational temperature is $\pm$ 50K. We call attention to the high quality of our experimental data. It far exceeds anything similar in the literature.

The calculated distributions which appear in Figs. 28-30 are for different temperatures, and it is seen that the best fit to the data is found in Fig. 30, with a rotational temperature of 350K.

## Data on Nitrogen Taken with $H_2^+$ Incident Particles

To gain further information about the nature of the collision mechanisms, we decided to use a different bombarding particle. The reason behind this decision was that $H_3^+$ carries two electrons with it, in a helium-like electronic arrangement. Now the ground state of $N_2$ is $X\ ^1\Sigma g^+$, while the excited states from which the 1P and 2P bands originate are triplets. Consequently, if the latter are excited by electron collisions with the former, there must be electron exchange. We thought this might be less likely with incident particles of $H_3^+$ than with $H_2^+$, since the latter is hydrogen-like in its electronic structure. Hence we elected to take spectra with $H_2^+$ as the bombarding particle. For a good comparison, we used the same particle velocity as in the $H_3^+$experiments.

The results of this investigation are given in Figs. 31-33. Two points may be made. One is that the data simply aren't very good. This was due to the fact that the beam was quite weak and unstable. The second point is, that insofar as one can tell, there is no significant difference in the relative band intensities for the two different kinds of incident particle.

We believe, in the face of this evidence, that, given the energy of the incident particles, the electrons in the $H_2^+$ case act independently of one another, so that the nominal similarity to He is of no consequence. What would be more instructive would be

bombardment with protons; had our contract not run out when it did, that work would have been carried out.

## Pressure Studies in Nitrogen

To obtain information about the excitation mechanism(s) operative in the collisions, we measured the yield of several spectral features as a function of target pressure. In our preliminary experiments, we took spectral scans at various pressures, with results as shown in Figs. 33-42. However, it was soon realized that a better way of finding the pressure dependence of the spectral features was at hand.

For this kind of measurement, the spectrometer was set to a particular wavelength, either at the peak of a monatomic line or on the most prominent peak within a molecular band, and the intensity measured as a function of pressure. However, such data require an important correction before they can be translated into the true pressure dependence of the feature.

The correction is due to the fact that the apparent current collected in the Faraday cup is not the actual current. When the beam passes through the gas target, ions are produced. Some are from the target gas, others from the fragmentation of the incident $H_3^+$ particles. For the latter charged particles, those with positive charges continue on their paths into the collector, whereas the electrons which are released are, for the most part, scattered or

absorbed, and do not reach the collector. Thus the effect is to increase the rate at which positive charge gets to the collector. This effect is pressure-dependent, and causes the apparent current to vary. A typical example appears in Fig. 43.

Consider, now, the way in which the collected current is used. For each of the data points, a definite amount of charge is collected, whereupon the pressure is changed and a new piece of data obtained. If, for example, the current to the collector is 10 microamp, it takes 20 seconds to acquire 200 microCoul of charge. If, then, the apparent current changes to 20 microamp, it takes only 10 seconds to accumulate that same charge, which means that

a) only half as many incident particles pass through the target gas in the second case as compared with the first, and

b) noise counts, which are proportional to the collection time, are more significant by a factor of two for one case relative to the other.

It is thus necessary to correct the raw data for the pressure dependence of the apparent current. With that correction made, the results for nitrogen appear in Figs. 44-47. Figure 48 is a summary of representative results.

From the general appearance of the curves in Figs. 44-47, we see that all states of a given initial type, i. e., 1P or 2P or 1N or monatomic, show the same kind of pressure variation, so there aren't any obvious differential effects caused by different excitation energies of the decaying states. As is well indicated in

Fig. 48, it seems likely that the same events, or at least similar kinds of events, are responsible for the production of the excited states in $N^+$ and $N_2^+$, and that a different kind of event causes the excitation of the neutral molecule, $N_2$. A discussion of what those events might be is given in the section on cross sections.

## Line Widths in Nitrogen

A high-resolution study was made of the nitrogen multiplet near 500 nm. The line width was 0.03 nm. The results appear in Fig. 24. The left-hand member of the multiplet is broadened because of the close proximity of two lines. However, the width is still considerably greater than the instrumental line width. This was initially attributed to faults in the spectrometer drive, but subsequent work showed that the cause is fundamental in nature.

For this purpose, we borrowed an echelle spectrograph from the Lunar and Planetary Laboratory. That instrument has in instrumental line width less than 0.01 nm, but it showed the same line width as we found with the Czerny-Turner spectrometer. The widths of the rotational lines in the 1N(0,0) band did not show any similar broadening.

This unexpected line width is ascribed to the precursor states whence the excited states of $N^{2+}$ emerge. If those states are predissociative or repulsive states in $N_2^+$, the molecular excitation energy is such that the emergent fragments have a kinetic energy of

the order of 10 eV. It is the Doppler broadening that arises from that kinetic energy that is responsible for the large line width in the emissions from states in $N^+$. A complete discussion of this effect and its fundamental meaning is given in a paper which has now been accepted for publication by Chemical Physics Letters, but we comment in passing that this is the first such observation. It was made possible by the high resolution of our work relative to that of previous experimenters.

## Observed Spectrum in Oxygen

The case of oxygen is considerably more complicated than that of nitrogen. This is because the molecular bands in oxygen are not nearly so well defined or so well separated as those in nitrogen. Thus there is a great deal of overlap, which makes it extremely difficult to sort out what features belong to a given transition. Possibly this accounts for the fact that few studies of oxygen have appeared in the literature. The complex situation is well illustrated by our spectra.

Figures 49-108 show the general spectrum obtained with a target gas of oxygen, and high-resolution spectra for selected regions. A line list is given in Table 4. The various figures represent data taken at different pressures, line widths, and other experimental parameters. There are, again, characteristic line shapes, which, along with the measured wavelengths, permit

identification of the main features. The identifications are given in Table 4. Figure 49 shows well the nature of the oxygen problem, for there one sees contributions from perhaps as many as 18 different vibrational transitions from the second negative system of $O_2^+$, all within a wavelength range of 75 nm.

Aside from the complexity in oxygen, there are two major differences between between the nitrogen and oxygen data. In the first place, there are no readily-identified transitions from $O_2$, whereas transitions from $N_2$ were prominent in the spectra taken with a target gas of nitrogen. This is easy to understand in terms of the potential-energy curves for $N_2$ and $O_2$; for the former, the curves are relatively narrow and show considerable overlap, but, for the latter, they are broad, fairly flat, and show little overlap with one another, especially for transitions in the visible part of the spectrum.

The second difference is that a number of fairly intense lines are seen from O I, although, as pointed out in the section on nitrogen line intensities, contributions from neutral nitrogen atoms were absent from the spectrum. It is, therefore, of considerable interest that there should be evidence of excited states in neutral oxygen. This distinction is further discussed later in this report.

Figure 91 illustrates a high-resolution scan of a small spectral range. The multiplet O I $3s\ ^5S^o$ - $3p\ ^5P$ is clearly resolved into its components; the relative line intensities were determined from the peak heights. They, along with similar data for other

oxygen lines, are listed in Table 5, which, as well, gives the relative transition probabilities calculated by WSG. Just as for nitrogen, we have omitted relative intensities as listed by SS; the agreement with the calculations of transition probabilities is satisfactory.

Figures 101-108 show the spectrum taken with a filter over the entrance slit to the spectrometer. This filter, by eliminating all lines with wavelengths below 500 nm, helped clarify the interpretation of the data.

It is obvious from the figures showing the presence of the various molecular bands that there is no point in attempting to determine relative intensities of the bands in the oxygen data.

## Pressure Studies in Oxygen

As for nitrogen, the apparent current to the Faraday cup was a function of pressure, and affected the interpretation of the pressure-dependent spectral studies. In Fig. 109, we exhibit the pressure dependence of the apparent current to the Faraday cup for a target of oxygen. These data were used to correct the raw data on the pressure variation of particular spectral features.

Figures 110-112 show the pressure-dependence of spectral features in O I, O II, and $O_2^+$. The curves are all quite similar in that they are concave downward and approach saturation at high pressure, although they don't reach a level value. These oxygen results indicate that a single type of process is responsible for the

observed excitations. This contrasts with the nitrogen data discussed earlier, where there was good evidence that two separate processes were involved. No explanation for the oxygen behavior is yet available.

## Cross Sections

A main purpose of these experiments was to determine absolute cross sections for the excitation of different states. The literature contains a number of papers in which such numbers are reported. However, those numbers are generally in wide disagreement with one another. Our work has found several good reasons why that should be the case, and we have further found that, as regards states in neutral molecules or singly-ionized oxygen, it is essentially impssible to obtain those numbers with any reasonable degree of accuracy. In fact, even for the monatomic states and the states in singly-ionized nitrogen molecules, for which the possibilities are best, it is still extremely difficult to determine cross sections in a reliable manner. We proceed to discuss the problems.

a) Target density.

Certain physical parameters must be known if the data are to yield cross-section information. One such parameter is the density of the targets, since it is obvious that changing the number of targets will change the number of interactions and therefore the

light intensity. The customary way of measuring the target density is to measure the gas pressure. However, that is unsatisfactory for the simple reason that the pressure at the manometer is not the same as that of the gas where the incident beam traverses the target volume. The beam causes local heating, which causes the gas density to be less than that in the adjacent volume. Moreover, that heating is a function of the kind of gas, the kind of incident particle, the energy of that particle, the nominal target pressure, and so forth. The result is that it is probably not possible, under the most restrictive of conditions, to determine the target density to better than 10 or 15%, and the "cross sections" cannot be better than that.

b) Number of incident particles

Another parameter which enters directly into the cross-section determination is the number of incident particles. However, as we have noted earlier in this report, that number is hard to measure, because of charge-changing events in the target gas. One way of improving this measurement would be to seal the Faraday cup off from the target gas, while permitting the incident particles to reach the collector. We have designed such a Faraday cup arrangement, but it has not been built because of lack of money.

c) Geometry

The geometry of the experimental system enters into cross-section data in three ways. First, the luminous part of the target is a cylinder of small diameter. One result of the collisions of interest is that the incident beam is scattered through a small

angle. That scattering adversely affects the efficiency with which the Faraday cup collects the incident beam, so the measured collected charge is less than the charge responsible for the excitation processes. Furthermore, if one attempts to improve the geometry by using a still smaller target diameter, the effect is to increase the loss of incident particles because of the small-angle scattering. This is a fundamental problem, which adds to the troubles encountered in the attempt to measure a cross section.

The second geometrical effect has to do with the collection of light from the luminous source. Obviously one wants the solid angle subtended at the source by the optical system to be constant. However, should the incident beam have a hot spot in it, or should it wander slightly over the target volume in the course of the measurements, the solid angle of interest will not be constant, but will vary in an erratic fashion. We do not know whether such hot spots or beam wandering are present in our system, and it would take an elaborate apparatus to check on such possibilities. Neither we nor any of the other investigators who have worked on this cross-section problem have accounted for such effects.

The third geometrical effect has to do with the focal properties of the collecting lens. As mentioned early in this report, the lens was made of quartz, and was put in a fixed position. Because the index of refraction of quartz is wavelength-dependent, we were not in focus for most of the incident light. An achromat and a good adjustable lens mount would have given better data. A

similar problem must also have affected the reports in the literature, but is not mentioned.

d) Spectroscopic resolution

Our data were taken with a line width of about 0.1 nm for the most part, and a factor of ten less for some special regions. Even so, there were important parts of the spectra in which different features were not resolved from one another. The inability to resolve those spectral components means that one cannot make proper measurements of the light yields from the excited states involved.

For the molecular states, the problem is compounded because the various bands overlap to such an extent that even infinite resolving power would not suffice to distinguish one from another. This is particularly evident in our data on oxygen, where a small spectral range may include contributions from as many as half a dozen different vibrational transitions. The only way to find out how much of the light yield can be attributed to a single vibrational transition is to make a model calculation which matches the experimental observations. While, as we have mentioned, that is possible for the first negative bands in $N_2^+$, it is presently not possible to do this in general, because the appropriate calculations are too complicated to have been carried out. So far as we have been able to determine, the requisite programs simply do not exist.

Even in the cases of the 1N bands in $N_2^+$ and the monatomic lines, the observed intensities are functions of the spectrometer's

slit width and the step size. We have used that information in our assessment of the rotational temperature of our nitrogen target, but such considerations have been routinely omitted by other authors. We point out that changing the width of the entrance slit into the spectrometer also changes the fraction of the target which is viewed by the spectrometer, so the observed light intensity is a function of the spectral resolution.

It is worth mentioning that other investigators used line widths one or more orders of magnitude worse than ours. Consequently it is not surprising that the reported cross-section values are widely disparate from paper to paper. We must also mention that those papers simply do not indicate how the light yields or the other factors we have mentioned above were determined. It is our conclusion that the cross sections in the literature are unreliable.

Still another serious problem arises in the analysis of the spectroscopic data for the purpose of determining cross sections. Consider that what one detects is the intensity of one or more spectral features. It is customary to think that that intensity is a measure of the excitation of the decaying state. However, that is simply incorrect, the reason being that the state in question may disappear from view by means other than the emission of radiation. Thus, the observed intensity is a number which results from a complex interaction, involving both excitation and de-excitation.

To be specific on this important point, we list below at least some of the likely excitation events, followed by de-excitation possibilities.

## Excitation Events

1. Direct interaction between the incident ions and the target molecules.

2. Direct interaction between the electrons which accompany the incident ions and the target molecules.

3. Excitation by electrons released from target molecules by ionization events.

4. Dissociation of the incident triatomic ion into ($H_2^+$ + p + e), ($H_2$ + p, (3p + 2e), (H + 2p + e), and/or (2H + p) prior to interaction in the region of observation, each element of which could then interact with target molecules.

5. Production of excited, neutral molecules by recombination of the molecular ions.

6. Dissociative recombination.

7. Dissociative excitation from pre-dissociative or repulsive states.

8. Three-particle interactions.

9. Excitation by electrons released from slit edges or other peripheral parts of the target system.

10. There is also the possibility that the primary process creates states which we cannot detect directly, but which then decay into those we do identify.

## Decay Modes

1. Radiative emission.
2. Recombination, as regards the monatomic and molecular ions.
3. Predissociation.
4. Dissociation from repulsive states.
5. Collisions of the second kind.
6. Diffusion out of the region of observation, which is effectively a decay mode for our method of observation. This can be especially significant for long-lived states, but it always introduces some difference among states of different lifetimes.

In view of the foregoing analysis, we are forced to conclude that it is inherently unusually difficult to measure cross sections for the excitation of states generated by the impact of positively charged particles on gas targets.

## Further Discussion

Certain additional points merit mention. We have called attention to the disparity between our nitrogen spectra and those reported from electron bombardment of nitrogen, especially the absence of lines from neutral nitrogen atoms in our experiment. On the other hand, we see a number of intense features from O I states, as is also reported from electron work. An important difference between the nitrogen and oxygen cases lies in the excitation cross sections. For nitrogen, the monatomic states are generated with cross sections of the order of $10^{-20}$ $cm^2$, whereas the comparable numbers for oxygen are about $10^{-18}$ $cm^2$. The question is, why are these numbers so different?

The answer lies, certainly, in the wave functions for the two systems. In searching for some physical distinction between the two atoms, we make the tentative suggestion that the difference might lie in the fact that N has seven electrons, whereas oxygen, of course, has eight. This offers the possibility that the difference between the two comes from the difference in electron correlation between the two atomic systems. If, for example, there should be a stronger coupling of electrons in oxygen than in nitrogen, that might explain why states in the former survive the collisions, whereas those in the latter do not. This suggestion is perhaps worthy of theoretical investigation.

We have also mentioned that the lines from well-resolved multiplets in N II are rather broad, certainly broader than the instrumental line width. We have sought the reason for this peculiarity. It is possible that this broadening, which, by the way, cannot be due to pressure effects even at the highest pressures we used, arises from the creation process. We offer the following argument.

We know from our data that excited states in $N_2^+$ are formed. It is reasonable to think, then, that the range of excitation of states in that system extends well into the region of pre-dissociative or even repulsive states. Excitation to the structure $N_2^{++}$ is also within the realm of possibility. Dissociation of the molecular ion must then occur; the decay products could well be $N^+$ and N. In work reported by others on the formation of excited states in hydrogen from electron bombardment of $H_2$, it is known that dissociation energies of 10 eV or so are characteristic of the decay products. Such energies are more than sufficient to account for the wavelength spread we observe. Furthermore, it appears that the breakup of excited $N_2^+$ into $N^+$ + N tends to leave the N in the ground state, which would be consistent with the failure to detect emissions from that system. It is still a puzzle, however, that our bombardments create less $N^*$ than the electron bombardments do.

Turning to the case for oxygen, one can make a comparison between the relative line intensities we measure and the cross sections for excitation of the same initial states by means of

electron collisions. For example, Schulman *et al.* , Phys. Rev. A 32, 2100 (1985), report on the emissions from oxygen atoms from the dissociative excitation of $O_2$ by electrons. We see many of the same lines they found, and we present a table (see Table 6) of the relative cross sections they give and the relative line intensities we determined. It must be kept in mind that our optical system was not calibrated for its dependence on wavelength. Furthermore, the slit settings for our work were less than optimal for this run. Nonetheless, the comparison is worth examining.

The comparison shows that there are some discrepancies between our results and those from electron bombardment. The most striking is the difference of a factor of 3, our yield being the smaller, for the transition 3s $^3S^o$ - 3p $^3P$. It would clearly be valuable to repeat these measurements.

## Work Still to be Done

Although this document is a final report, it is perhaps worth pointing out that certain further experiments - and calculations - would be of great value. On the experimental side, it would clarify some of our observations if we were to use protons, rather than $H_3^+$ particles. This would eliminate any interaction between the incoming electrons and the target molecules.

It would be of further help if one could look at other target gases, since one might then discover systematic effects in the interaction and decay mechanisms.

A particularly useful experiment would be to determine the spectra in the vacuum ulatra-violet. We have the requisite apparatus, but lack the financial support to do this work.

As to calculations, we pointed out that models are needed if one is to obtain reliable numbers for the yields under the different bands. We further noted that a program for such a calculation is available for the first negative system of $N_2^+$, but for nothing else. However, with sufficient support, it would be possible to build programs applicable to other systems.

Our work shows that a much more extensive investigation of oxygen is needed. For this substance, much higher resolving power than we were able to obtain is essential if the several important transitions are to be identified with certainty. It would be especially interesting to know if bands from $O_2$ are produced by ion bombardment. If not, one could perhaps distinguish between electron-induced and proton-induced auroras in terms of the intensities of the $O_2$ bands.

## Data Presentations

Reports on parts of our work have been reported at four major conferences, namely:

1. P.Sercel, S. Bashkin, R. Bruch, D. DeWitt, and S. Fuelling, "High Resolution Study of Optical Emission Induced by Bombarding Nitrogen Gas with Energetic $H^+$, $H_2^+$, and $H_3^+$ Projectiles," Fifteenth International Conference on the Physics of Electronic and Atomic Collisions (ICPEAC), Brighton, United Kingdom, 1987.
2. P. C. Sercel, S. Bashkin, J. A. Anderson, D. A. Thiede, R. F. Bruch, D. DeWitt, and S. Fuelling, "Excitation of Gases with Positive Ions," Symposium on the Atomic Spectroscopy of Highly Ionized Atoms, Nucl. Instr. Meth. B31, 241 (1988).
3. S. Bashkin, D. A. Thiede, M.-L. Li, P.-C. Lin, D. G. Jenkins, D. E. Shemansky, and E. Träbert, "Excitation of Nitrogen by Energetic Particles," Tenth Conference on the Application of Accelerators to Research and Industry, Denton, Texas, Nov. 7-9, 1988, Nucl. Instr. Meth., B40/41, 239 (1989)
4. S. Bashkin, M.-L. Li, P.-C. Lin, D. A. Thiede, D. G. Jenkins, and E. Träbert, "Excitation of Oxygen by Ion Bombardment," First Asia-Pacific Conference on Atomic and Molecular Physics, Taipei, Taiwan, Nov. 25-29, 1988, Chinese Journal of Physics 27, 126 (1989) .

In addition, two major papers on nitrogen and oxygen, are in preparation for submission to research journals.

## Personnel

The Principal Investigator was Professor Stanley Bashkin. Professor D. E. Shemansky, of the Lunar and Planetary Laboratory, contributed to certain aspects of the data analysis. There were no technical persons on the project, all the developmental and repair work being done by Professor Bashkin and his Arizona students. Arizona students who significantly assisted in this project are listed below:

| Undergraduate Students | Graduate Students |
|---|---|
| John A. Anderson | Ming-Liang Li |
| Peter C. Sercel | Po-Chuan Lin |
| David G. Jenkins | |
| Carol Kenney | |
| David A. Thiede | |

There were also a number of visitors, who worked with us for periods ranging from a few days to a month. They were:

From the University of Nevada at Reno:

Professor Reinhard Bruch

David DeWitt (undergraduate student)

Stefan Fuelling (graduate student)

From the Ruhr University of Bochum in West Germany:

Dr. Elmar Träbert

## Tables

Table 1. Following is a list of observed spectral features from our work on nitrogen. All wavelengths are in nm. For bands, the value listed is for the band head.

Monatomic lines from N I and N II

| Transition | Wavelength (nm) |
|---|---|
| **N I** | |
| $3s\ ^2P_{3/2}$ - $4p\ ^2S^o_{3/2}$ | 493.5 |
| **N II** | |
| $3d\ ^3F_3$ - $4f\ G(9/2)_4$ | 453.04 |
| $3p\ ^3D_1$ - $3d\ ^3F^o_2$ | 500.11, unresolved from next entry |
| $3p\ ^3D_2$ - $3d\ ^3F^o_3$ | 500.15, well resolved from next entry |
| $3p\ ^3D_3$ - $3d\ ^3F^o_4$ | 500.51 |
| $3s\ ^3P^o_1$ - $3p\ ^3P_0$ | 462.14 |
| $3s\ ^3P^o_2$ - $3p\ ^3P_2$ | 463.05 |
| $2p^3\ ^1D^o_2$ - $3p\ ^1P_1$ | 489.51 |
| $3s\ ^3P^o_1$ - $3p\ ^3D_2$ | 566.66 |
| $3s\ ^3P^o_0$ - $3p\ ^3D_1$ | 567.60 |
| $3s\ ^3P^o_2$ - $3p\ ^3D_3$ | 567.96 |
| $3s\ ^3P^o_1$ - $3p\ ^3D_1$ | 568.62 |
| $3s\ ^3P^o_2$ - $3p\ ^3D_2$ | 571.08 |
| $3s\ ^3P^o_{1,0}$ - $3p\ ^3D_{2,1}$ | 589.73, 589.98, unresolved |

| | | | |
|---|---|---|---|
| | $3s\ ^3P^o_1$ - $3p\ ^1P_1$ | 648.21 | Blend with 2P(5,5) in second order |
| | $3s\ ^1P^o_1$ - $3p\ ^3D_2$ | 574.73 | |
| | $3s\ ^1P^o_1$ - $3p\ ^3D_1$ | 576.74 | |
| $N_2$ | | | |
| 1P | (2,0) | 775.32 | |
| | (3,0) | 687.50 | |
| | (3,1) | 762.62 | |
| | (4,1) | 678.86 | |
| | (4,2) | 750.39 | |
| | (5,1) | 612.74 | |
| | (5,2) | 670.48 | |
| | (5,3) | 738.66 | |
| | (6,2) | 606.97 | |
| | (6,4) | 727.33 | |
| | (7,3) | 601.36 | |
| | (7,4) | 654.48 | |
| | (7,5) | 716.48 | Blend with 1N(1,0) seen in 2nd order |
| | (8,4) | 595.90 | |
| | (8,5) | 646.85 | |
| | (9,4) | 547.85 | |
| | (9,5) | 590.60 | |
| | (9,6) | 639.47 | |
| | (10,5) | 544.23 | |

| | | | |
|---|---|---|---|
| | (10,6) | 585.44 | |
| | (10,7) | 632.29 | |
| | (11,6) | 540.71 | |
| | (11,7) | 580.43 | |
| | (11,8) | 625.28 | |
| | (12,7) | 537.28 | |
| | (12,8) | 575.52 | Blend with 1N(1,5) |
| | (12,9) | 618.52 | |
| 2P | (0,0) | 337.13 | Also seen in 2nd order |
| | (0,1) | 357.69 | Also seen in 2nd order |
| | (0,2) | 380.49 | Also seen in 2nd order |
| | (0,3) | 405.94 | Also seen in 2nd order |
| | (0,4) | 434.36 | |
| | (1,0) | 315.93 | Seen in 2nd order |
| | (1,1) | 333.9 | Also seen in 2nd order |
| | (1,2) | 353.67 | Also seen in 2nd order |
| | (1,3) | 375.54 | Also seen in 2nd order |

| | |
|---|---|
| (1,4) | 399.84 Also seen in 2nd order |
| (1,5) | Not seen. Overwhelmed by 1N(0,1) |
| (1,6) | 457.43 |
| (1,7) | 491.68 |
| (2,1) | 313.60 Seen in 2nd order |
| (2,2) | 330.9, blend with 1N(2,0) Also seen in 2nd order blended with 2nd order1N(2,0) |
| (2,3) | 350.05 Also seen in 2nd order |
| (2,4) | 371.05 Also seen in 2nd order |
| (2,5) | 394.30 Also seen in 2nd order |
| (2,6) | 420.05 Blend with 1N(2,3) |
| (2,7) | 449.02 |
| (2,8) | 481.47 |
| (3,3) | 328.53 |
| (3,4) | 346.9 Also seen in 2nd order |
| (3,5) | 367.19 |

| | | |
|---|---|---|
| (3,6) | Not seen. Overwhelmed by 1N(0,0) | |
| (3,7) | 414.18 | |
| (3,8) | 441.67 | |
| (3,9) | 472.35 | |
| $N_2^+$ | | |
| 1N (0,0) | 391.44 | Also seen in 2nd order |
| (0,1) | 427.81 | |
| (0,2) | 470.92 | |
| (0,3) | 522.83 | |
| (0,4) | 586.47 | |
| (1,0) | 358.21 | Also seen in 2nd order |
| (1,1) | 388.43 | Also seen in 2nd order |
| (1,2) | 423.65 | |
| (1,3) | 465.18 | |
| (1,4) | 514.88 | |
| (1,5) | 575.44 | |
| (2,0) | 3308.0 | Blend with 2P(2,2). Also seen in 2nd order |
| (2,1) | 3563.9 | |
| (2,2) | 385.79 | |

| | | |
|---|---|---|
| (2,3) | 419.91 | Blend with 2P(2,6) |
| (2,4) | 459.97 | |
| (2,5) | 507.66 | |
| (3,5) | 455.41 | |
| (5,4) | 353.26 | Perhaps seen in 2nd order |

Table 2. Nitrogen I transitions expected in our wavelength range. The transitions are listed in the order in which they appear in the A-value compilation by Wiese, Smith, and Glennon. Average values are used for the wavelengths and transition probabilities, as in WSG. While most of the entries are listed as being possibly obscured (generally by molecular bands), there is no question but that those transitions, even if present, are extremely weak. It is impressive to compare these data with those for the comparable situation in oxygen, as discussed in the text.

| λ (nm) | Transition | A ($x10^{-8}$s) | Comments |
|---|---|---|---|
| 534.9 | $2s2p^4\ ^4P$ - $2s^22p^2(^3P)4p\ ^4D^o$ | 0.00252 | Possibly obscured |
| 529.5 | $^4P$ - $^4P^o$ | 0.00373 | Possibly obscured |
| 517.7 | $^4P$ - $^4S^o$ | 0.00427 | Possibly obscured |
| 745.2 | $2p^23s\ ^4P$ - $2p^2(^3P)3p\ ^4S^o$ | 0.318 | Possibly obscured |
| 410.7 | $2p^2(^3+)3s\ ^2P$ - $2p(^1D)3p'\ ^2D^o$ | 0.041 | Very small indication |
| 425.6 | $2p^23s\ ^4P$ - $2p^2(^3P)4p\ ^4D^o$ | 0.02 | Possibly obscured |
| 422.2 | $^4P$ - $^4P^o$ | 0.073 | Possibly obscured |

| | | | |
|---|---|---|---|
| 414.6 | $^4P$ - $^4S^o$ | 0.025 | No sign |
| 492.8 | $^2P$ - $^2S^o$ | 0.0234 | Slight indication of component at 493.5 nm. |
| 540.8 | $2p^2(^3P)3p\ ^2P^o$ - $2p^2(^1S)3''\ ^2S$ | 0.0111 | Possibly obscured |
| 438.9 | $^2P^o$ - $2p^2(^1D)3d'\ ^2S$ | 0.0153 | No sign |
| 664.4 | $2p^23p\ ^4D^o$ - $2p^2(^3P)5s\ ^4P$ | 0.0389 | Possibly obscured |
| 695.5 | $^4P^o$ - $^4P$ | 0.0212 | No sign |
| 520.0 | $^2S^o$ - 5d $^2P$ | 0.023 | Possibly obscured |
| 583.6 | $^4P^o$ - 6s $^4P$ | 0.0092 | Possibly obscured |

Table 3. Relative intensities for the transition array N II 3s $^3P^o$ - 3p $^3D$ from our nitrogen data and the relative transition probabilities, from WSG.

| $J_i$ - $J_f$ | Our Data | WSG |
|---|---|---|
| 1 - 2 | 56 | 54 |
| 0 - 1 | 23 | 24 |
| 2 - 3 | 100 | 100 |
| 1 - 1 | 15 | 18 |
| 2 - 2 | 19 | 18 |
| 2 - 1 | _ | 1.2 |

Table 4. Transitions identified from the spectra taken with oxygen as the target gas. We list in order of wavelength only those transitions which were seen cleanly. Sometimes a transition is seen more clearly in second order than in first, partly because of the improved resolution, partly because the spectrometer is more efficient in second order than in first. Approximate wavelengths are listed for lines in nm; however, the bands from $O_2^+$ are so much overlapped that it doesn't help to list wavelengths for them. Quite a few of the bands were seen in second order.

Monatomic lines from O I and O II

| Transition | Wavelength (nm) |
|---|---|
| O I | |
| $3p\ ^3P$ - $3s''\ ^3P^o$ | 395.3 |
| $3s\ ^3S^o$ - $4p\ ^3P$ | 436.8 |
| $3p\ ^5P$ - $5d\ ^5D^o$ | 533.0 |
| $3p\ ^5P$ - $4d\ ^5D^o$ | 615.7 |
| $3p\ ^5P$ - $5s\ ^5S^o$ | 645.4 |
| $3p\ ^3P$ - $4d\ ^3D^o$ | 700.2 |
| $3s''\ ^3P^o$ - $3p''\ ^3D$ | 748 |
| $3s\ ^5S^o$ - $3p\ ^5P$ | 777 |
| $3p\ ^5S^o$ - $4p\ ^5P$ | 394.8 (seen in second order) |
| $3s\ ^3S^o$ - $3p\ ^3P$ | 844.3 |

O II

| | |
|---|---|
| 3s $^2P$ - 3p $^2P^o$ | 397.3 Seen in 1st and 2nd orders |
| 3p $^4D^o$ - 3d $^4F$ | 409.3 Seen in 1stand 2nd orders |
| 3p $^4P^o$ - 3d $^4D$ | 411.1 Weak in 2nd order |
| 3p' $^2F^o$ - 3d' $^2G$ | 418 Seen in 1st and 2nd orders |
| 3d' $^2G$ - 4f' $^2H^o$ | 425.4 |
| 3d $^4D$ - 4f $^2F^o$ | 427 blend |
| 3d $^4D$ - 4f $^4F^o$ | 427 blend |
| 3d $^4P$ - 4p $^4D^o$ | 428,429 blend |
| 3d $^4D$ - 4f $^4F^o$ | 428,429 blend |
| 3d $^4P$ - 4f $^4D^o$ | 428,429 blend |
| 3d $^2F$ - 4f $^4F^o$ | 428,429 blend |
| 3d' $^2G$ - 4f' $^2G^o$ | 430 |
| 3d $^2F$ - 4f $^2F^o$ | 431,432 blend |
| 3d $^2F$ - 4f $^4F^o$ | 431,432 blend |
| 3d $^4D$ - 4f $^4D^o$ | 431,432 blend |
| 3d $^4D$ - 4f $^4F^o$ | 431,432 blend |
| 3s $^4P$ - 3p $^4P^o$ | 431,432 blend |
| 3d $^4P$ - 4f $^2D^o$ | 431,432 blend |
| 3s $^4P$ - 3p $^4P^o$ | 437 blend |
| 3p $^2D^o$ - 3d $^2D$ | 437 blend |
| 3d' $^2D$ - 4f' $^2F^o$ | 438 blend |
| 3d $^2F$ - 4f $^4G^o$ | 437 blend |
| 3d $^2D$ - 4f' $^2F^o$ | 437 blend |
| 3p' $^2P^o$ - 4d $^2P$ | 441 blend |

| | |
|---|---|
| $3s\ ^2P - 3p\ ^2D^o$ | 441 blend |
| $3s'\ ^2D - 3p'\ ^2F^o$ | 459 |
| $3d\ ^2D - 4f\ ^2F^o$ | 460 |
| $3s\ ^4P - 3p\ ^4D^o$ | 464 |
| $3s\ ^2P - 3p\ ^2S^o$ | 664 |
| $3d\ ^2P - 4p\ ^2P^o$ | 667 |
| $3s\ ^2P - 3p\ ^2S^o$ | 672 |
| $3p\ ^2S^o - 3d\ ^2P$ | 339 Seen in second order |
| $3d\ ^4F - 4p\ ^4D^o$ | 690 |
| $3p'\ ^2P^o - 4s'\ ^2D$ | 373 Seen in second order |
| $3p\ ^4S^o - 4s\ ^4P$ | 374 Seen in second order |
| $3s\ ^4P - 3p\ ^4S^o$ | 375 Seen in second order |
| $3s'\ ^2D - 3p'\ ^2P^o$ | 391 Seen in second order |
| $3s\ ^2P - 3p\ ^2P^o$ | 395 Seen in second order |
| $3d\ ^4F - 4f\ ^4D^o$ | 410 Seen in second order |
| $3p\ ^4P^o - 3d\ ^2F$ | 411 Seen in second order |
| $3p'\ ^2F^o - 3d'\ ^2D$ | 411 Seen in second order |

$O_2^+$

**2N $A\ ^2\Pi_u - X\ ^2\Pi_g$**

(0,6i), (0,6ii), (0,7i), (0,7ii), (0,8i), (0,8ii),
(0,9i),(0,9ii),(0,11ii)

(1,6ii), (1,8i), (1,8ii), (1,12i)

(2,7i), (2,7ii), (2,8i), (2,8ii)

**1N $b^4\Sigma_g - a\,^4\Pi_u$**

(0,0), (0,1), (0,2), (0,3)

(1,0), (1,1), (1,2), (1,4)

(2,0), (2,1), (2,2)

(3,0), (3,1), (3,2), (3,3)

(4,1), (4,2), (4,3), (4,4)

(5,2), (5,3), (5,4), (5,5)

(6,4)

(7,5)

Table 5. Relative intensities from some of our oxygen data and the relative transition probabilities, from WSG. It will be seen that, as in the case of nitrogen, our measured relative intensities within any multiplet are in excellent agreement with the calculated values.

| Transition in O I | Wavelength (nm) | Our Data | WSG |
|---|---|---|---|
| $3s\ ^5S^o - 3p\ ^5P$ | | | |
| $J_f - J_i$ | | | |
| 2 - 3 | 777.2 | 100 | 100 |
| 2 - 2 | 777.4 | 72 | 71 |
| 2 - 1 | 777.5 | 43 | 43 |
| Transitions in O II | | | |
| $3s\ ^2P_{3/2} - 3p\ ^2P_{3/2}^o$ | 397.32 | 100 | 100 |
| 3/2 - 1/2 | 398.27 | 18 | 18 |
| $3s'\ ^2D_{5/2} - 3p'\ ^2F_{7/2}^o$ | 459.10 | 100 | 100 |
| 3/2 - 5/2 | 459.62 | 77 | 70 |
| $3s\ ^4P_{1/2} - 3p\ ^4D_{3/2}^o$ | 463.89 | 27 | 20 |
| 3/2 - 5/2 | 464.18 | 57 | 57 |
| 5/2 - 7/2 | 464.91 | 100 | 100 |
| 1/2 - 1/2 | 465.08 | 23 | 20 |
| 3/2 - 3/2 | 466.16 | 23 | 25 |

Table 6. Comparison of electron excitation cross sections and our measured relative intensities for monatomic lines from neutral oxygen. For conformity with the electron excitation data, we give our relative intensities in terms of the sums of the individual peak line intensities for all members of the multiplets studied. For simplicity in making the comparisons, we have normalized our intensities to the highest value (430) given for the electron data. The two columns labeled N are normalized to 100 for the most intense feature. However, we caution that our measurements have not been corrected for the wavelength response of our system. Furthermore, the slit settings for the run of interest were less than optimal.

| Multiplet | Cross Section ($\times 10^{-20}$ cm$^2$) | N | Our Relative Intensities Counts | N |
|---|---|---|---|---|
| 3p $^5$P - 5s $^5$S$^o$ | 3.7 | 0.9 | 4,200 | 1.5 |
| 3p $^5$S$^o$ - 3p $^5$P | 430 | 100 | 283,700 | 100 |
| 3p $^5$P - 4d $^5$D$^o$ | 11 | 2.6 | 8,019 | 2.8 |
| - 5d $^5$D$^o$ | 3.4 | 0.8 | | |
| 3s $^3$S$^o$ - 3p $^3$P | 200 | 47 | 44,810 | 15 |
| 3p $^3$P - 3s" $^3$P$^o$ | <0.01 | <0.002 | | |
| 3p $^3$P - 4d $^3$D$^o$ | 1.4 | 0.3 | 2,037 | 0.7 |
| 3s' $^3$D$^o$ - 3p' $^3$D | 8.6 | 2 | 4,750 | 1.7 |
| 3s" $^3$P$^o$ - 3p" $^3$D | < 1.1 | <0.26 | 1,150 | 0.4 |

## Figure Captions

1. Schematic representation of the target chamber. When the beam exits from the chamber, it is collected in an unshielded Faraday cup (not shown). The pressure in the vacuum system can be measured both before and after the gas cell. Light passes through a vertical quartz plate (not shown) and is focussed onto the entrance slit of an air Czerny-Turner scanning monochromator. A photomultiplier tube is located beyond the exit slit of the monochromator.
2. Spectrum obtained from the bombardment of 200 mTorr of $N_2$ with ions of $H_3^+$ at 1 MeV. The line width was about 0.1 nm. The spectral range extends from 3200 to 3600 A. Identifications of the prominent features are found from the shapes, which are clear signatures that molecular excitations are being seen, and the wavelengths of the band heads. Reading from left to right, the four prominent features are due to 2P(0,0), 2P(1,2), 2P(0,1), and 1N(1,0), respectively.
3. As in Fig. 2, but with a different ordinate, so as to exhibit weak components of the spectrum.
4. As in Fig. 2, but for the range 3665 to 4065 A. The 1N(0,0) band is well exhibited here. It is the strongest feature we see.
5. As in Fig. 4, but with a different ordinate. Many 2P bands are evident. From left to right, they are 2P(3,5), 2P(2,4), 2P(1,3),

2P(0,2), 1N(2,2), 1N(1,1), 1N(0,0) (off scale), 2P(2,5), 2P(1,4), and 2P(0,3). Comparison of Figs. 4 and 5 shows how dominant the 1N(0,0) band is.

6. As in Fig. 2, but for the range 4100 to 4550 A. Here we find the bands 1N(1,2) at 423.65 nm and 1N(0,1) at 427.81 nm.

7. As in Fig. 6, but with a different ordinate. A monatomic line can be seen here. It is from N II 3d $^1F^o$ - 4f $G(9/2)_4$ at 453.04 nm. The weak bands are mostly from the 2P series, although 1N(2,3) is present at 419.91 nm, blended with 2P(2,6) at 420.05 nm.

8. As in Fig. 2, but for the range 4550 to 4950 A. The main features are from 1N(1,3) at 465.18 nm and 1N(0,2) at 470.92 nm, both of whose rotational lines are clearly displayed.

9. Primarily as in Fig. 8, but with a different ordinate; the range is from 4550 to 4950 A, and the ordinate is expanded so as to show minor spectral features.

10. As in Fig. 2, but for the range 4995 to 5445 A. Strong monatomic lines appear; they are from N II 3p $^3D$ - 3d $^3F^o$ near 500 nm. Additional 1N bands (1,4) at 514.88 nm and (0,3) at 522.83 nm are also obvious.

11. As in Fig. 10, but with a different ordinate. One can identify 1N(2,5), 1P(12,7), 1P(11,6), and 1P(10,5), but they are weak and badly blended.

12. As in Fig. 2, but for the range 5498 to 5898 A. Many more transitions from $N^+$ states are found here, along with further

bands of the 1N and 1P character. The N II 3s $^3P^o$ - 3p $^3D$ appears between 565 and 570 nm.

13. As in Fig. 12, but for the range 5648 to 5898 A, showing some of the molecular transitions in greater detail.

14. Much as in Fig. 13, but with a different ordinate. Additional weak features are seen.

15. As in Fig. 2, but for the range 5900 to 6350 A. The five weak features on the left-hand portion of the figure are from the 1P series, while, at the right, there is the 2P(2,1) band adjacent to the blend of the 2P(1,0) band, seen in second order, and the 1P(10,7) band.

16. As in Fig. 15, but with a different ordinate. In addition to the five 1P bands mentioned in caption 15, the 1P(12,9) band at 618.5 nm can also be distinguished.

17. As in Fig. 2, but for the range 6350 to 6800 A. Nine bands from 1P, 2P, and 1N appear here, some in second order. Some blending is also apparent.

18 As in Fig. 17, but with a different ordinate. This allows one to see the 1P(9,6) band at 639.47 nm, which has only half the intensity of the 1P(8,5) band at 646.85 nm, itself quite weak. It is instructive to compare Figs. 17 and 18, for that comparison indicates how far down into the noise we can go and still detect spectral contributions.

19. As in Fig. 2, but for the range 6800 to 7200 A. The strongest feature shown is from 2P(0,1) at 357.69 nm, which is seen in second order.

20. As in Fig. 19, but with a different ordinate so as to exhibit weak components of the spectrum. Some of the bands are in second order.

21. As in Fig. 2, but for the range 7250 to 7650 A. Numerous 1P and 2P bands show up, some in second order.

22. As in Fig. 2, but for the range 7685 to 7835 A. The prominent peaks arise from 1N(0,0), seen in second order, with its accompanying rotational structure.

23. As in Fig. 22, but with a different ordinate and a somewhat expanded abscissa. The three features to the right of 1N(0,0) are from 2P(2,5), 2P(1,4), and 2P(0,3), respectively, all in second order.

24. High-resolution scan of the N II transition array 3p $^3D_2$ - 3d $^3F^o_2$. Note that the width of the left-hand feature is greater than that of the right-hand part. That is because the left "line" includes two components, which are only 0.03 nm apart. However, the width of the isolated member is considerably wider than the instrumental line width, and gives evidence for the Doppler broadening from which we deduce the excitation mechanism, and which is discussed in the text.

25. High-resolution scan of the N II transition array 3s $^3P^o_1$ -

$3p\ ^3D_2$. Five components of this array are clearly seen. Measurements of the relative intensities of these components are used in our comparison with values in the experimental literature and with the calculated transition probabilities.

26. High-resolution scan of the 1N(0,0) band at 391.4 nm, taken in second order. The target pressure was 150 mTorr; the instrumental line width was about 0.15 A, far better than anything comparable in the literature. Still, one could hope for improvements, particularly with the wavelength drive, which was not as constant as one would like. The variations in drive show up as variations in line width for the rotational lines.
27. As in Fig. 26, but for a pressure of 200 mTorr.
28. Model calculation of the rotational structure of the 1N(0,0) band for the 200 mTorr data, assuming a temperature of 300 K and excitation from electrons on $N_2$. Comparison of these relative intensities with those observed shows that the fit could be improved.
29. As in Fig. 28, but with an assumed temperature of 350 K. This yields the best fit to the data.
30. As in Fig. 28, but with an assumed temperature of 400 K. This fit to the data is not as good as that of Fig. 29. It is instructive to make a detailed comparison of the relative peak heights of the rotational feratures for the three calculated figures, for they show the effect of changing the temperature.

31. Spectral scan using an incident beam of $H_2^+$at an energy of 667 keV. This energy was selected so as to have the same particle velocity as in the $H_3^+$ data. The target pressure was 100 mTorr. The data for the $H_2^+$ runs were not very good.
32. As in Fig. 29, but for a longer wavelength range.
33. As in Fig. 29, but for a longer wavelength range.
34. Scans over several lines and bands for a target pressure of 10 mTorr. The lines, all from N II are, respectively, 3p $^3D_1$ - 3d $^3Fo_2$ and 3p $^3D_2$ - 3d $^3Fo_3$ at 500.11 and 500.15 nm, 3p $^3D_3$ - 3d $^3Fo_2$ at 500.51 nm, 3s $^3Po_2$ - 3p $^3D_3$ at 567.96 nm, and 3s $^3Po_1$ - 3p $^1P_1$ at 648.21 nm. The bands arise from 2P(0,0) and 1N(0,0), both seen in second order. These data were taken as part of the study of the pressure-dependence of various radiations. The abscissa is NOT proportional to the wavelength of the features. Note, further, that to obtain the proper pressure-dependence from these and the next following curves requires correction for both the dependence of the apparent current as a function of target pressure and the collected charge. The pressure-corrected curves appear in Figs. 44 - 47, with a summary set of curves in Fig. 48.
35. As in Fig. 34, but for a target pressure of 20 mTorr.
36. As in Fig. 35, but with a different ordinate.
37. As in Fig. 34, but for a target pressure of 40 mTorr.
38. As in Fig. 37, but with a different ordinate.
39 As in Fig. 34, but for a target pressure of 80 mTorr.

40. As in Fig. 39, but with a different ordinate.

41. As in Fig. 34, but for a target pressure of 200 mTorr.

42. As in Fig. 41, but with a different ordinate.

43. Measurement of the apparent current collected in the Faraday cup as a function of nitrogen pressure in the target cell.

44. Pressure-variation of a number of 1P band heads. These data, which were obtainee by setting the spectrometer on the peak yield of each band, have been corrected for pressure- and time-dependence of the method of collecting data, as discussed in the text. The shapes are all quite similar.

45. Pressure-variation of a number of 2P band heads. These shapes are similar to one another and also to those of the 1P curves of Fig. 44.

46. Pressure-variation of a number of monatomic lines from N II. These curves are quite different from those of Figs. 44 and 45.

47. Pressure-variation of a number of 1N band heads. These data resemble those of Fig. 46.

48. Summary of representative pressure-variations of monatomic lines and band heads. It is clear that the 1P and 2P bands have a similar pressure-dependence. So do the 1N and N II features. However, the latter and former pairs obviously have different pressure responses.

49. The first in a series of spectral scans taken with oxygen as the target gas. The pressure was 100 mTorr, and the incident particle was again $H_3^+$ at 1 MeV. The spectral range was from

3225 to 3925 A. Although the yield is low, the oscillations that appear are physically significant. It is quite possible that there are contributions from $O_2^+$ 2N(2,6i) all the way to (0,8ii), in addition to the $O_2$ Herzberg System I and night-sky bands in this spectrum. The blending is severe.

50. As in Fig. 49, the range being continued to 4200 A. In this region of the spectrum, lines from O II are clearly present; the strongest are from O II 3p $^4D^o$ - 3d $^4F$, 3p $^4D^o$ - 3d $^4F$ near 407 nm, and 3p' $^2F^o$ - 3d' $^2G$ near 418 nm.

51. A small part of Fig. 50 is shown here so as to clarify the relative intensities of the transition array O II 3s $^2P$ - 3p $^2P^o$ near 397 nm.

52. The spectrum from 4050 to 4130 A.. Here the multiplet O II 3p $^4D^o$ - 3d $^4F$, near 407 nm, is well defined.

53. Resolution of the multiplet O II 3p' $^2F^o$ - 3d' $^2G$ near 419 nm.

54. The spectrum from 430.0 to 467.5 nm. The strongest lines, all from transitions in $O^+$, are from 3p' $^2P^o$ - 4f $^2P$ and 3s' $^2P$ - 3p $^2D^o$ near 441 nm; 3d $^2D$ - 3p' $^2F^o$ and 3d $^2D$ - 4f $^2F^o$; and 3s $^4P$ - 4f $^2F^o$ near 464 nm.

55. A continuation of the spectrum out to 5100 A. A complicated band structure is evident. Apparently, contributions from 2N(0,11ii), 2N(1,12i), 1N(5,2), 1N(4,1), and 1N(3,0) are present.

56. The spectrum from 5145 to 5545 A. The large structure comes from a blend of six different vibrational transitions in the 1N system. Near 530 nm, one sees a line from O I 3p $^5P$ - 5d $^5D^o$.

57. In the wavelength interval 5525 to 5675 A there is another example of overlapping bands in $O_2^+$, these arising from the 1N(5,4), (4,3), (3,2), (2,1), and (1,0) transitions.

58. A high-resolution scan of part of the band structure shown in Fig. 57. The target pressure was changed from 100 to 200 mTorr so as to increase the yield.

59. A continuation of Fig. 58.

60. A further extension of Fig. 58.

61. An extension of Fig. 58 to 5870 A.

62. An extension of Fig. 58 to 5896 A.

63. An extension of Fig 58 to 5936 A.

64. An extension of Fig. 58 to 6030 A.

65. The spectrum for the range between 5900 and 6300 A. The strong line is from O I 3p $^5P$ - 4d $^5D^o$ near 615 nm.

66. An extension of Fig. 65 out to 6500 A.

67. Resolution of the O I 3p $^5P$ - 4d $^5D^o$ quintet seen in Figs. 65 and 66.

68. High-resolution scan of the range from 6310 to 6460 A.

69. High-resolution scan of the range from 6630 to 6680 A The strong line is from O II 3p $^2P_{1/2}$ - 3p $^2S^0_{1/2}$ at 664 nm. The 3/2-1/2 component is at 672 nm, and is also seen..

70. As in Fig. 69, but extended in wavelength.

71. An expanded portion of Fig. 70, from 6670 to 6720 A.

72. An extension of Fig. 71 to 6760 A.

73. An extension of Fig. 72 to 6800 A.

74. An extension of Fig. 73 to 6840 A.

75. An extension of Fig. 74 to 6880 A.

76. An extension of Fig. 75 to 6915 A. The strongest feature is from O II 3d $^4F$ - 4p $^4D^o$.

77. Scan of the range from 6705 to 7105 A at a pressure of 100 mTorr. The strong line near 700 nm is from O I 3p $^3P$ - 4d $^3D^o$.

78. The line O I 3p $^3P$ - 4d $^3D^o$. Here the pressure was 200 mTorr, but the line width one/third that of Fig. 77. This effort to resolve the triplet was not too successful, since the line spacing is only 0.03 nm.

79. The spectrum from 6980 to 7030 A.

80. Extension of the scan from 7100 to 7700 A.

81. An expansion of part of Fig. 80. Most of the structure is from 2N bands, seen in second order.

82. An extension of Fig. 81.

83. An extension of Fig. 82.

84. An extension of Fig. 83. The strong lines are from O II (3p' $^2P^o$ - 4s' $^2D$ and 3s $^4$ P - 3p $^4S^o$) and O I (3s" $^5S^o$ - 3p" $^3D$), the former lines seen in second order, the latter, in first order.

85. An expansion of part of Fig. 84. This further illustrates the difficulty of resolving the individual contributions of oxygen bands to the spectrum.

86. An extension of Fig. 85. The lines referred to in the caption to Fig. 84 are more clearly delineated here.

87. An extension of Fig. 86 to 7680 A.

88. The spectrum from 7600 to 8200 A. There are some O I transitions here (3s $^5S^o$ - 3p $^5P$ near 777 nm and 3p $^5S^o$ - 4p $^5P$ near 395 nm seen in second order), but most are from O II (3s $^2P$ - 3p $^2P^o$ near 397 nm and 3p $^4D^o$ - 3d $^4F$ near 409 nm, both seen in second order).

89. Fig. 88 with a reduced ordinate. This illustrates the large intensity of O I 3s $^5S^o$ - 3p $^5P$, relative to other features.

90. An expanded version of Fig. 89, showing resolution of the components of the O I 3s $^5S^o$ - 3p $^5P$ transition array.

91. A high-resolution scan of the multiplet O I 3s $^5S^o$ - 3p $^5P$.

92. The scan from 7600 to 8200 A. The ordinate is changed from that of Fig. 88.

93. An expanded version of Fig. 92, from 7800 to 7900 A. The lines are all second-order from O II (3s' $^2D$ - 3p' $^2P^o$ at 391 nm and 3s $^2P$ - 3p $^2P^o$ near 395 nm).

94. A continuation of Fig. 93 out to 7980 A; one of the lines is from O I (3p $^3P$ - 3s" $^3P^o$ near 395.3 nm, seen in second order). The others are from O II (3s $^2P$ - 3p $^2P^o$ near 397.3 nm, also in second order).

95. The spectrum from 8125 to 8250 A. The lines are from O I (3s' $^3D^o$ - 3p' $^3D$ near 823 nm in first order) and O II (3p $^4D^o$ - 3d $^4F$ near 407 nm in second order).

96. A continuation of Fig. 95 to 8290 A. Once again, molecular bands appear.

97. A continuation of Fig. 96 to 8340 A.

98. The scan from 8240 to 8490 A. This region is devoid of molecular features, but lines from O II and O I are strong The most intense feature is from O I 3s $^3S^o$ - 3p $^3P$ near 845 nm.

99. An enlarged view of part of Fig. 98. The lines are from O II, 3p' $^2F^o$ - 3d' $^2G^o$, *in second order.*

100. High-resolution scan of the multiplet O II 3p' $^2F^o$ - 3d' $^2G$.

101 - 108. These are scans taken with a filter in front of the entrance slit of the spectrometer. The filter cut out all light with wavelengths shorter than 500 nm, so that all second-order features were eliminated from the observed spectrum. This was of great assistance in identifying the components of the spectrum. For example, much of the structure of Figs. 70-75 is missing from Fig. 101, but the effect is particularly striking in a comparison of Figs. 84 and 101. Again, Fig. 86 shows a number of lines which are gone from Fig. 101, and so forth.

109. Apparent current to the Faraday cup vs. pressure for the oxygen target gas.

110. Corrected pressure-dependence of the transition O I 3p $^5P$ - 4d $^5D^o$.

111. Corrected pressure-dependence of the transition O II 3s $^4P$ - 3p $^4D^o$.

112. Corrected pressure-dependence of a number of overlapping bands of the first negative system in $O_2^+$.

# TARGET CHAMBER
## (sub-assembly)

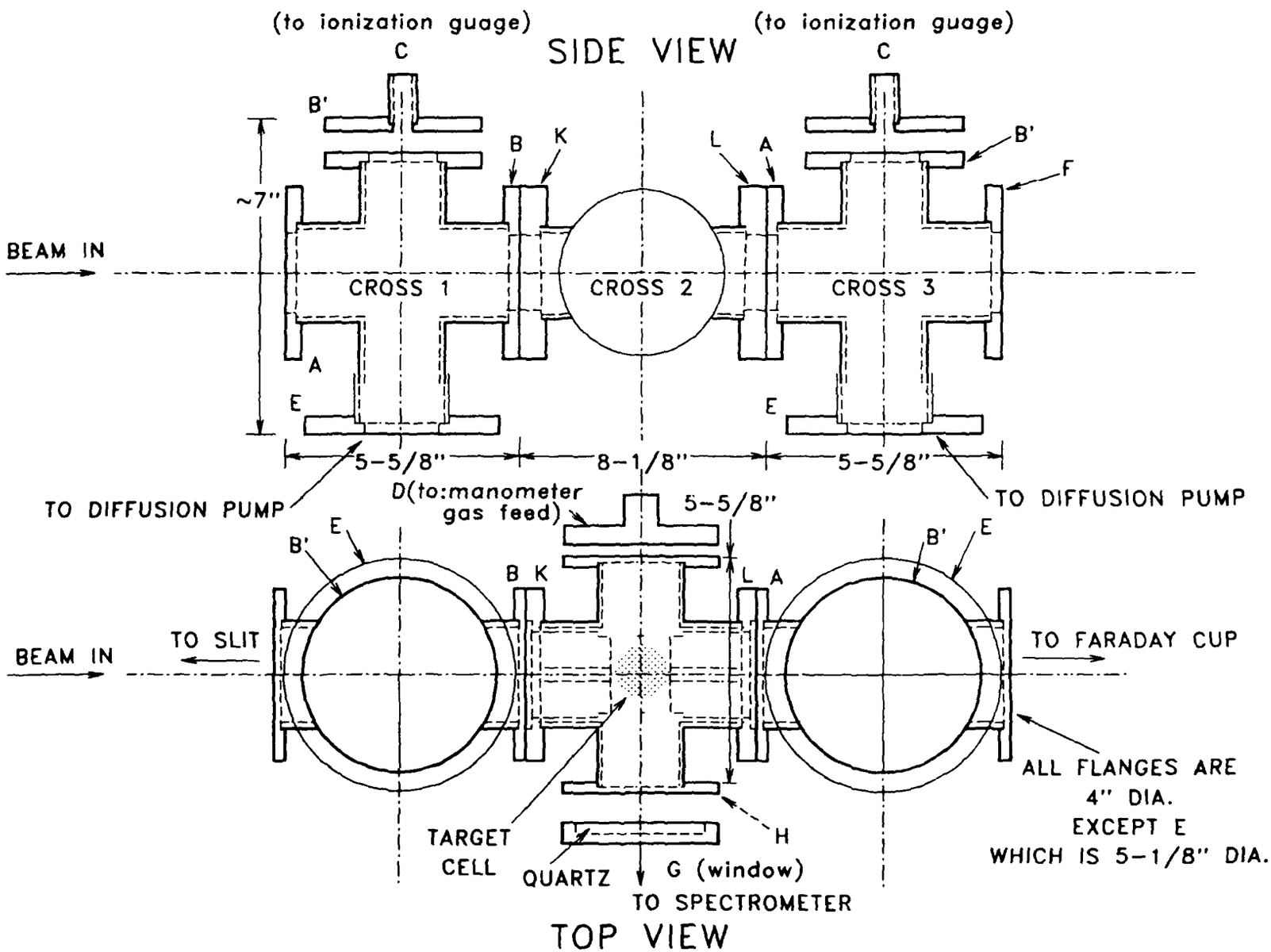


**Figure 1**

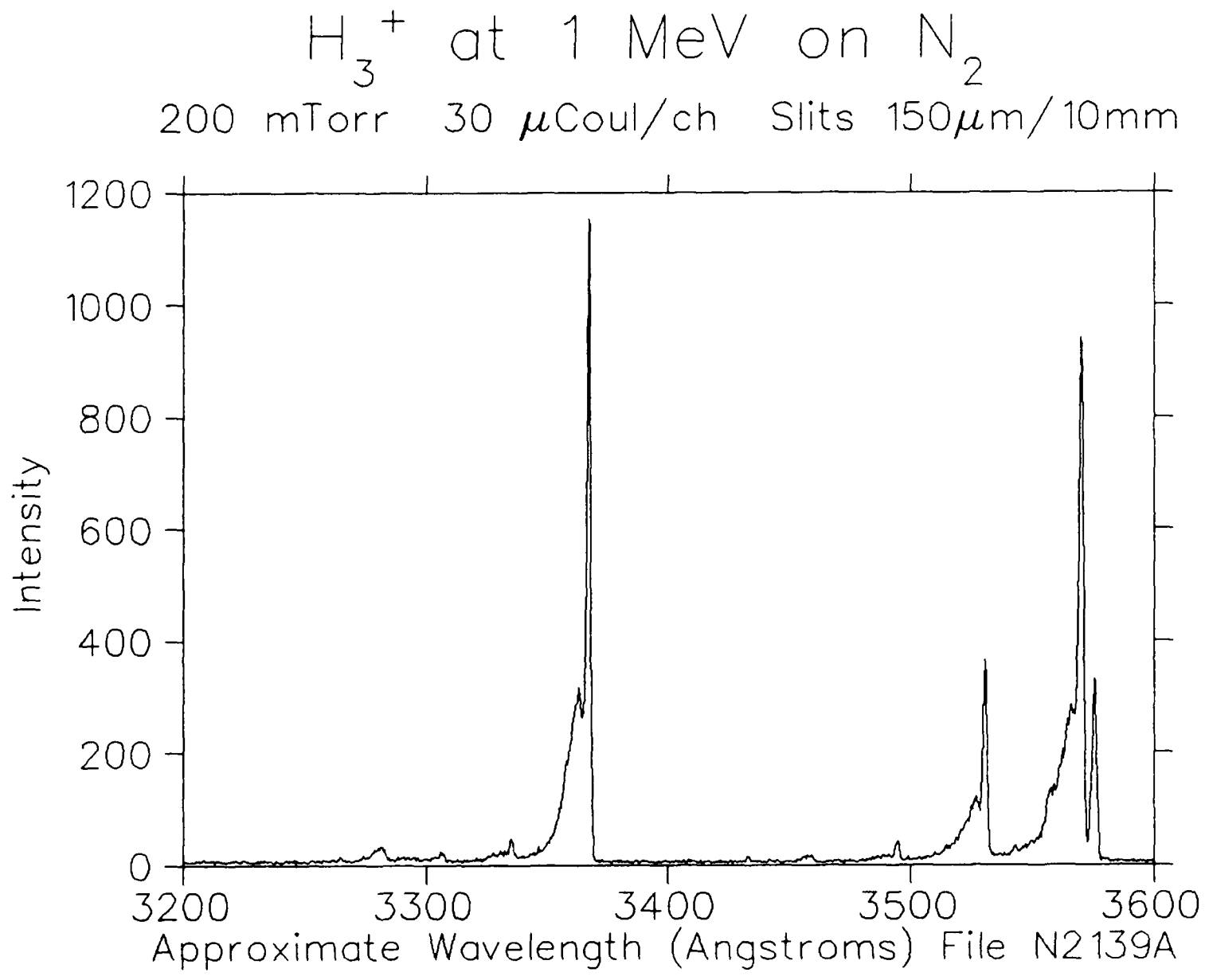
$H_3^+$ at 1 MeV on $N_2$
200 mTorr 30 μCoul/ch Slits 150μm/10mm
Intensity
1200
1000
800
600
400
200
0
3200
3300
3400
3500
3600
Approximate Wavelength (Angstroms) File N2139A

Fig. 2

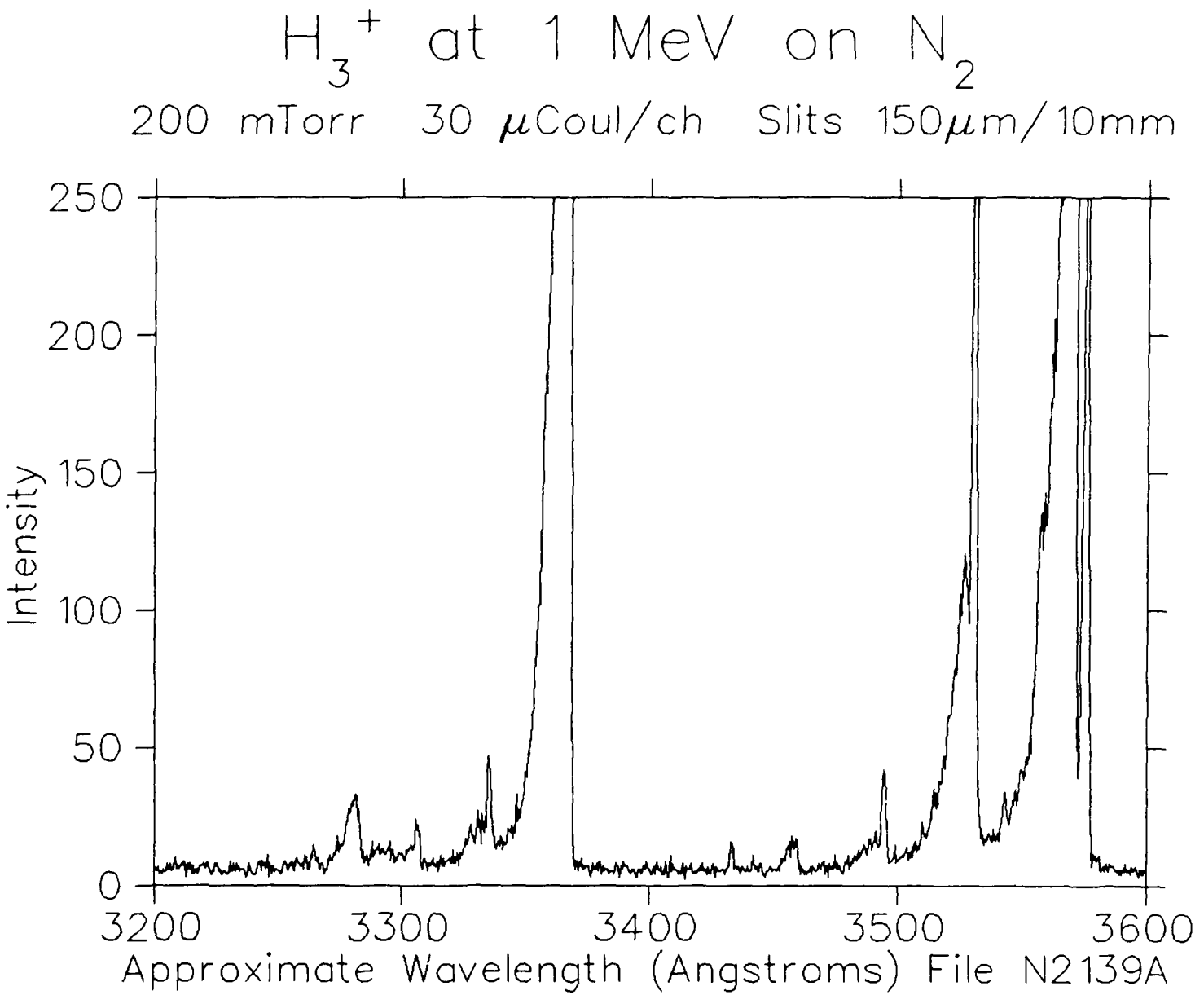
$H_3^+$ at 1 MeV on $N_2$
200 mTorr 30 μCoul/ch Slits 150μm/10mm
Intensity
250
200
150
100
50
0
3200
3300
3400
3500
3600
Approximate Wavelength (Angstroms) File N2139A

Fig. 3

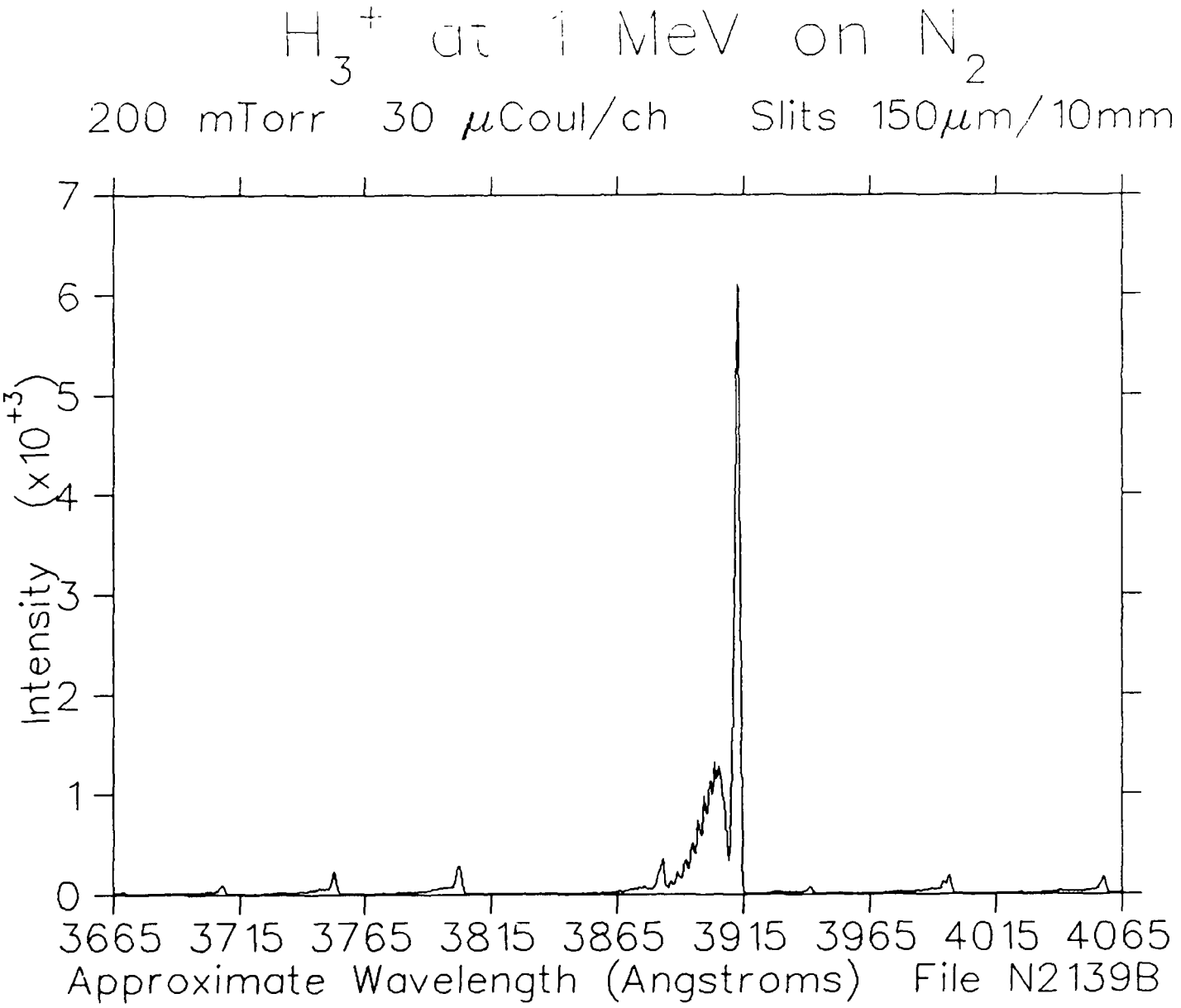
$H_3^+$ at 1 MeV on $N_2$
200 mTorr 30 μCoul/ch Slits 150μm/10mm
Intensity (x10^+3)
0
1
2
3
4
5
6
7
3665 3715 3765 3815 3865 3915 3965 4015 4065
Approximate Wavelength (Angstroms) File N2139B

Fig. 4

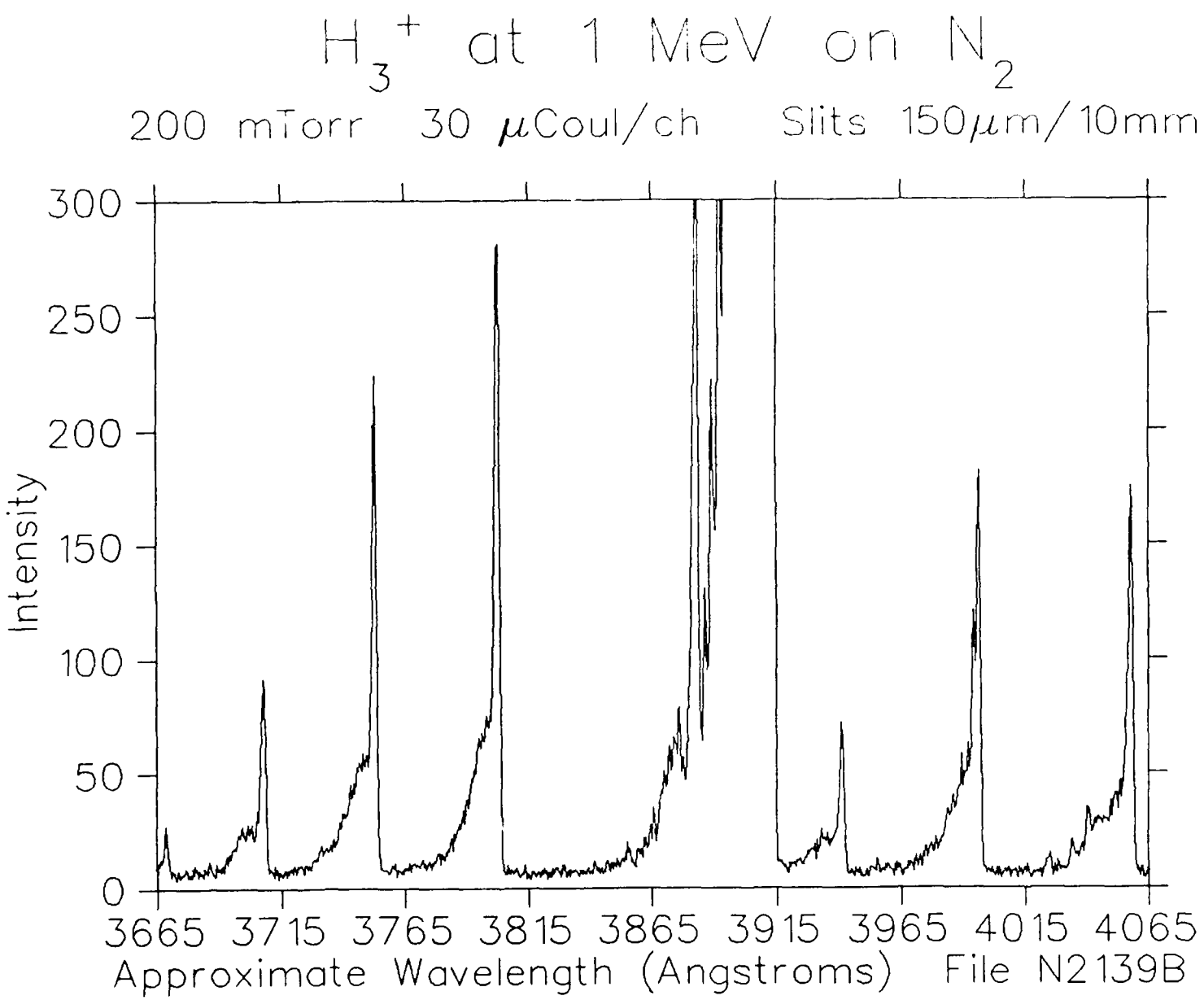
$H_3^+$ at 1 MeV on $N_2$
200 mTorr 30 μCoul/ch Slits 150μm/10mm
Intensity
300
250
200
150
100
50
0
3665 3715 3765 3815 3865 3915 3965 4015 4065
Approximate Wavelength (Angstroms) File N2139B

Fig. 5

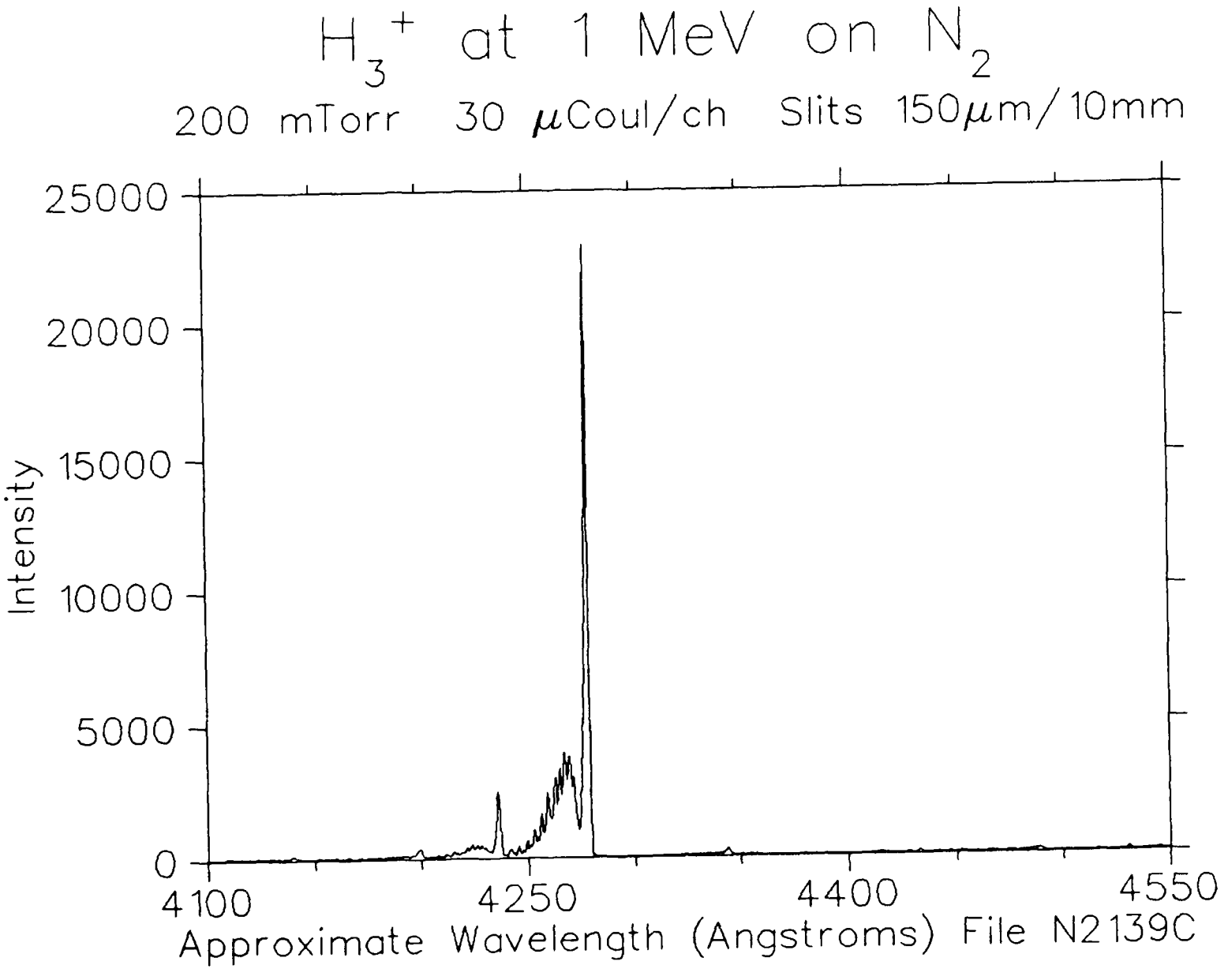
$H_3^+$ at 1 MeV on $N_2$
200 mTorr 30 μCoul/ch Slits 150μm/10mm
25000
20000
15000
10000
5000
0
Intensity
4100
4250
4400
4550
Approximate Wavelength (Angstroms) File N2139C

Fig. 6

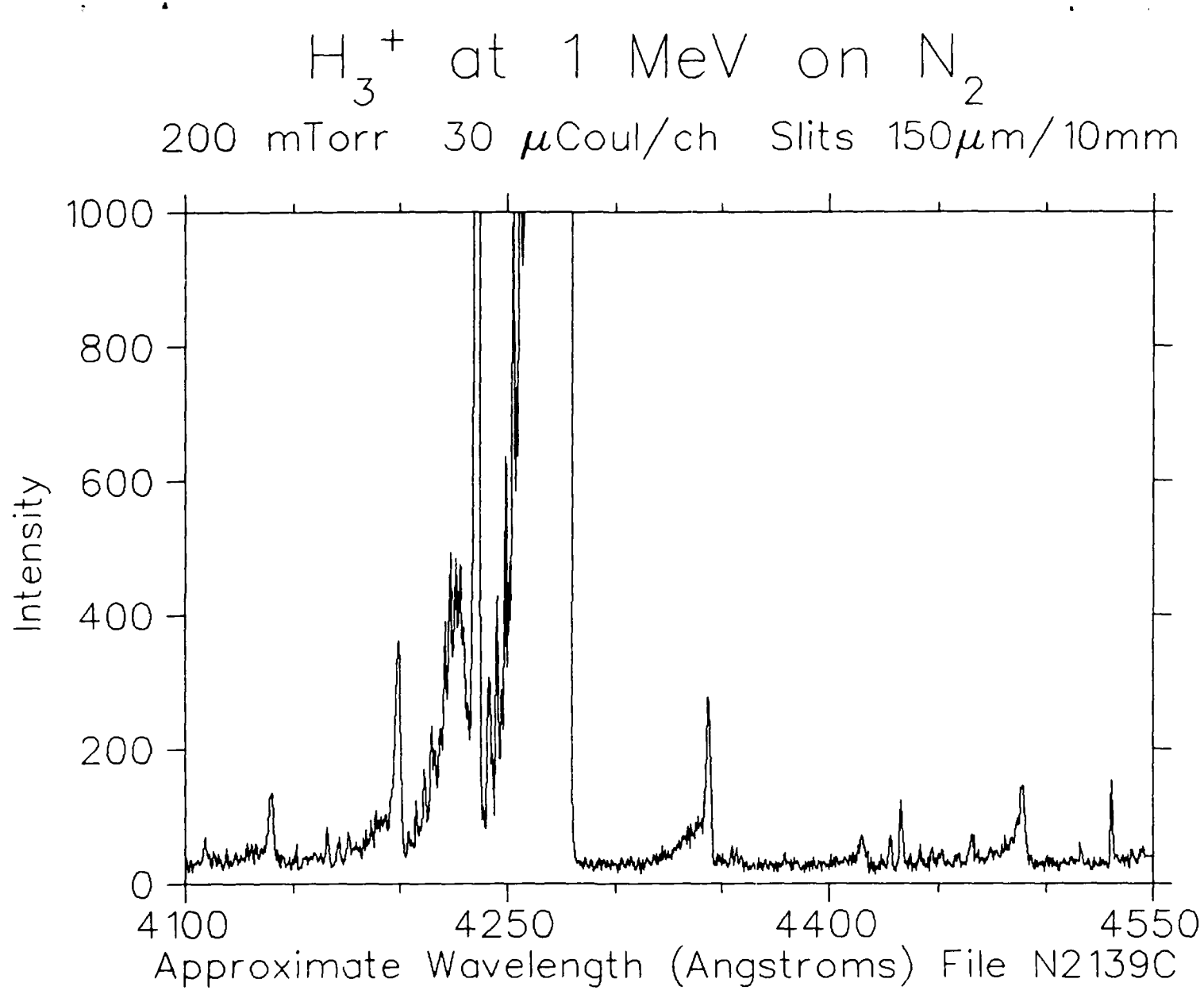
$H_3^+$ at 1 MeV on $N_2$
200 mTorr 30 μCoul/ch Slits 150μm/10mm
Intensity
1000
800
600
400
200
0
4100
4250
4400
4550
Approximate Wavelength (Angstroms) File N2139C

Fig. 7

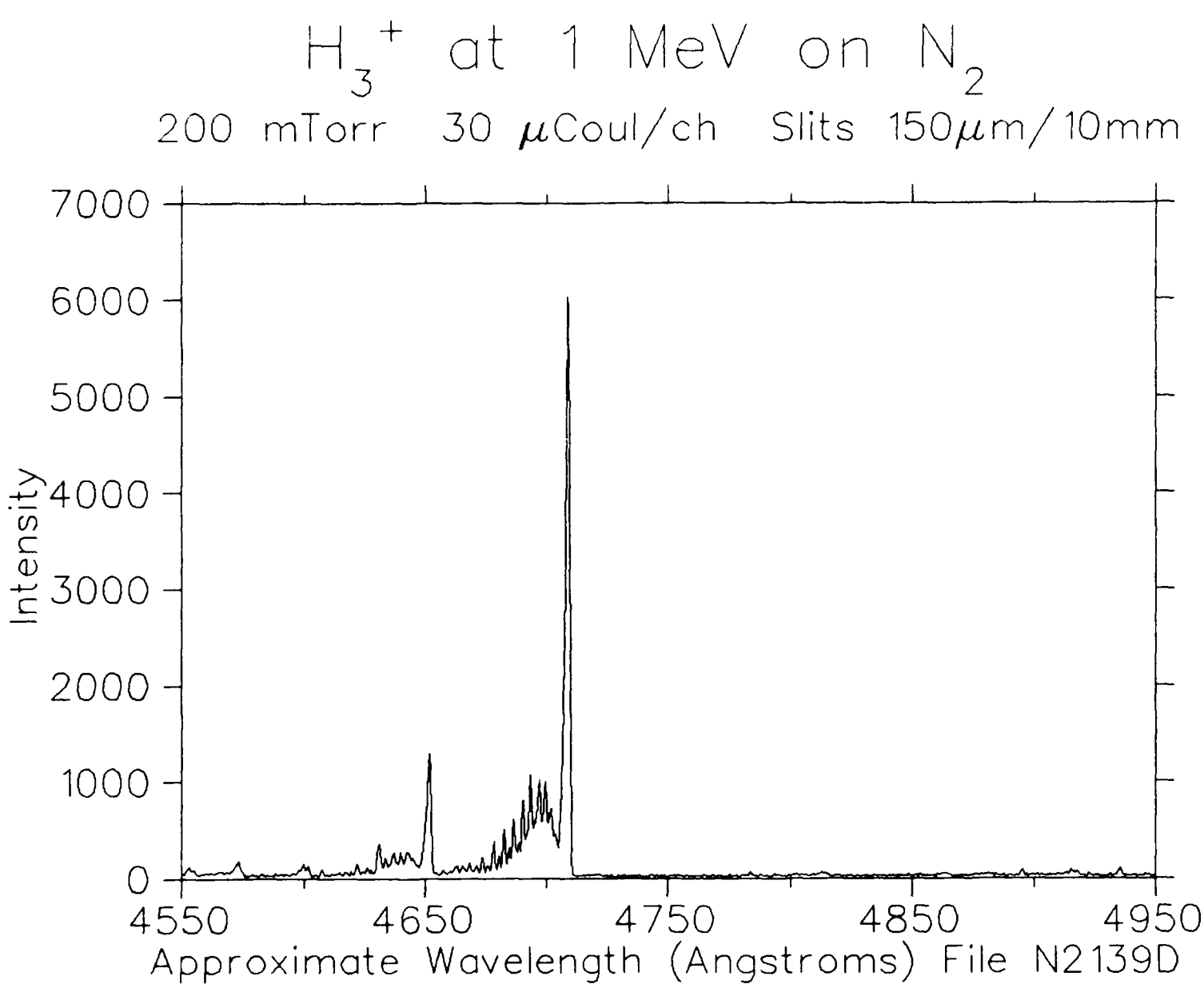
$H_3^+$ at 1 MeV on $N_2$
200 mTorr 30 μCoul/ch Slits 150μm/10mm
Intensity
7000
6000
5000
4000
3000
2000
1000
0
4550
4650
4750
4850
4950
Approximate Wavelength (Angstroms) File N2139D

Fig. 8

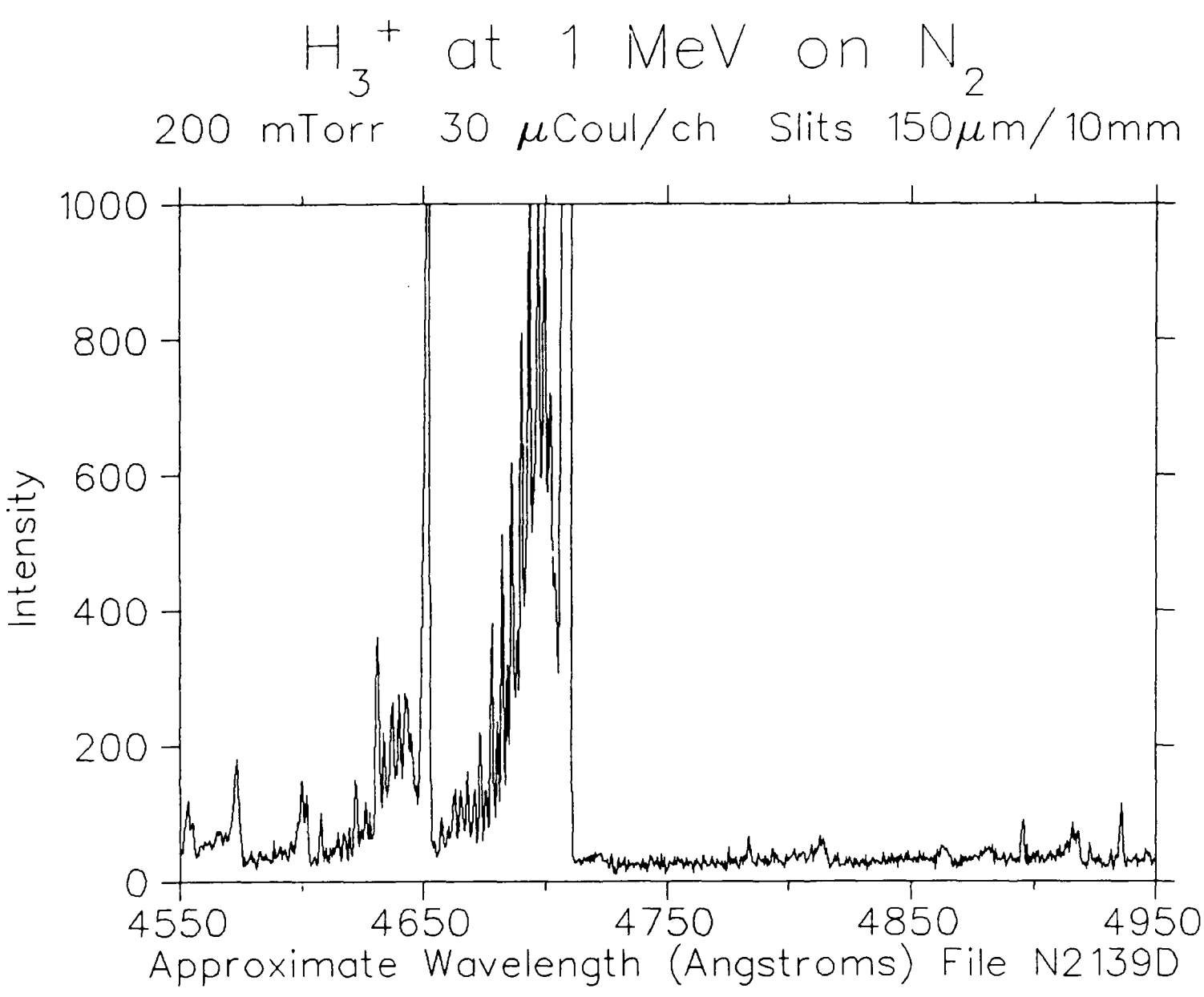
$H_3^+$ at 1 MeV on $N_2$
200 mTorr 30 μCoul/ch Slits 150μm/10mm
Intensity
1000
800
600
400
200
0
4550
4650
4750
4850
4950
Approximate Wavelength (Angstroms) File N2139D

Fig. 9

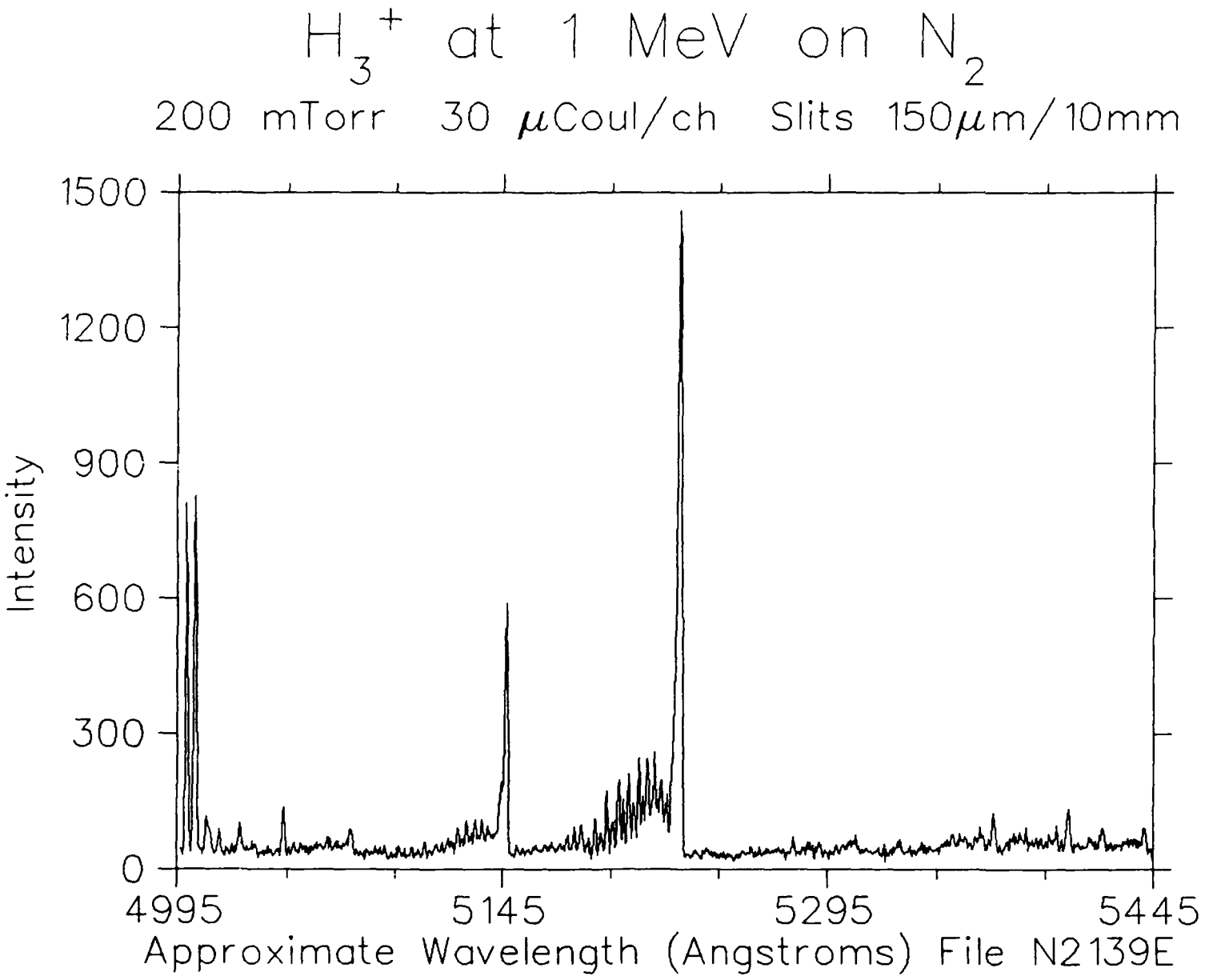
$H_3^+$ at 1 MeV on $N_2$
200 mTorr 30 μCoul/ch Slits 150μm/10mm
Intensity
1500
1200
900
600
300
0
4995
5145
5295
5445
Approximate Wavelength (Angstroms) File N2139E

Fig. 10

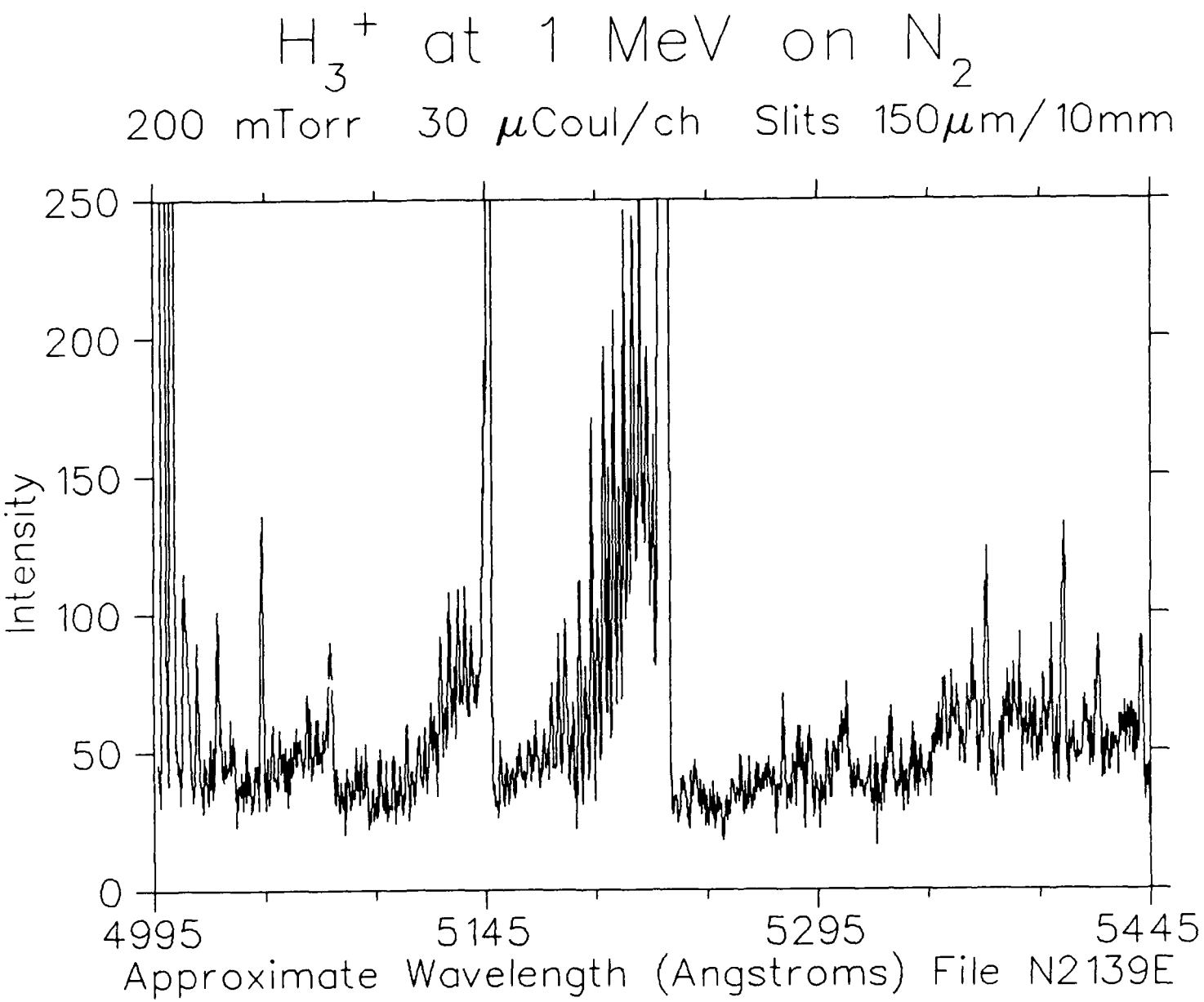
$H_3^+$ at 1 MeV on $N_2$
200 mTorr 30 μCoul/ch Slits 150μm/10mm
Intensity
250
200
150
100
50
0
4995
5145
5295
5445
Approximate Wavelength (Angstroms) File N2139E

Fig. 11

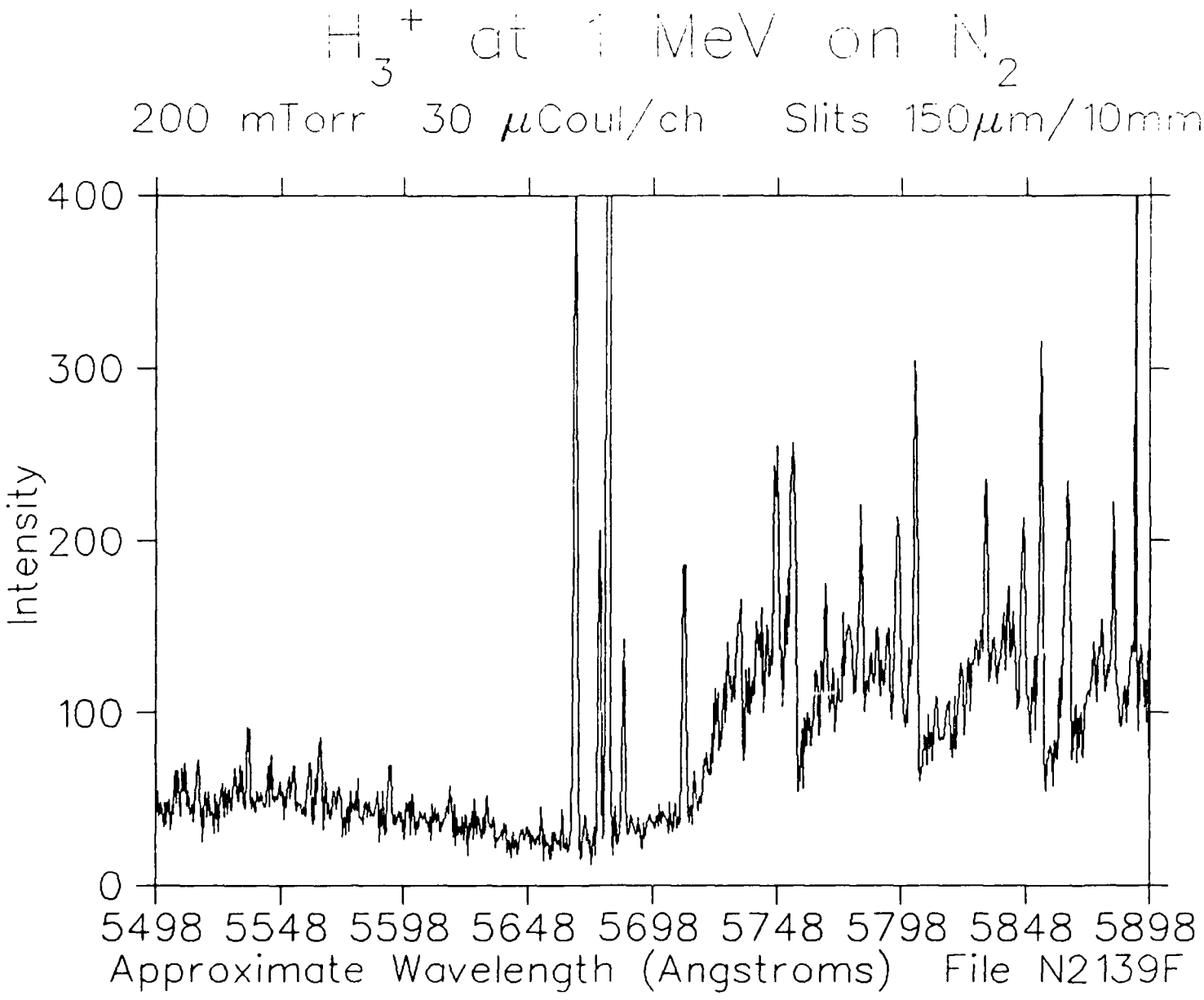
$H_3^+$ at 1 MeV on $N_2$
200 mTorr 30 μCoul/ch Slits 150μm/10mm
Intensity
400
300
200
100
0
5498 5548 5598 5648 5698 5748 5798 5848 5898
Approximate Wavelength (Angstroms) File N2139F

Fig. 12

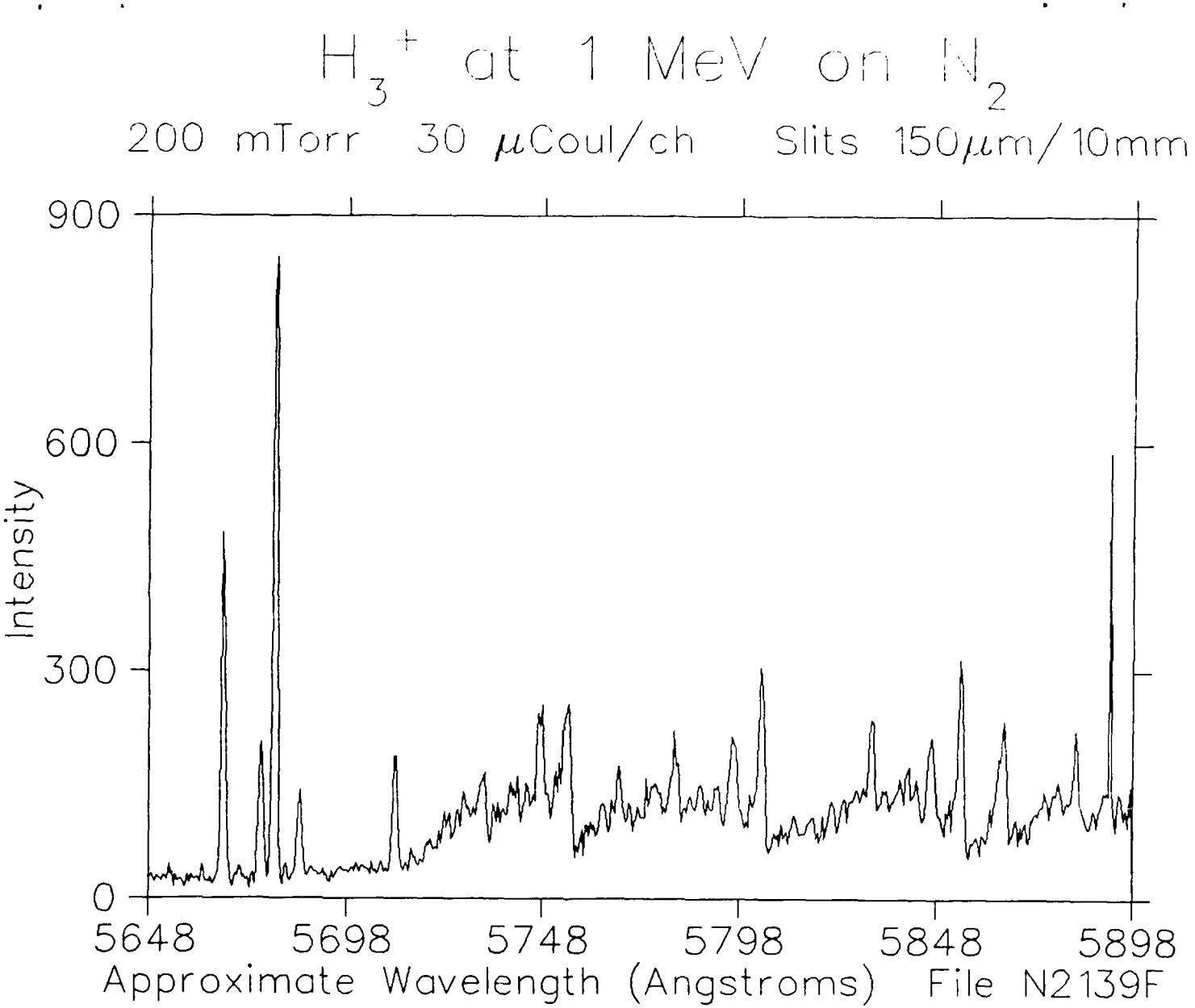
$H_3^+$ at 1 MeV on $N_2$
200 mTorr 30 μCoul/ch Slits 150μm/10mm
900
600
300
0
Intensity
5648
5698
5748
5798
5848
5898
Approximate Wavelength (Angstroms) File N2139F

Fig. 13

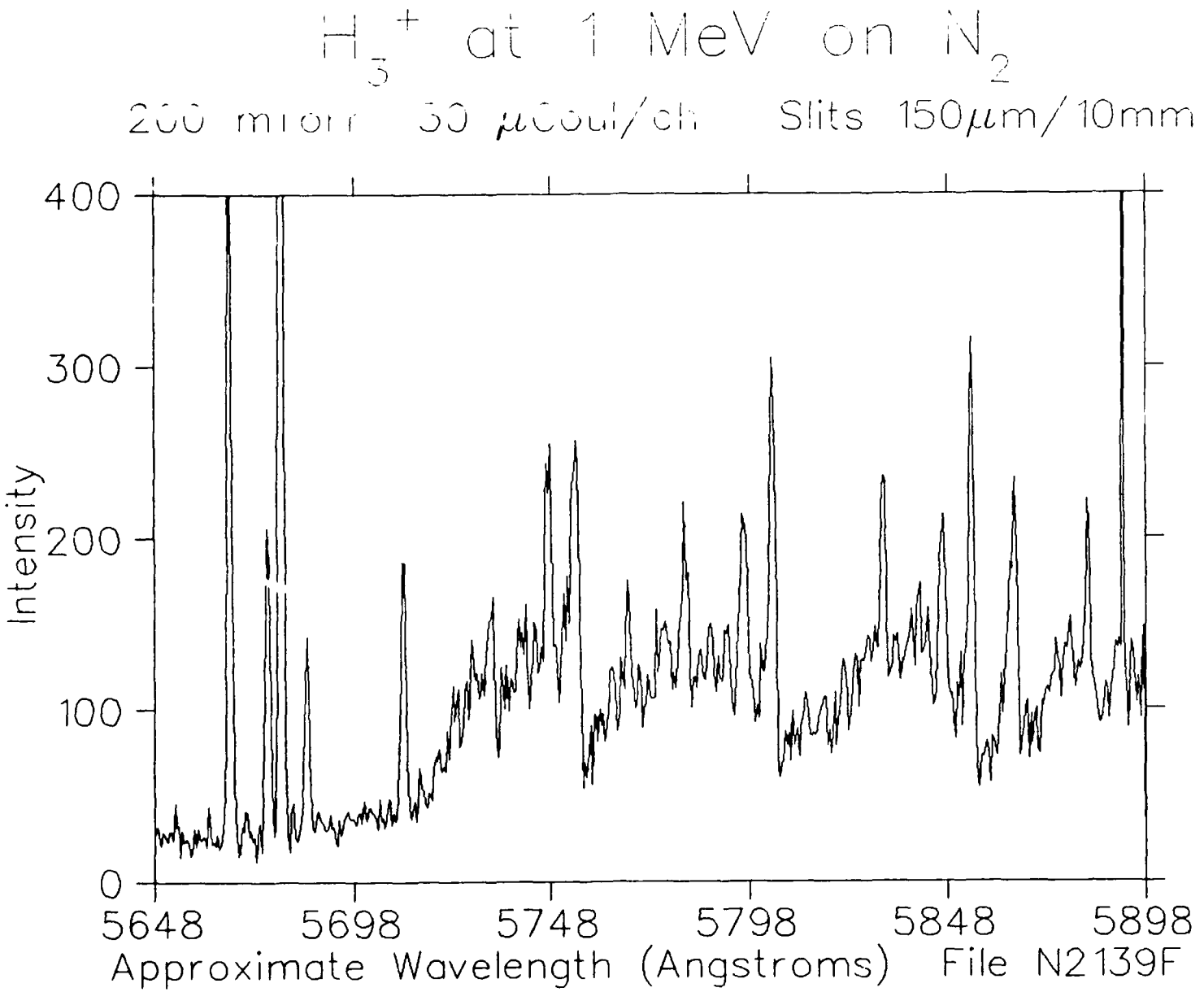
$H_3^+$ at 1 MeV on $N_2$
200 mTorr 30 μCoul/ch Slits 150μm/10mm
Intensity
400
300
200
100
0
5648
5698
5748
5798
5848
5898
Approximate Wavelength (Angstroms) File N2139F

Fig. 14

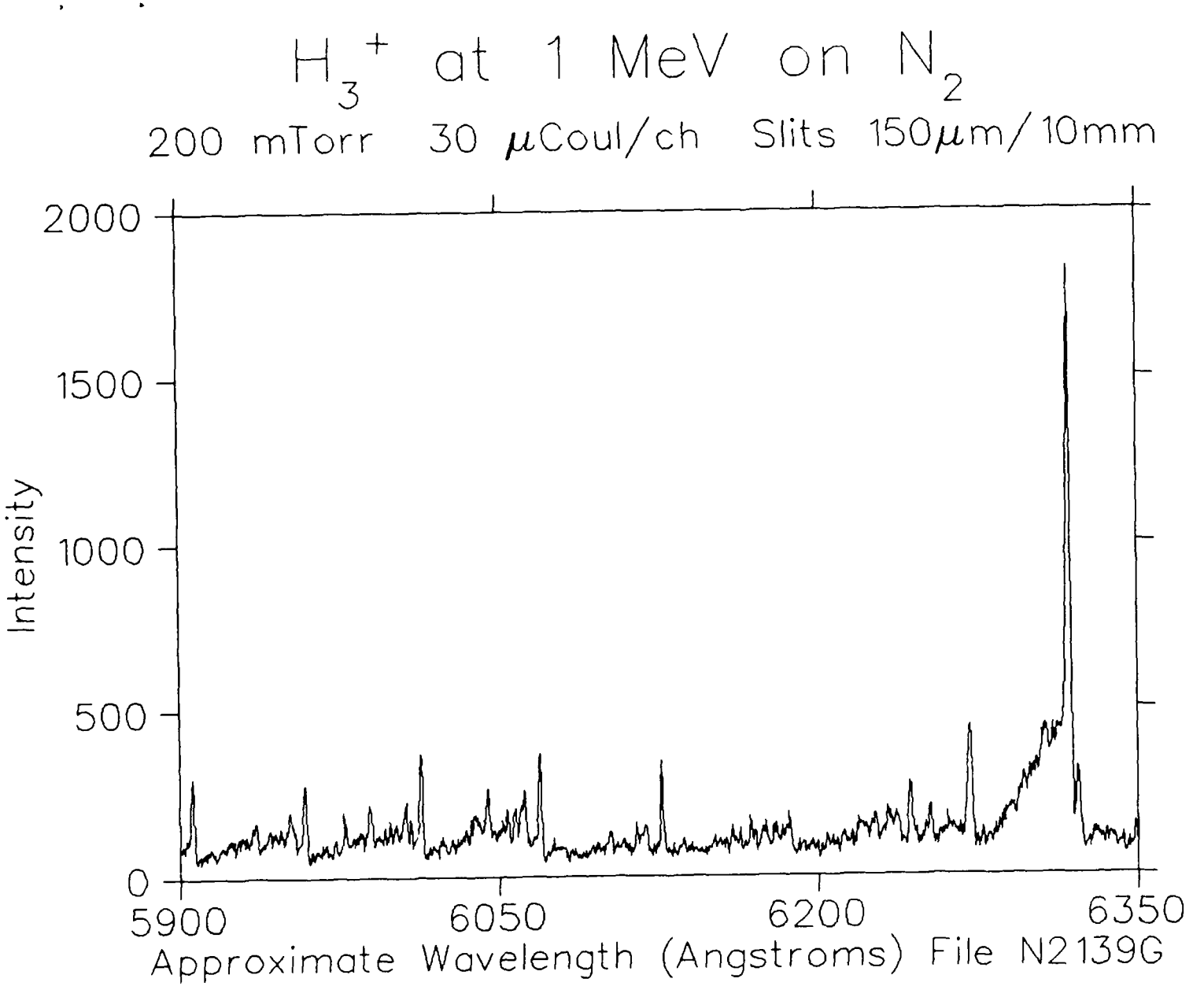
$H_3^+$ at 1 MeV on $N_2$
200 mTorr 30 μCoul/ch Slits 150μm/10mm
2000
1500
1000
500
0
Intensity
5900
6050
6200
6350
Approximate Wavelength (Angstroms) File N2139G

Fig. 15

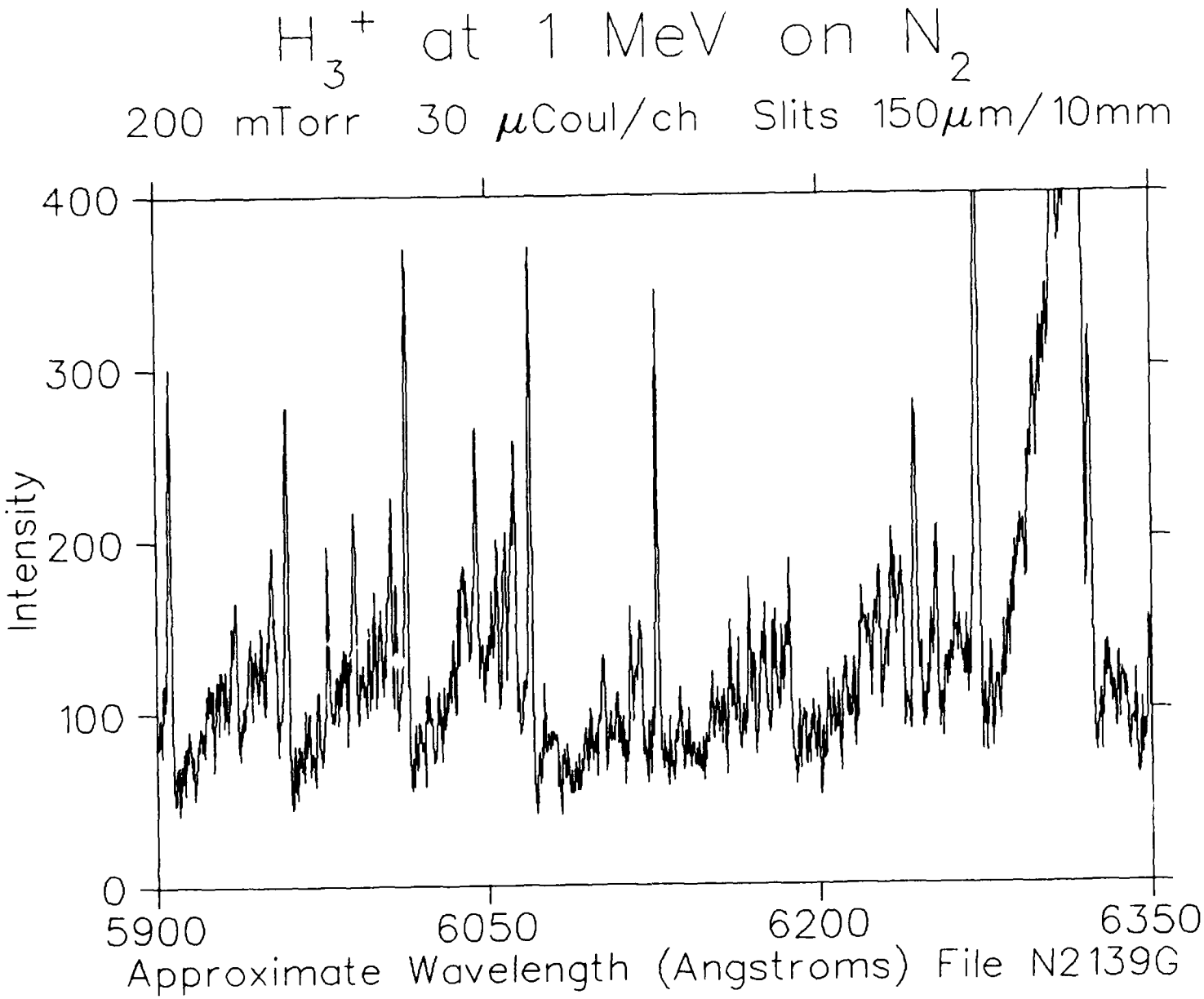
$H_3^+$ at 1 MeV on $N_2$
200 mTorr 30 μCoul/ch Slits 150μm/10mm
Intensity
400
300
200
100
0
5900
6050
6200
6350
Approximate Wavelength (Angstroms) File N2139G

Fig. 16

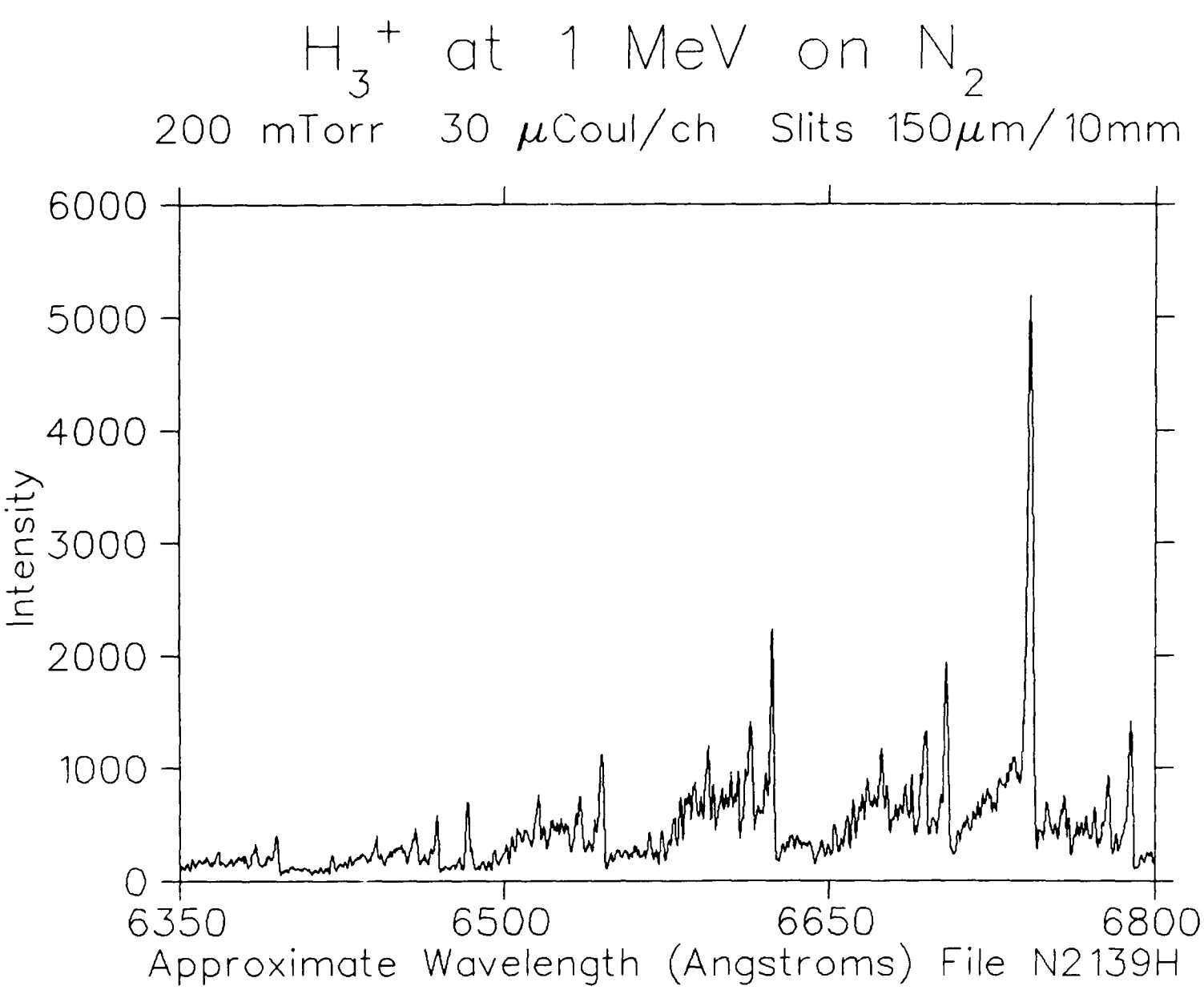
$H_3^+$ at 1 MeV on $N_2$
200 mTorr 30 μCoul/ch Slits 150μm/10mm
Intensity
6000
5000
4000
3000
2000
1000
0
6350
6500
6650
6800
Approximate Wavelength (Angstroms) File N2139H

Fig. 17

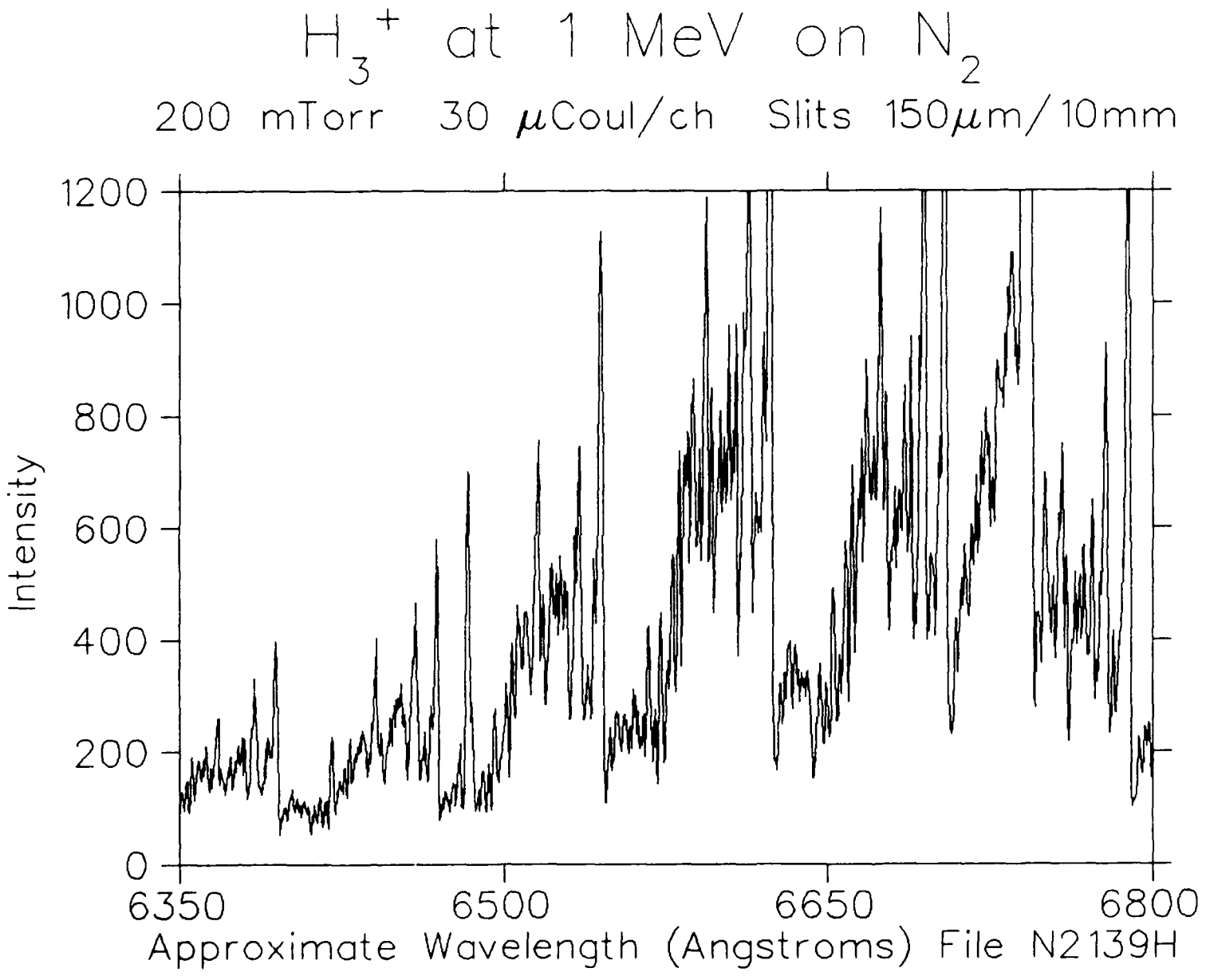
$H_3^+$ at 1 MeV on $N_2$
200 mTorr 30 μCoul/ch Slits 150μm/10mm
Intensity
1200
1000
800
600
400
200
0
6350
6500
6650
6800
Approximate Wavelength (Angstroms) File N2139H

Fig. 18

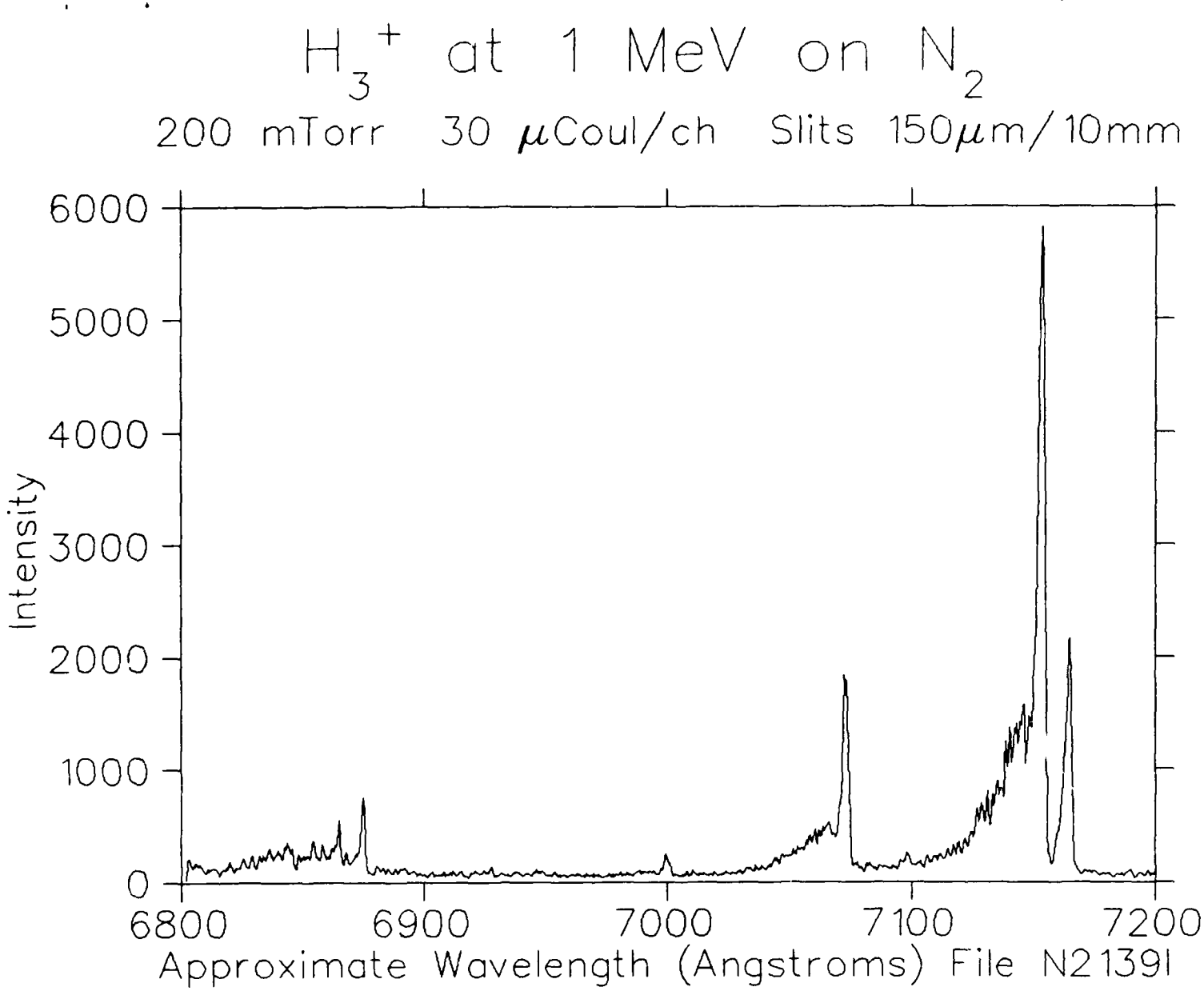
$H_3^+$ at 1 MeV on $N_2$
200 mTorr 30 μCoul/ch Slits 150μm/10mm
6000
5000
4000
3000
2000
1000
0
Intensity
6800
6900
7000
7100
7200
Approximate Wavelength (Angstroms) File N2139I

Fig. 19

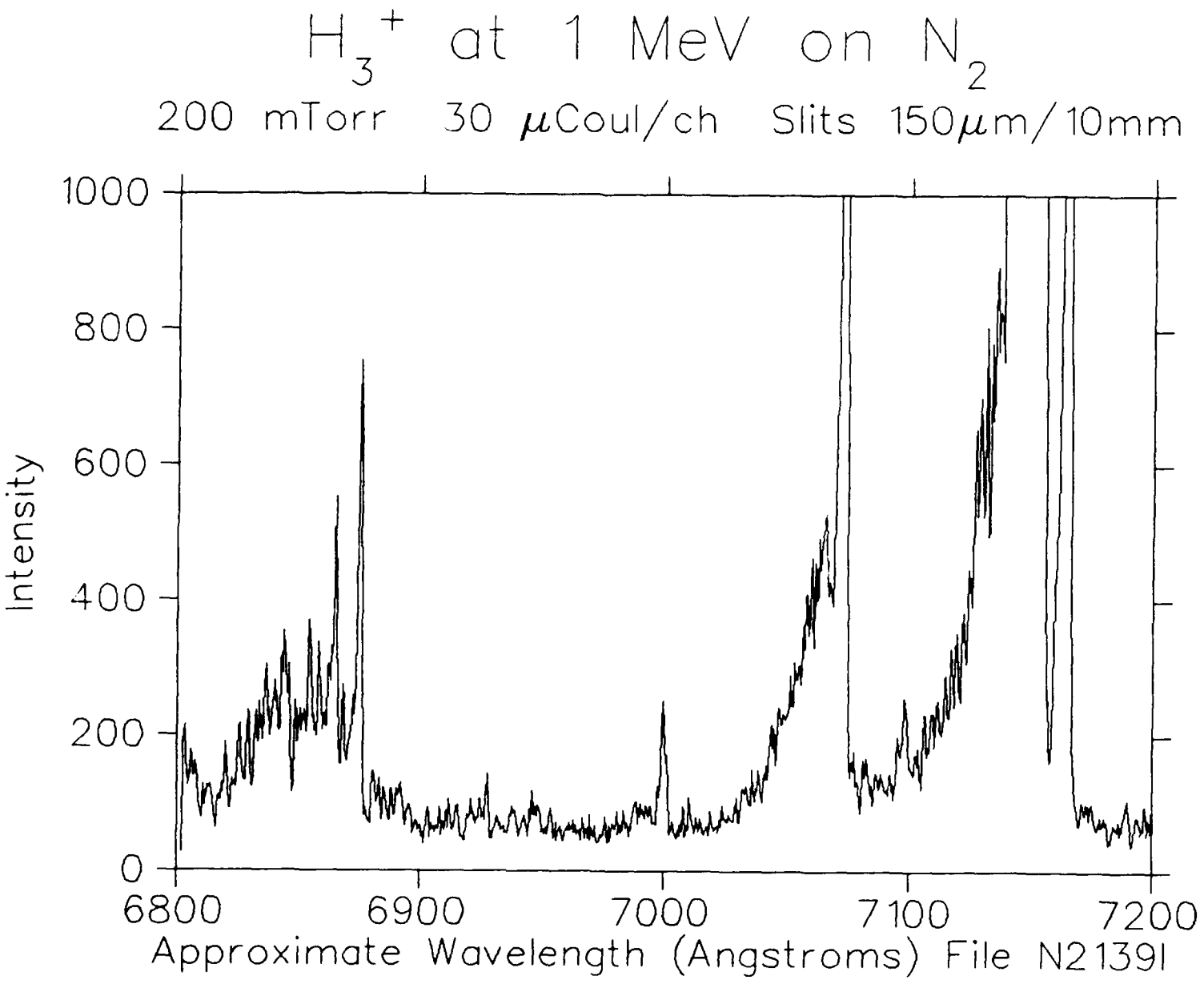
$H_3^+$ at 1 MeV on $N_2$
200 mTorr 30 μCoul/ch Slits 150μm/10mm
Intensity
1000
800
600
400
200
0
6800
6900
7000
7100
7200
Approximate Wavelength (Angstroms) File N21391

Fig. 20

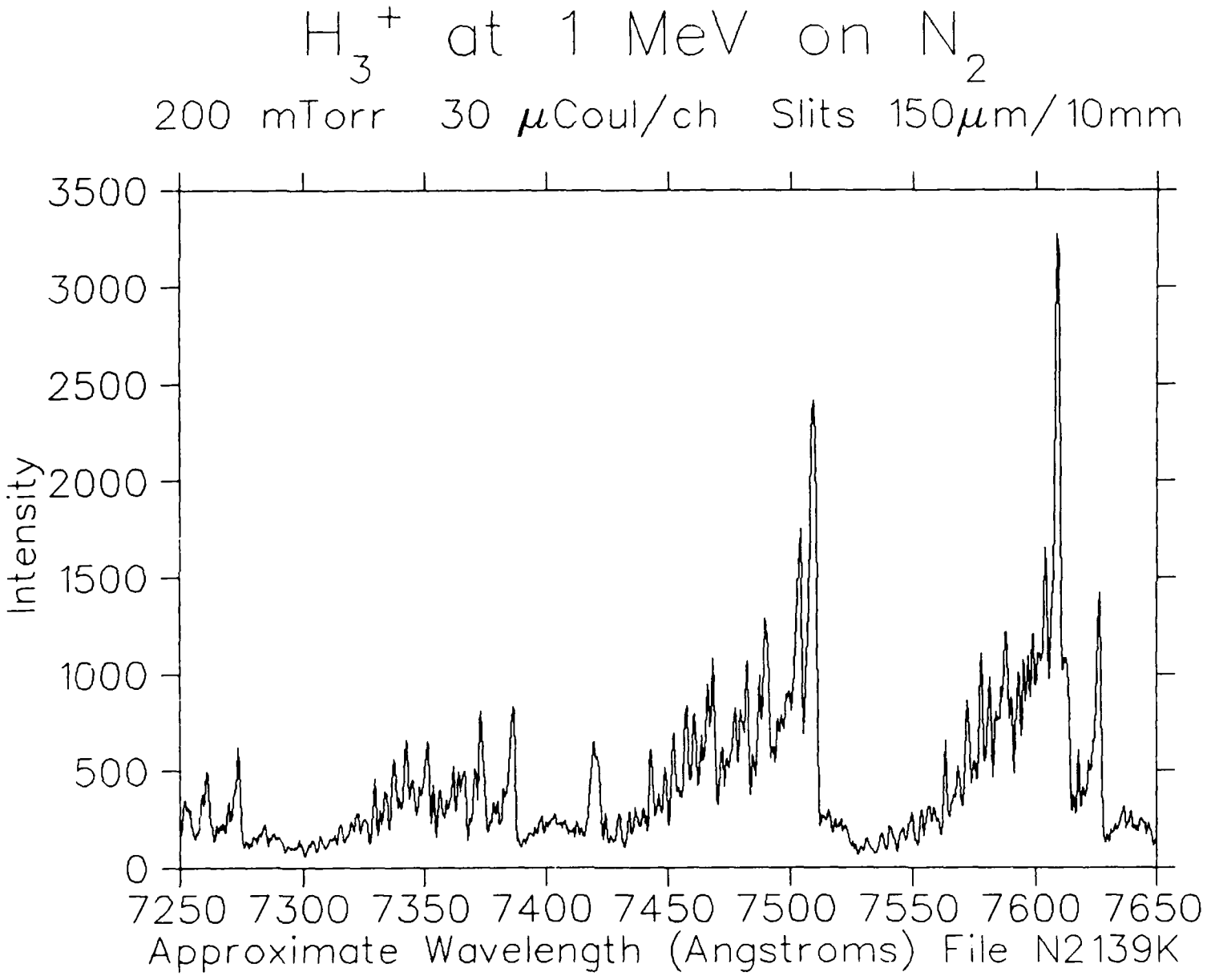
$H_3^+$ at 1 MeV on $N_2$
200 mTorr 30 μCoul/ch Slits 150μm/10mm
Intensity
3500
3000
2500
2000
1500
1000
500
0
7250 7300 7350 7400 7450 7500 7550 7600 7650
Approximate Wavelength (Angstroms) File N2139K

Fig. 21

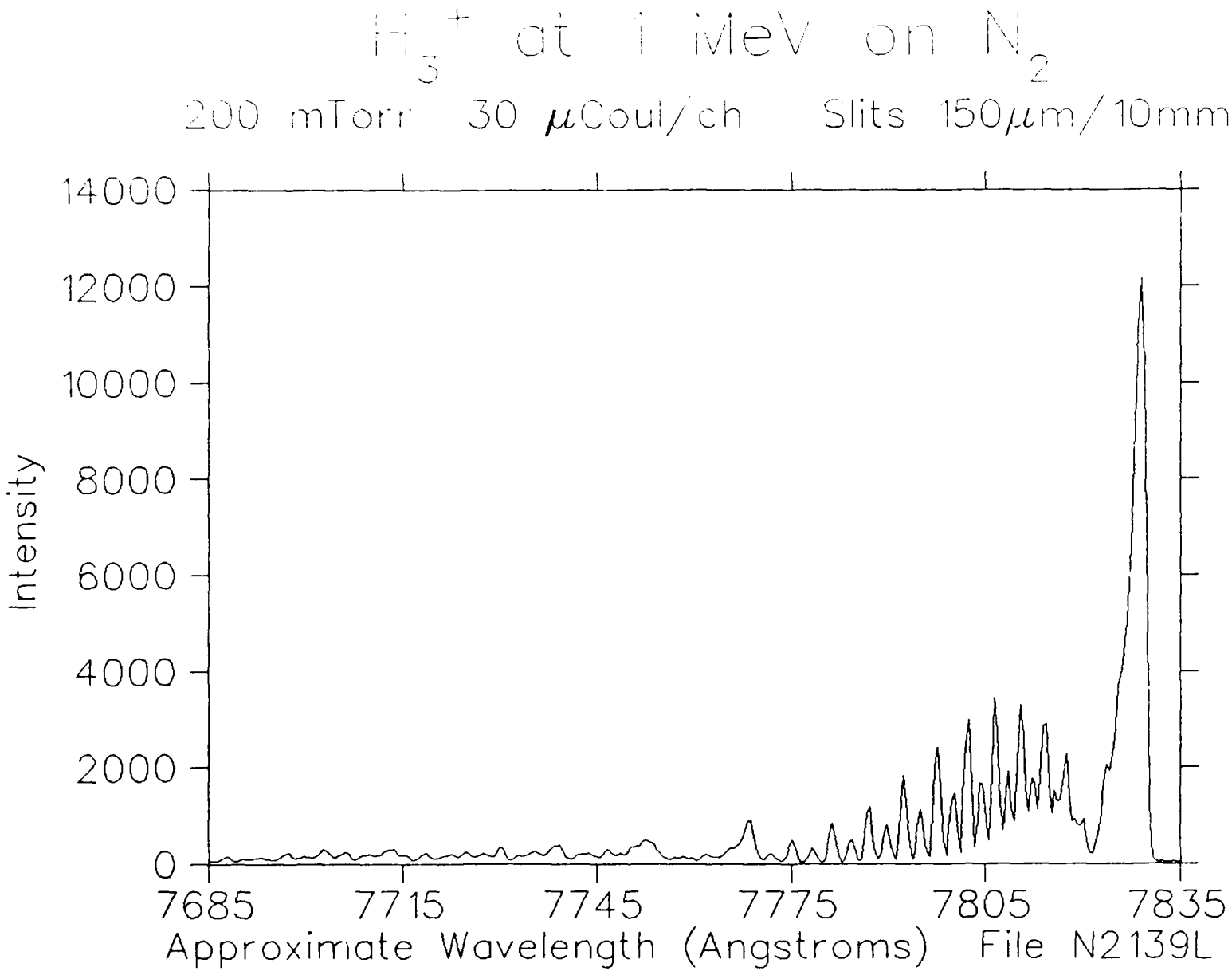
$H_3^+$ at 1 MeV on $N_2$
200 mTorr 30 μCoul/ch Slits 150μm/10mm
Intensity
14000
12000
10000
8000
6000
4000
2000
0
7685
7715
7745
7775
7805
7835
Approximate Wavelength (Angstroms) File N2139L

Fig. 22

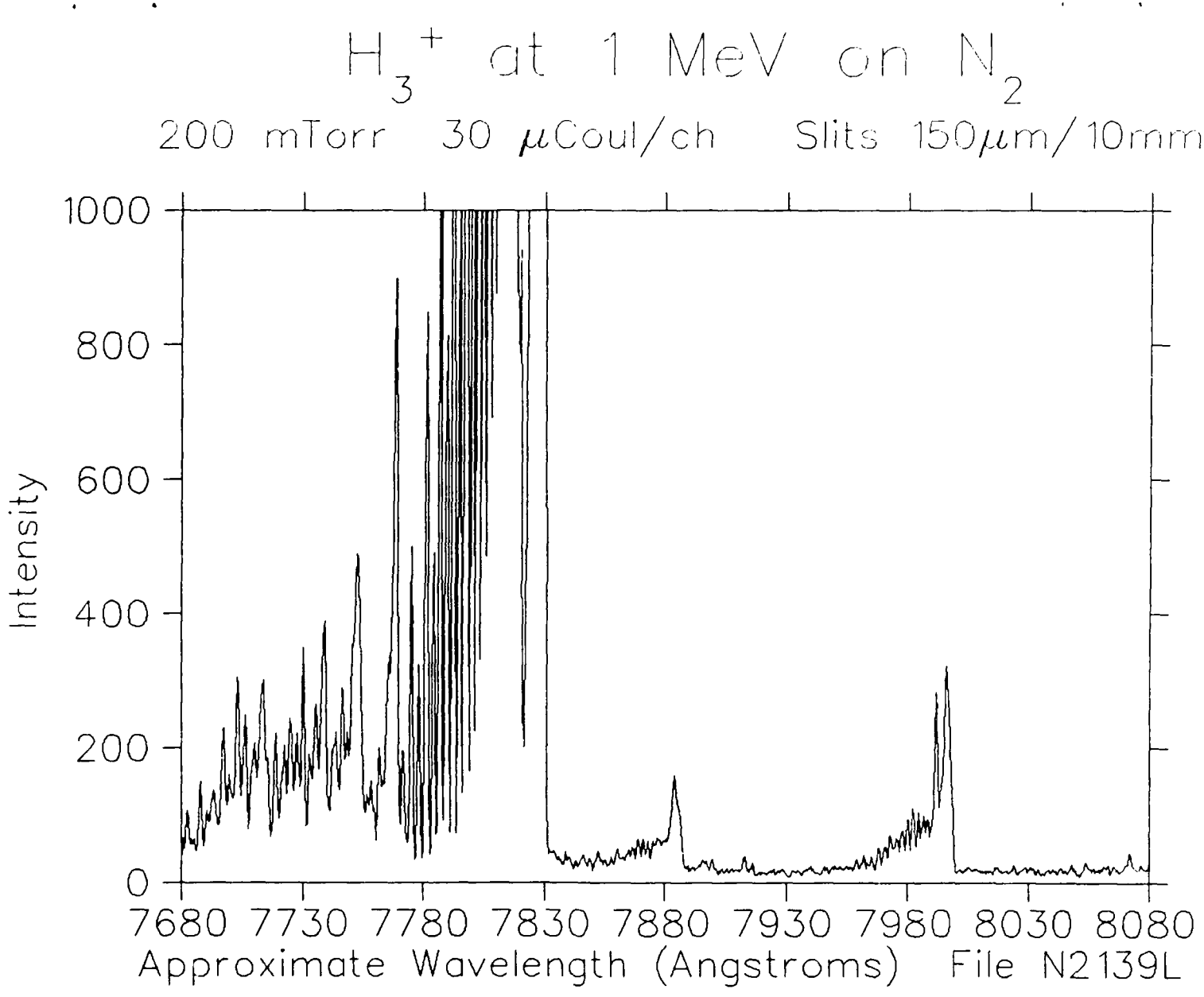
$H_3^+$ at 1 MeV on $N_2$
200 mTorr 30 μCoul/ch Slits 150μm/10mm
Intensity
1000
800
600
400
200
0
7680 7730 7780 7830 7880 7930 7980 8030 8080
Approximate Wavelength (Angstroms) File N2139L

Fig. 23

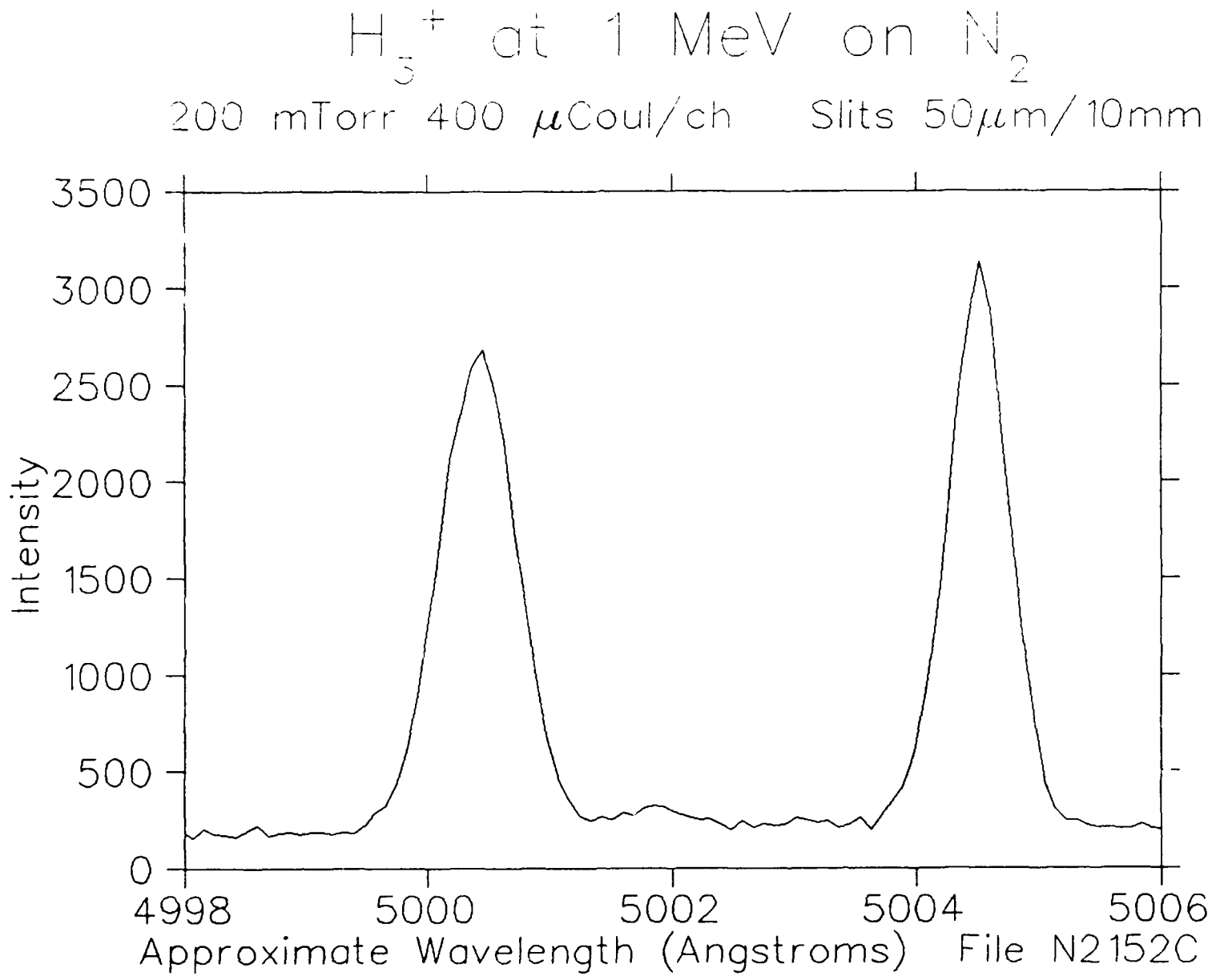
$H_3^+$ at 1 MeV on $N_2$
200 mTorr 400 μCoul/ch Slits 50μm/10mm
Intensity
3500
3000
2500
2000
1500
1000
500
0
4998
5000
5002
5004
5006
Approximate Wavelength (Angstroms) File N2152C

Fig. 24

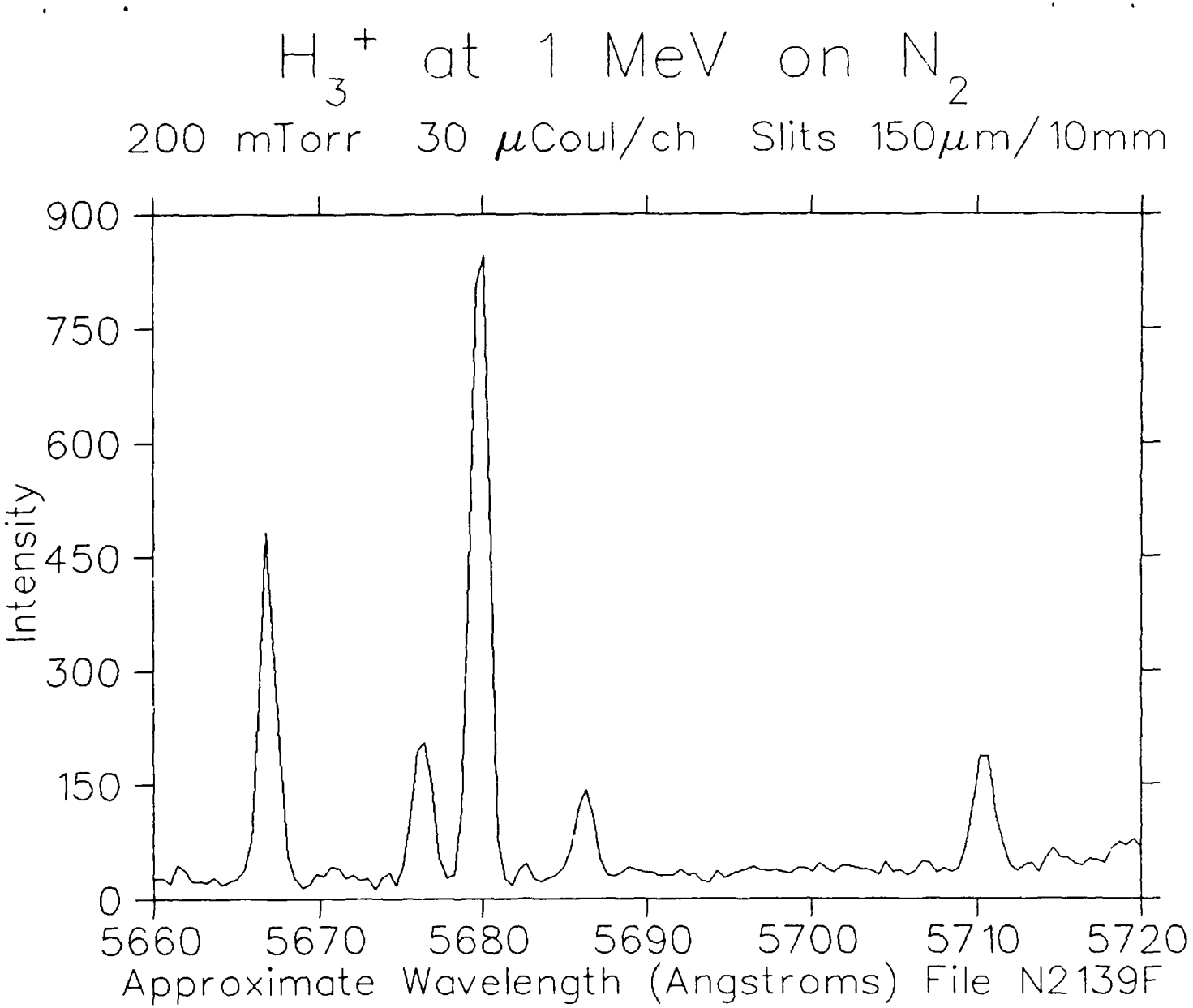
$H_3^+$ at 1 MeV on $N_2$
200 mTorr 30 μCoul/ch Slits 150μm/10mm
900
750
600
450
300
150
0
Intensity
5660
5670
5680
5690
5700
5710
5720
Approximate Wavelength (Angstroms) File N2139F

Fig. 25

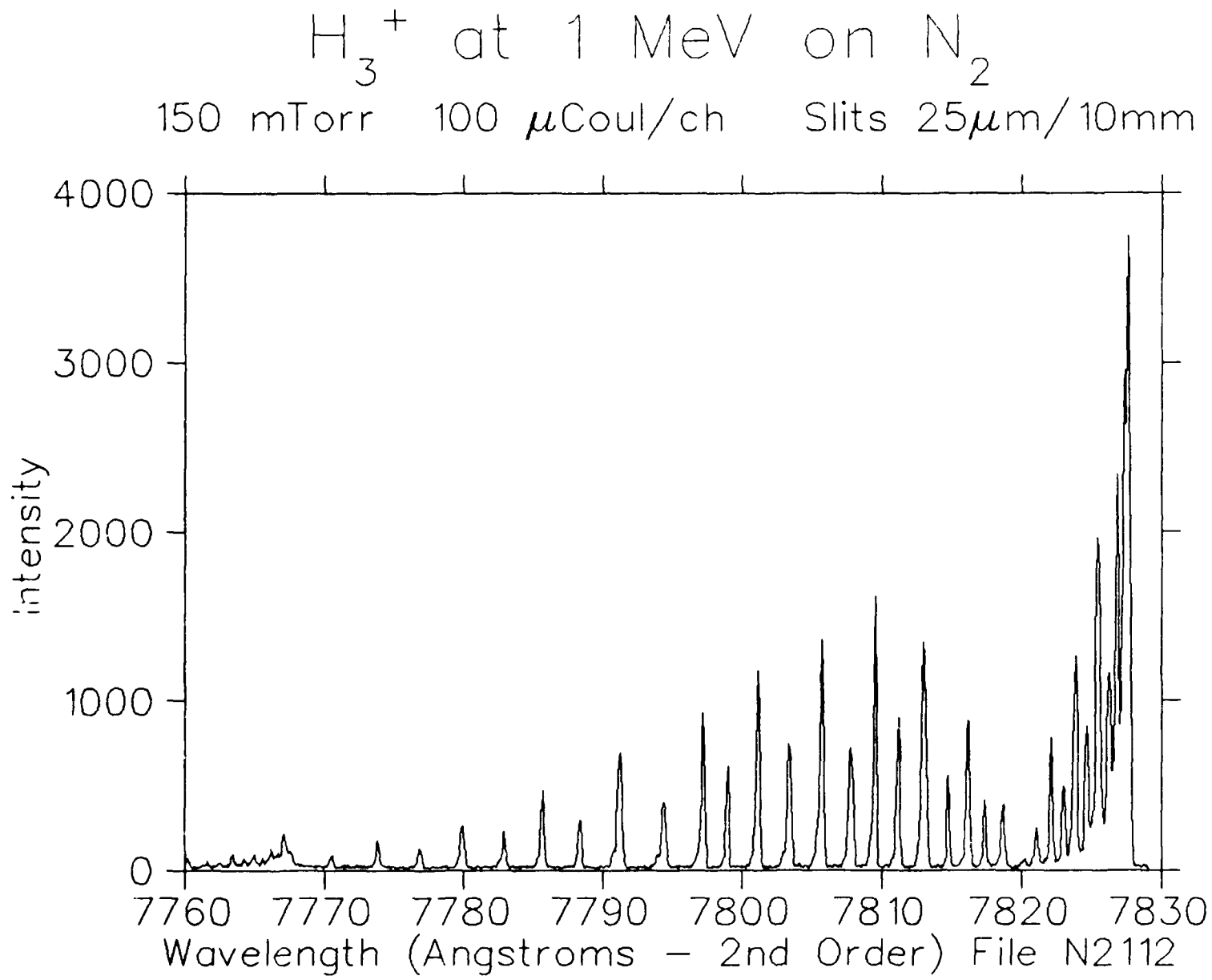
$H_3^+$ at 1 MeV on $N_2$
150 mTorr 100 μCoul/ch Slits 25μm/10mm
4000
3000
2000
1000
0
Intensity
7760 7770 7780 7790 7800 7810 7820 7830
Wavelength (Angstroms – 2nd Order) File N2112

Fig. 26

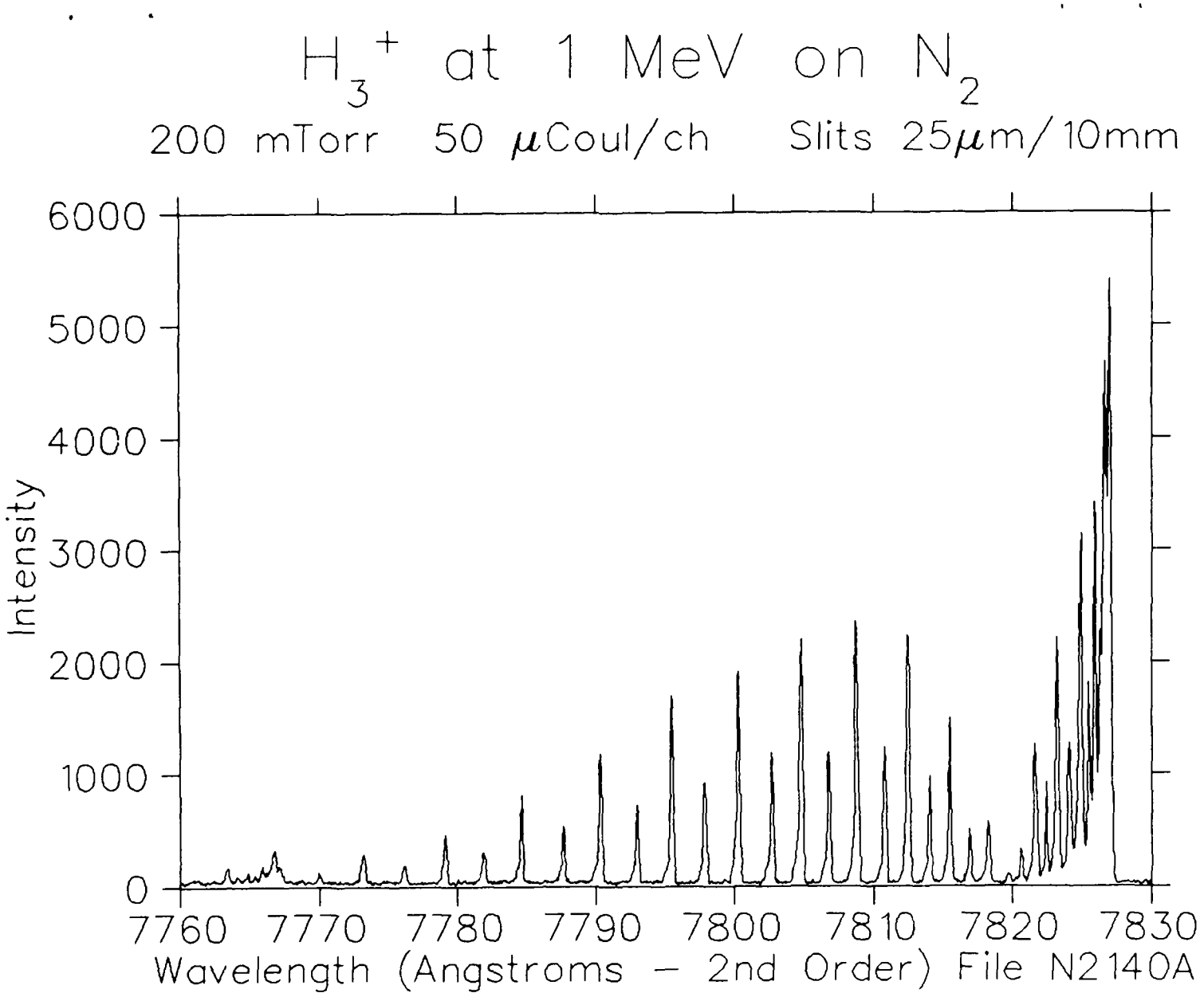
$H_3^+$ at 1 MeV on $N_2$
200 mTorr 50 μCoul/ch Slits 25μm/10mm
6000
5000
4000
3000
2000
1000
0
Intensity
7760 7770 7780 7790 7800 7810 7820 7830
Wavelength (Angstroms – 2nd Order) File N2140A

Fig. 27

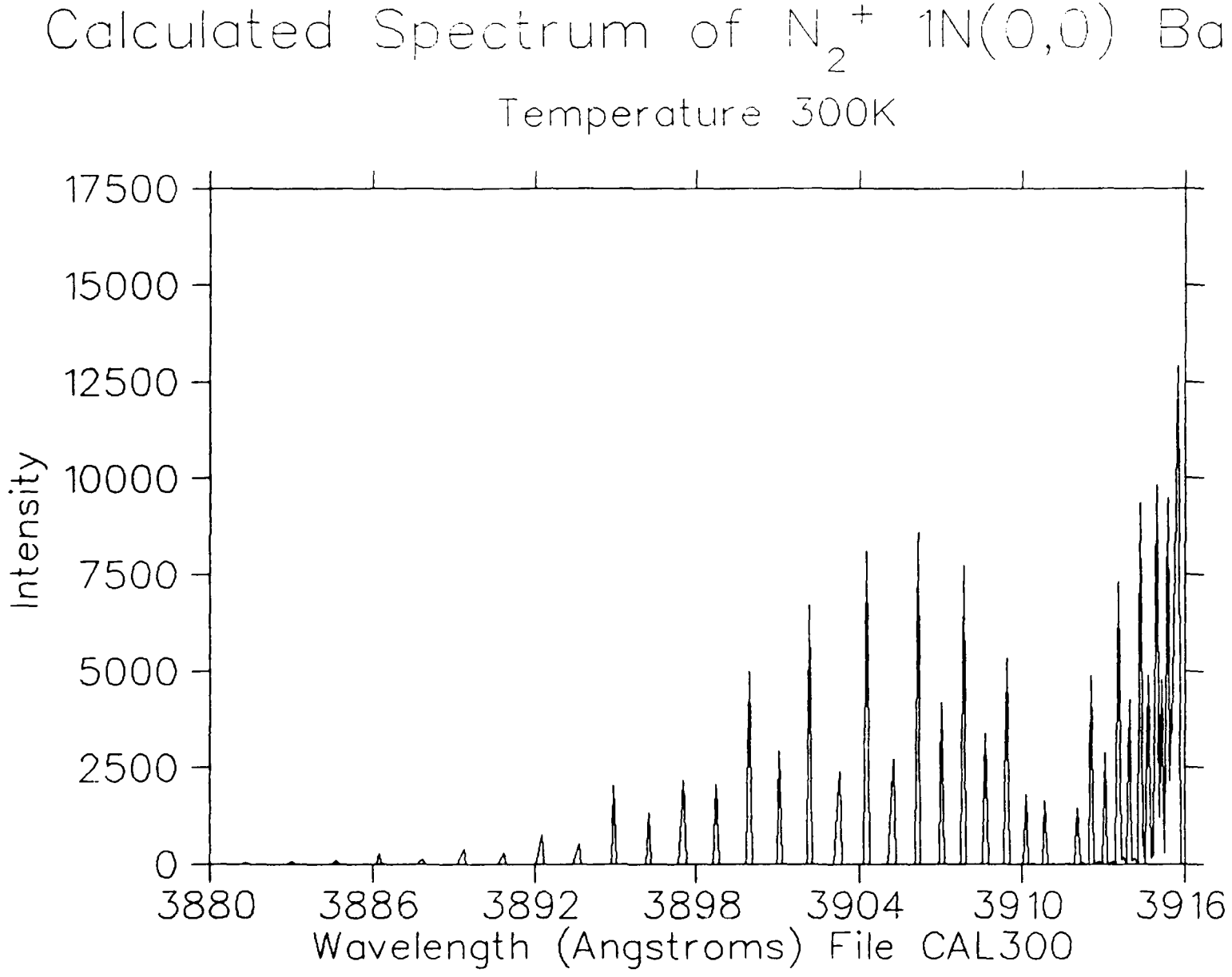
Calculated Spectrum of $N_2^+$ 1N(0,0) Band
Temperature 300K
Intensity
17500
15000
12500
10000
7500
5000
2500
0
3880
3886
3892
3898
3904
3910
3916
Wavelength (Angstroms) File CAL300

Fig. 28

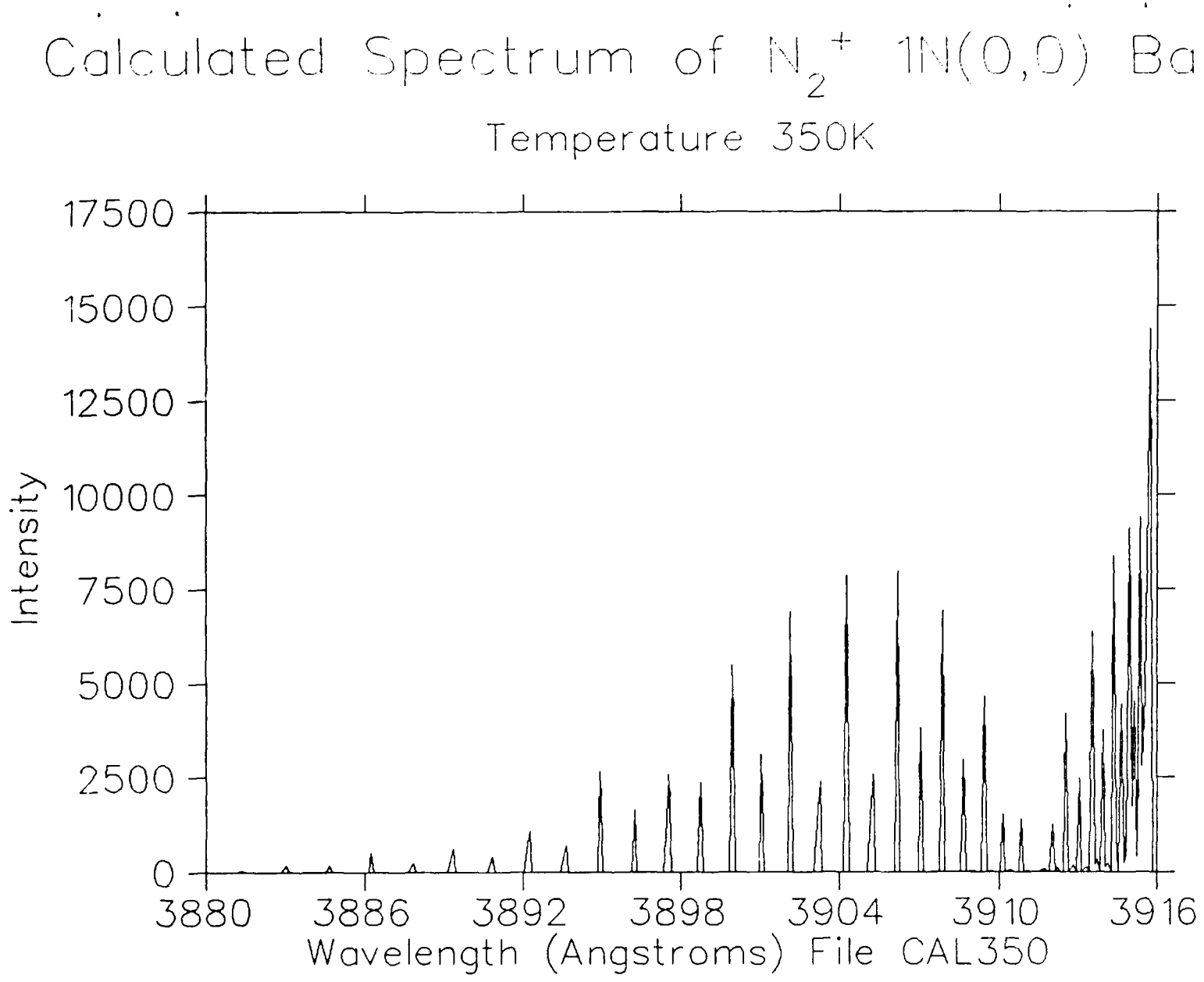
Calculated Spectrum of $N_2^+$ 1N(0,0) Band
Temperature 350K
Intensity
17500
15000
12500
10000
7500
5000
2500
0
3880
3886
3892
3898
3904
3910
3916
Wavelength (Angstroms) File CAL350

Fig. 29

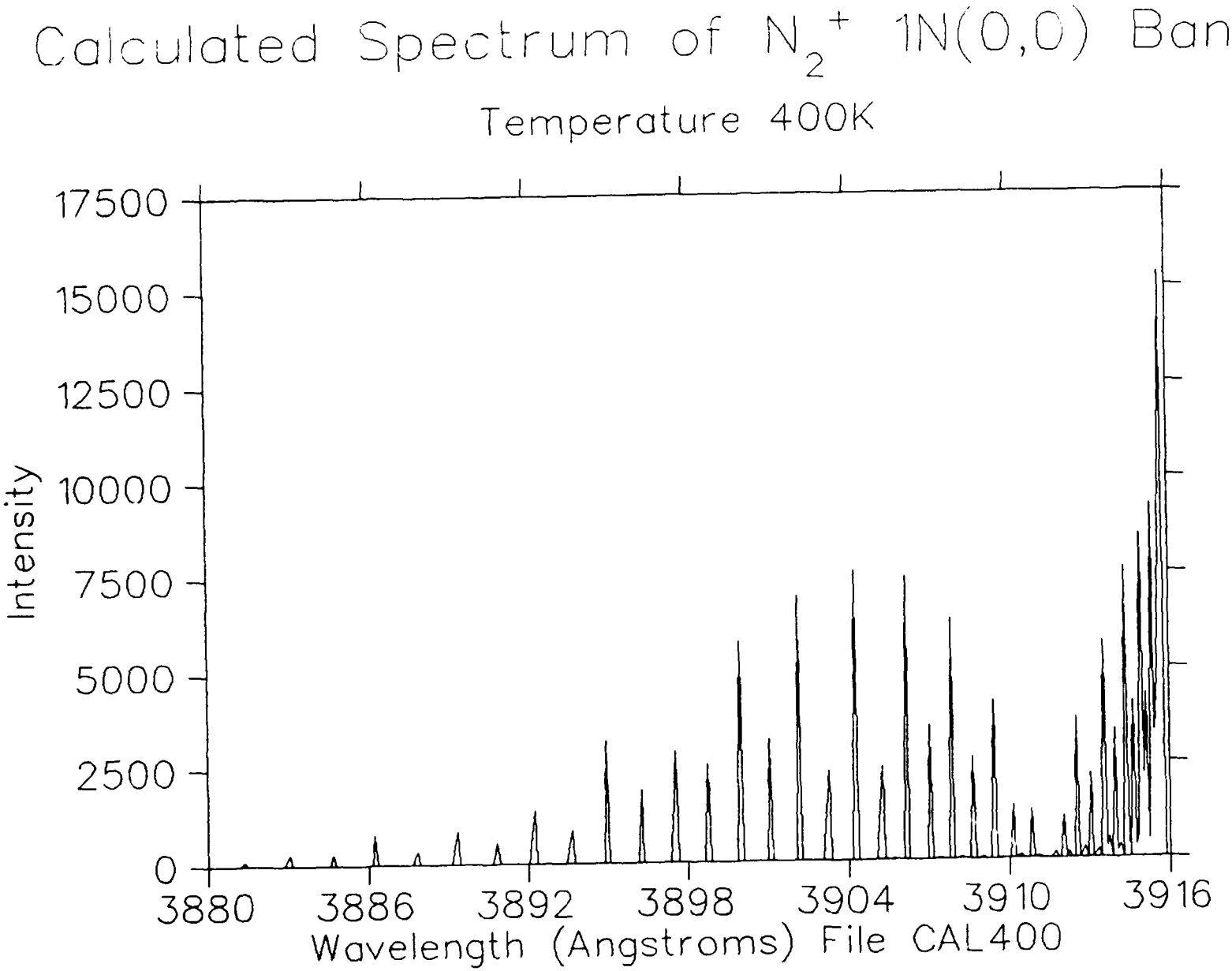
Calculated Spectrum of $N_2^+$ 1N(0,0) Band
Temperature 400K
17500
15000
12500
10000
7500
5000
2500
0
Intensity
3880
3886
3892
3898
3904
3910
3916
Wavelength (Angstroms) File CAL400

Fig. 30

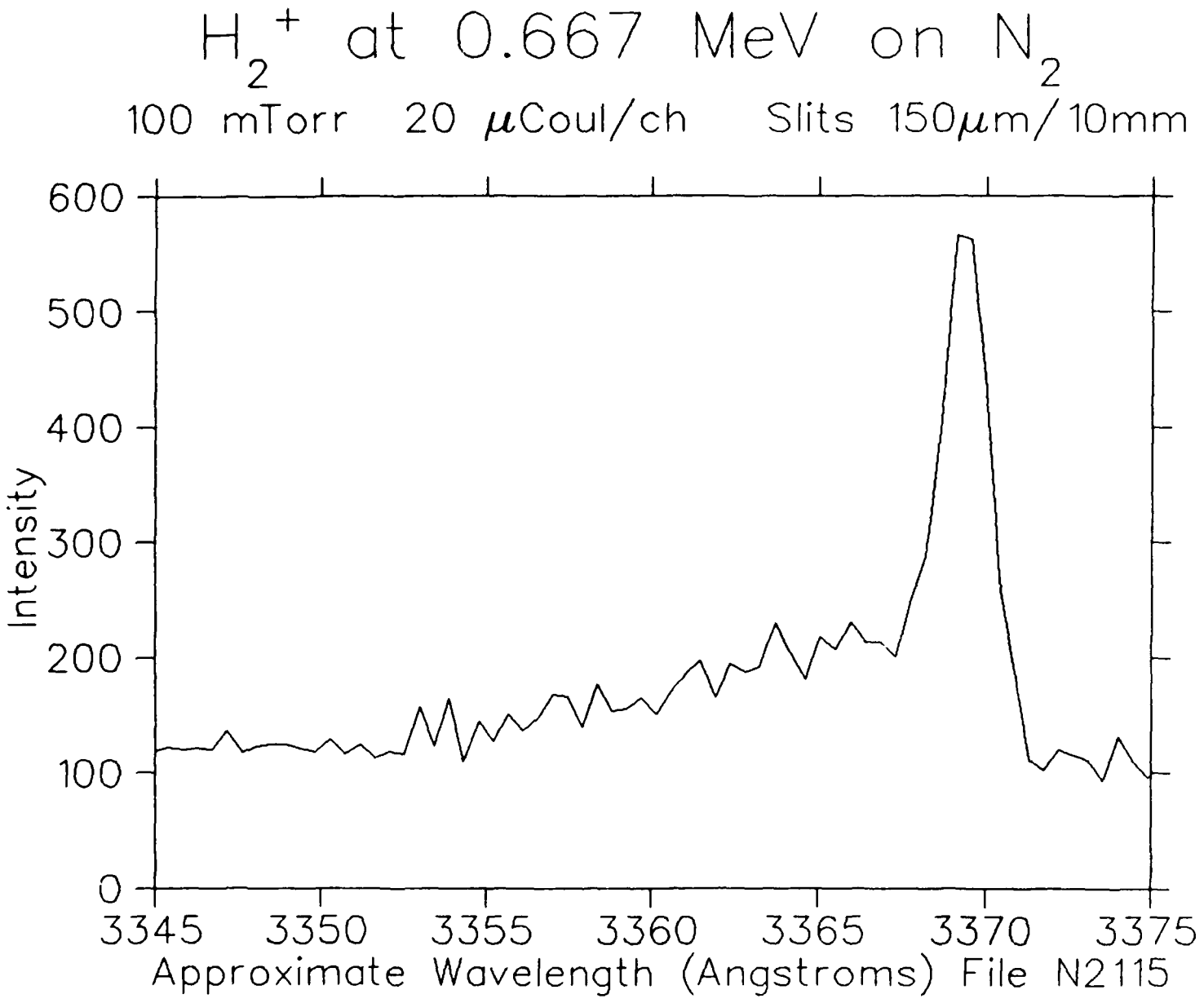
$H_2^+$ at 0.667 MeV on $N_2$
100 mTorr 20 μCoul/ch Slits 150μm/10mm
Intensity
600
500
400
300
200
100
0
3345
3350
3355
3360
3365
3370
3375
Approximate Wavelength (Angstroms) File N2115

Fig. 31

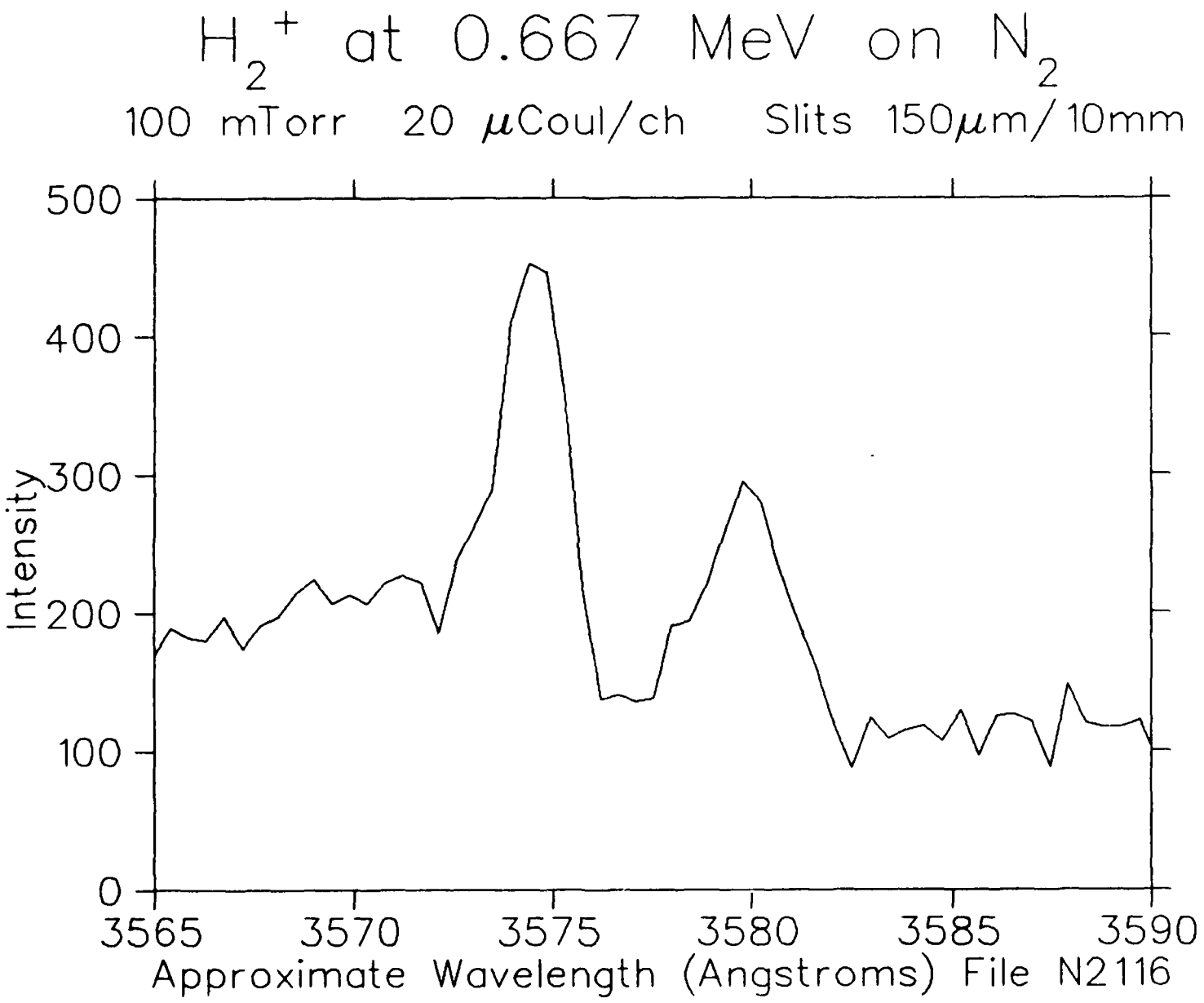
$H_2^+$ at 0.667 MeV on $N_2$
100 mTorr 20 μCoul/ch Slits 150μm/10mm
Intensity
500
400
300
200
100
0
3565
3570
3575
3580
3585
3590
Approximate Wavelength (Angstroms) File N2116

Fig. 32

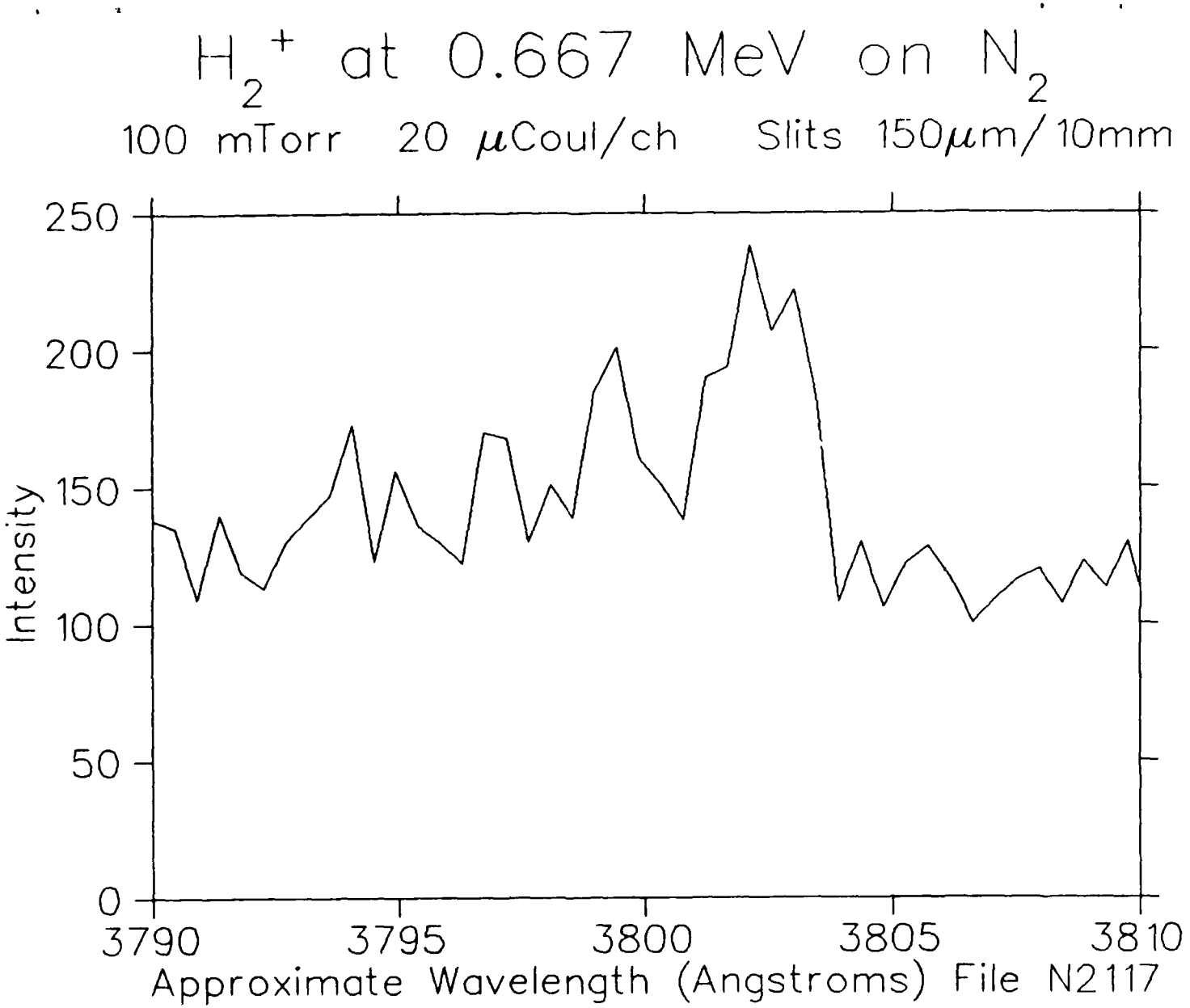
$H_2^+$ at 0.667 MeV on $N_2$
100 mTorr 20 μCoul/ch Slits 150μm/10mm
Intensity
250
200
150
100
50
0
3790
3795
3800
3805
3810
Approximate Wavelength (Angstroms) File N2117

Fig. 33

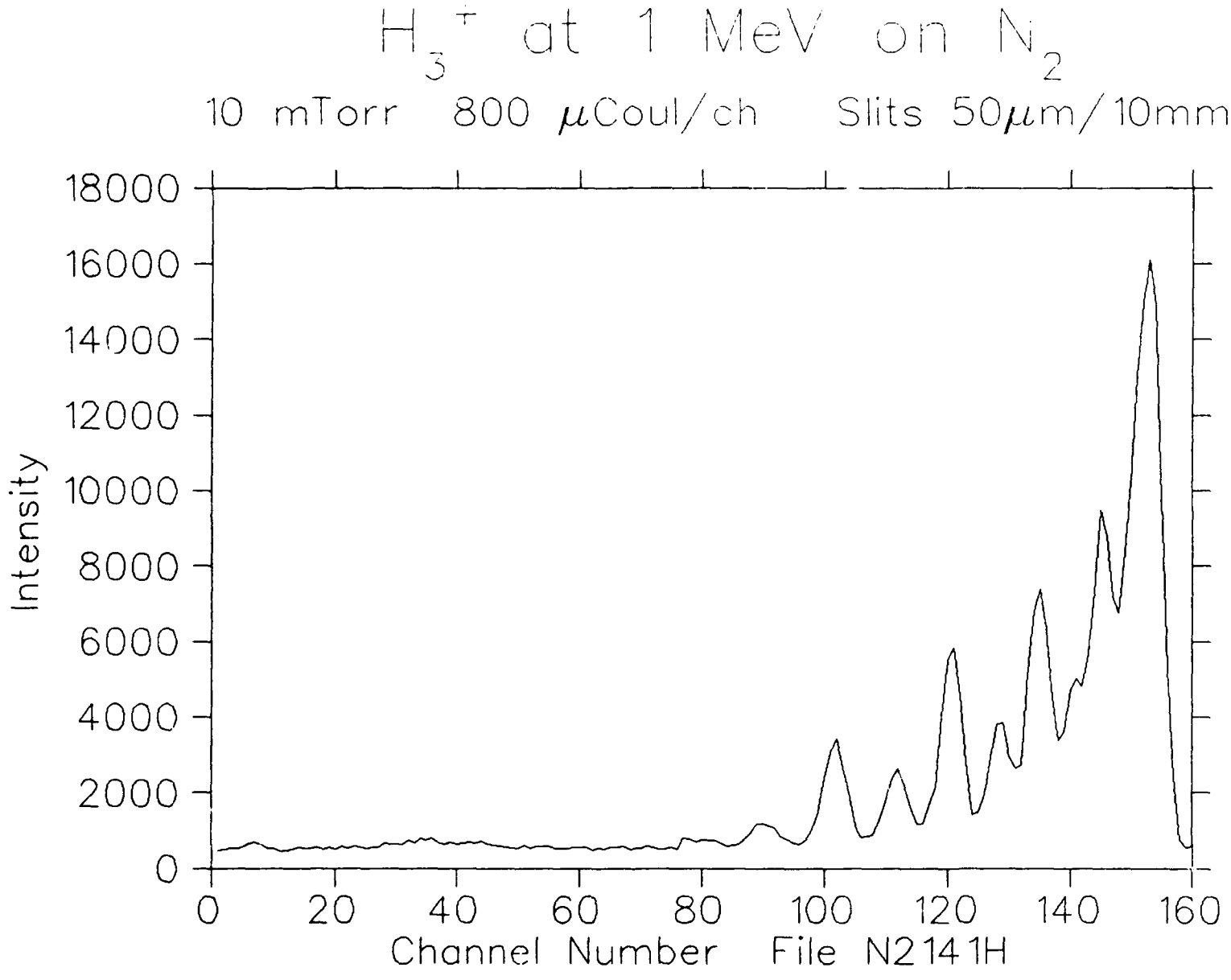
$H_3^+$ at 1 MeV on $N_2$
10 mTorr 800 μCoul/ch Slits 50μm/10mm
Intensity
18000
16000
14000
12000
10000
8000
6000
4000
2000
0
0 20 40 60 80 100 120 140 160
Channel Number File N2141H

Fig. 34

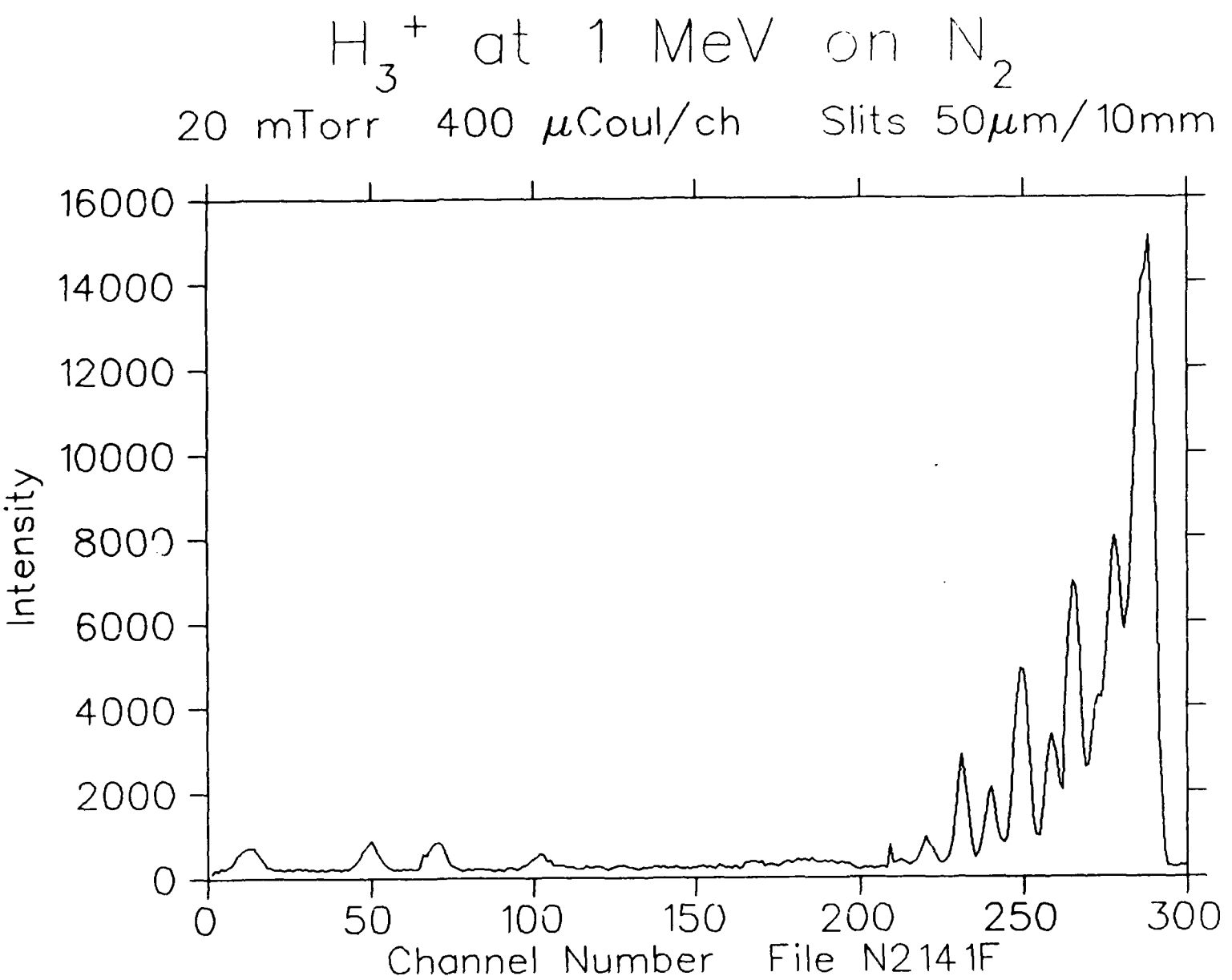
$H_3^+$ at 1 MeV on $N_2$
20 mTorr 400 μCoul/ch Slits 50μm/10mm
Intensity
16000
14000
12000
10000
8000
6000
4000
2000
0
0
50
100
150
200
250
300
Channel Number File N2141F

Fig. 35

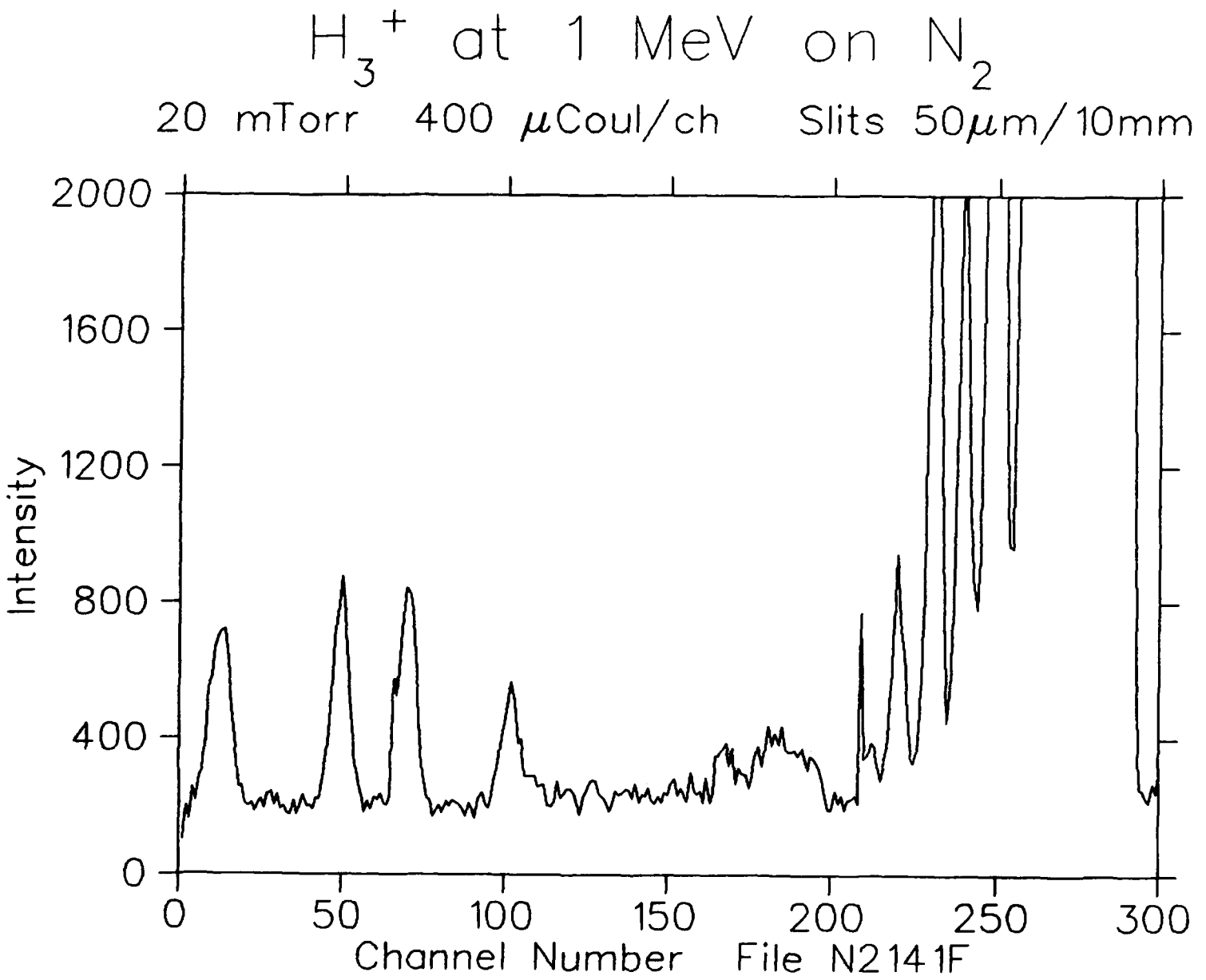
$H_3^+$ at 1 MeV on $N_2$
20 mTorr 400 μCoul/ch Slits 50μm/10mm
2000
1600
1200
800
400
0
Intensity
0
50
100
150
200
250
300
Channel Number File N2141F

Fig. 36

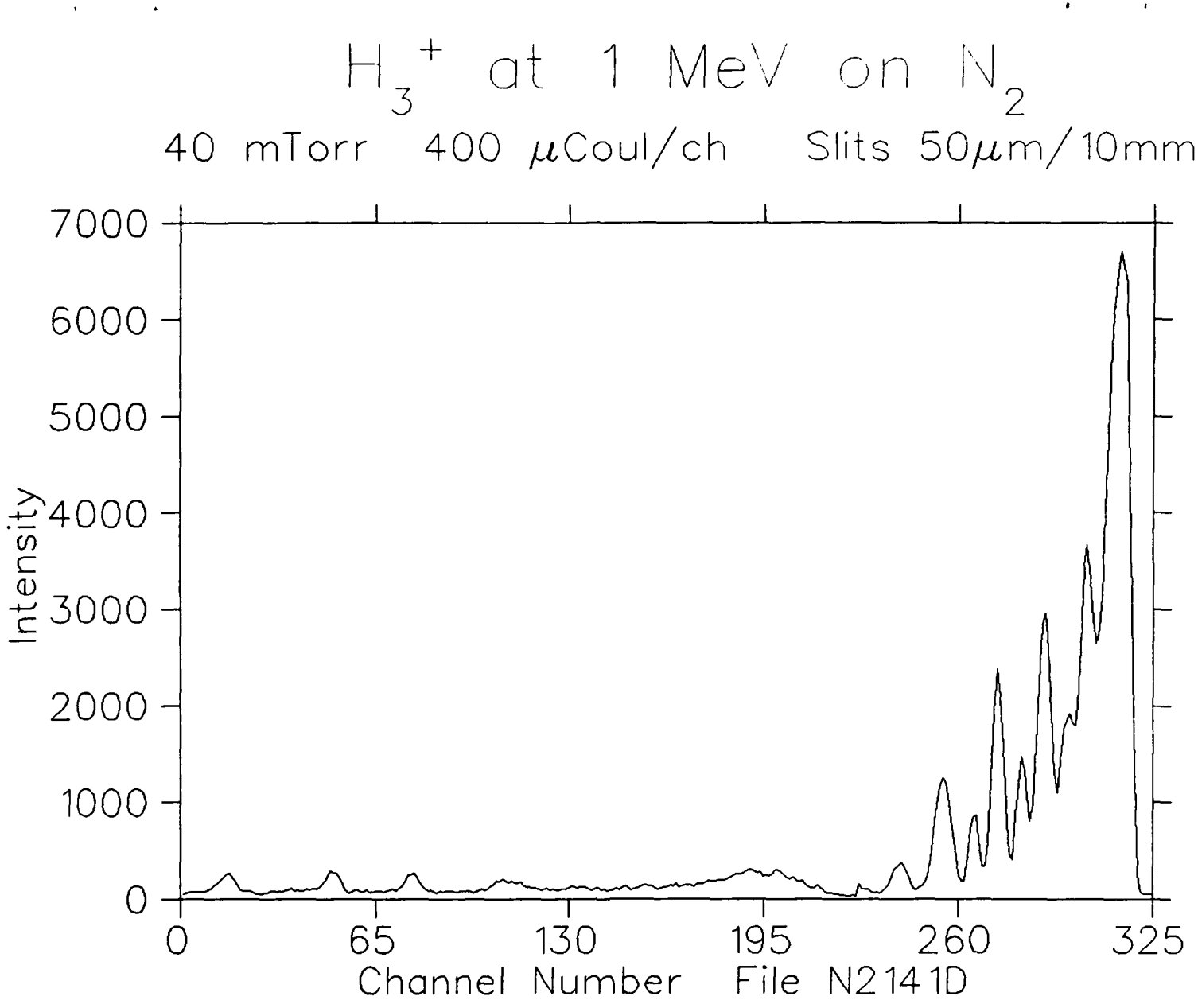
$H_3^+$ at 1 MeV on $N_2$
40 mTorr 400 μCoul/ch Slits 50μm/10mm
Intensity
7000
6000
5000
4000
3000
2000
1000
0
0
65
130
195
260
325
Channel Number File N2141D

Fig. 37

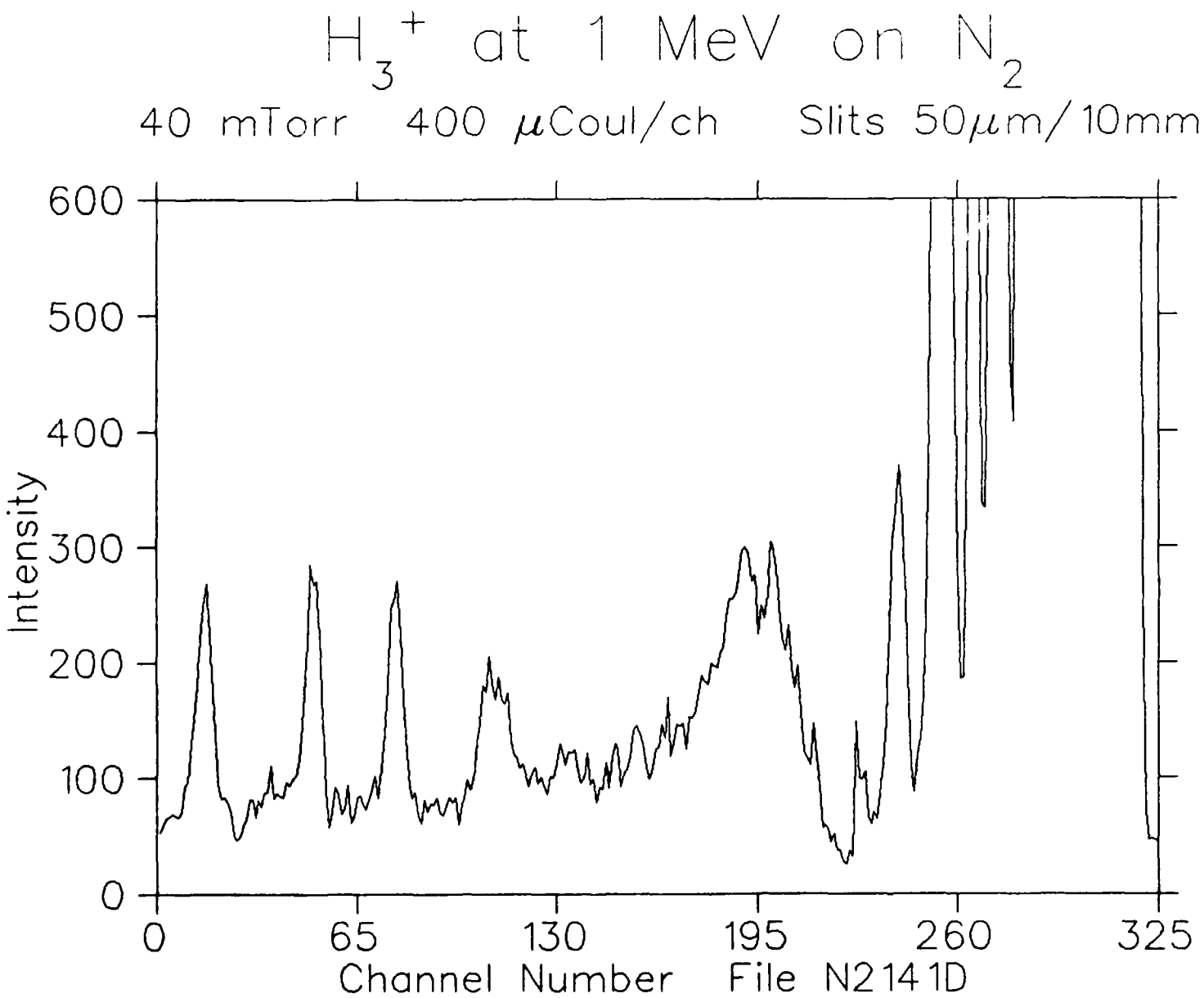
$H_3^+$ at 1 MeV on $N_2$
40 mTorr 400 μCoul/ch Slits 50μm/10mm
Intensity
600
500
400
300
200
100
0
0
65
130
195
260
325
Channel Number File N2141D

Fig. 38

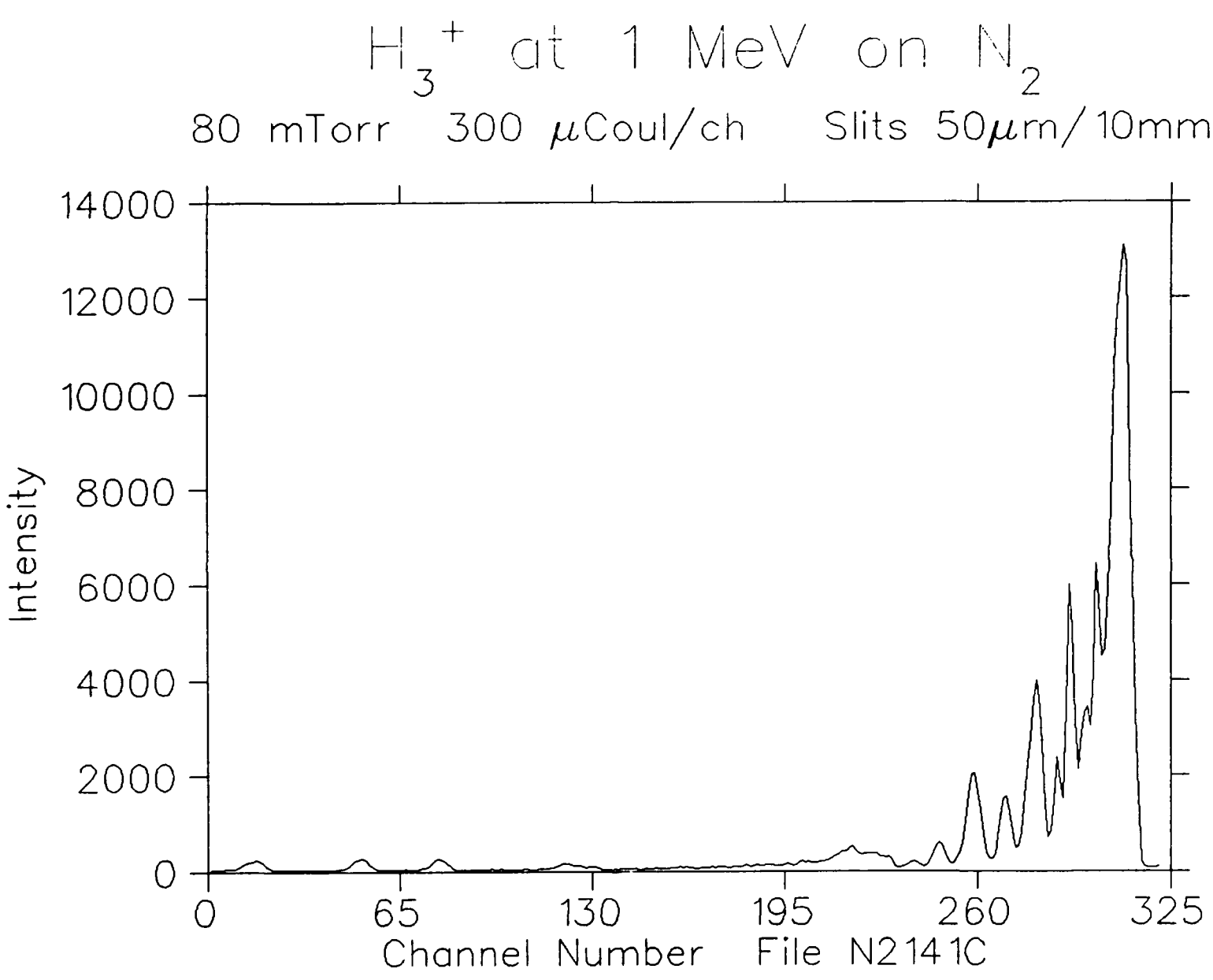
$H_3^+$ at 1 MeV on $N_2$
80 mTorr 300 μCoul/ch Slits 50μm/10mm
14000
12000
10000
8000
6000
4000
2000
0
Intensity
0
65
130
195
260
325
Channel Number File N2141C

Fig. 39

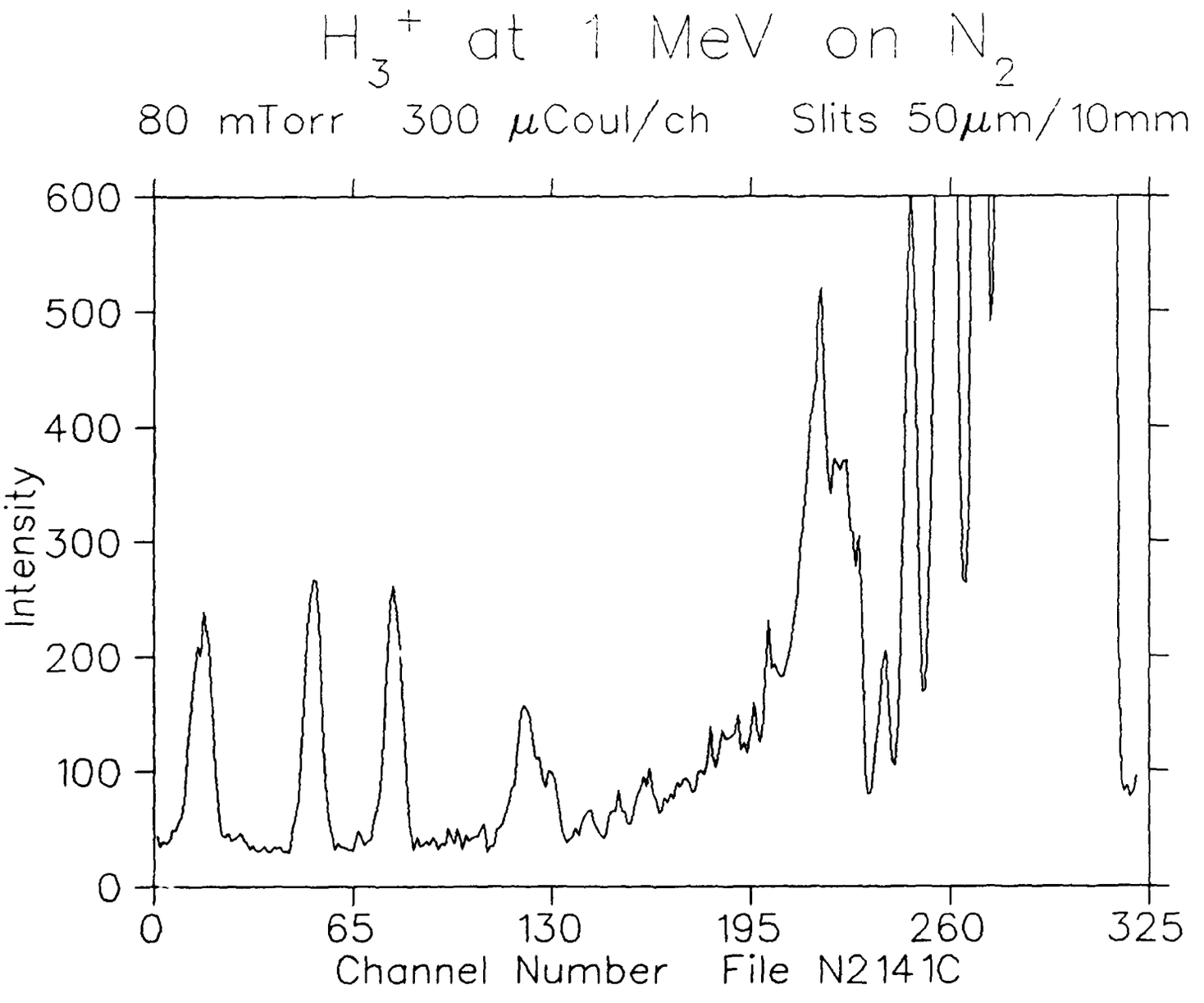
$H_3^+$ at 1 MeV on $N_2$
80 mTorr 300 μCoul/ch Slits 50μm/10mm
Intensity
600
500
400
300
200
100
0
0
65
130
195
260
325
Channel Number File N2141C

Fig. 40

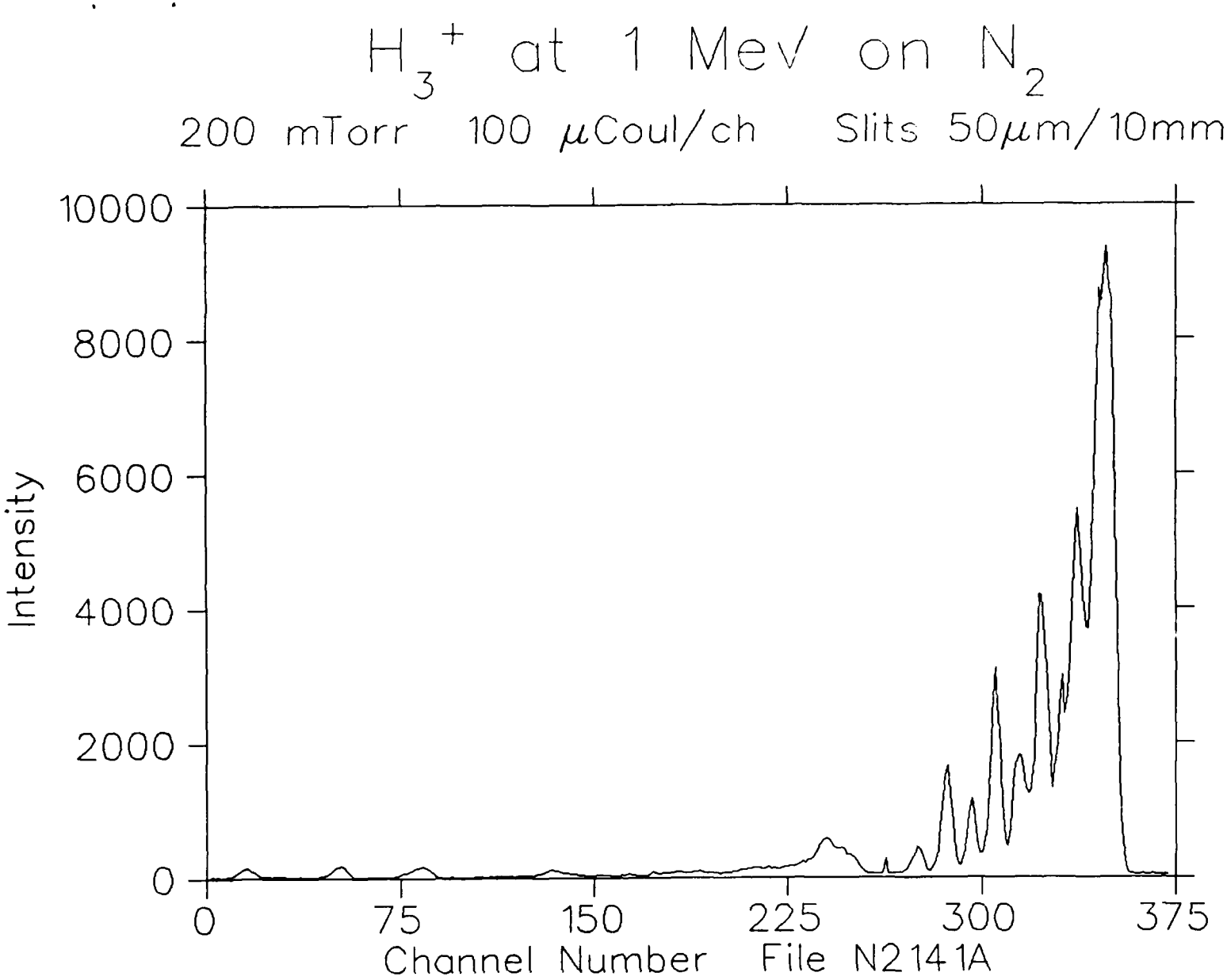
$H_3^+$ at 1 MeV on $N_2$
200 mTorr 100 μCoul/ch Slits 50μm/10mm
Intensity
10000
8000
6000
4000
2000
0
0
75
150
225
300
375
Channel Number File N2141A

Fig. 41

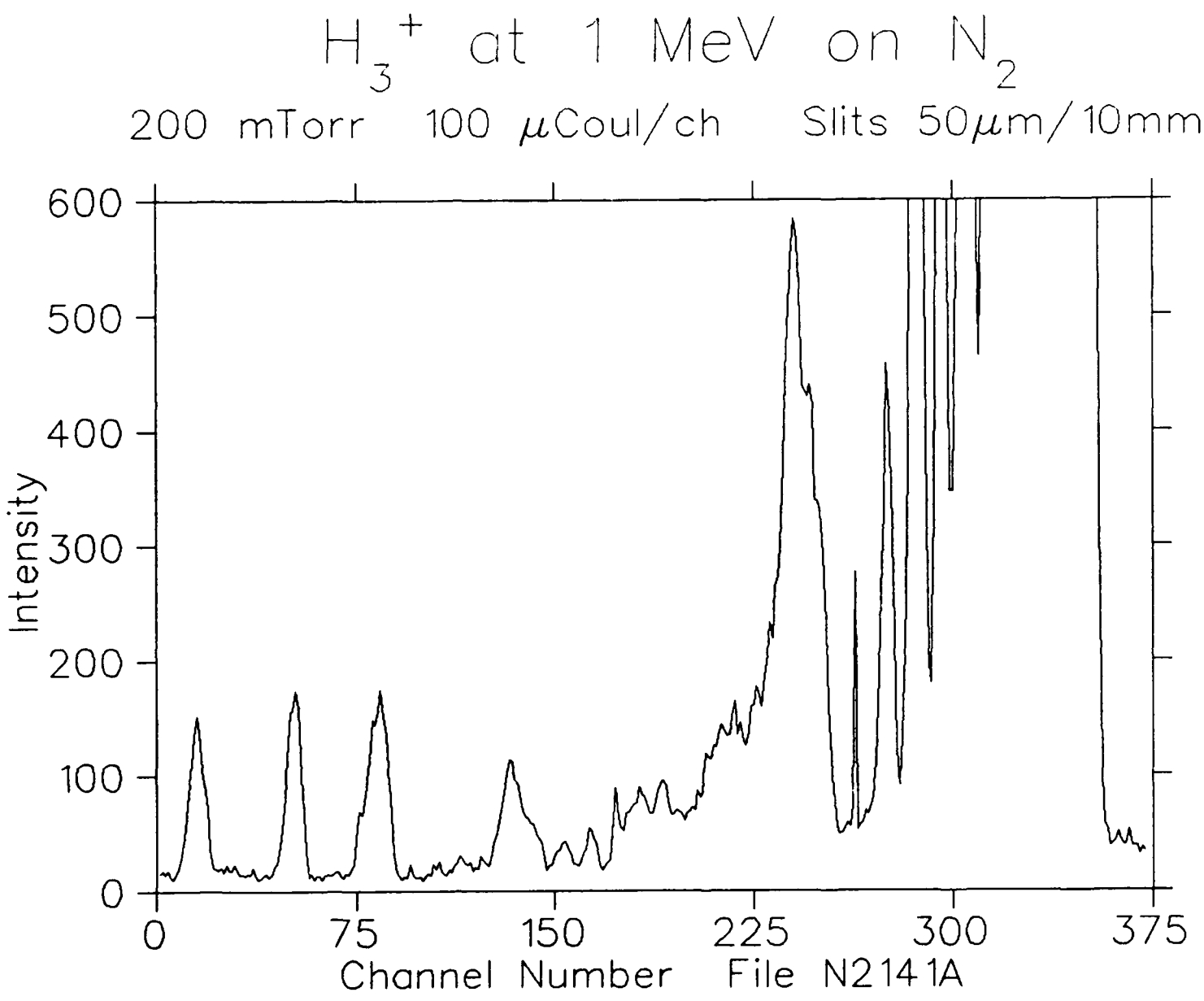
$H_3^+$ at 1 MeV on $N_2$
200 mTorr 100 μCoul/ch Slits 50μm/10mm
Intensity
600
500
400
300
200
100
0
0
75
150
225
300
375
Channel Number File N2141A

Fig. 42

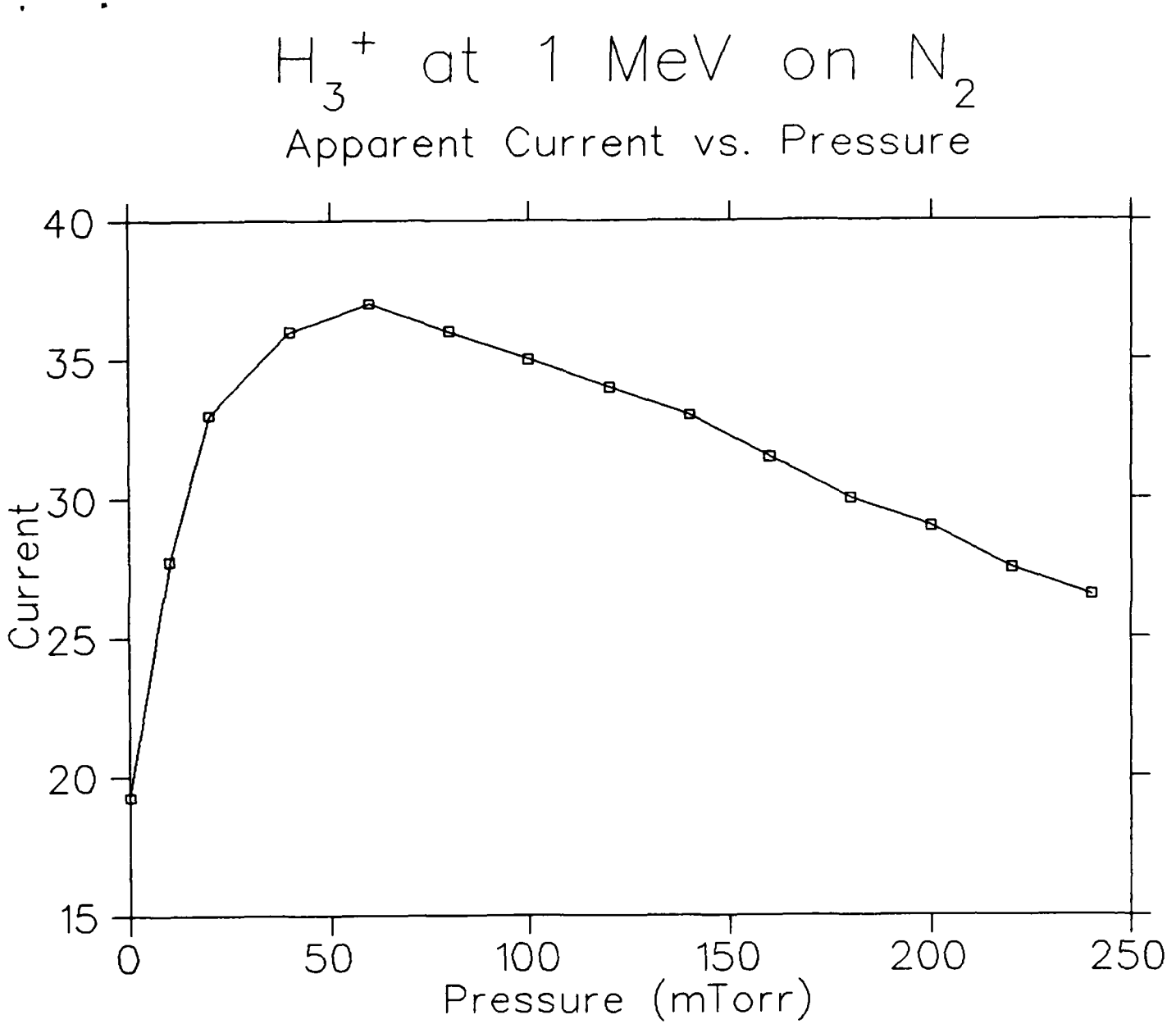
$H_3^+$ at 1 MeV on $N_2$
Apparent Current vs. Pressure
Current
40
35
30
25
20
15
0
50
100
150
200
250
Pressure (mTorr)

Fig. 43

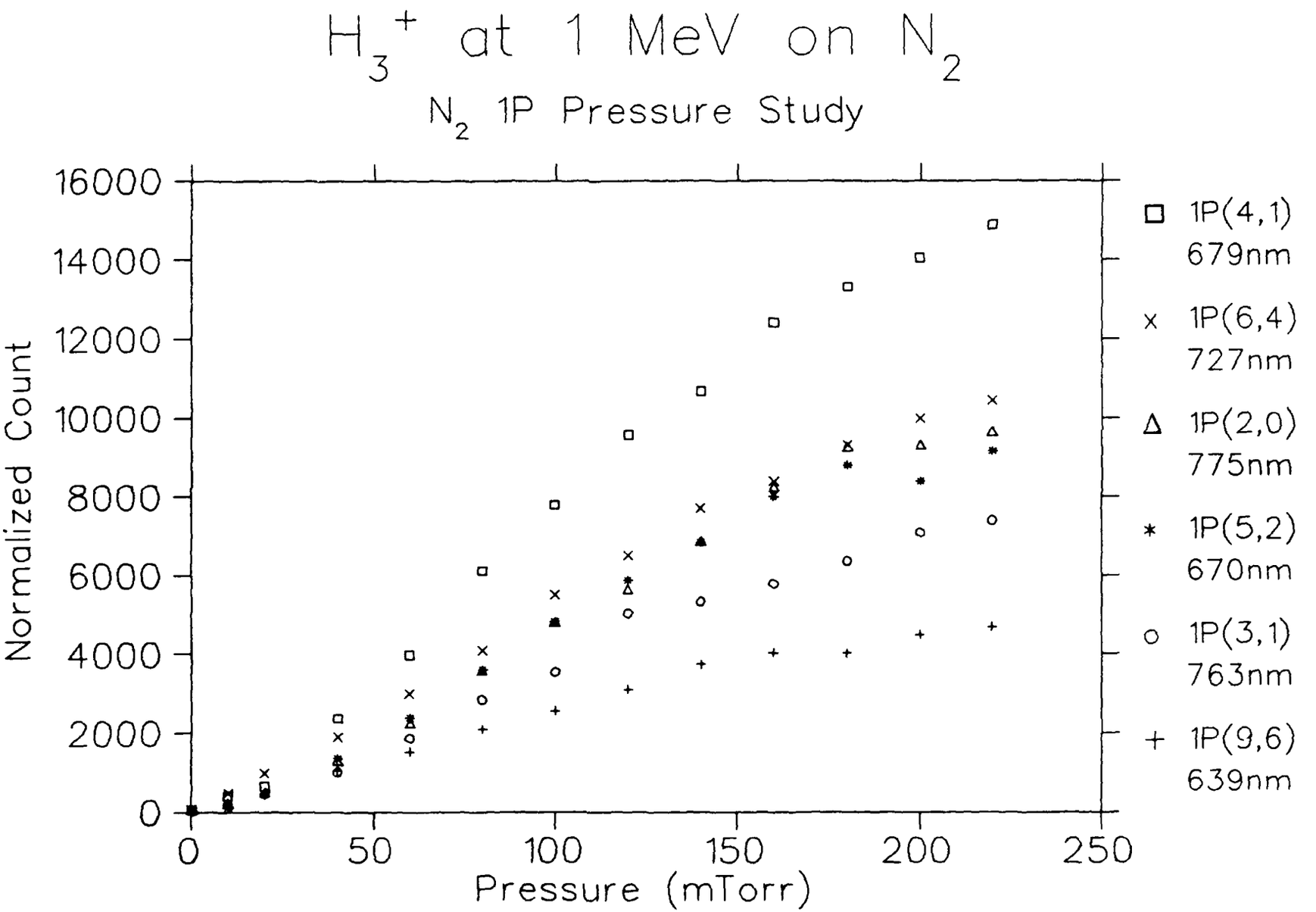
$H_3^+$ at 1 MeV on $N_2$
$N_2$ 1P Pressure Study
Normalized Count
16000
14000
12000
10000
8000
6000
4000
2000
0
0
50
100
150
200
250
Pressure (mTorr)
1P(4,1) 679nm
1P(6,4) 727nm
1P(2,0) 775nm
1P(5,2) 670nm
1P(3,1) 763nm
1P(9,6) 639nm

Fig. 44

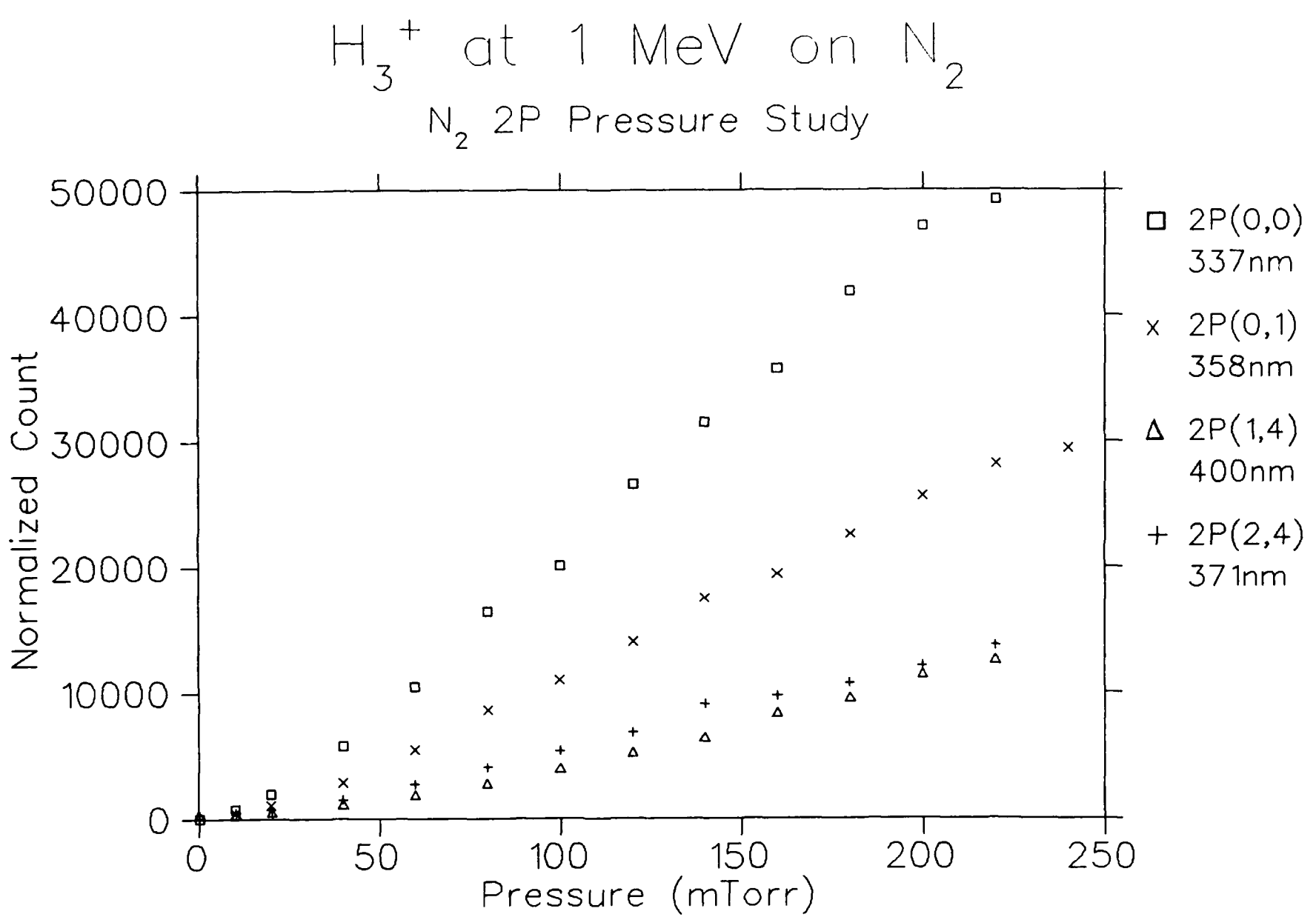
$H_3^+$ at 1 MeV on $N_2$
$N_2$ 2P Pressure Study
Normalized Count
50000
40000
30000
20000
10000
0
0
50
100
150
200
250
Pressure (mTorr)
2P(0,0) 337nm
2P(0,1) 358nm
2P(1,4) 400nm
2P(2,4) 371nm

Fig. 45

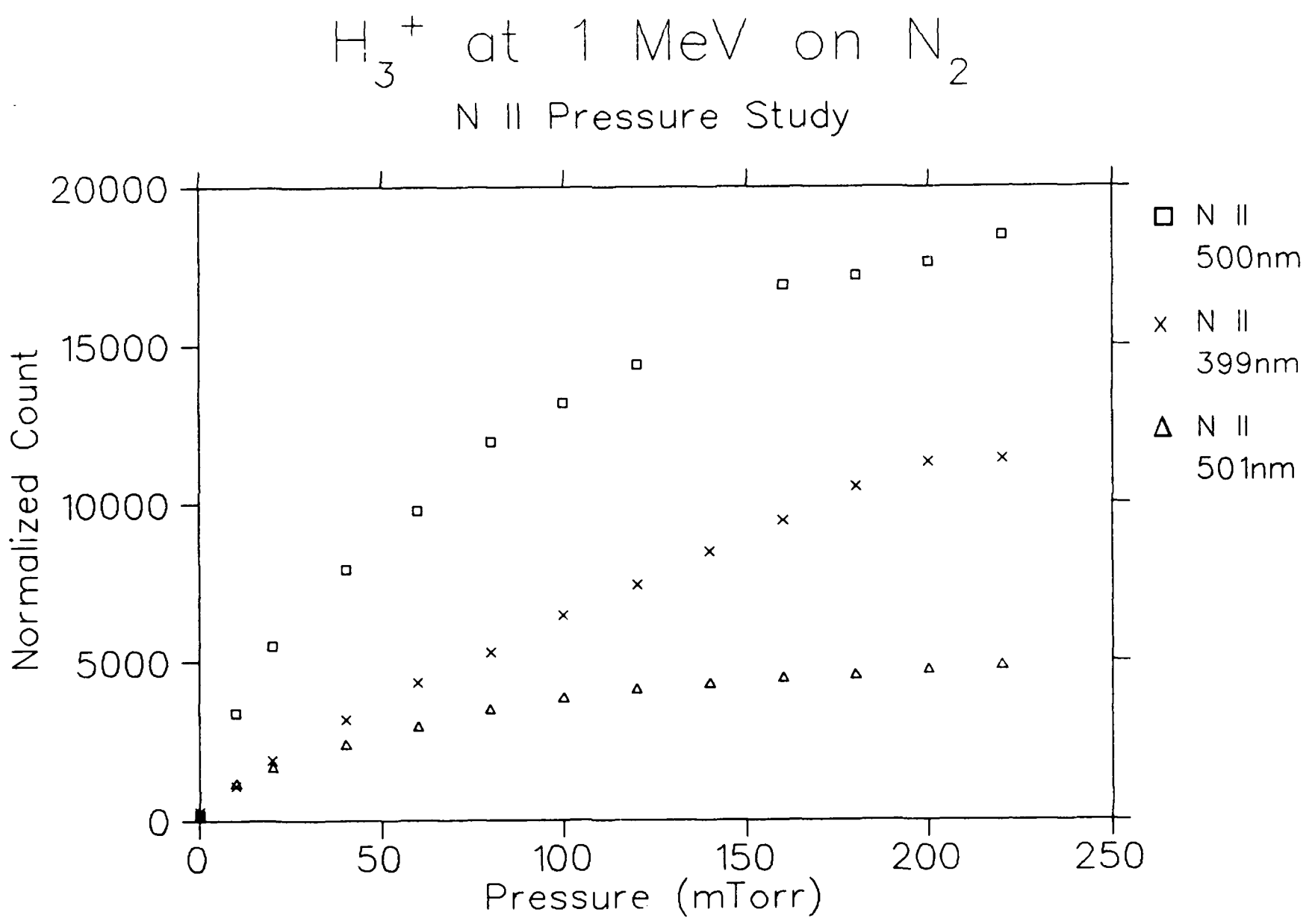
$H_3^+$ at 1 MeV on $N_2$
N II Pressure Study
Normalized Count
20000
15000
10000
5000
0
0
50
100
150
200
250
Pressure (mTorr)
N II 500nm
N II 399nm
N II 501nm

Fig. 46

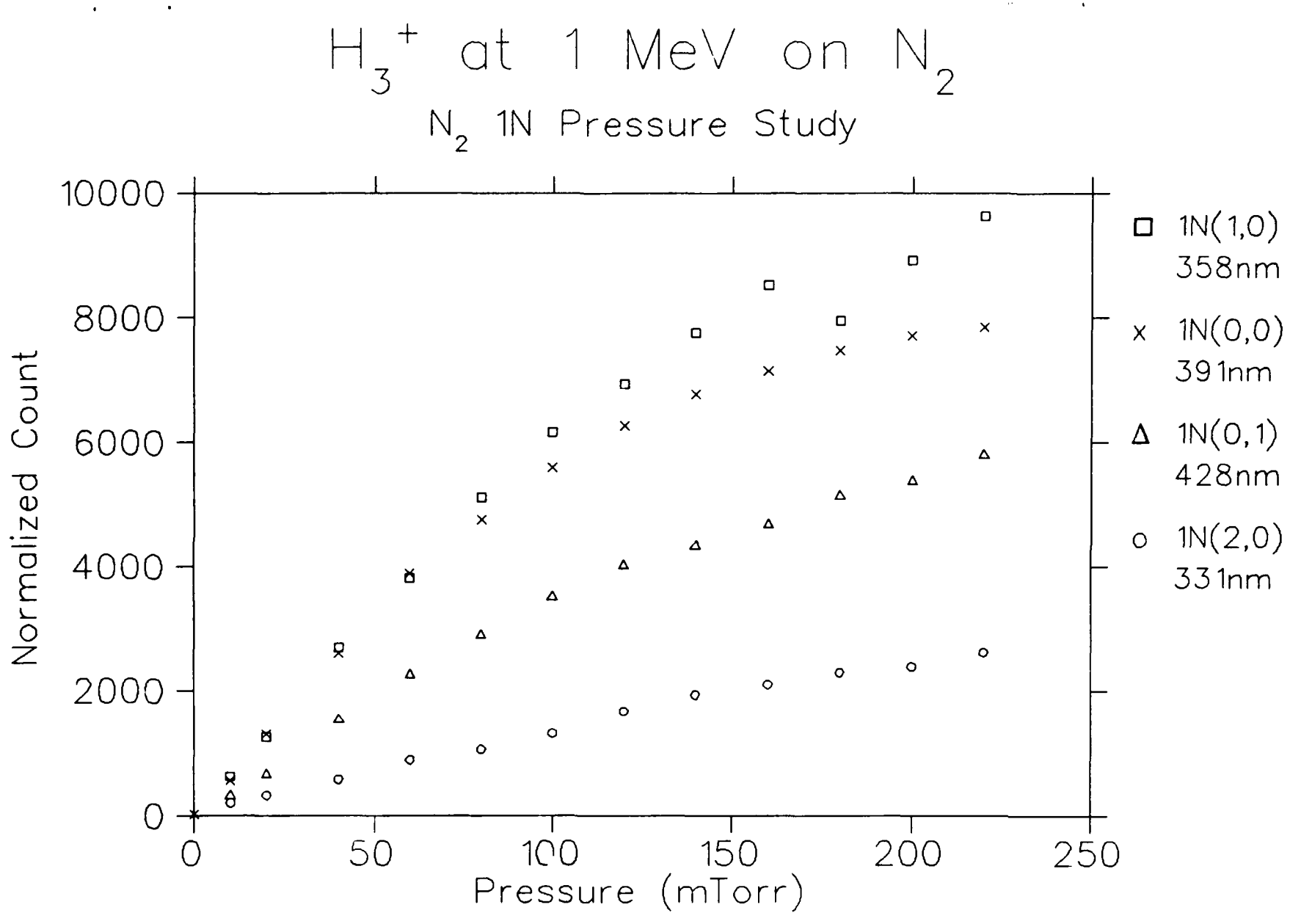
$H_3^+$ at 1 MeV on $N_2$
$N_2$ 1N Pressure Study
Normalized Count
10000
8000
6000
4000
2000
0
0
50
100
150
200
250
Pressure (mTorr)
1N(1,0) 358nm
1N(0,0) 391nm
1N(0,1) 428nm
1N(2,0) 331nm

Fig. 47

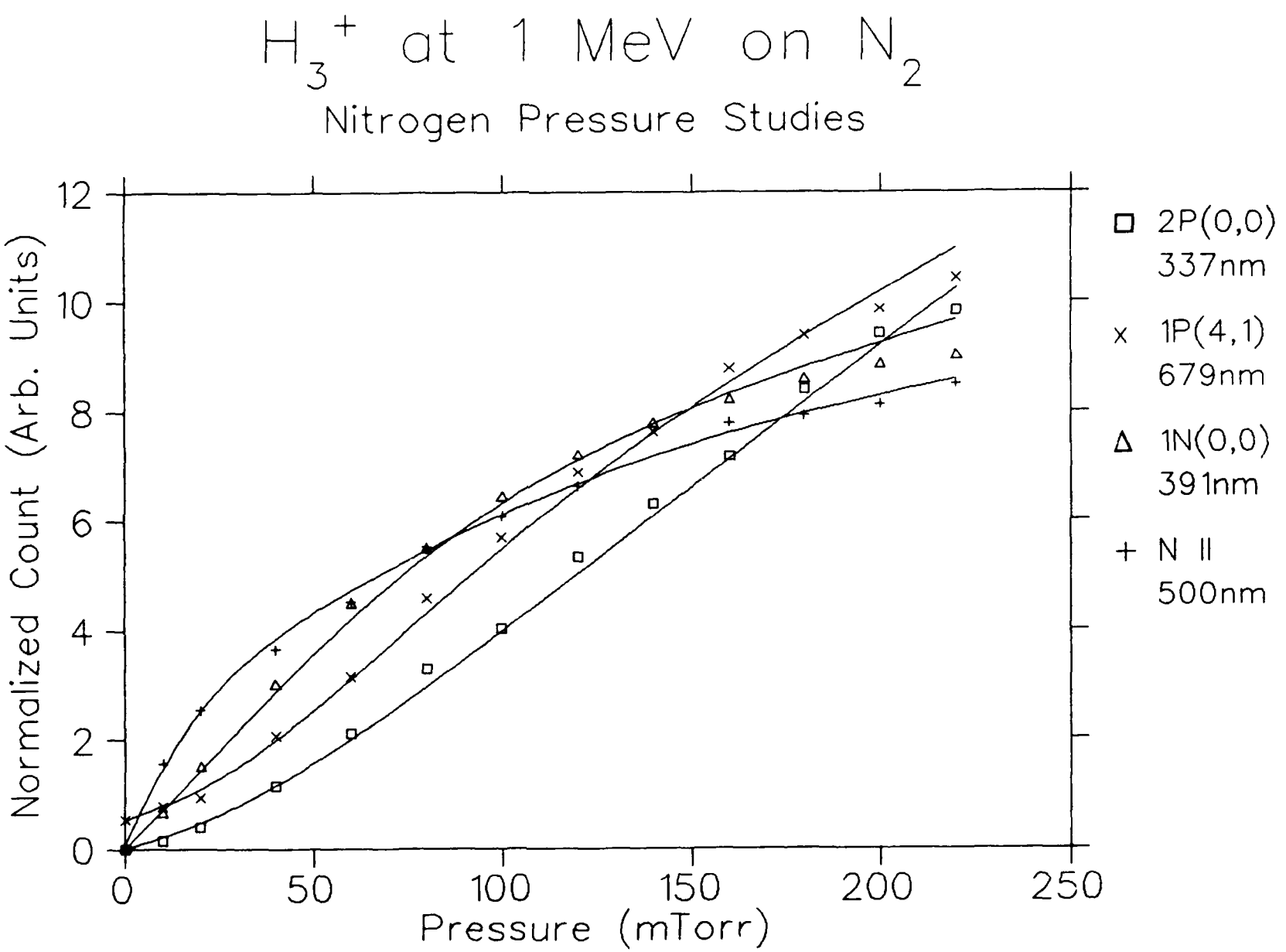
$H_3^+$ at 1 MeV on $N_2$
Nitrogen Pressure Studies
Normalized Count (Arb. Units)
Pressure (mTorr)
0
2
4
6
8
10
12
0
50
100
150
200
250
2P(0,0) 337nm
1P(4,1) 679nm
1N(0,0) 391nm
N II 500nm

Fig. 48

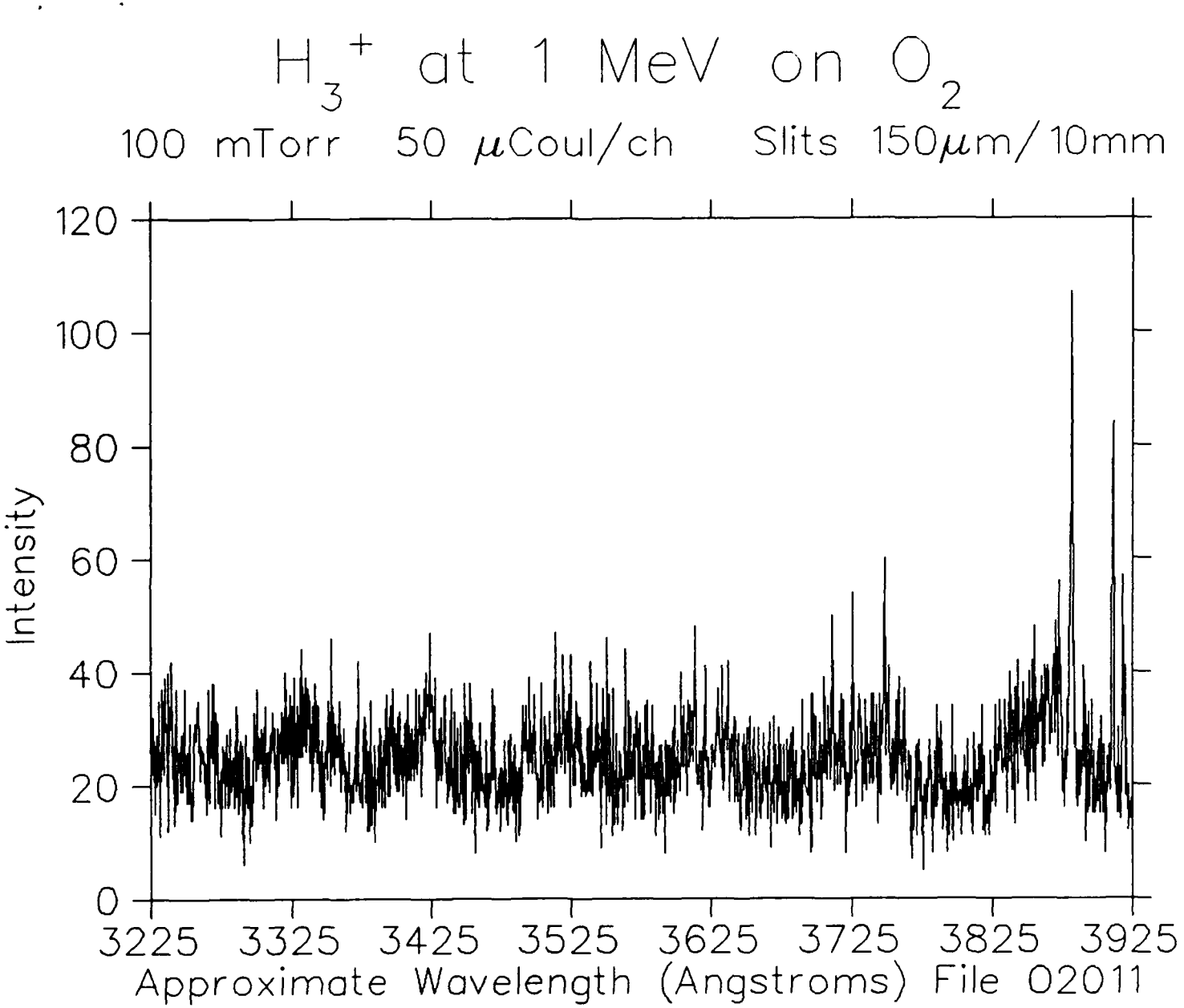
$H_3^+$ at 1 MeV on $O_2$
100 mTorr 50 μCoul/ch Slits 150μm/10mm
Intensity
120
100
80
60
40
20
0
3225 3325 3425 3525 3625 3725 3825 3925
Approximate Wavelength (Angstroms) File 02011

Fig. 49

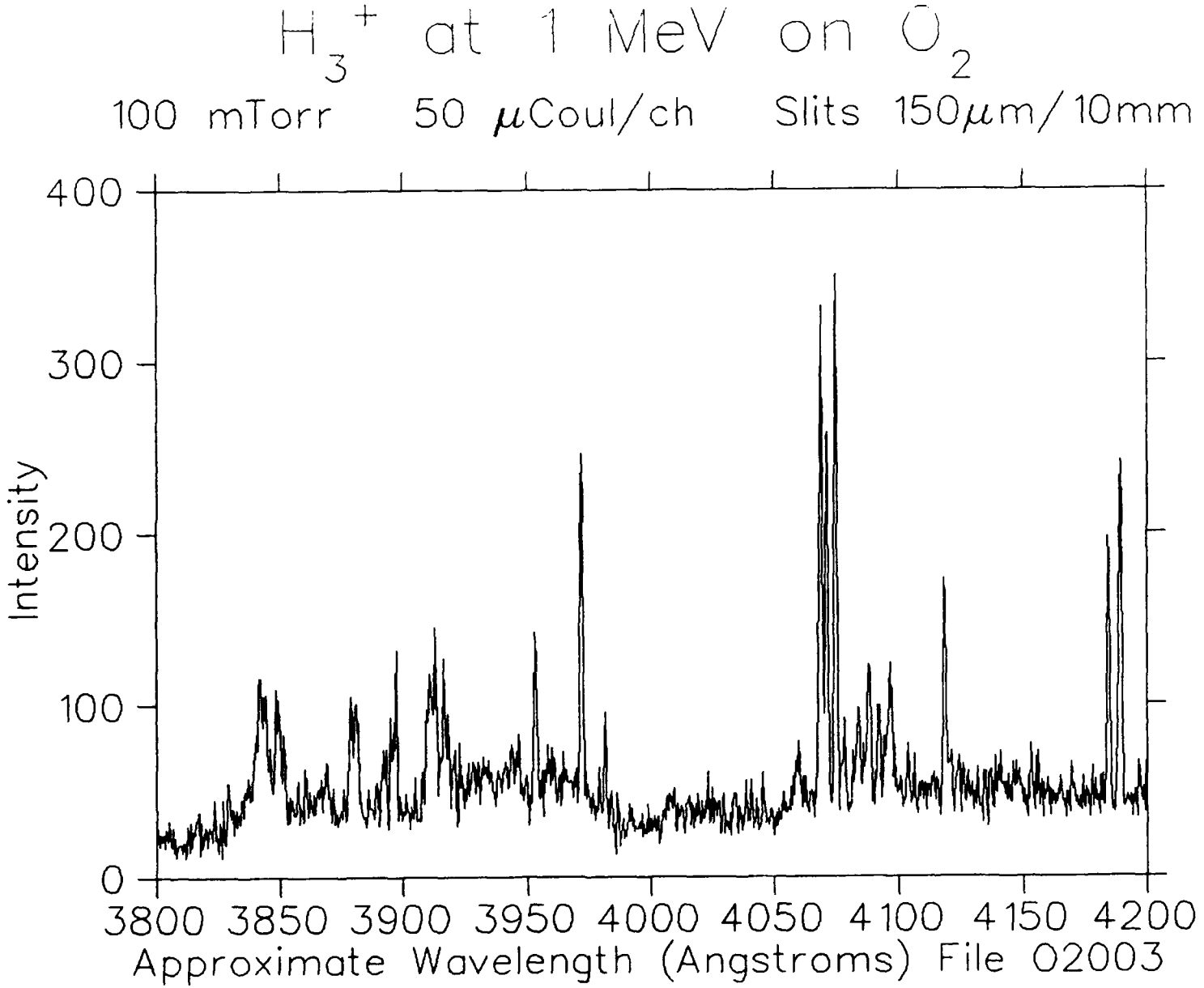
$H_3^+$ at 1 MeV on $O_2$
100 mTorr 50 μCoul/ch Slits 150μm/10mm
Intensity
400
300
200
100
0
3800 3850 3900 3950 4000 4050 4100 4150 4200
Approximate Wavelength (Angstroms) File 02003

Fig. 50

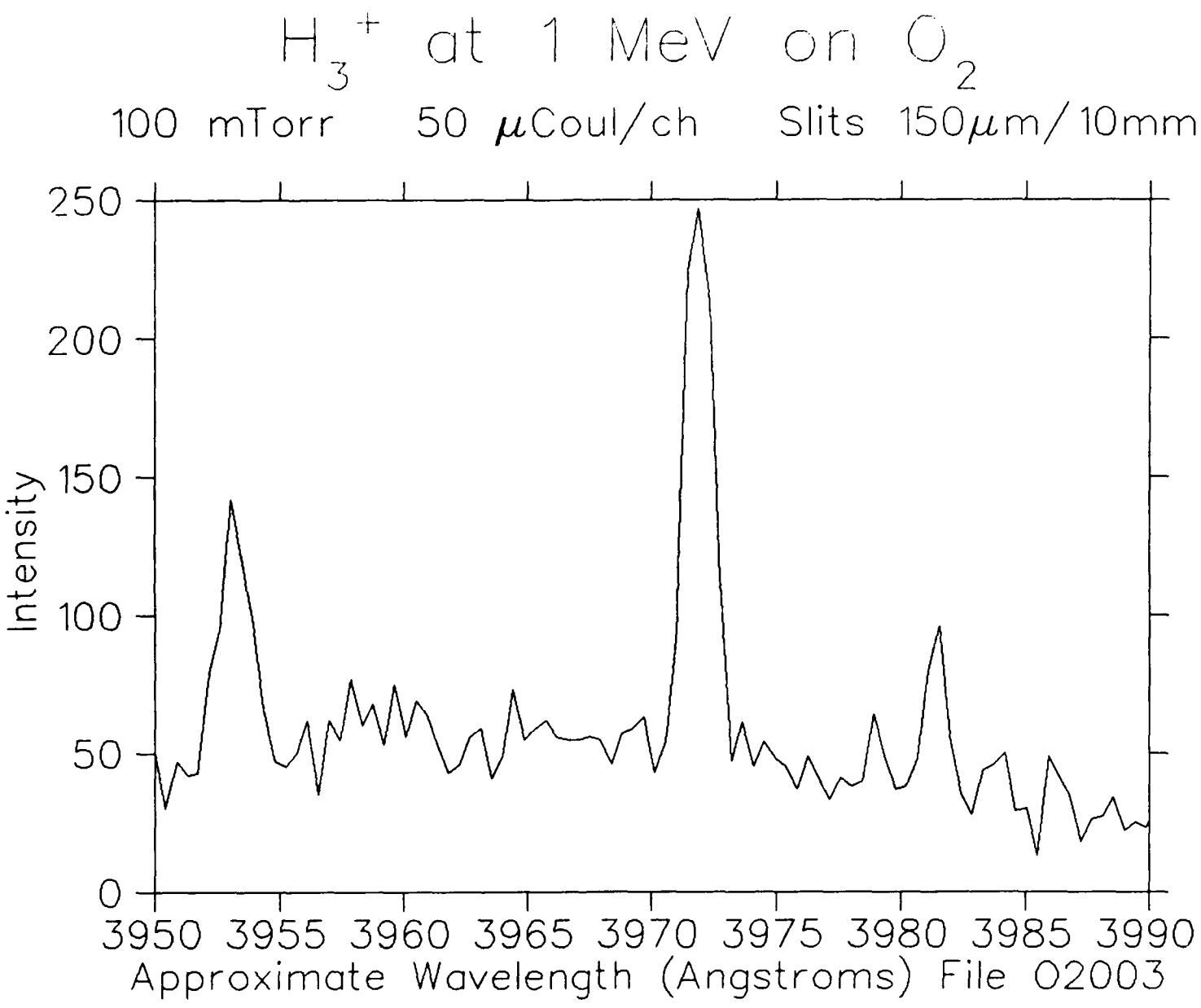
$H_3^+$ at 1 MeV on $O_2$
100 mTorr 50 μCoul/ch Slits 150μm/10mm
Intensity
250
200
150
100
50
0
3950 3955 3960 3965 3970 3975 3980 3985 3990
Approximate Wavelength (Angstroms) File 02003

Fig. 51

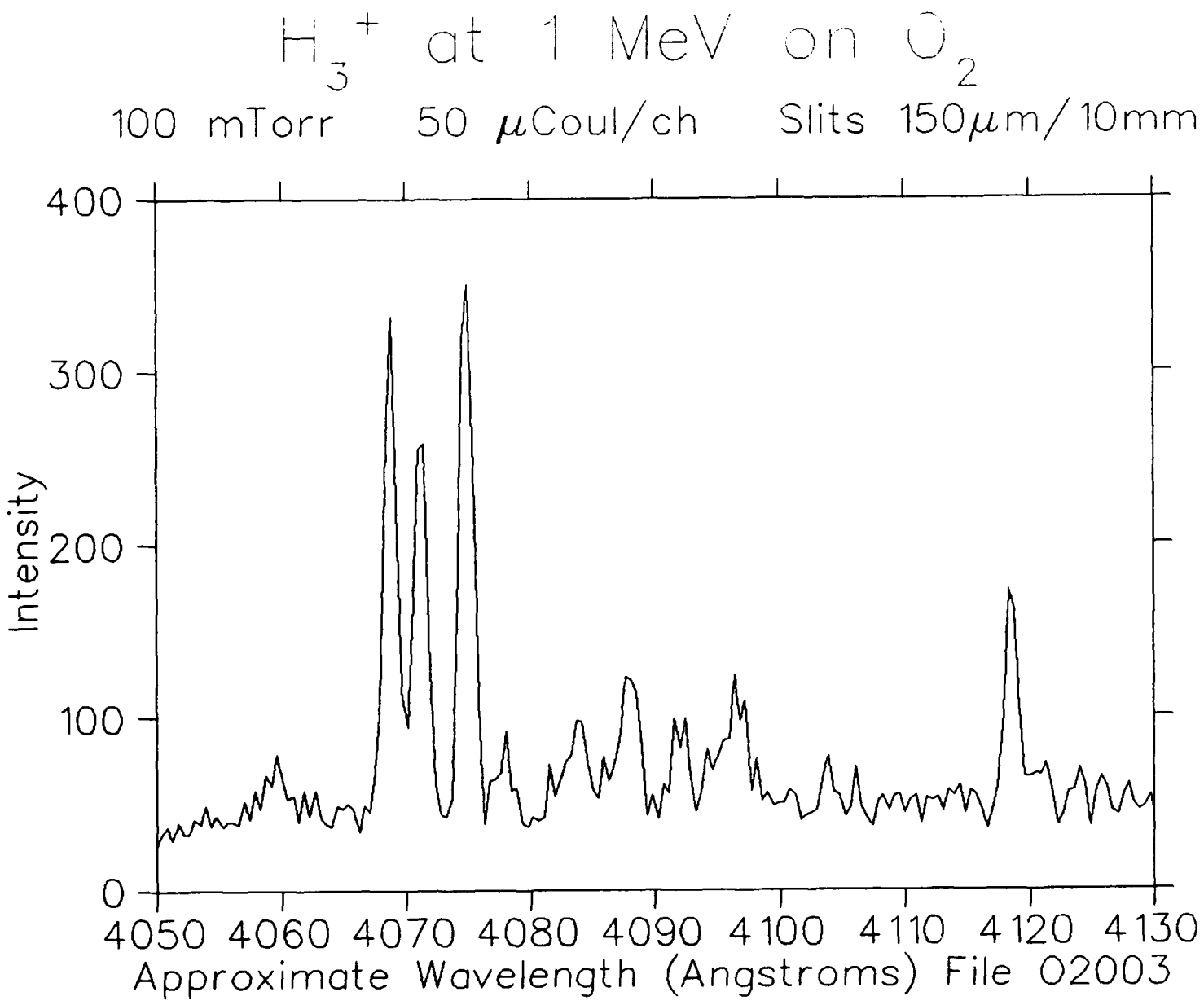
$H_3^+$ at 1 MeV on $O_2$
100 mTorr 50 μCoul/ch Slits 150μm/10mm
Intensity
400
300
200
100
0
4050 4060 4070 4080 4090 4100 4110 4120 4130
Approximate Wavelength (Angstroms) File 02003

Fig. 52

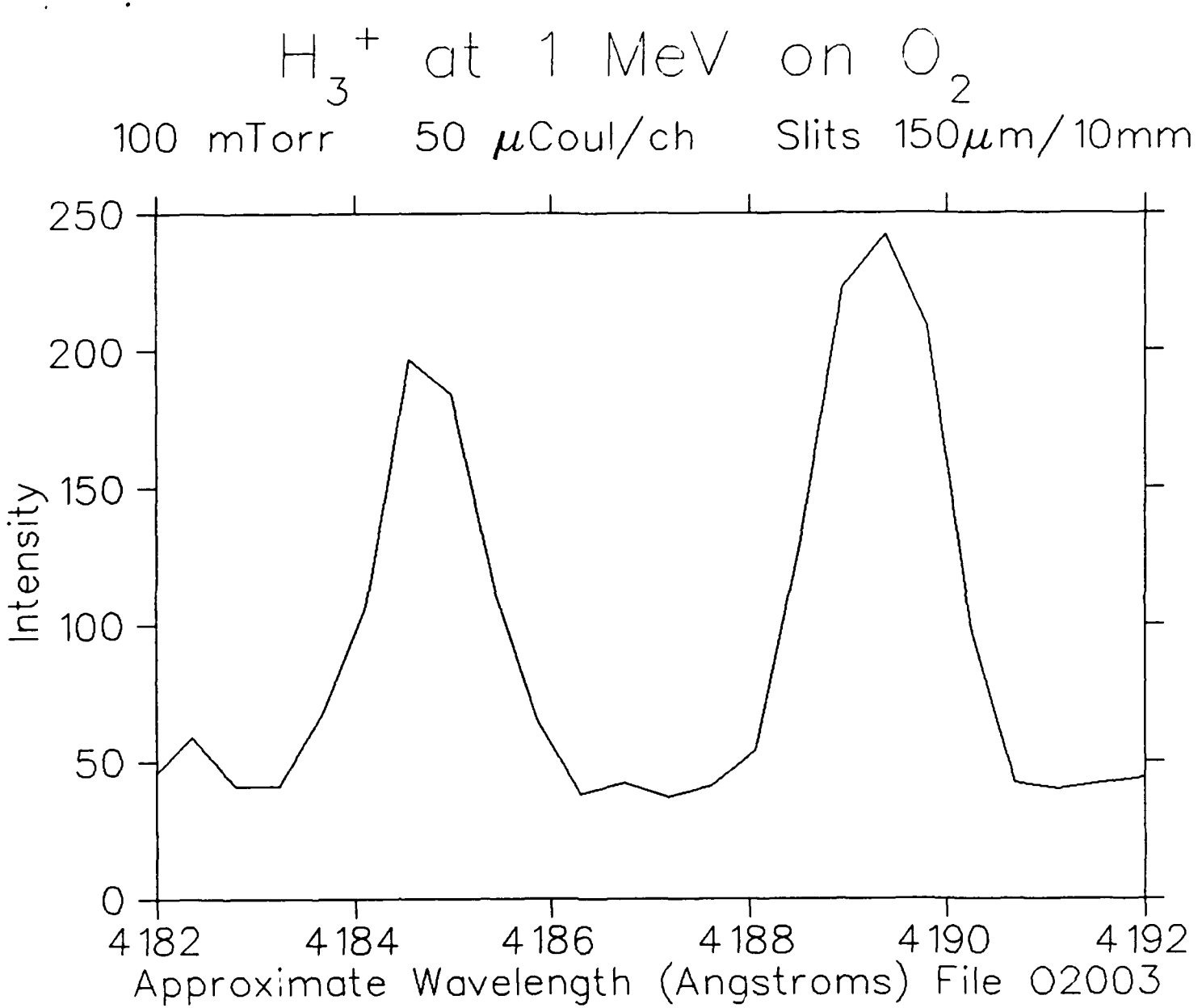
$H_3^+$ at 1 MeV on $O_2$
100 mTorr 50 μCoul/ch Slits 150μm/10mm
250
200
150
100
50
0
Intensity
4182
4184
4186
4188
4190
4192
Approximate Wavelength (Angstroms) File 02003

Fig. 53

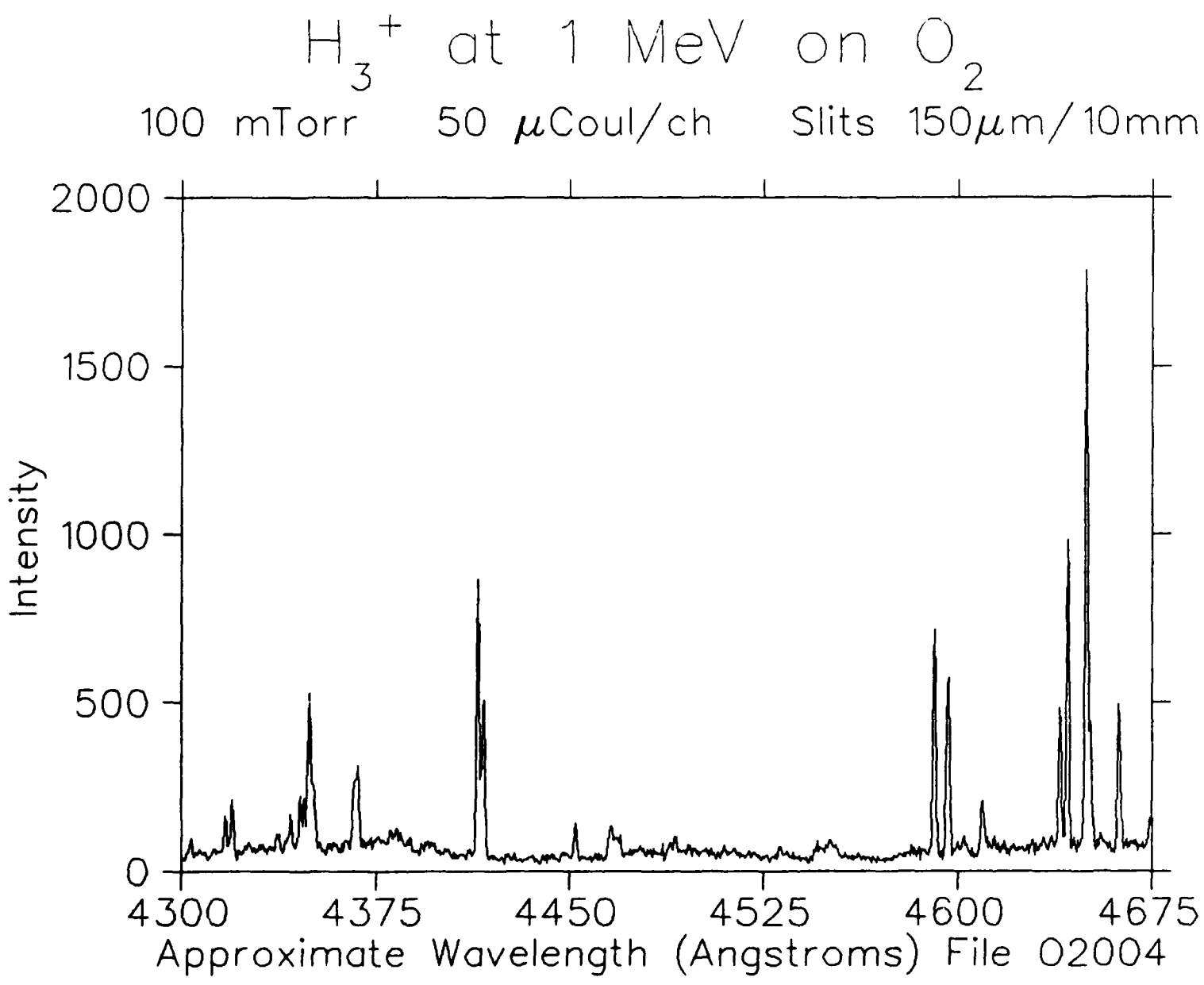
$H_3^+$ at 1 MeV on $O_2$
100 mTorr 50 μCoul/ch Slits 150μm/10mm
2000
1500
1000
500
0
Intensity
4300
4375
4450
4525
4600
4675
Approximate Wavelength (Angstroms) File 02004

Fig. 54

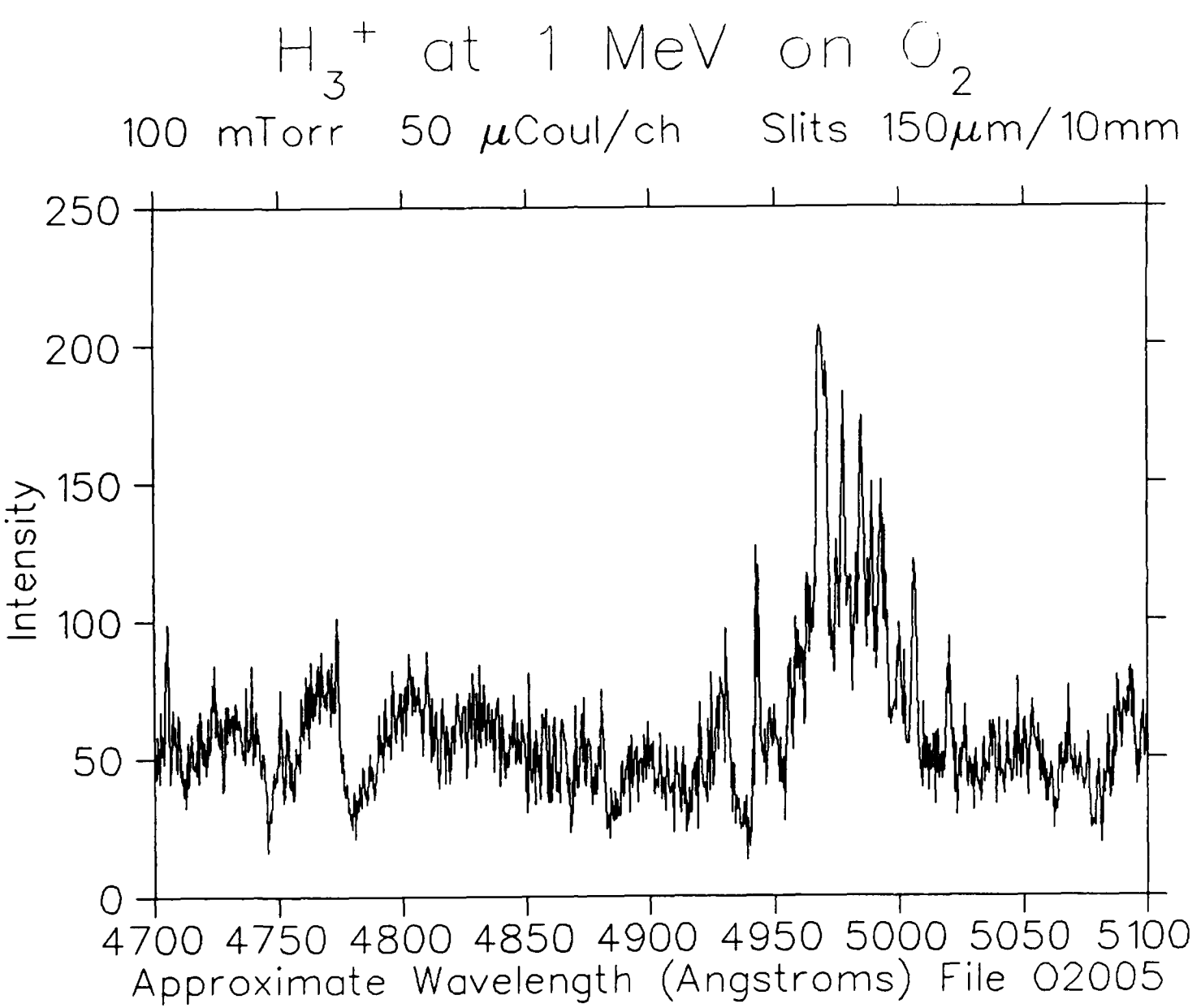
$H_3^+$ at 1 MeV on $O_2$
100 mTorr 50 μCoul/ch Slits 150μm/10mm
Intensity
250
200
150
100
50
0
4700 4750 4800 4850 4900 4950 5000 5050 5100
Approximate Wavelength (Angstroms) File 02005

Fig. 55

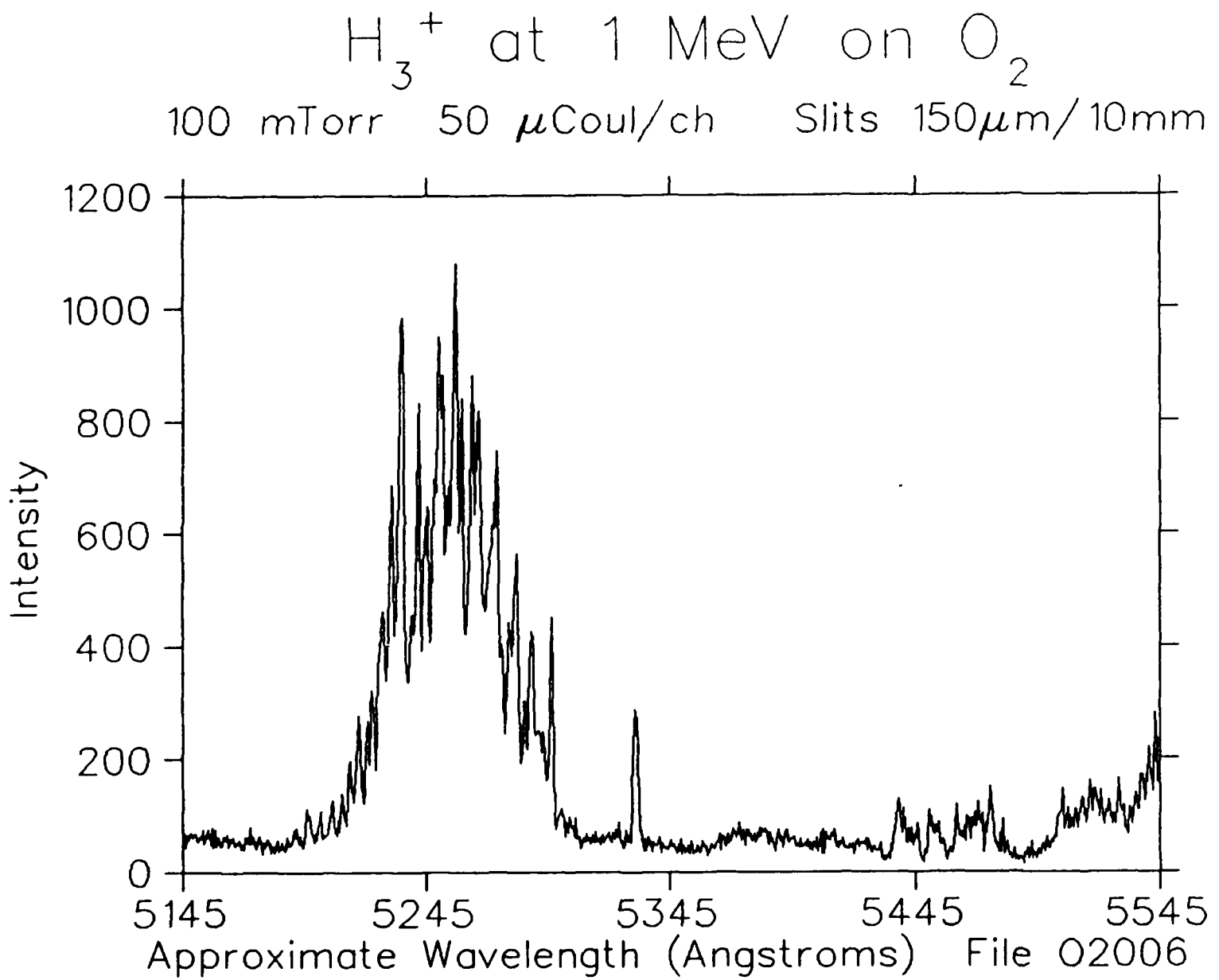
$H_3^+$ at 1 MeV on $O_2$
100 mTorr 50 μCoul/ch Slits 150μm/10mm
Intensity
1200
1000
800
600
400
200
0
5145
5245
5345
5445
5545
Approximate Wavelength (Angstroms) File 02006

Fig. 56

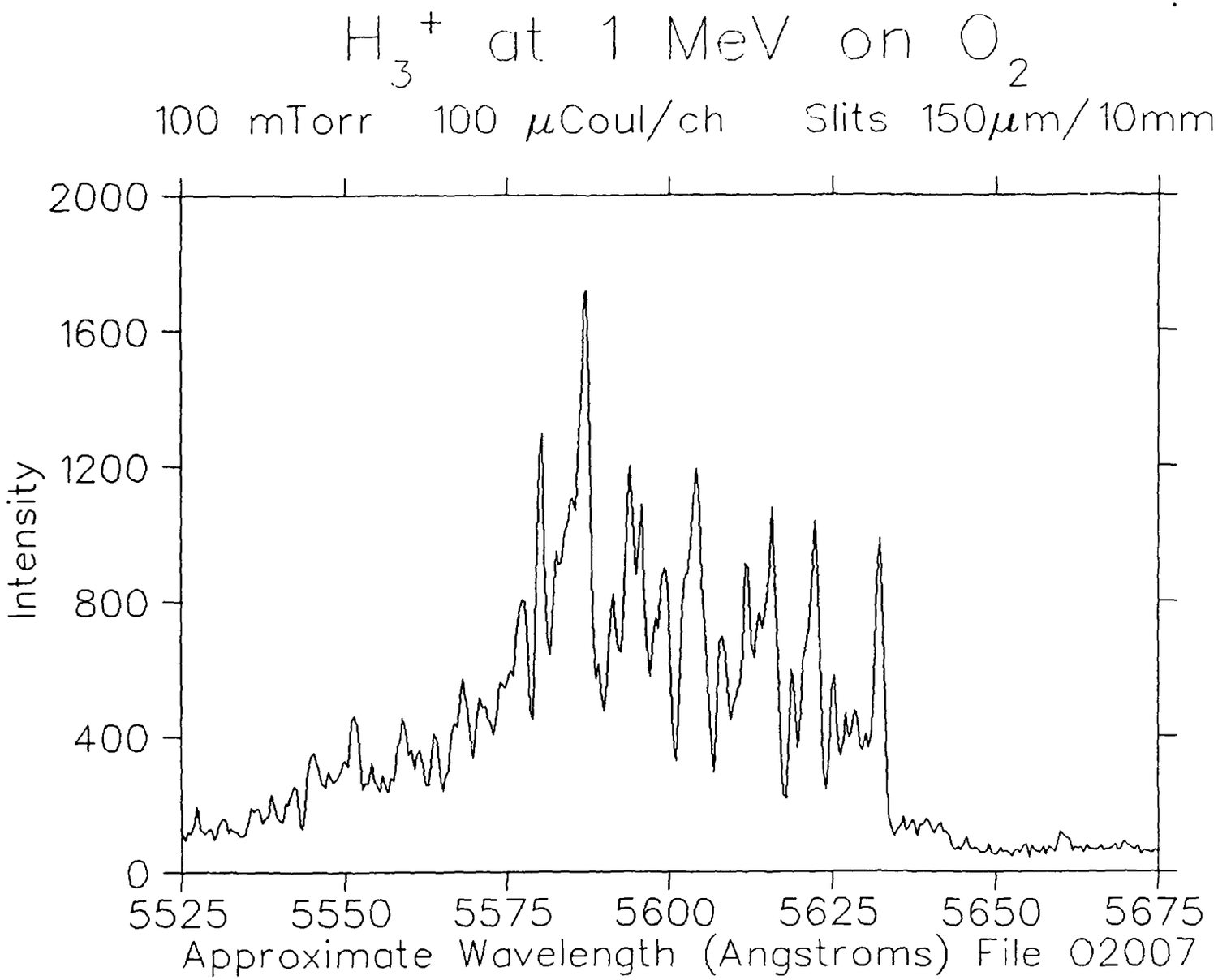
$H_3^+$ at 1 MeV on $O_2$
100 mTorr 100 μCoul/ch Slits 150μm/10mm
Intensity
2000
1600
1200
800
400
0
5525
5550
5575
5600
5625
5650
5675
Approximate Wavelength (Angstroms) File 02007

FIG. 57

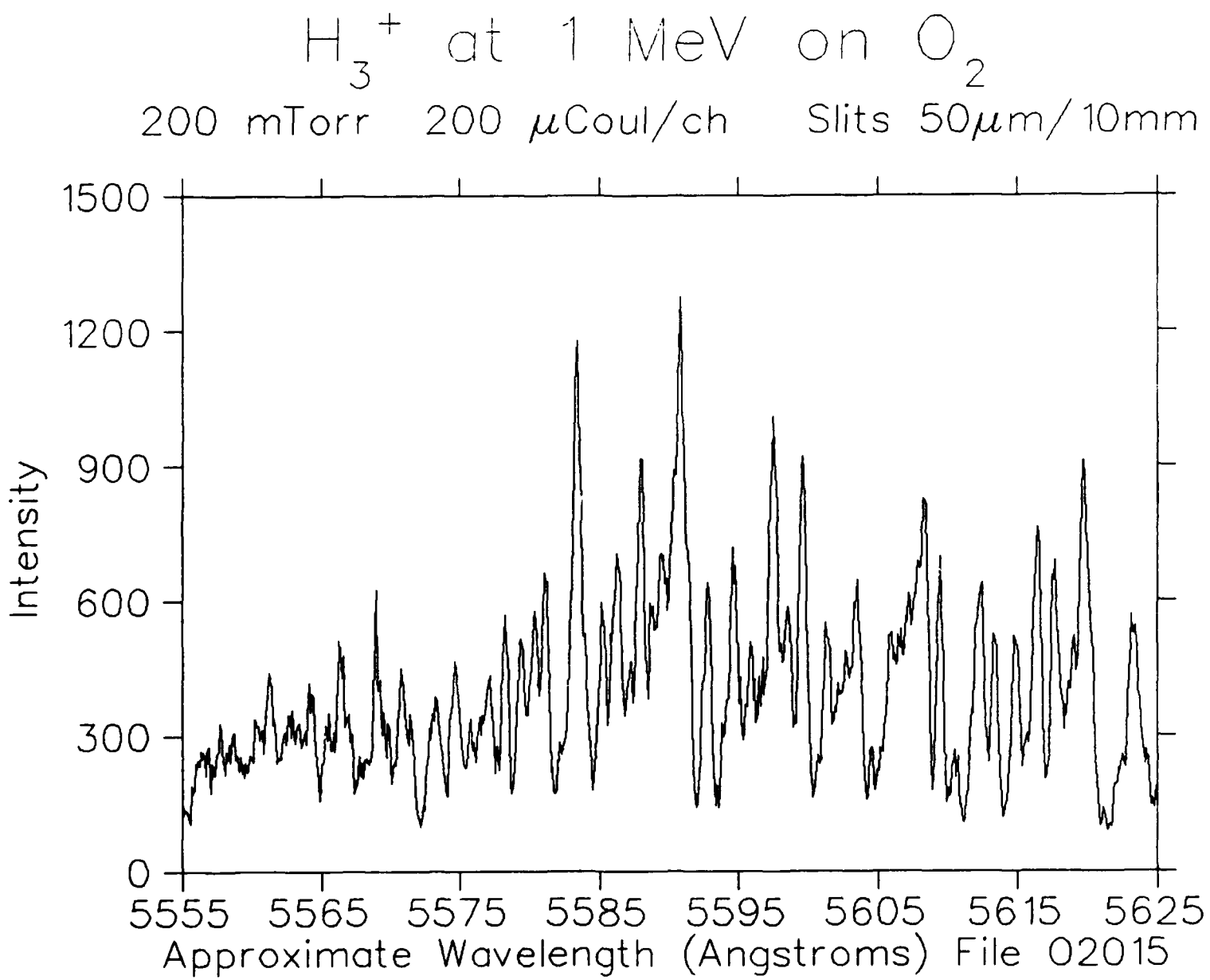
$H_3^+$ at 1 MeV on $O_2$
200 mTorr 200 μCoul/ch Slits 50μm/10mm
Intensity
1500
1200
900
600
300
0
5555 5565 5575 5585 5595 5605 5615 5625
Approximate Wavelength (Angstroms) File 02015

Fig. 58

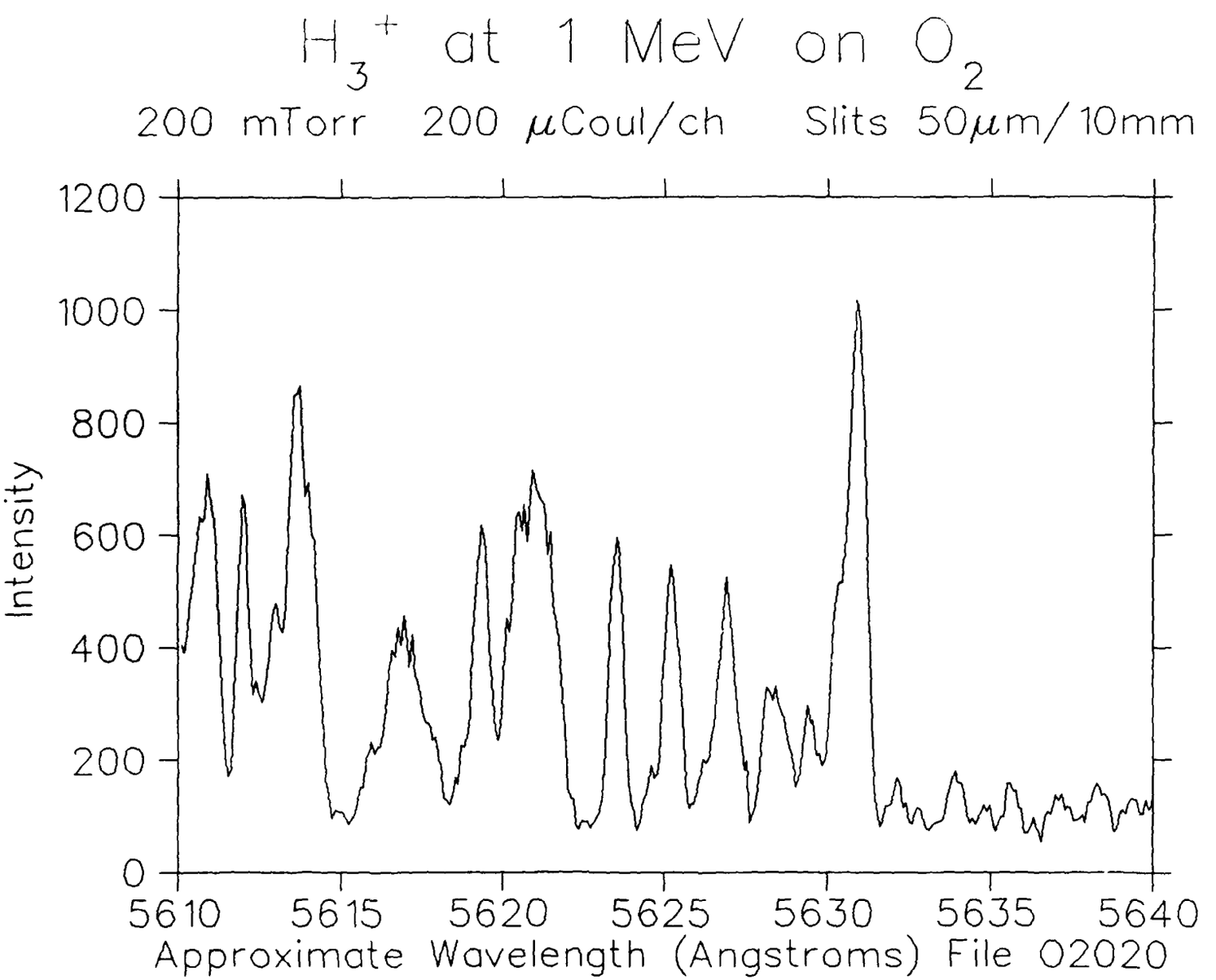
$H_3^+$ at 1 MeV on $O_2$
200 mTorr 200 μCoul/ch Slits 50μm/10mm
Intensity
1200
1000
800
600
400
200
0
5610
5615
5620
5625
5630
5635
5640
Approximate Wavelength (Angstroms) File 02020

Fig. 59

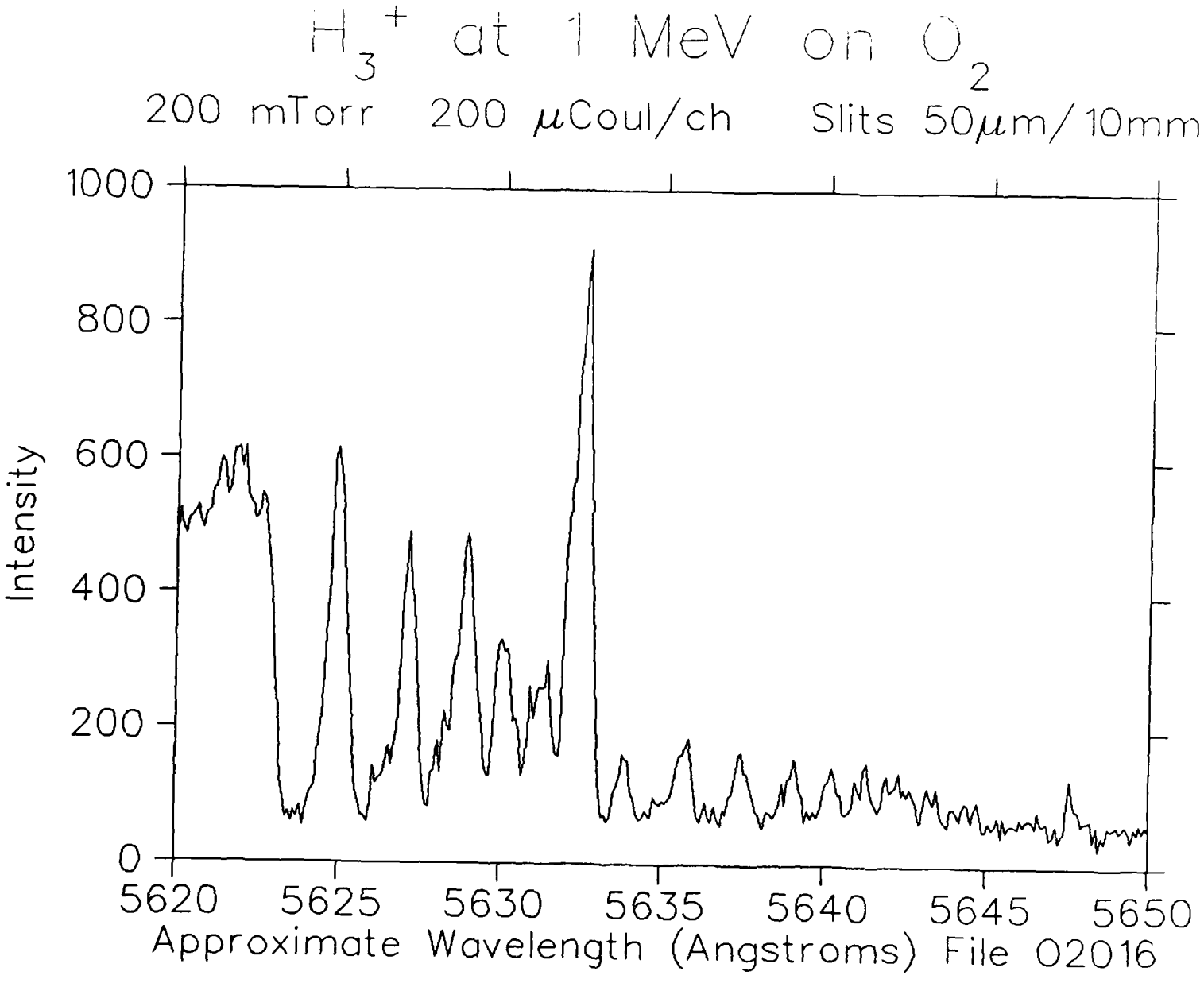
$H_3^+$ at 1 MeV on $O_2$
200 mTorr 200 μCoul/ch Slits 50μm/10mm
Intensity
1000
800
600
400
200
0
5620
5625
5630
5635
5640
5645
5650
Approximate Wavelength (Angstroms) File 02016

Fig. 60

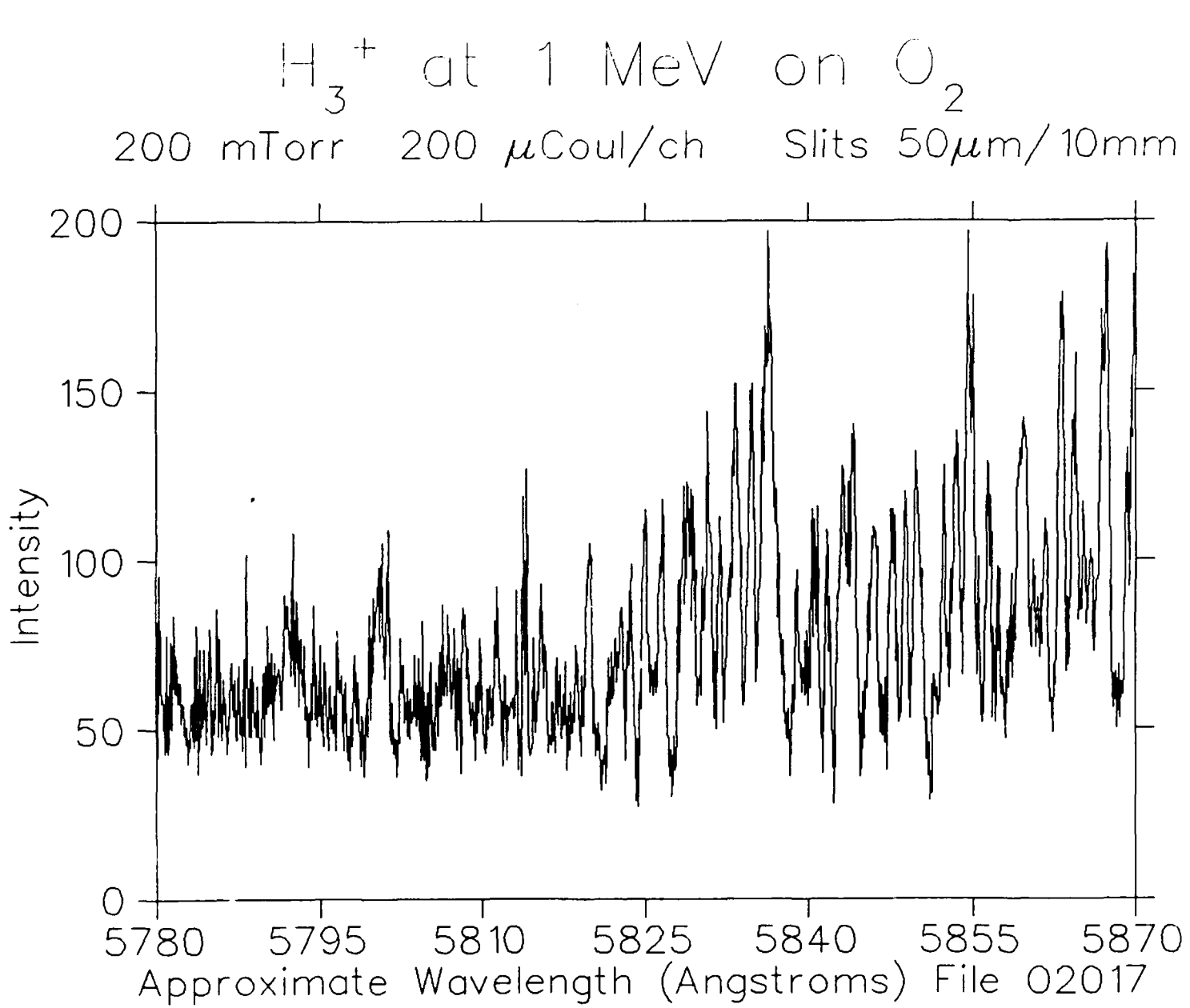
$H_3^+$ at 1 MeV on $O_2$
200 mTorr 200 μCoul/ch Slits 50μm/10mm
Intensity
200
150
100
50
0
5780
5795
5810
5825
5840
5855
5870
Approximate Wavelength (Angstroms) File 02017

Fig. 61

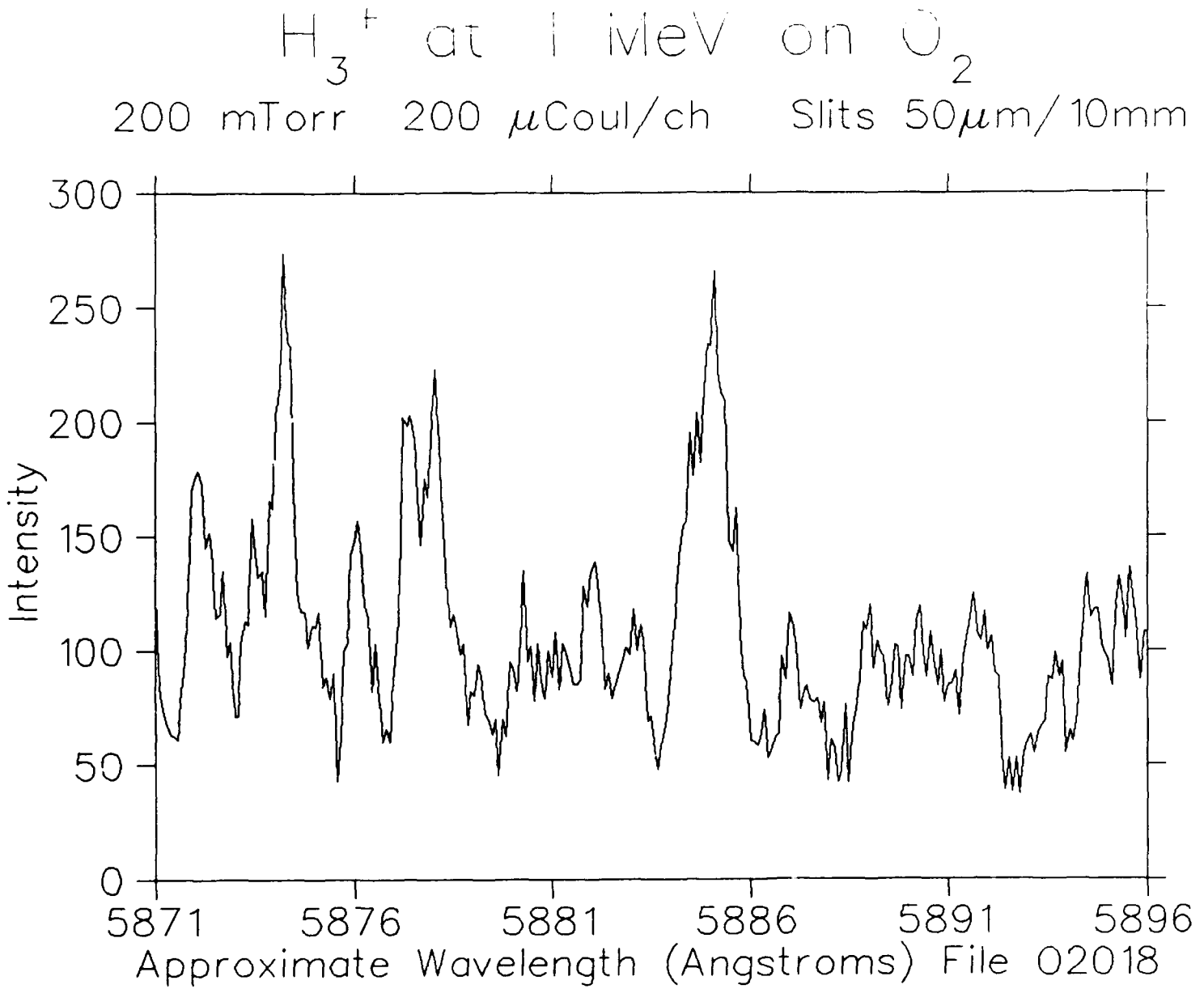
$H_3^+$ at 1 MeV on $O_2$
200 mTorr 200 μCoul/ch Slits 50μm/10mm
Intensity
300
250
200
150
100
50
0
5871
5876
5881
5886
5891
5896
Approximate Wavelength (Angstroms) File 02018

Fig. 62

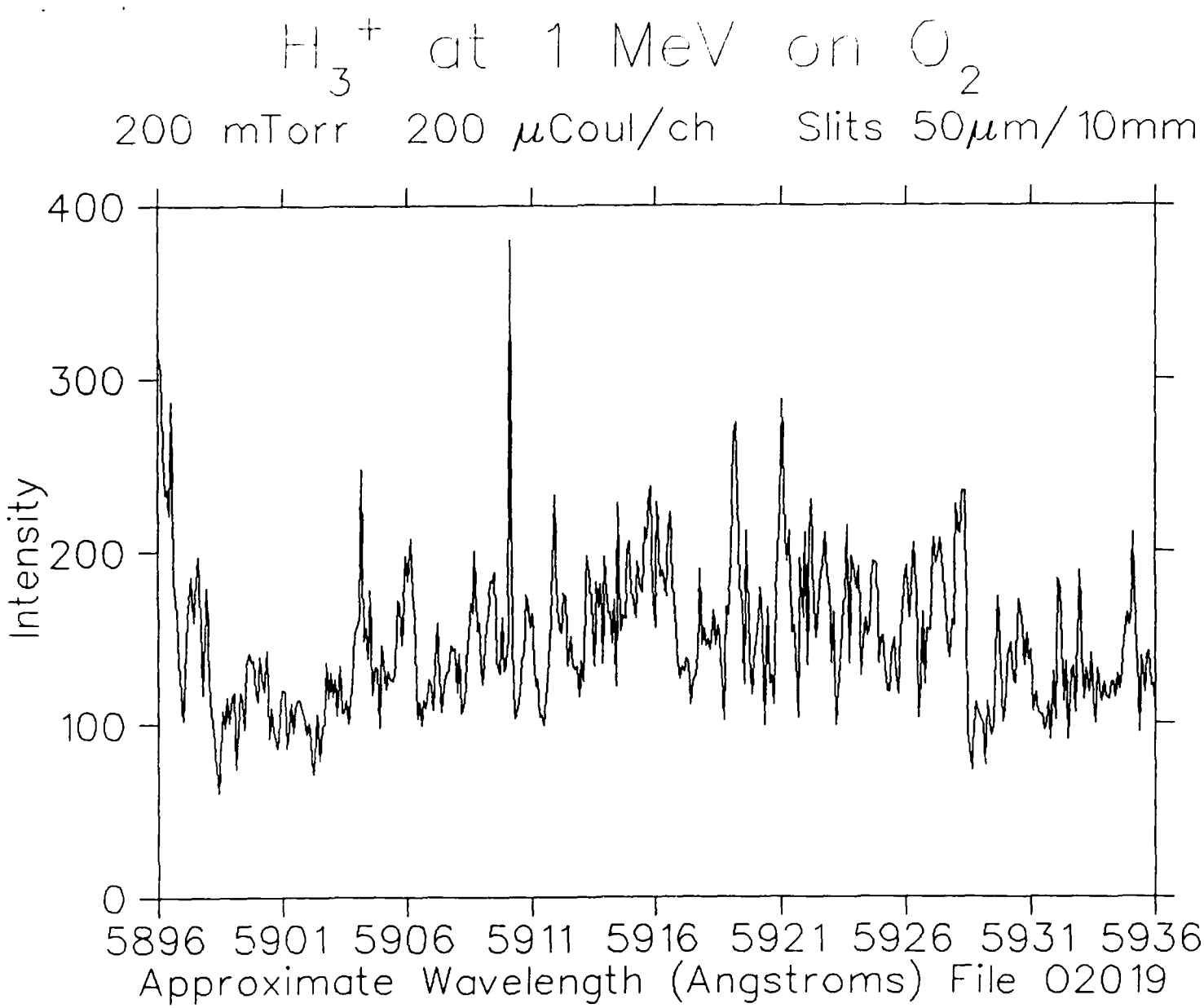
$H_3^+$ at 1 MeV on $O_2$
200 mTorr 200 μCoul/ch Slits 50μm/10mm
Intensity
400
300
200
100
0
5896 5901 5906 5911 5916 5921 5926 5931 5936
Approximate Wavelength (Angstroms) File 02019

Fig. 63

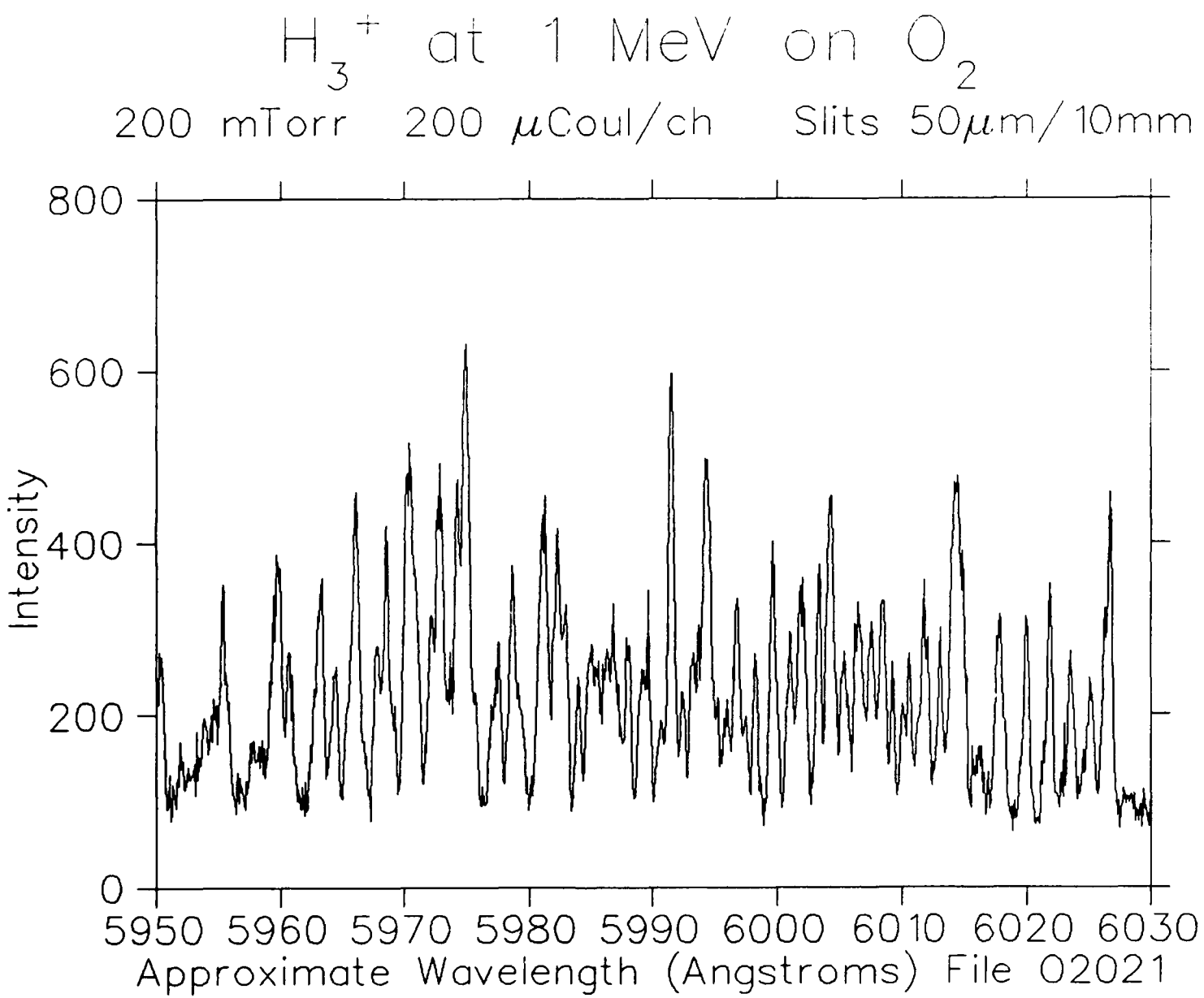
$H_3^+$ at 1 MeV on $O_2$
200 mTorr 200 μCoul/ch Slits 50μm/10mm
Intensity
800
600
400
200
0
5950 5960 5970 5980 5990 6000 6010 6020 6030
Approximate Wavelength (Angstroms) File 02021

Fig. 64

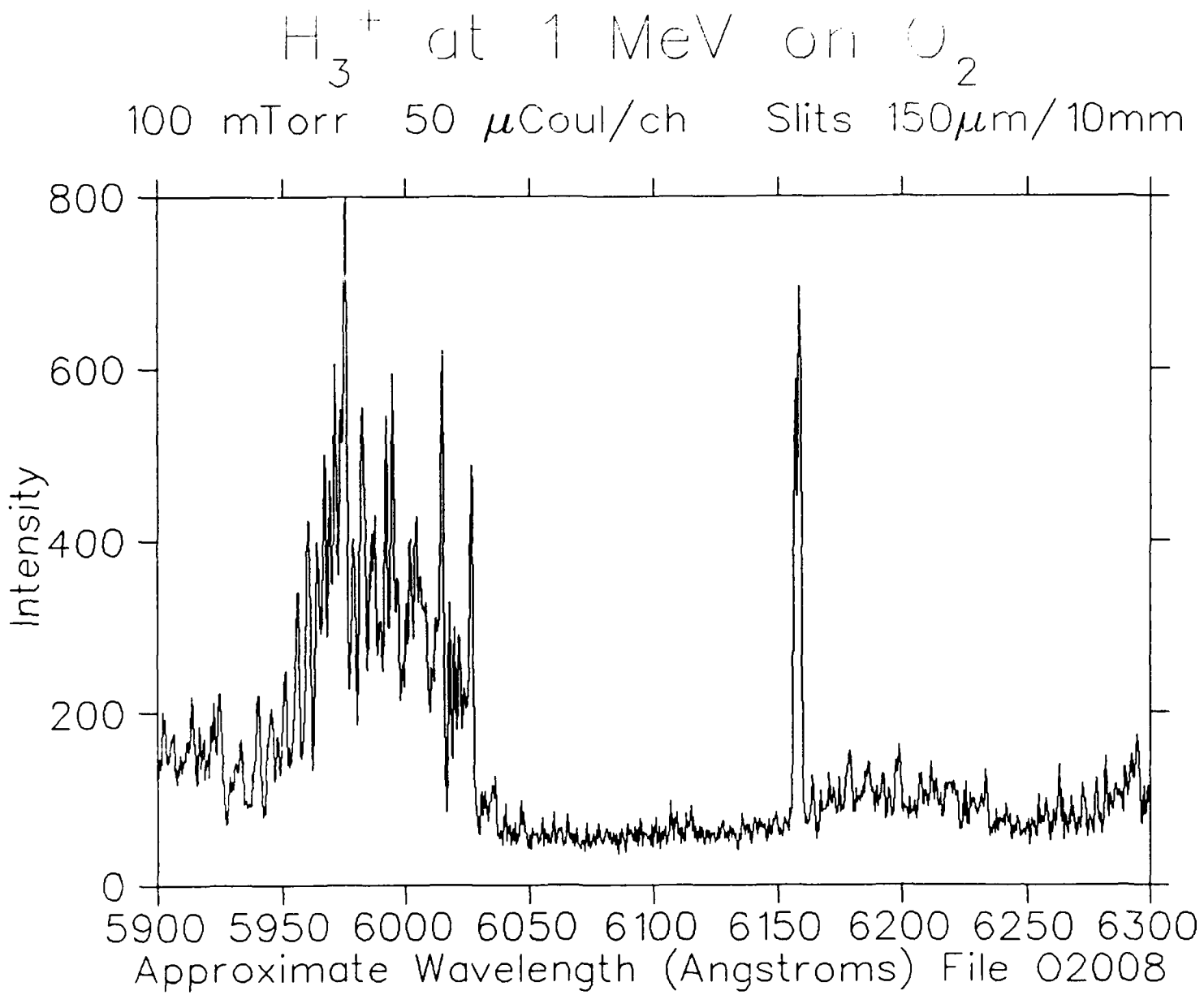
$H_3^+$ at 1 MeV on $O_2$
100 mTorr 50 μCoul/ch Slits 150μm/10mm
Intensity
800
600
400
200
0
5900 5950 6000 6050 6100 6150 6200 6250 6300
Approximate Wavelength (Angstroms) File 02008

Fig. 65

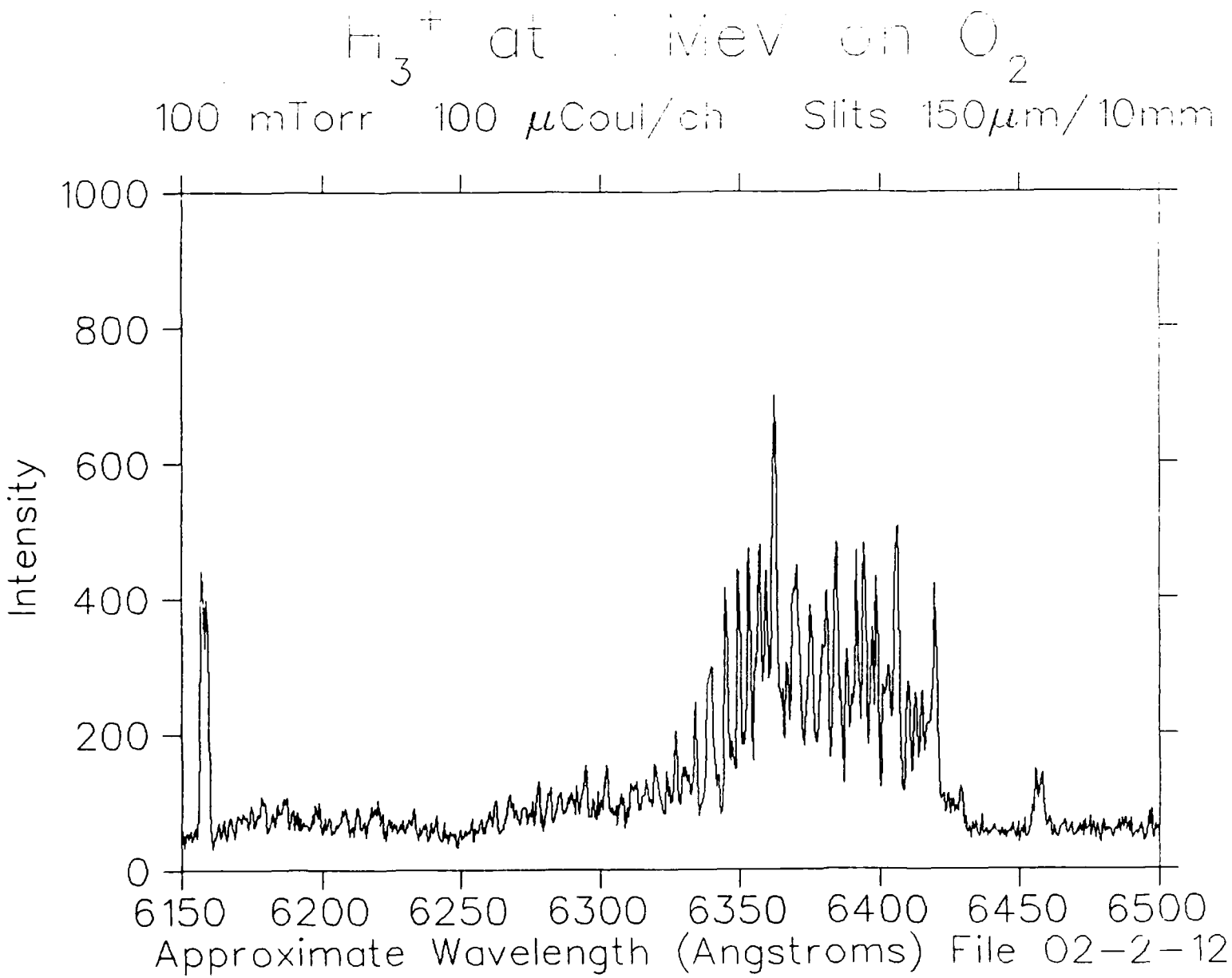
$H_3^+$ at 1 Mev on $O_2$
100 mTorr 100 μCoul/ch Slits 150μm/10mm
Intensity
1000
800
600
400
200
0
6150 6200 6250 6300 6350 6400 6450 6500
Approximate Wavelength (Angstroms) File 02-2-12

FIG. 66

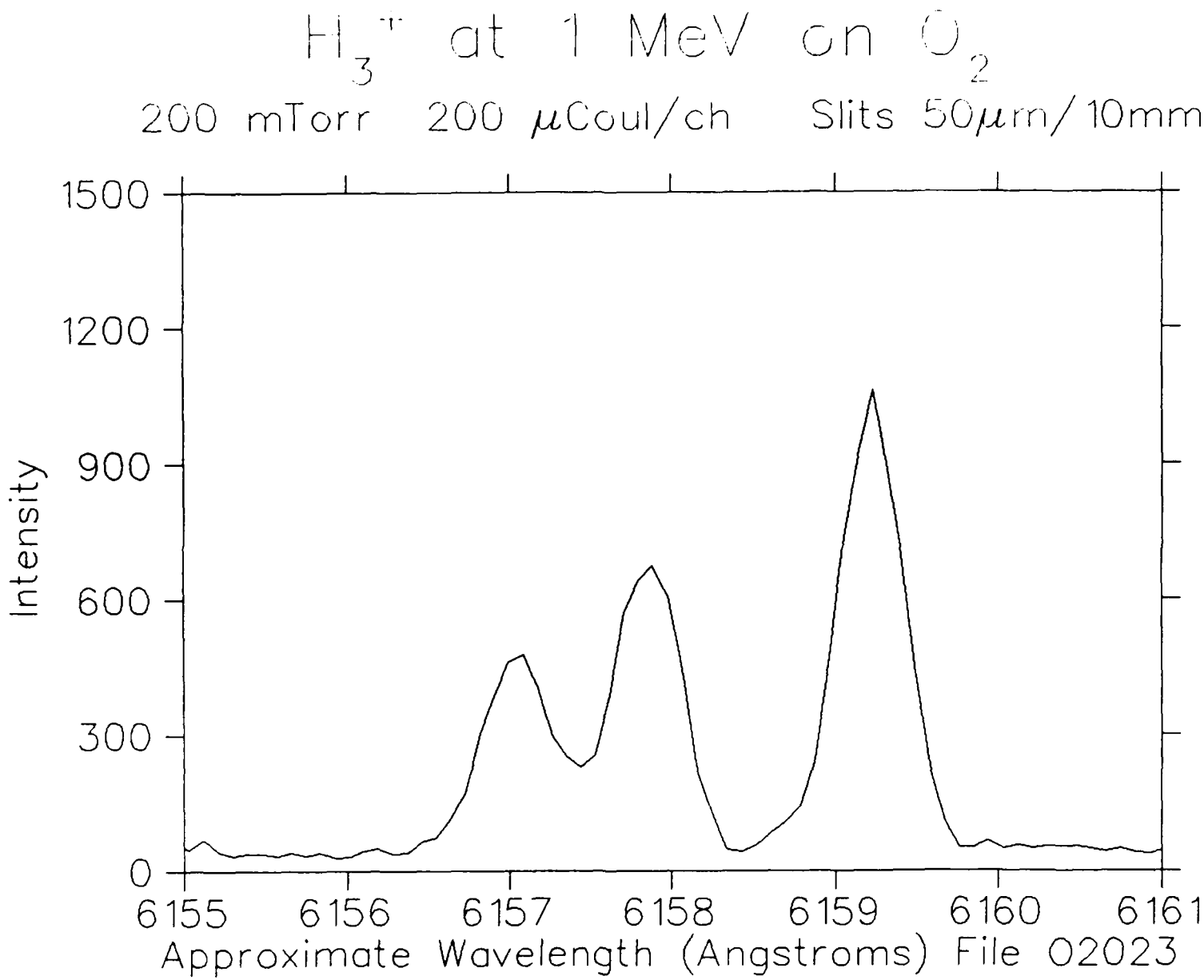
$H_3^+$ at 1 MeV on $O_2$
200 mTorr 200 μCoul/ch Slits 50μm/10mm
Intensity
1500
1200
900
600
300
0
6155
6156
6157
6158
6159
6160
6161
Approximate Wavelength (Angstroms) File 02023

Fig. 67

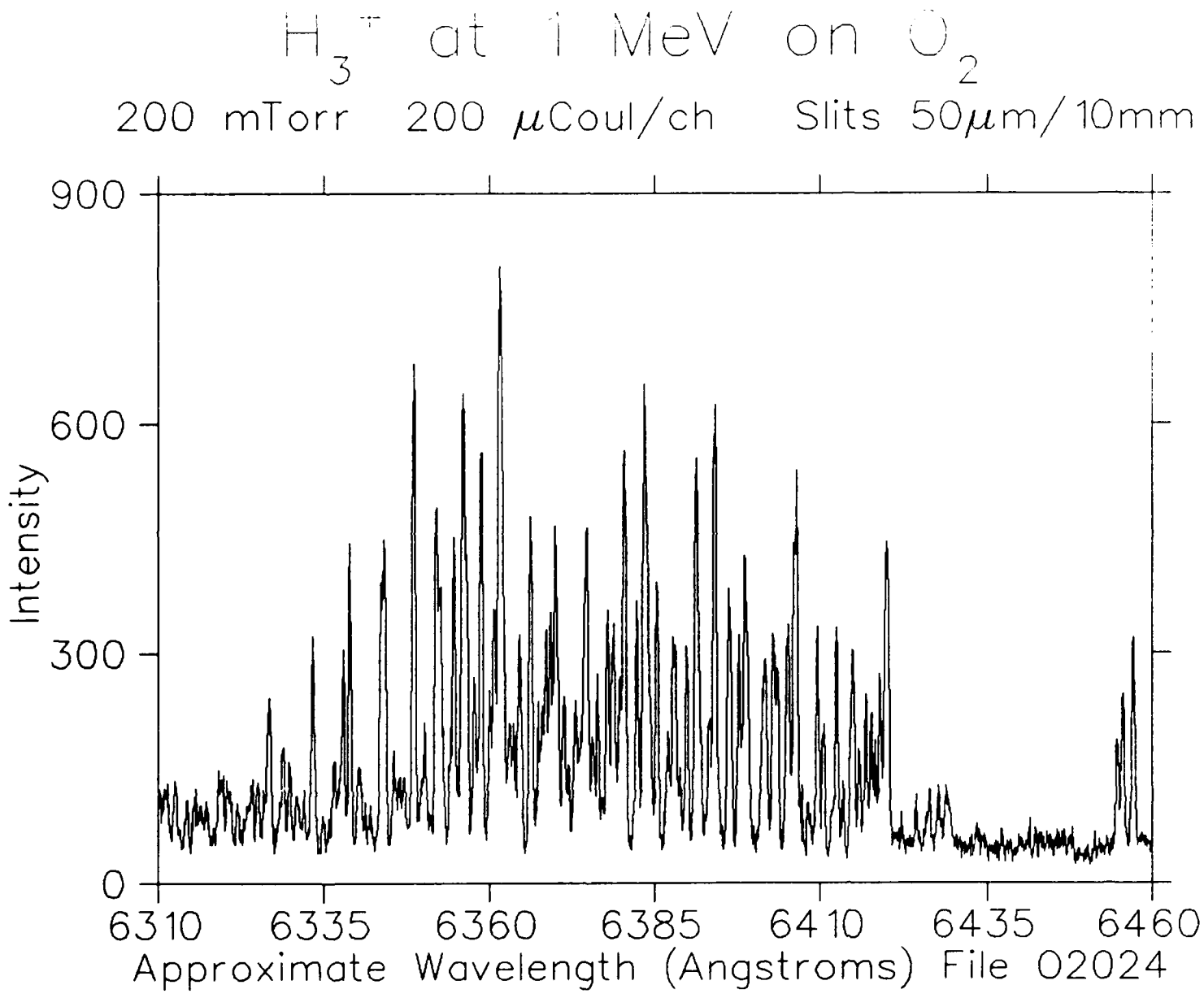
$H_3^+$ at 1 MeV on $O_2$
200 mTorr 200 μCoul/ch Slits 50μm/10mm
900
600
300
0
Intensity
6310
6335
6360
6385
6410
6435
6460
Approximate Wavelength (Angstroms) File 02024

Fig. 68

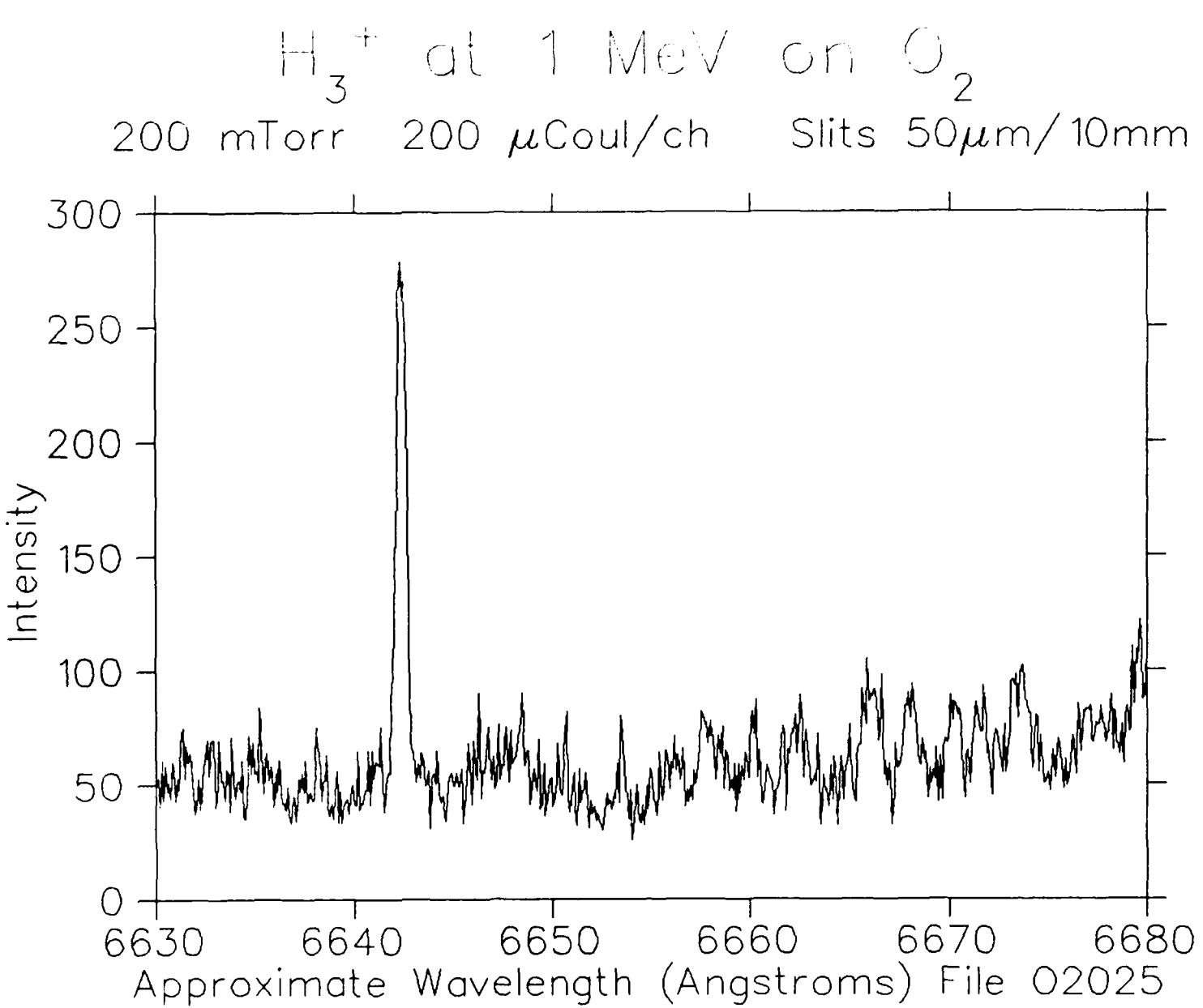
$H_3^+$ at 1 MeV on $O_2$
200 mTorr 200 μCoul/ch Slits 50μm/10mm
Intensity
300
250
200
150
100
50
0
6630
6640
6650
6660
6670
6680
Approximate Wavelength (Angstroms) File 02025

Fig. 69

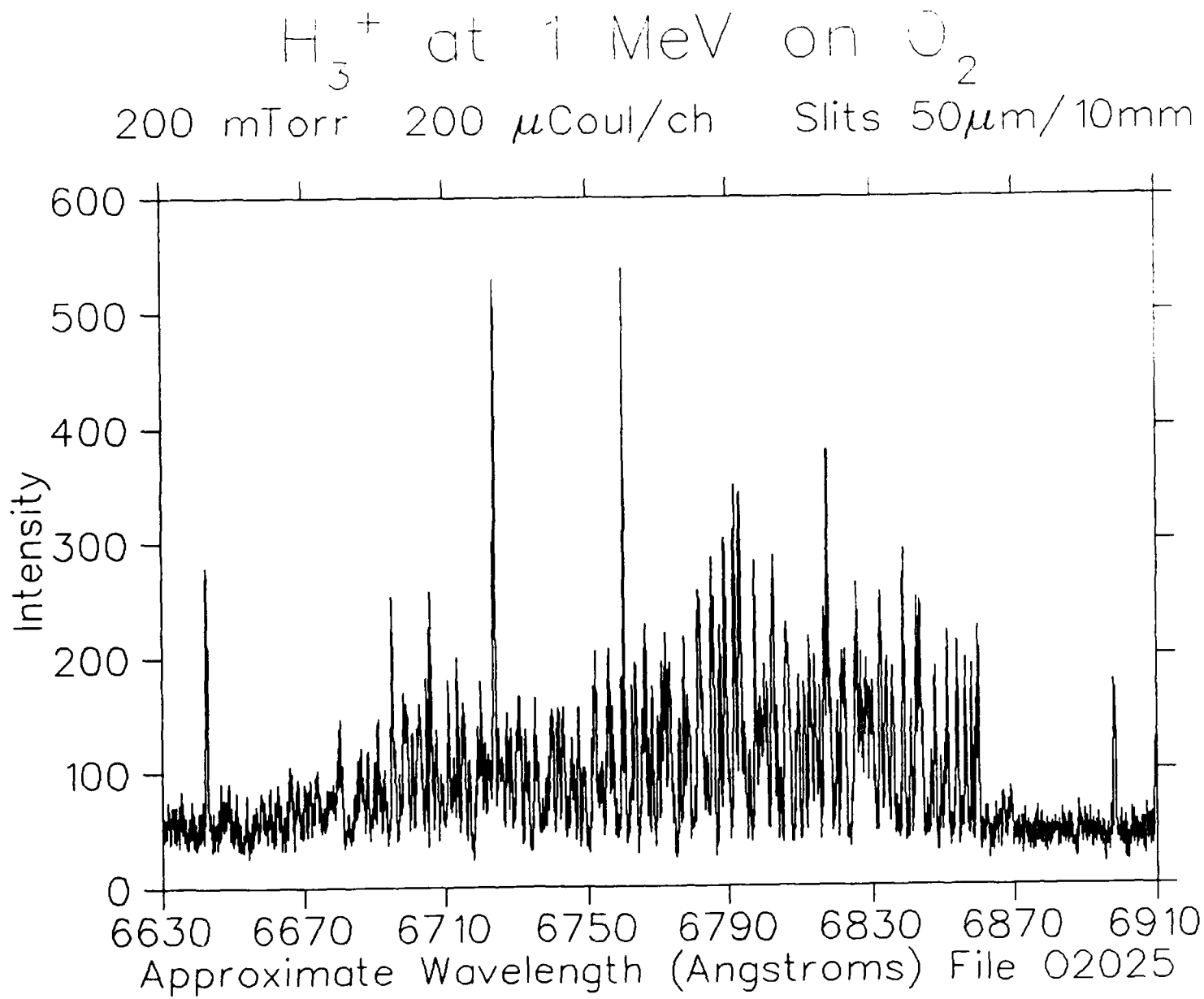
$H_3^+$ at 1 MeV on $O_2$
200 mTorr 200 μCoul/ch Slits 50μm/10mm
Intensity
600
500
400
300
200
100
0
6630 6670 6710 6750 6790 6830 6870 6910
Approximate Wavelength (Angstroms) File 02025

Fig. 70

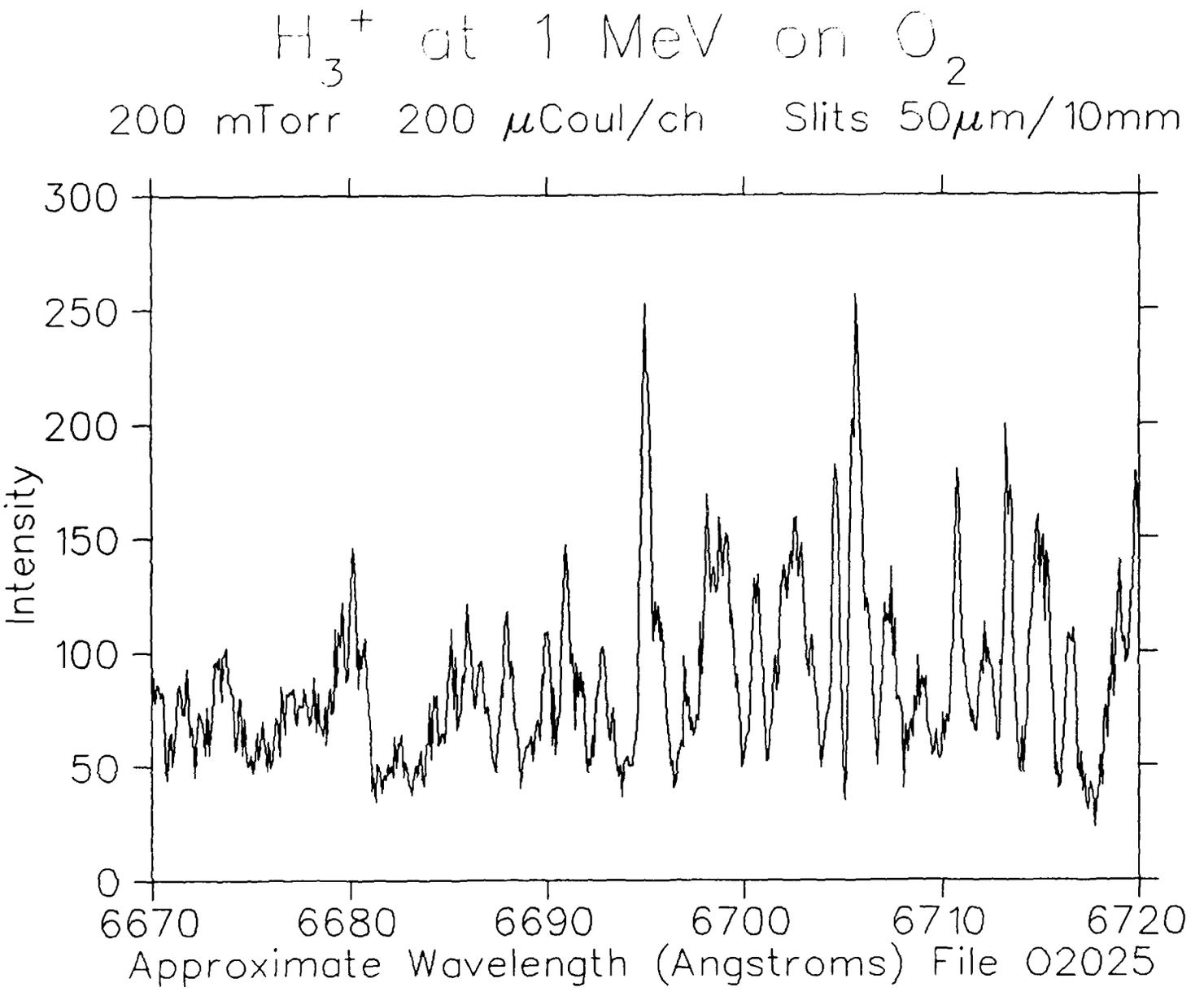
$H_3^+$ at 1 MeV on $O_2$
200 mTorr 200 μCoul/ch Slits 50μm/10mm
Intensity
300
250
200
150
100
50
0
6670
6680
6690
6700
6710
6720
Approximate Wavelength (Angstroms) File 02025

Fig. 71

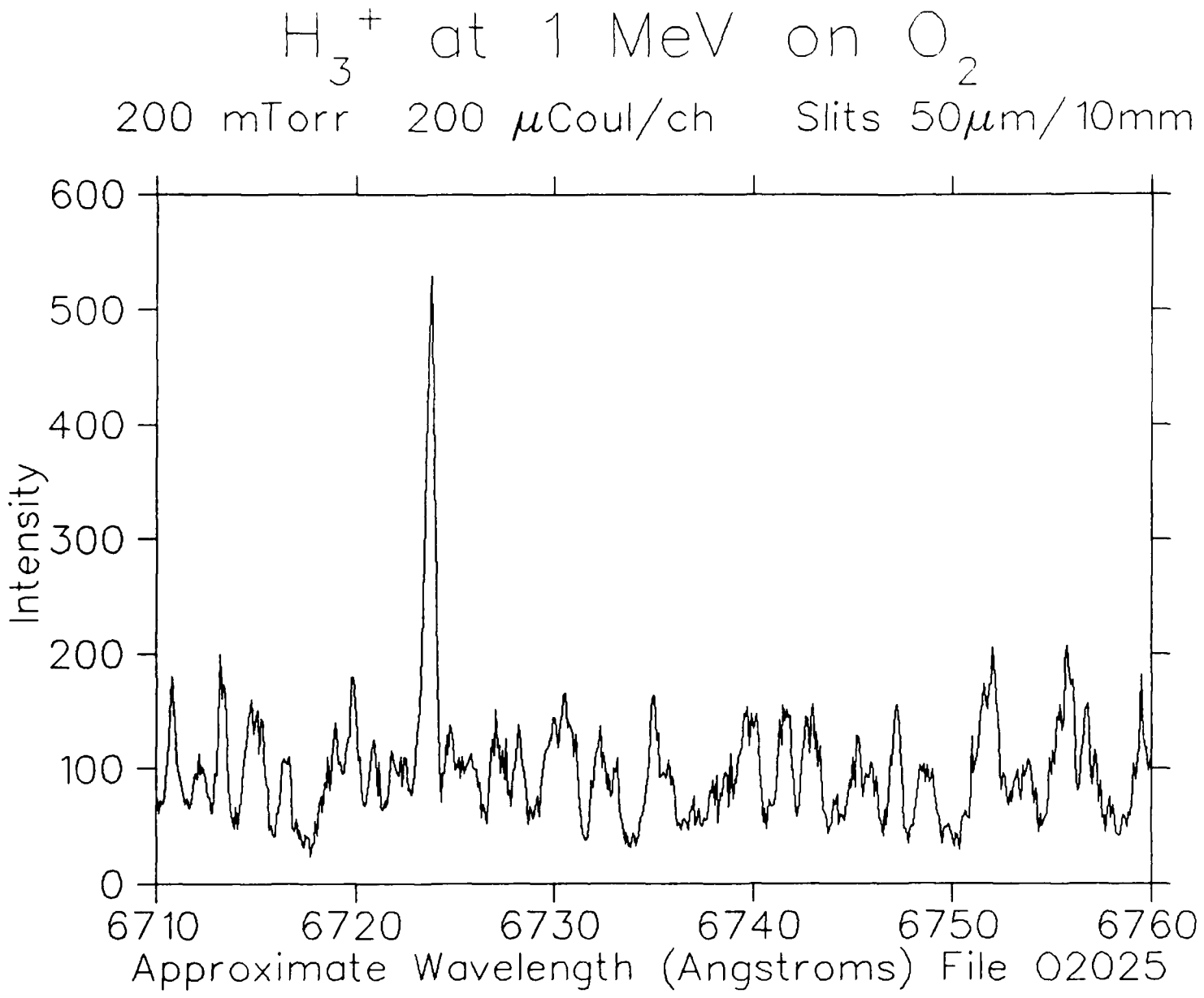
$H_3^+$ at 1 MeV on $O_2$
200 mTorr 200 μCoul/ch Slits 50μm/10mm
600
500
400
300
200
100
0
Intensity
6710
6720
6730
6740
6750
6760
Approximate Wavelength (Angstroms) File 02025

Fig. 72

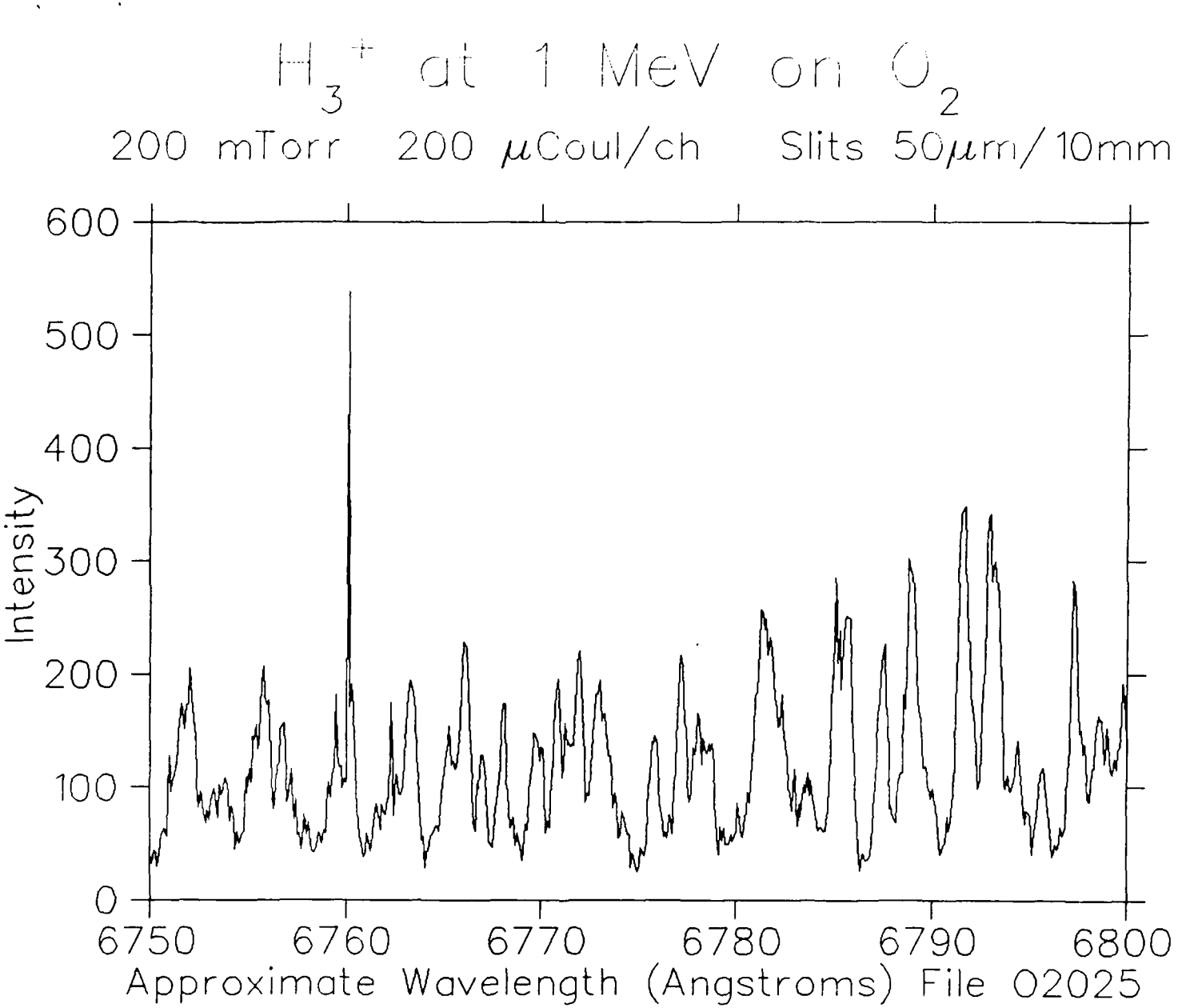
$H_3^+$ at 1 MeV on $O_2$
200 mTorr 200 μCoul/ch Slits 50μm/10mm
Intensity
600
500
400
300
200
100
0
6750
6760
6770
6780
6790
6800
Approximate Wavelength (Angstroms) File 02025

Fig. 73

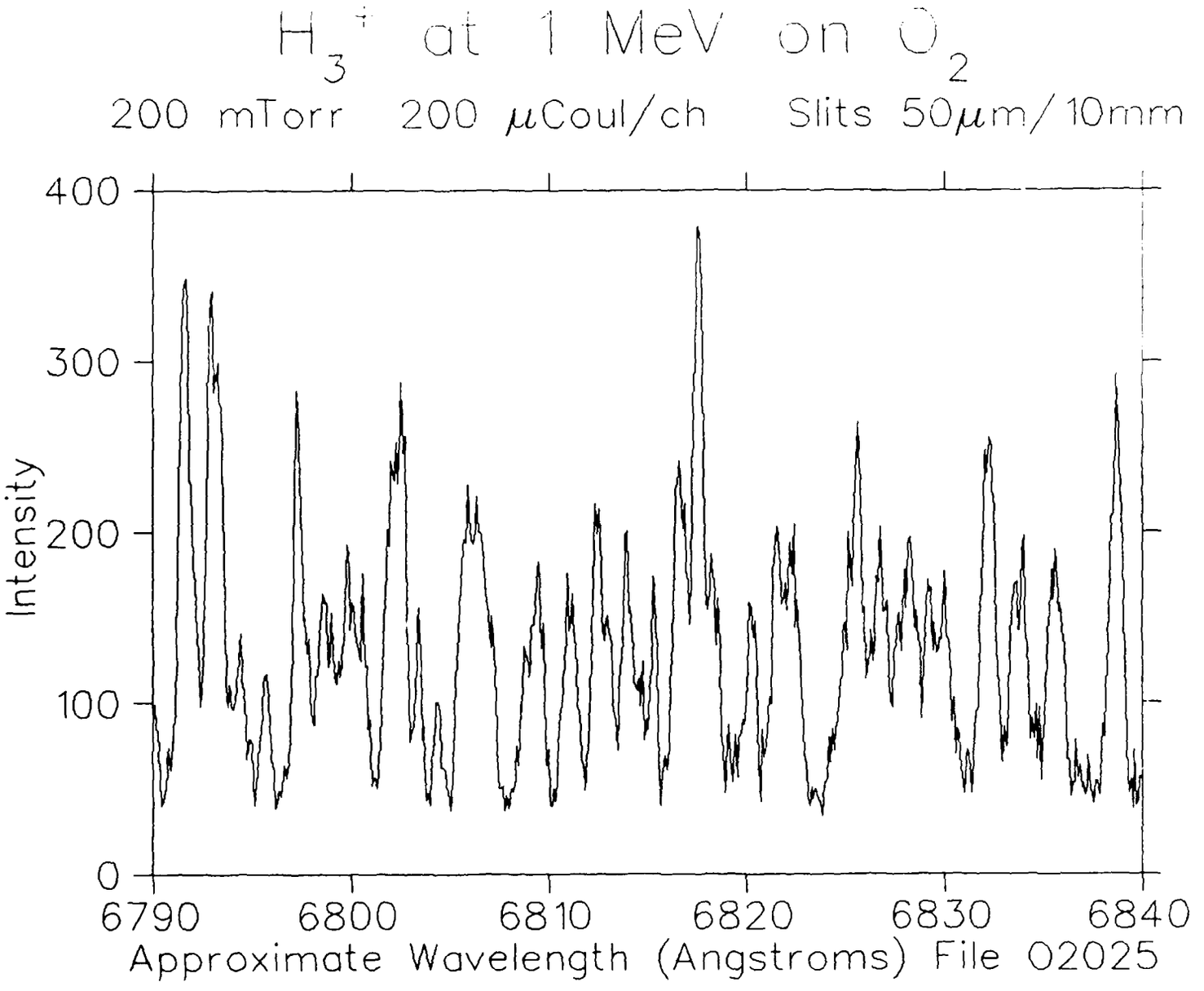
$H_3^+$ at 1 MeV on $O_2$
200 mTorr 200 μCoul/ch Slits 50μm/10mm
Intensity
400
300
200
100
0
6790
6800
6810
6820
6830
6840
Approximate Wavelength (Angstroms) File 02025

Fig. 74

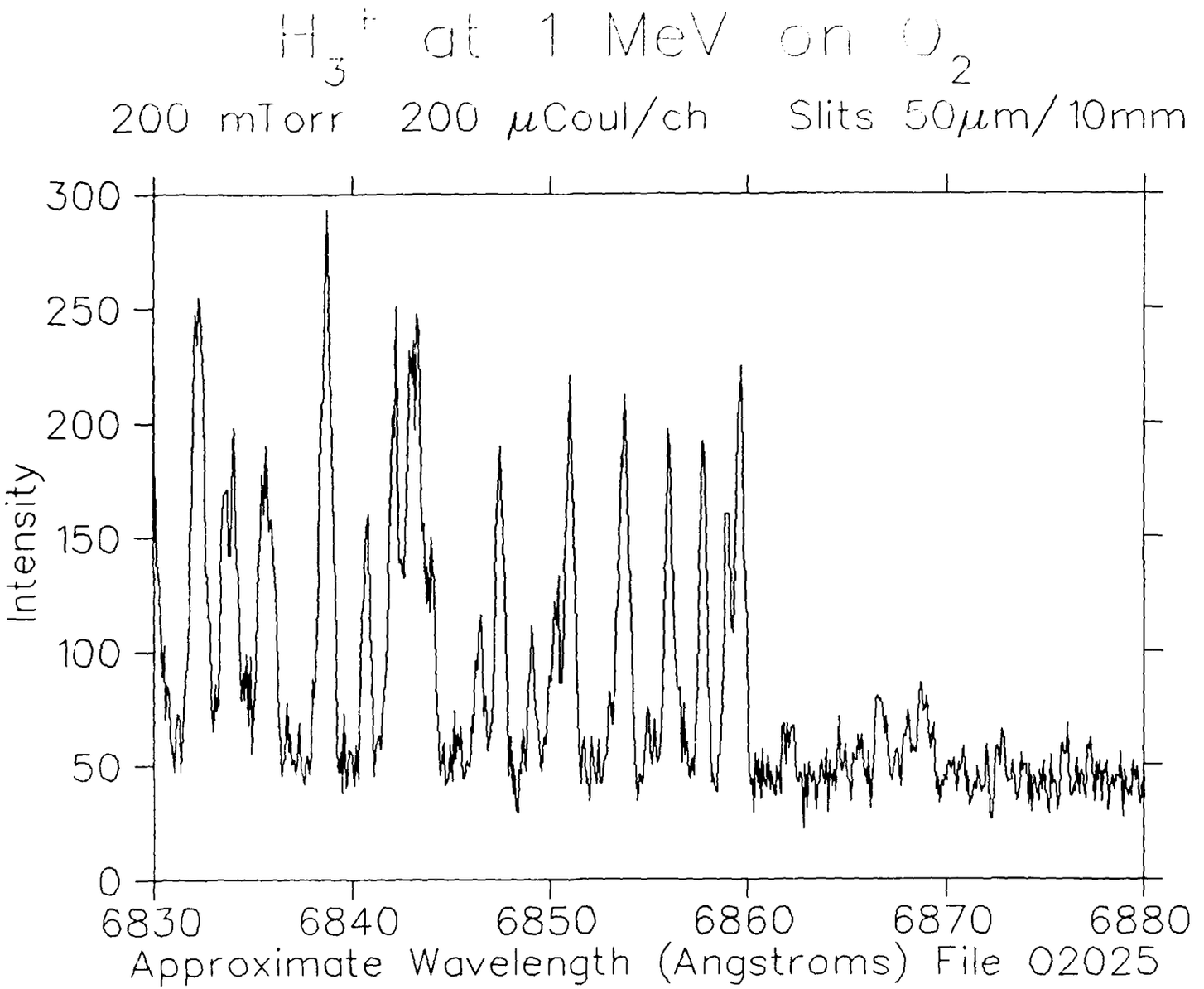
$H_3^+$ at 1 MeV on $O_2$
200 mTorr 200 μCoul/ch Slits 50μm/10mm
Intensity
300
250
200
150
100
50
0
6830
6840
6850
6860
6870
6880
Approximate Wavelength (Angstroms) File 02025

Fig. 75

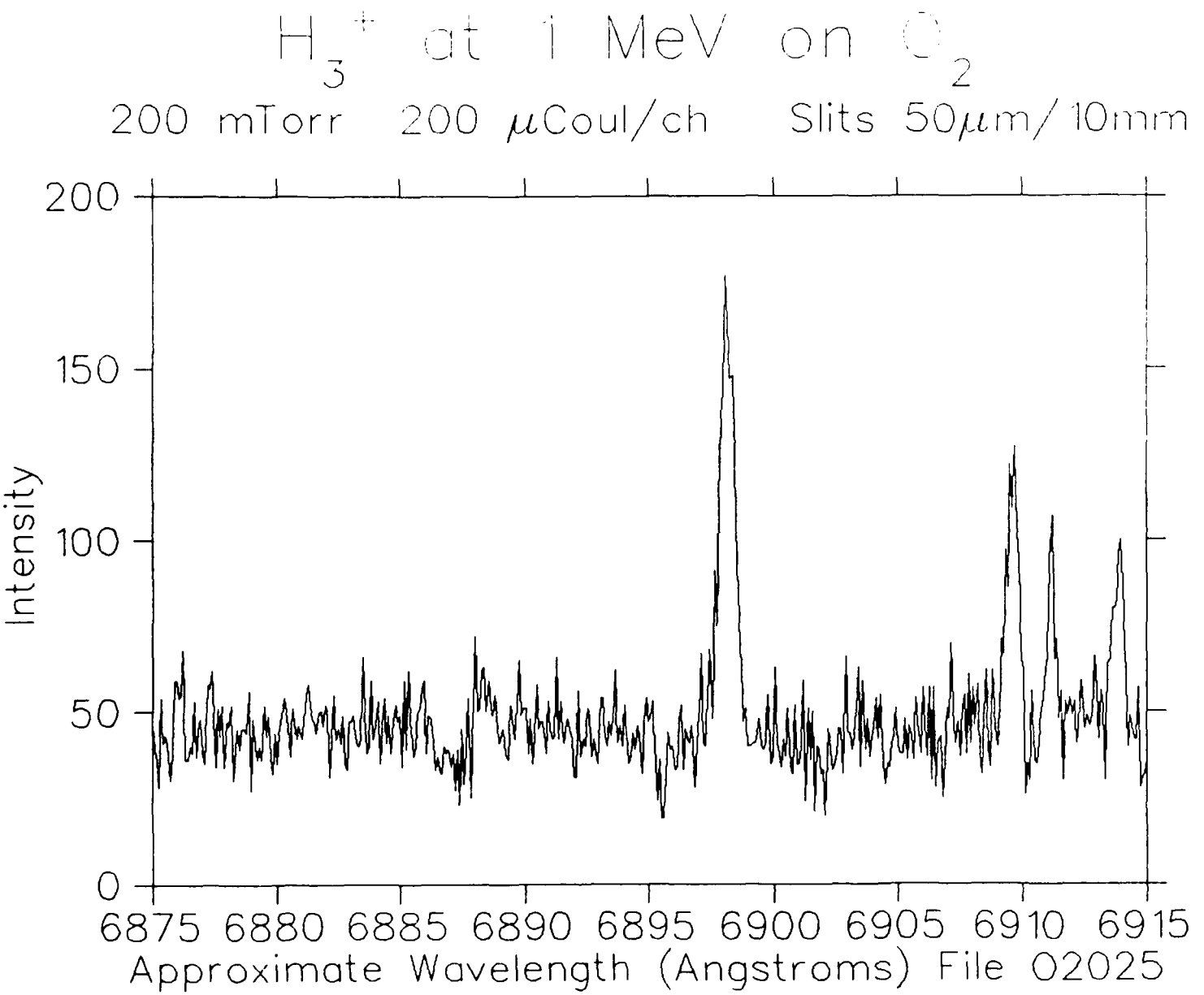
$H_3^+$ at 1 MeV on $O_2$
200 mTorr 200 μCoul/ch Slits 50μm/10mm
Intensity
200
150
100
50
0
6875 6880 6885 6890 6895 6900 6905 6910 6915
Approximate Wavelength (Angstroms) File 02025

Fig. 76

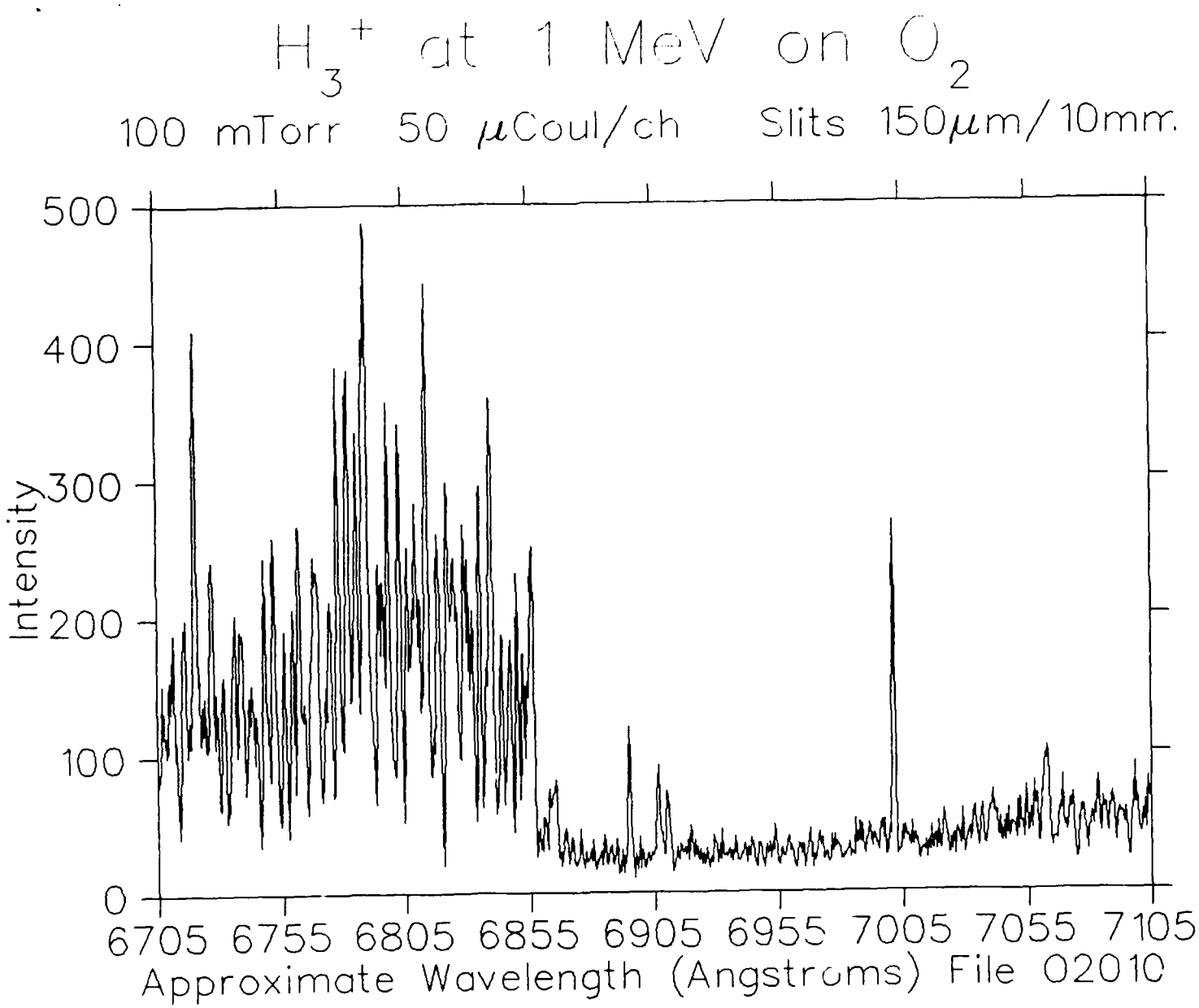
$H_3^+$ at 1 MeV on $O_2$
100 mTorr 50 μCoul/ch Slits 150μm/10mm.
Intensity
500
400
300
200
100
0
6705 6755 6805 6855 6905 6955 7005 7055 7105
Approximate Wavelength (Angstroms) File 02010

Fig. 77

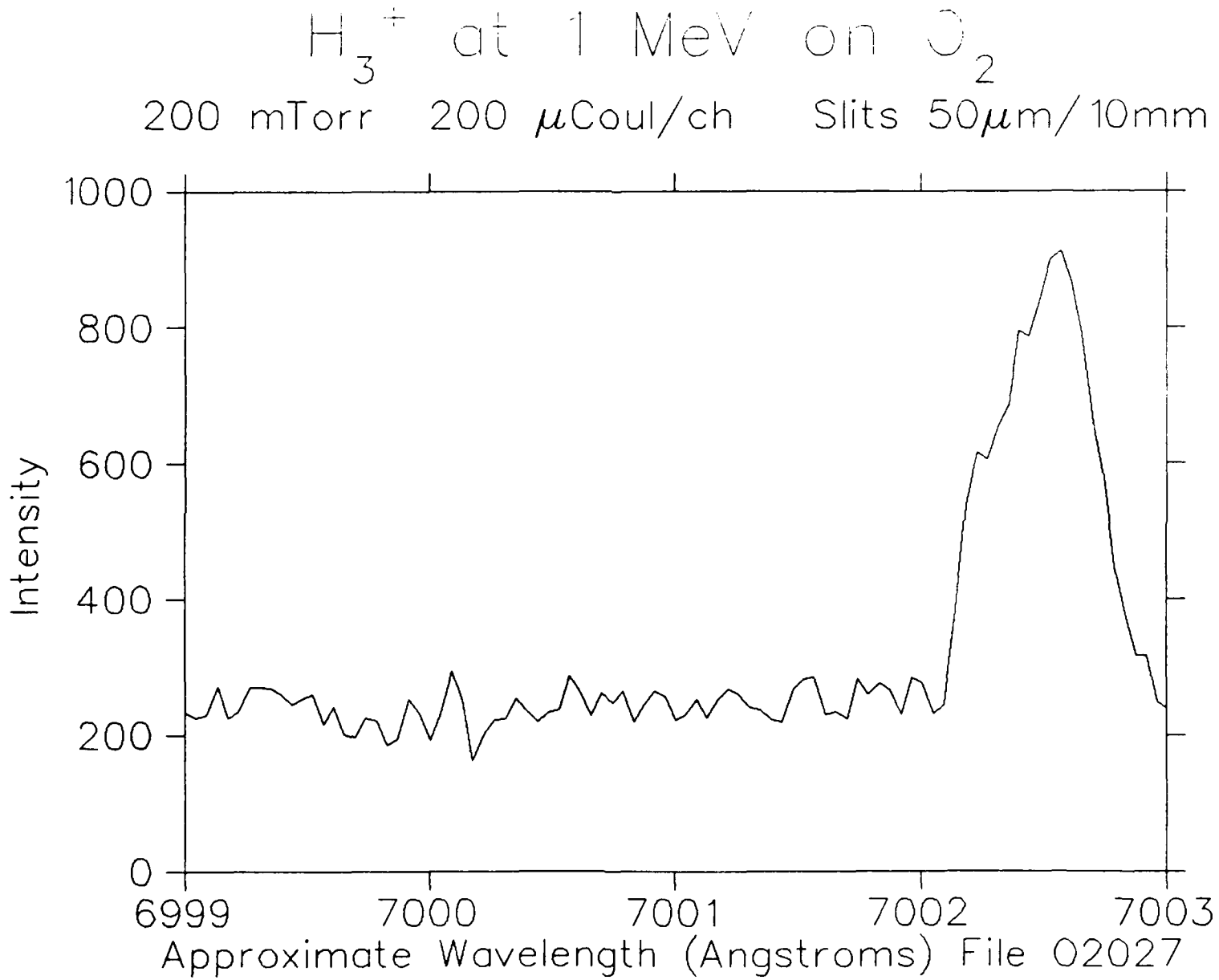
$H_3^+$ at 1 MeV on $O_2$
200 mTorr 200 μCoul/ch Slits 50μm/10mm
1000
800
600
400
200
0
Intensity
6999
7000
7001
7002
7003
Approximate Wavelength (Angstroms) File 02027

Fig. 78

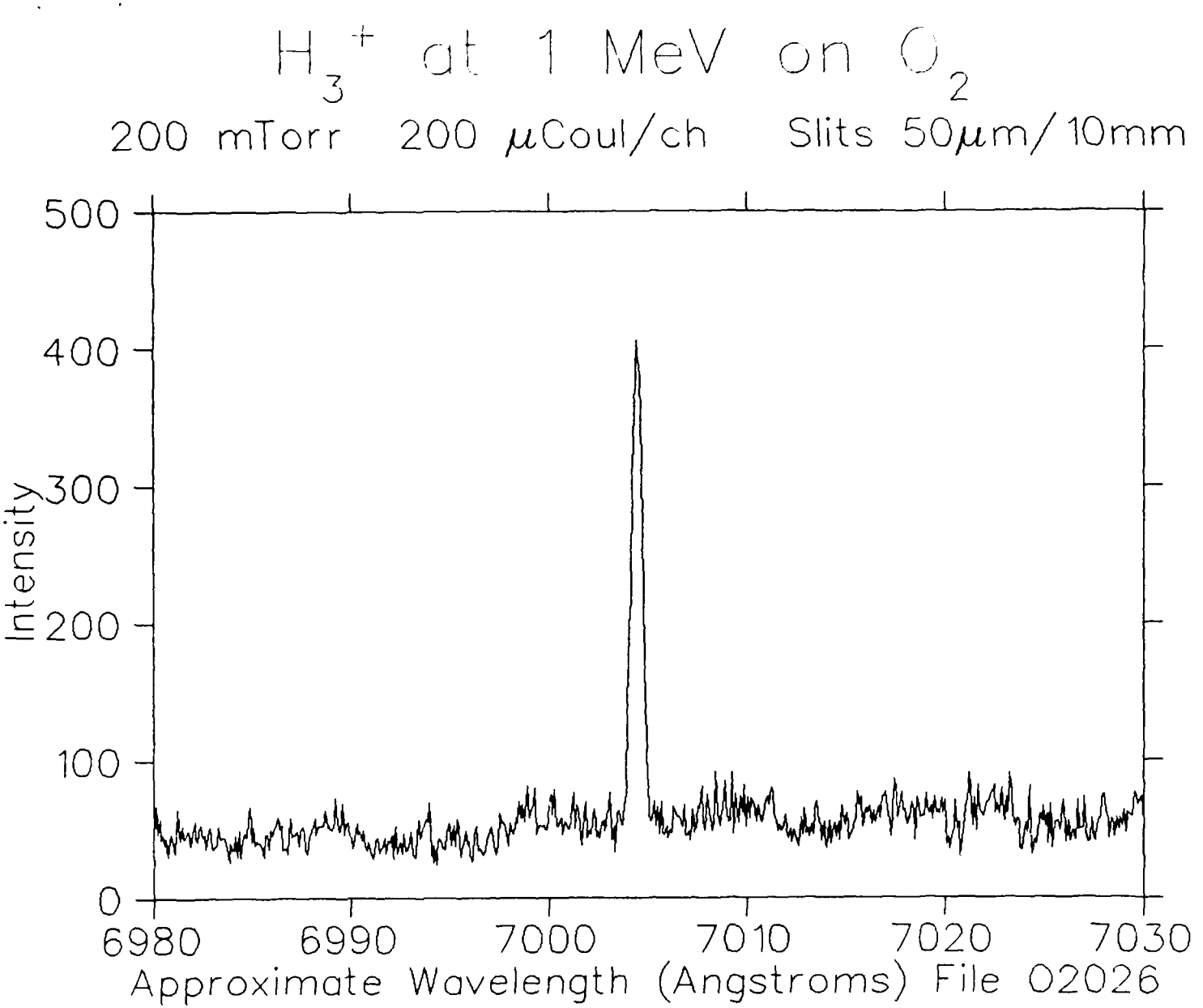
$H_3^+$ at 1 MeV on $O_2$
200 mTorr 200 μCoul/ch Slits 50μm/10mm
Intensity
500
400
300
200
100
0
6980
6990
7000
7010
7020
7030
Approximate Wavelength (Angstroms) File 02026

Fig. 79

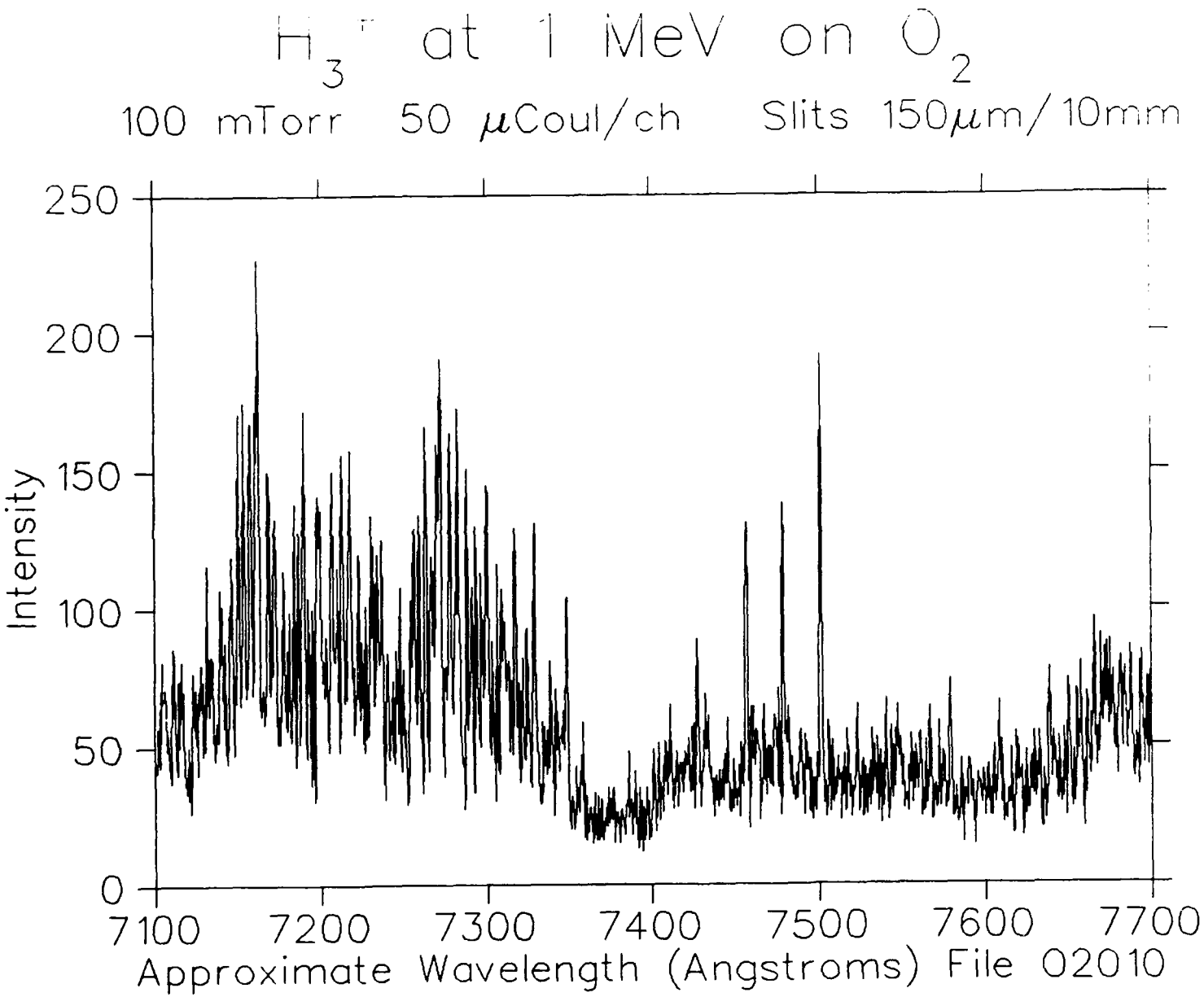
$H_3^+$ at 1 MeV on $O_2$
100 mTorr 50 μCoul/ch Slits 150μm/10mm
Intensity
250
200
150
100
50
0
7100
7200
7300
7400
7500
7600
7700
Approximate Wavelength (Angstroms) File 02010

Fig. 80

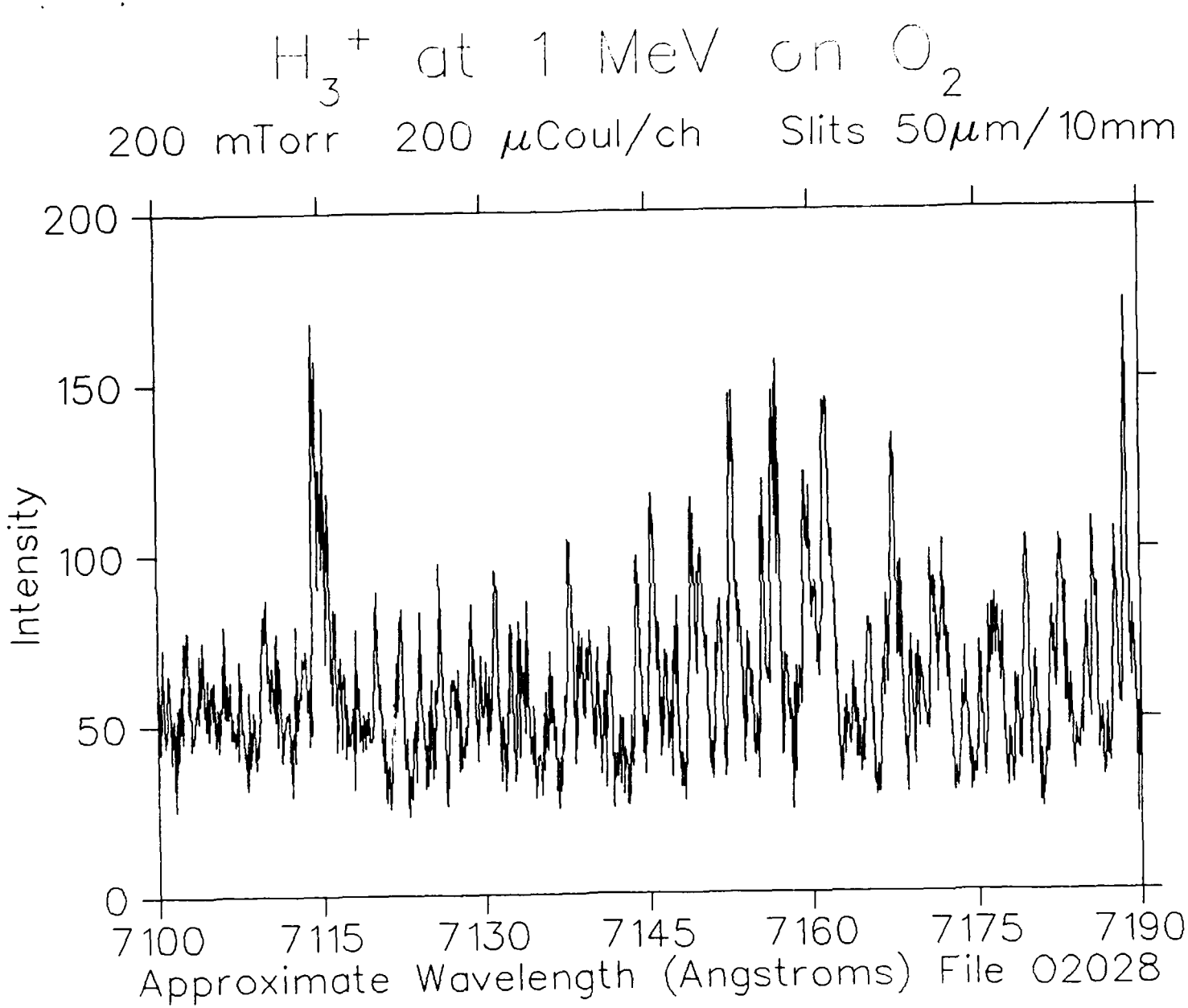
$H_3^+$ at 1 MeV on $O_2$
200 mTorr 200 μCoul/ch Slits 50μm/10mm
Intensity
200
150
100
50
0
7100
7115
7130
7145
7160
7175
7190
Approximate Wavelength (Angstroms) File 02028

Fig. 81

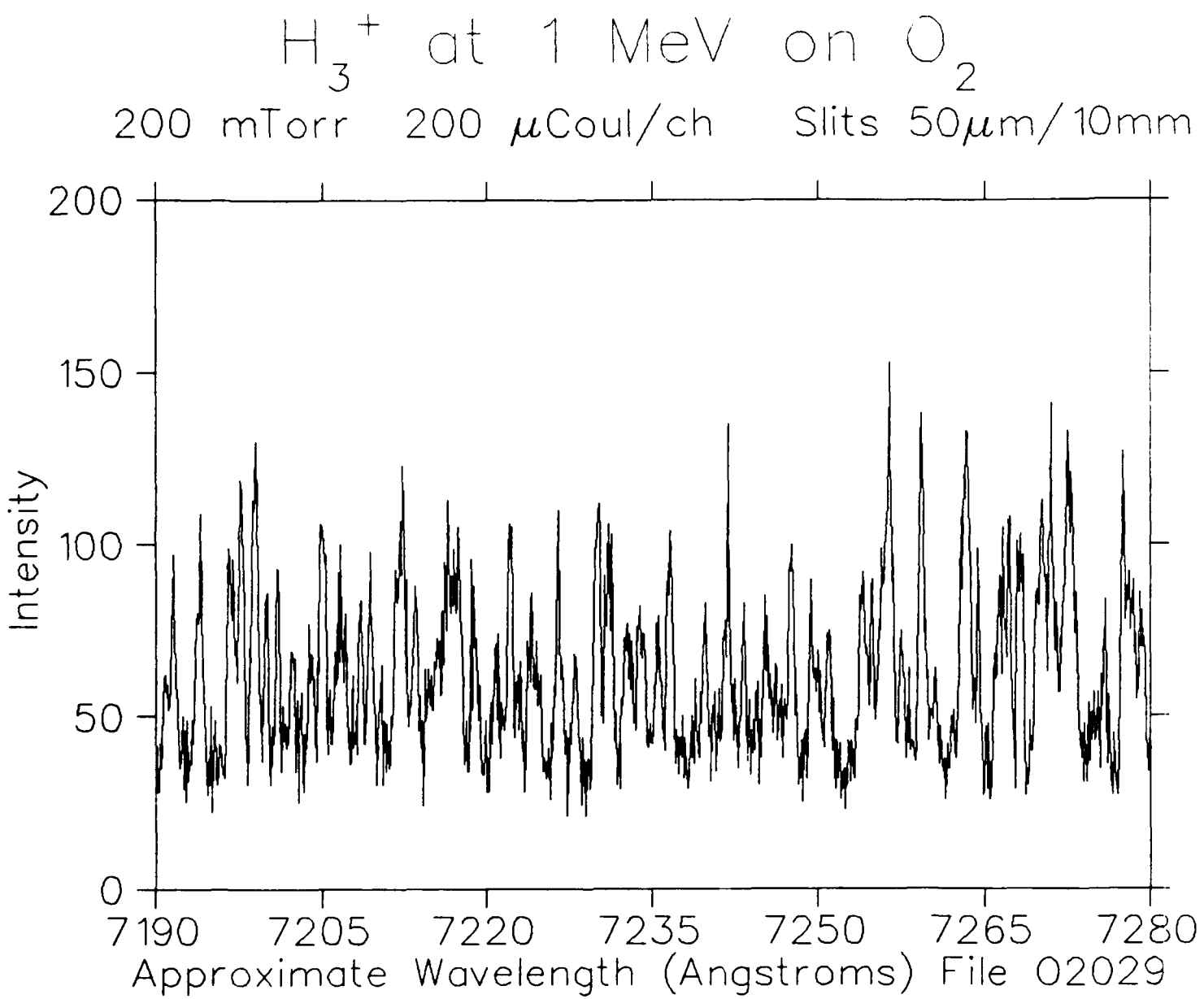
$H_3^+$ at 1 MeV on $O_2$
200 mTorr 200 μCoul/ch Slits 50μm/10mm
Intensity
200
150
100
50
0
7190
7205
7220
7235
7250
7265
7280
Approximate Wavelength (Angstroms) File 02029

Fig. 82

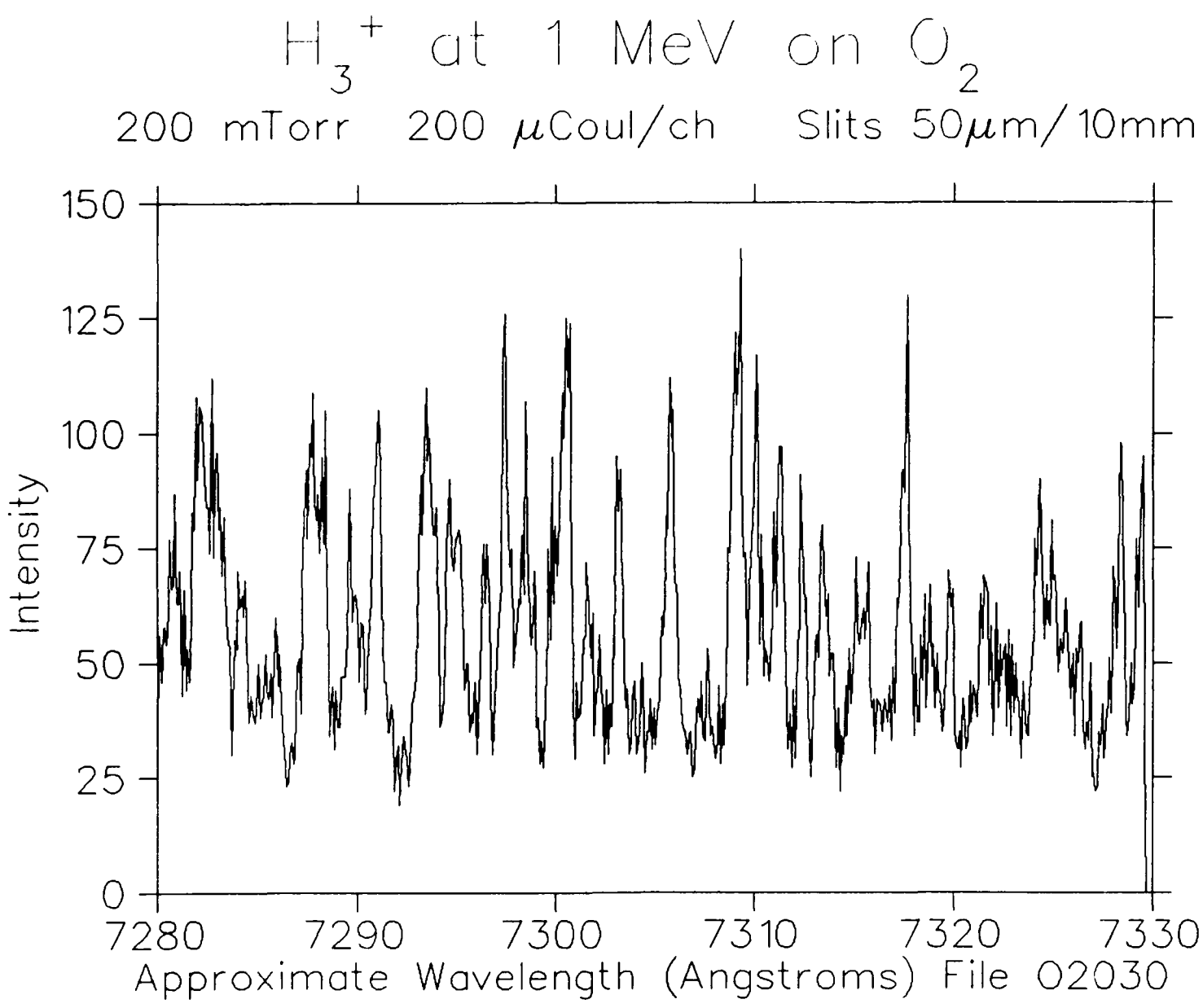
$H_3^+$ at 1 MeV on $O_2$
200 mTorr 200 μCoul/ch Slits 50μm/10mm
Intensity
150
125
100
75
50
25
0
7280
7290
7300
7310
7320
7330
Approximate Wavelength (Angstroms) File 02030

Fig. 83

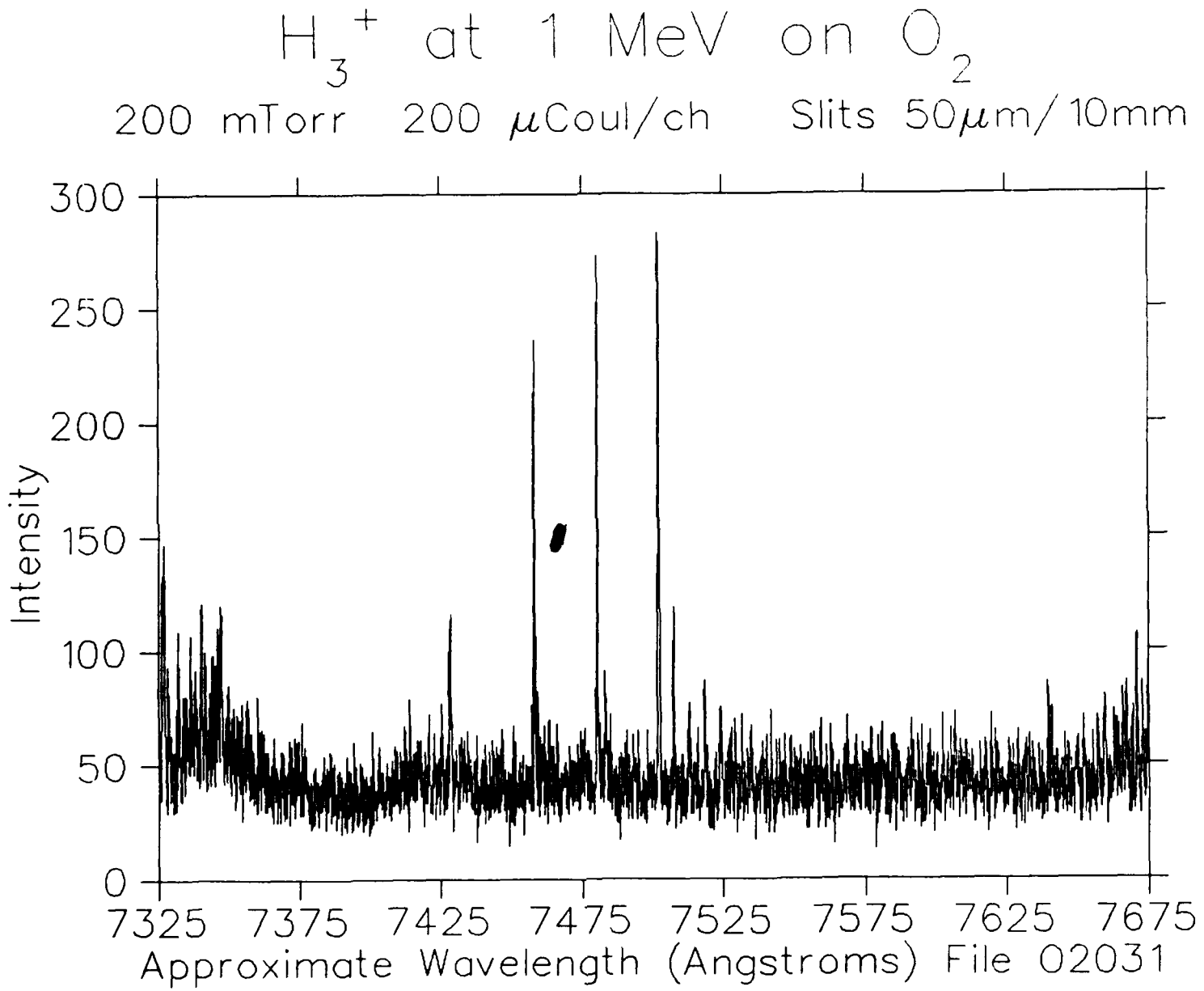
$H_3^+$ at 1 MeV on $O_2$
200 mTorr 200 μCoul/ch Slits 50μm/10mm
Intensity
300
250
200
150
100
50
0
7325 7375 7425 7475 7525 7575 7625 7675
Approximate Wavelength (Angstroms) File 02031

Fig. 84

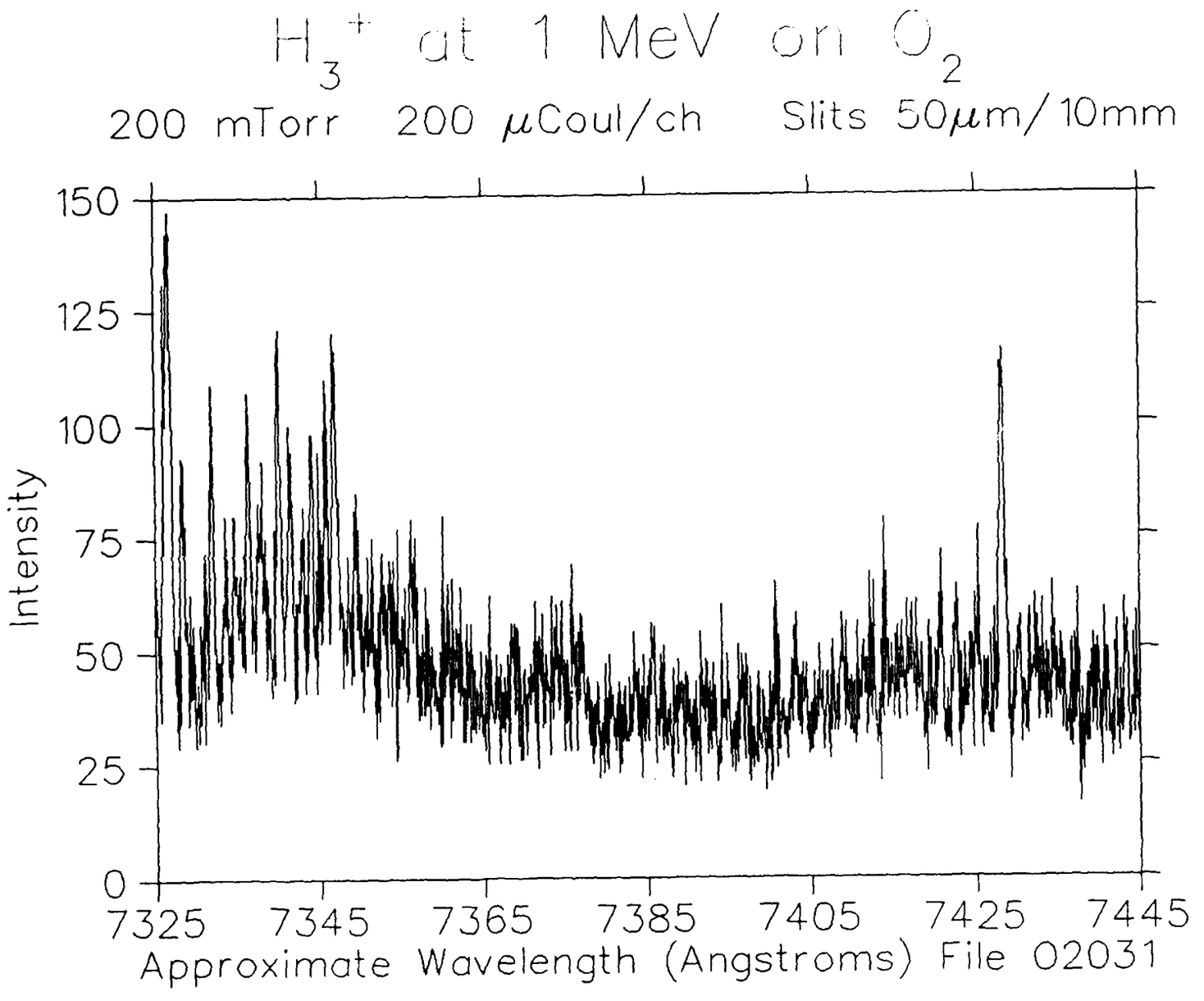
$H_3^+$ at 1 MeV on $O_2$
200 mTorr 200 μCoul/ch Slits 50μm/10mm
Intensity
150
125
100
75
50
25
0
7325
7345
7365
7385
7405
7425
7445
Approximate Wavelength (Angstroms) File 02031

Fig. 85

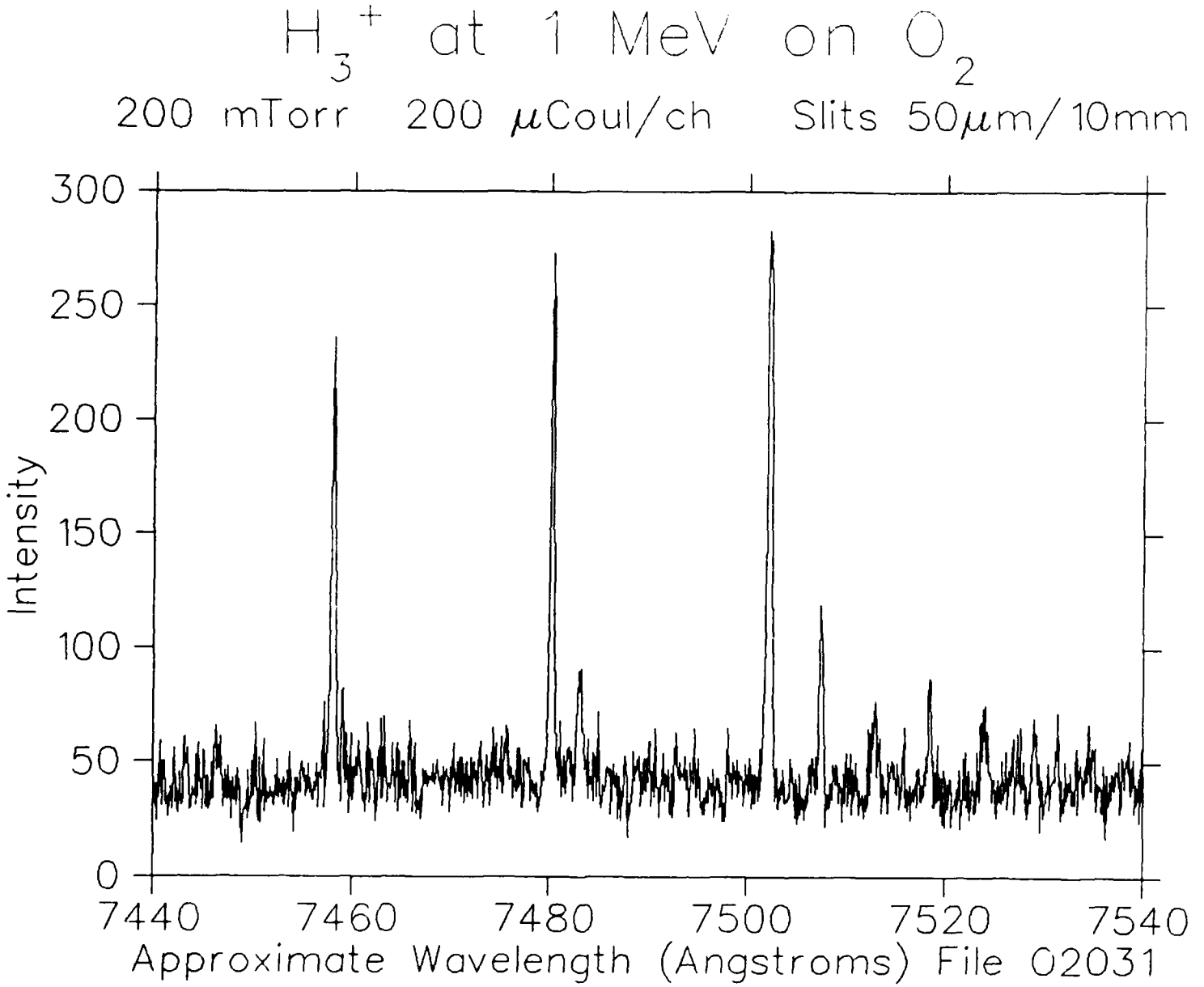
$H_3^+$ at 1 MeV on $O_2$
200 mTorr 200 μCoul/ch Slits 50μm/10mm
Intensity
300
250
200
150
100
50
0
7440
7460
7480
7500
7520
7540
Approximate Wavelength (Angstroms) File 02031

Fig. 86

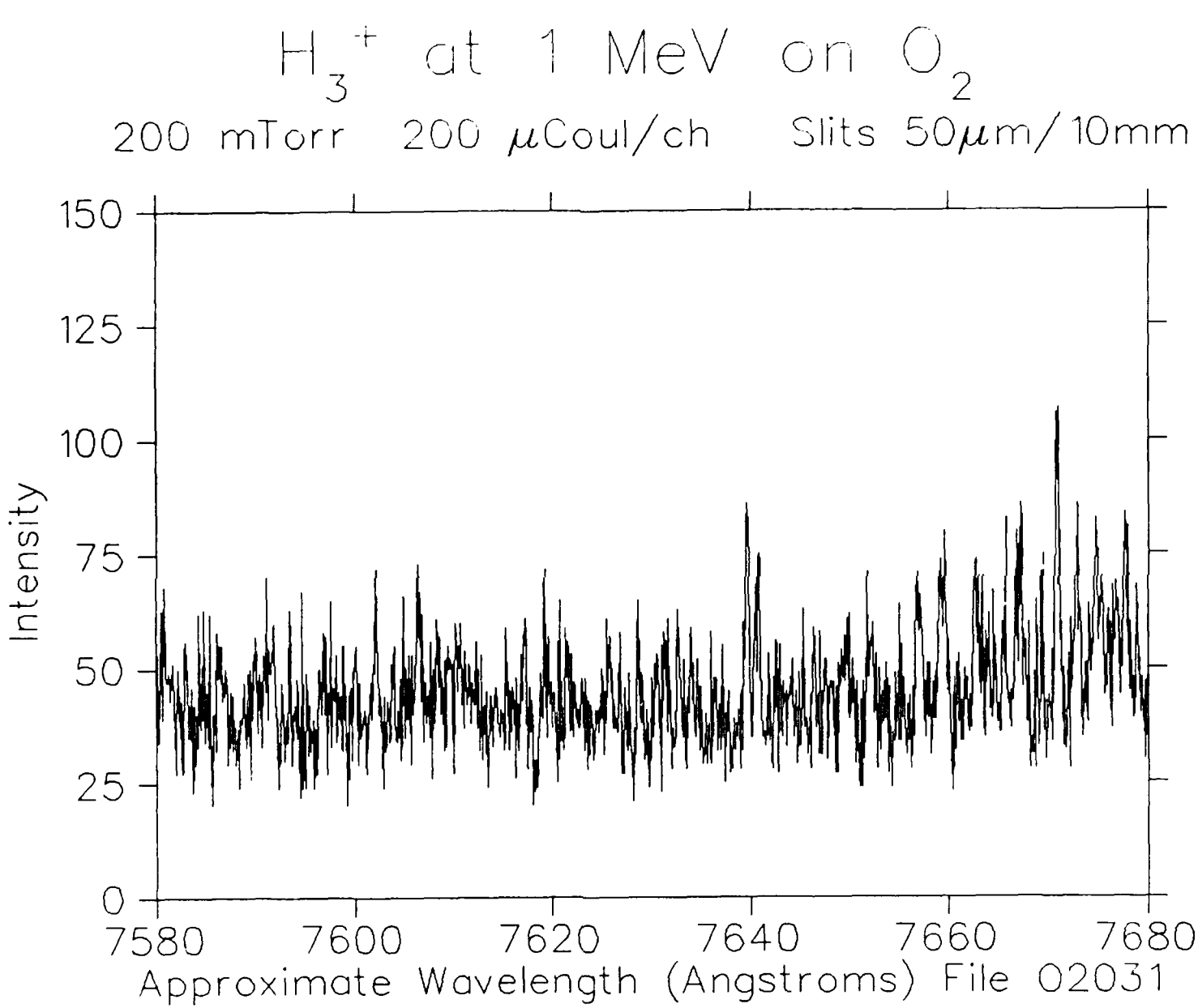
$H_3^+$ at 1 MeV on $O_2$
200 mTorr 200 μCoul/ch Slits 50μm/10mm
Intensity
150
125
100
75
50
25
0
7580
7600
7620
7640
7660
7680
Approximate Wavelength (Angstroms) File 02031

Fig. 87

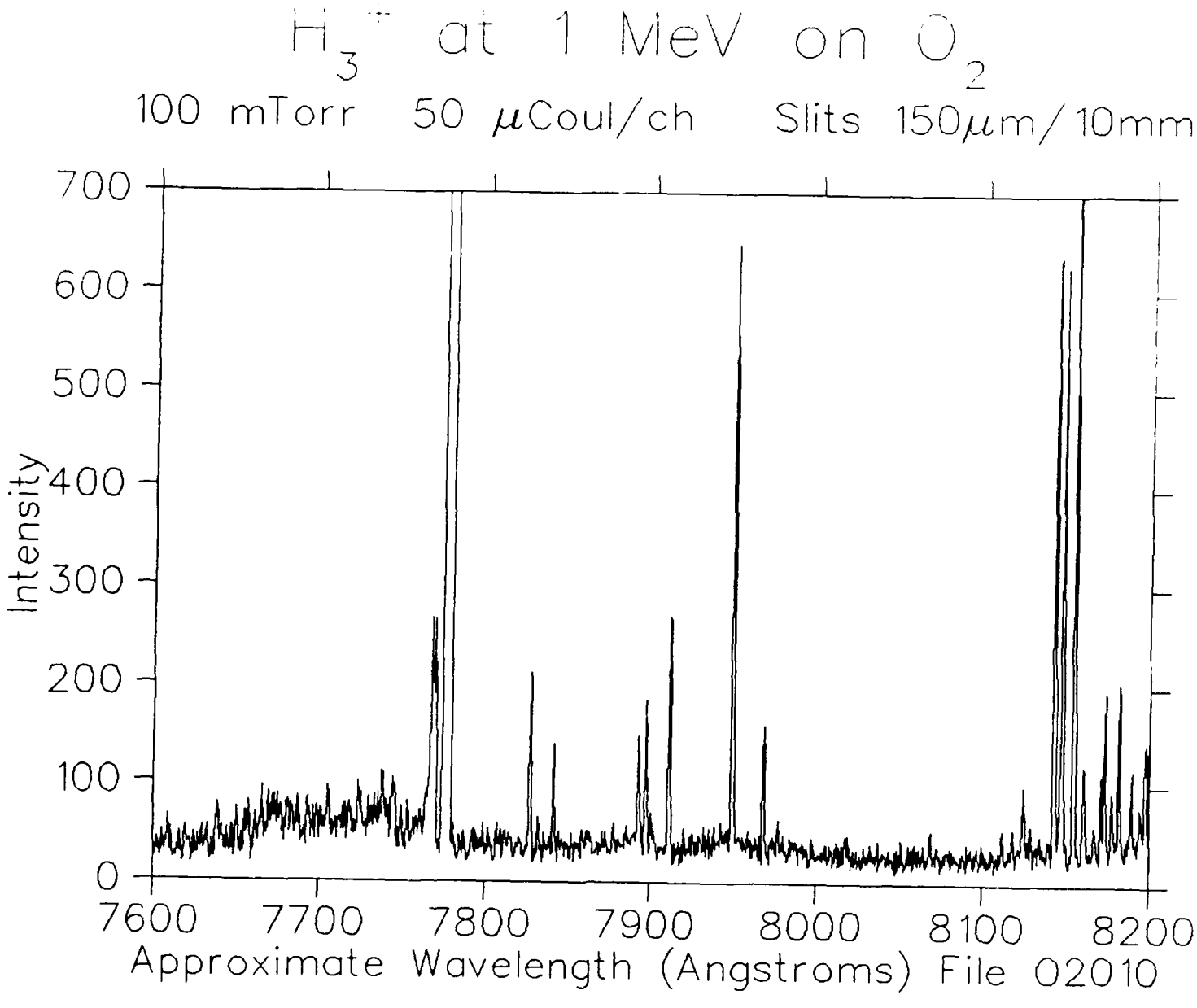
$H_3^+$ at 1 MeV on $O_2$
100 mTorr 50 μCoul/ch Slits 150μm/10mm
Intensity
700
600
500
400
300
200
100
0
7600
7700
7800
7900
8000
8100
8200
Approximate Wavelength (Angstroms) File 02010

Fig. 88

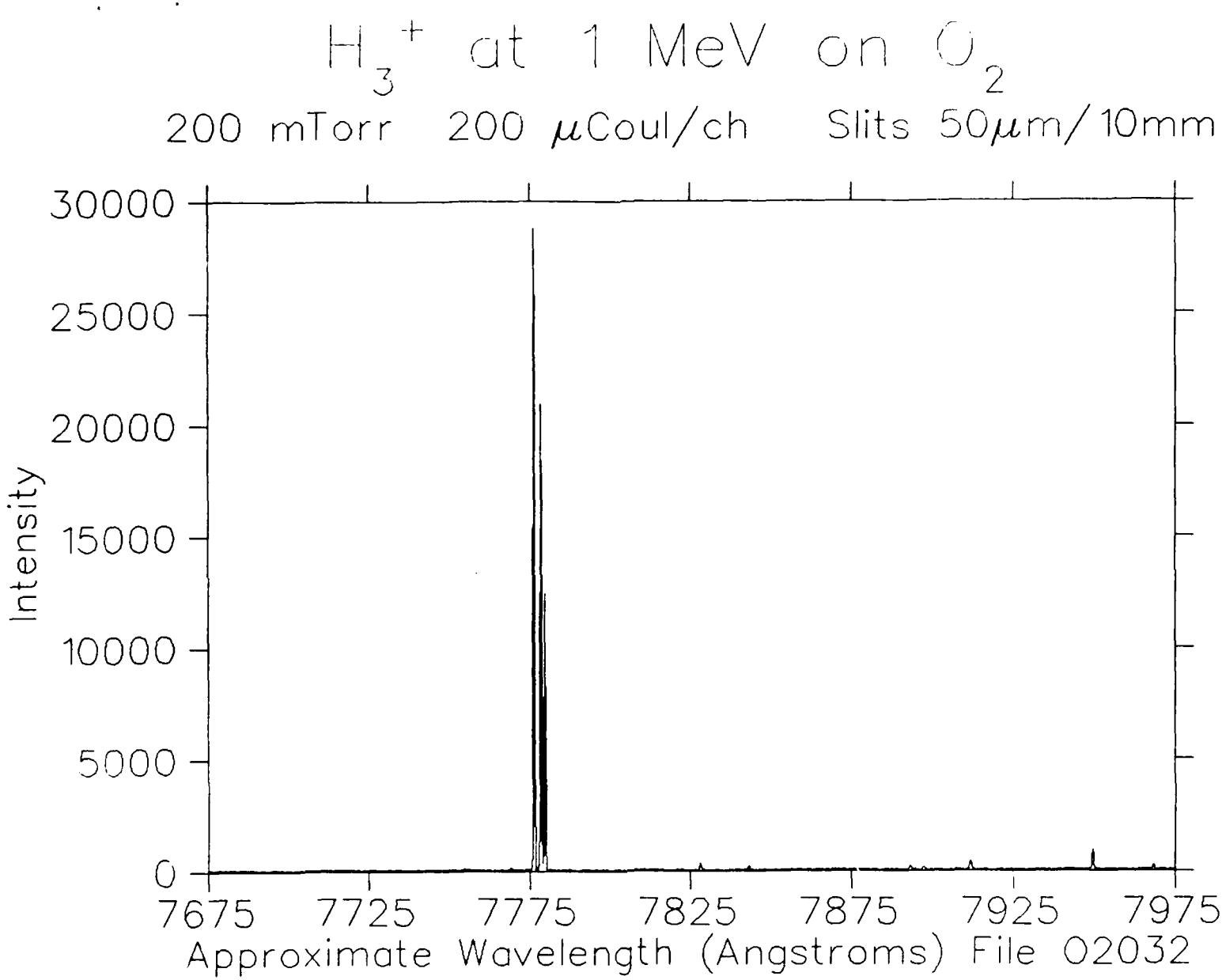
$H_3^+$ at 1 MeV on $O_2$
200 mTorr 200 μCoul/ch Slits 50μm/10mm
30000
25000
20000
15000
10000
5000
0
Intensity
7675
7725
7775
7825
7875
7925
7975
Approximate Wavelength (Angstroms) File 02032

Fig. 89

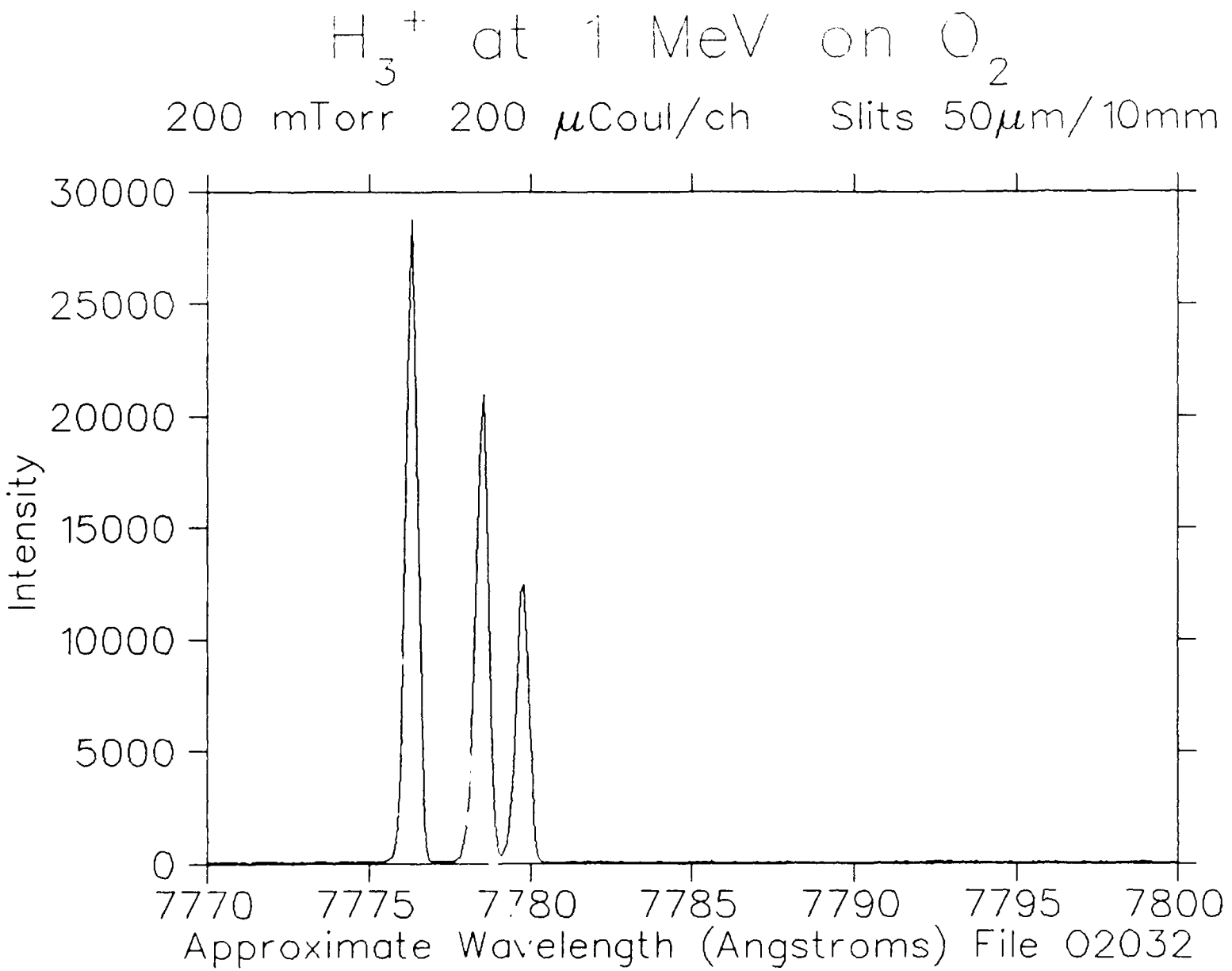
$H_3^+$ at 1 MeV on $O_2$
200 mTorr 200 μCoul/ch Slits 50μm/10mm
30000
25000
20000
15000
10000
5000
0
Intensity
7770
7775
7780
7785
7790
7795
7800
Approximate Wavelength (Angstroms) File 02032

Fig. 90

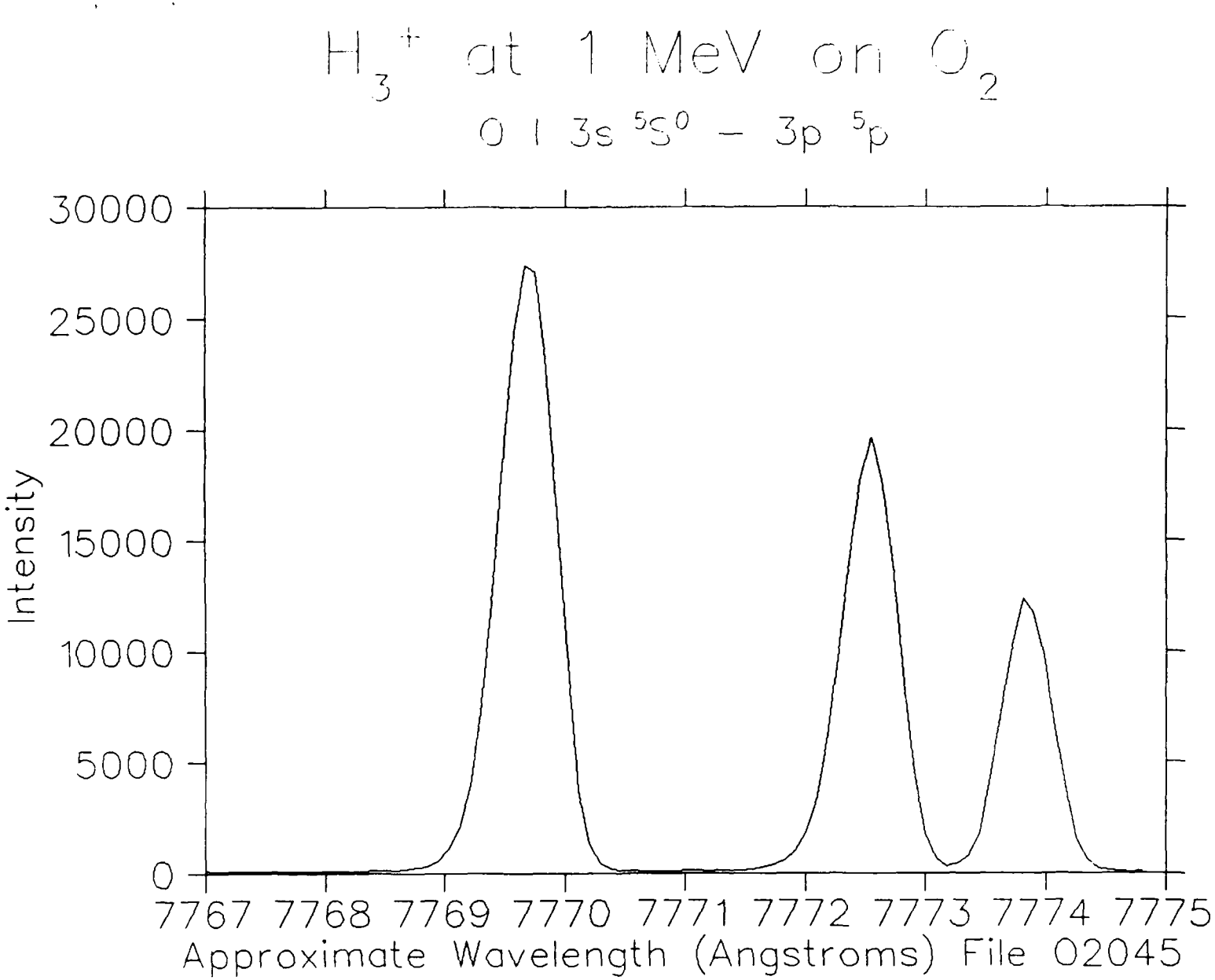
$H_3^+$ at 1 MeV on $O_2$
O I 3s $^5S^0$ – 3p $^5p$
30000
25000
20000
15000
10000
5000
0
Intensity
7767 7768 7769 7770 7771 7772 7773 7774 7775
Approximate Wavelength (Angstroms) File 02045

Fig. 91

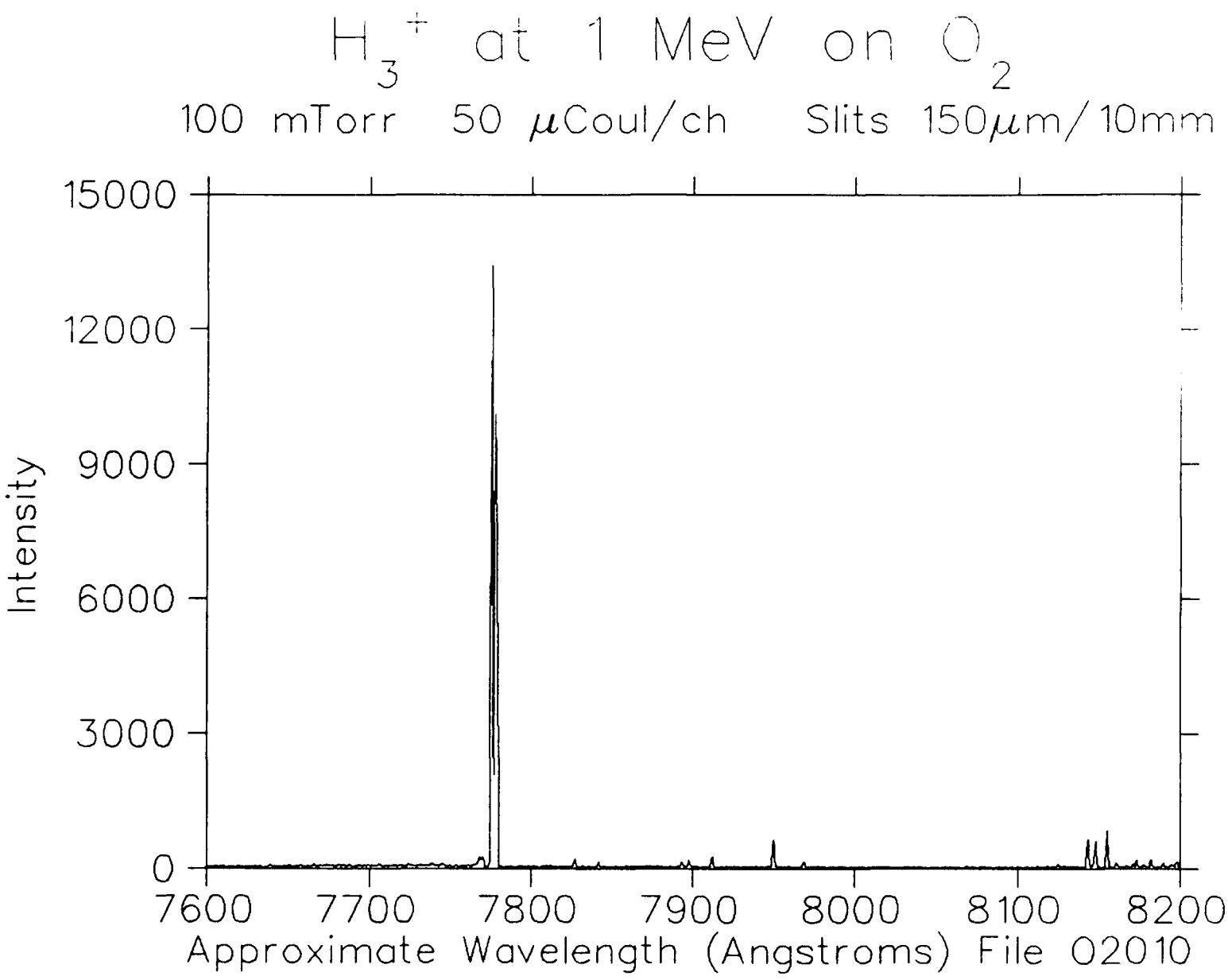
$H_3^+$ at 1 MeV on $O_2$
100 mTorr 50 μCoul/ch Slits 150μm/10mm
15000
12000
9000
6000
3000
0
Intensity
7600
7700
7800
7900
8000
8100
8200
Approximate Wavelength (Angstroms) File 02010

Fig. 92

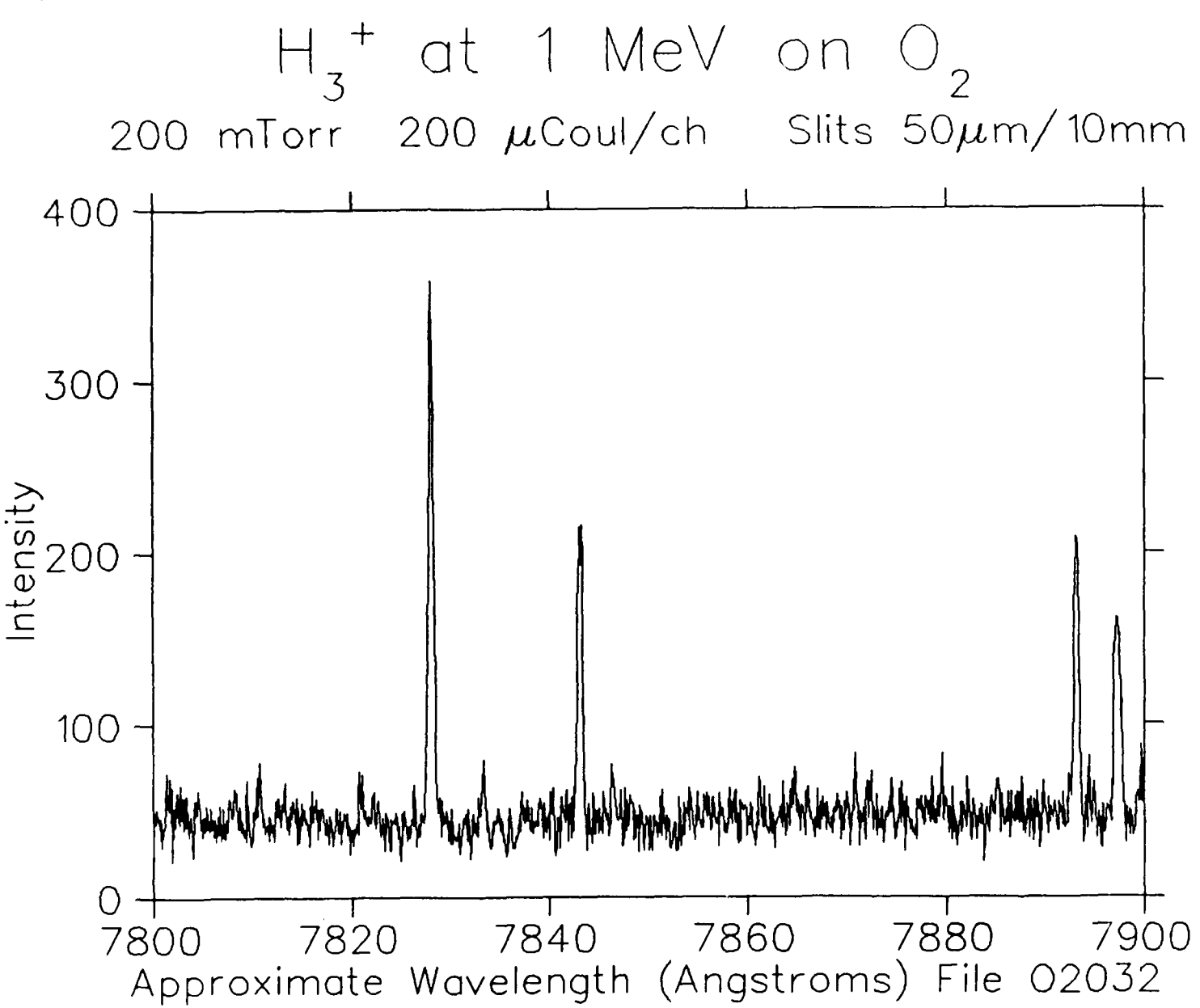
$H_3^+$ at 1 MeV on $O_2$
200 mTorr 200 μCoul/ch Slits 50μm/10mm
Intensity
400
300
200
100
0
7800
7820
7840
7860
7880
7900
Approximate Wavelength (Angstroms) File 02032

Fig. 93

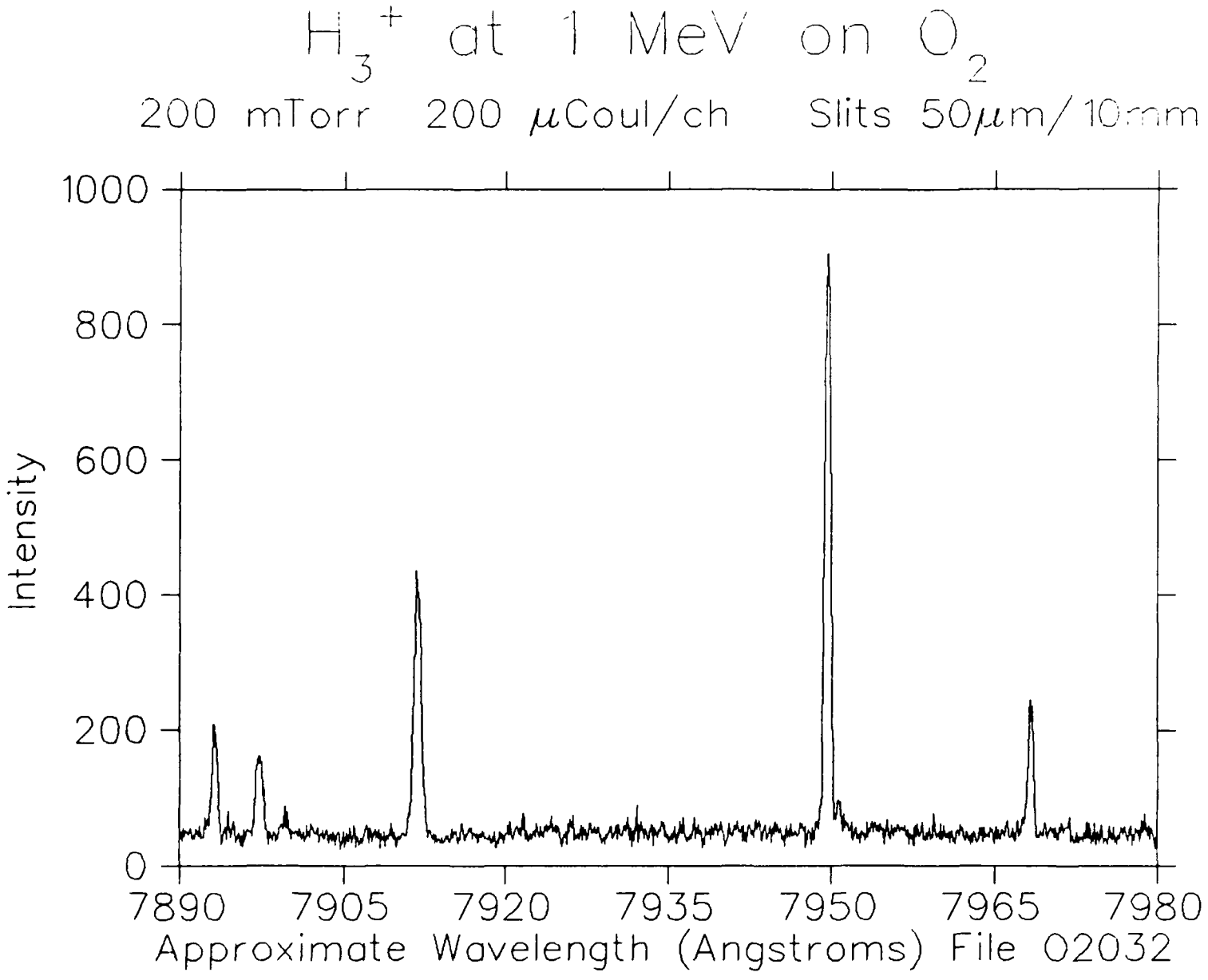
$H_3^+$ at 1 MeV on $O_2$
200 mTorr 200 μCoul/ch Slits 50μm/10mm
Intensity
1000
800
600
400
200
0
7890
7905
7920
7935
7950
7965
7980
Approximate Wavelength (Angstroms) File 02032

Fig. 94

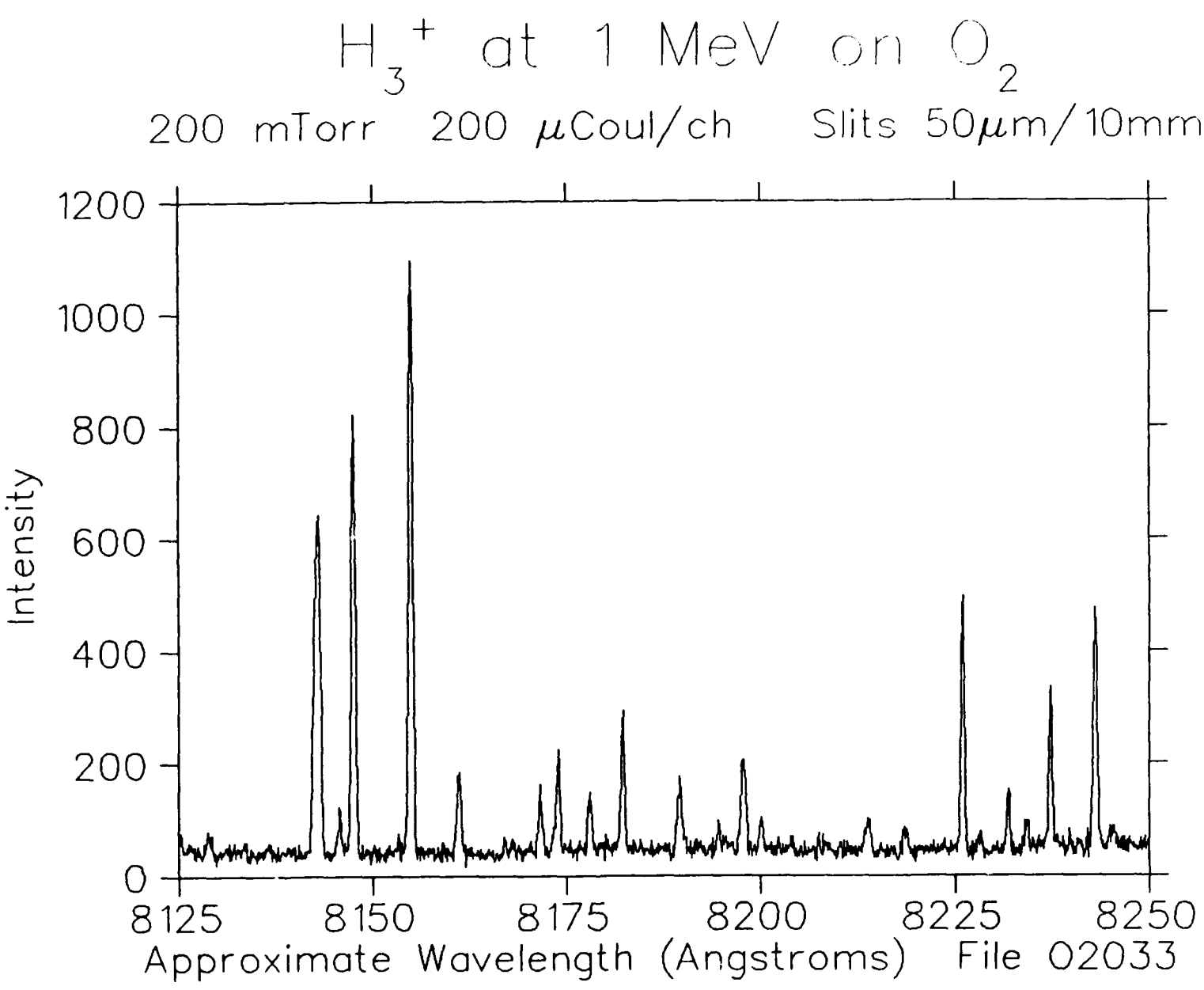
$H_3^+$ at 1 MeV on $O_2$
200 mTorr 200 μCoul/ch Slits 50μm/10mm
Intensity
1200
1000
800
600
400
200
0
8125
8150
8175
8200
8225
8250
Approximate Wavelength (Angstroms) File 02033

Fig. 95

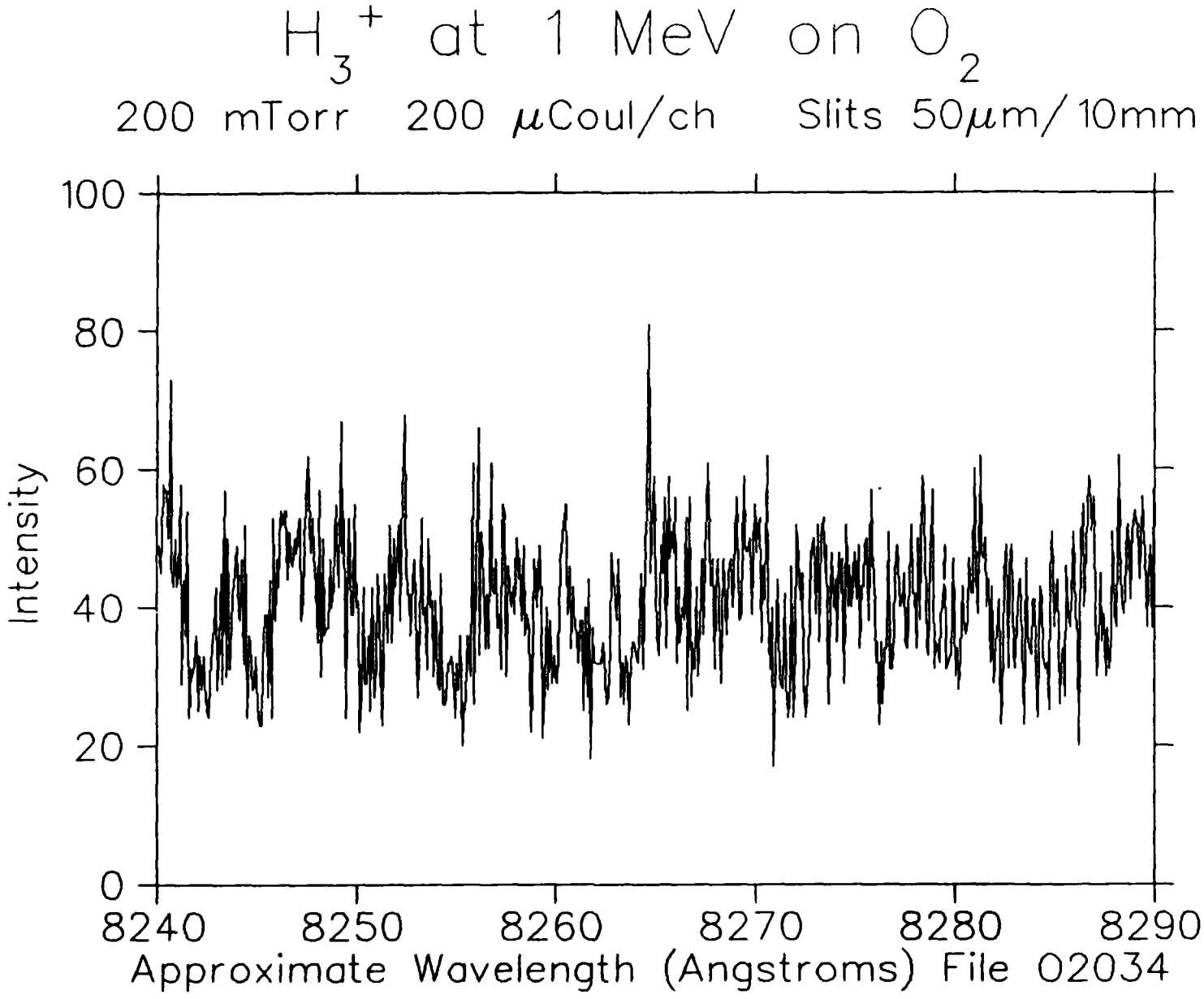
$H_3^+$ at 1 MeV on $O_2$
200 mTorr 200 μCoul/ch Slits 50μm/10mm
Intensity
100
80
60
40
20
0
8240
8250
8260
8270
8280
8290
Approximate Wavelength (Angstroms) File 02034

Fig. 96

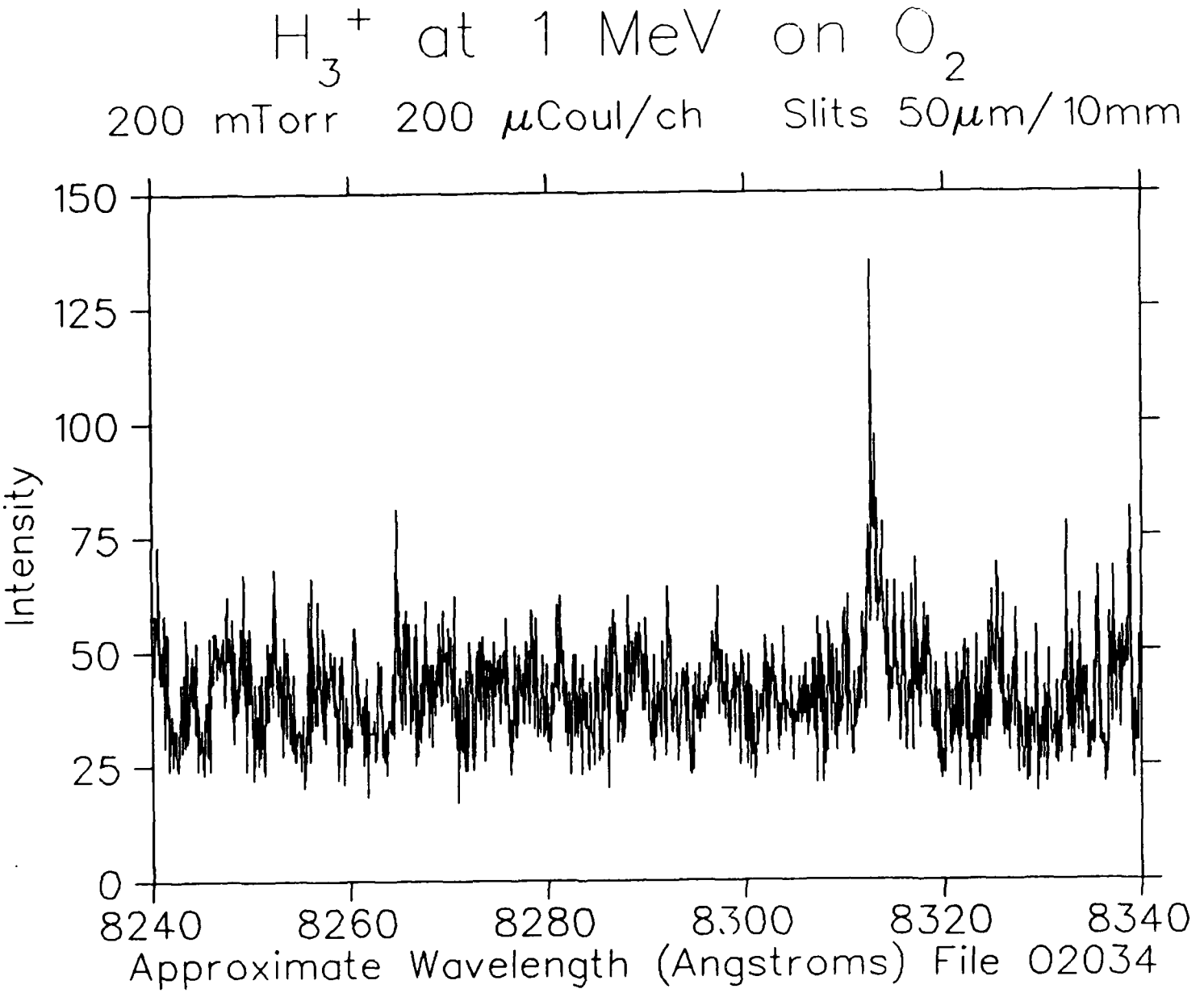
$H_3^+$ at 1 MeV on $O_2$
200 mTorr 200 μCoul/ch Slits 50μm/10mm
Intensity
150
125
100
75
50
25
0
8240
8260
8280
8300
8320
8340
Approximate Wavelength (Angstroms) File 02034

Fig. 97

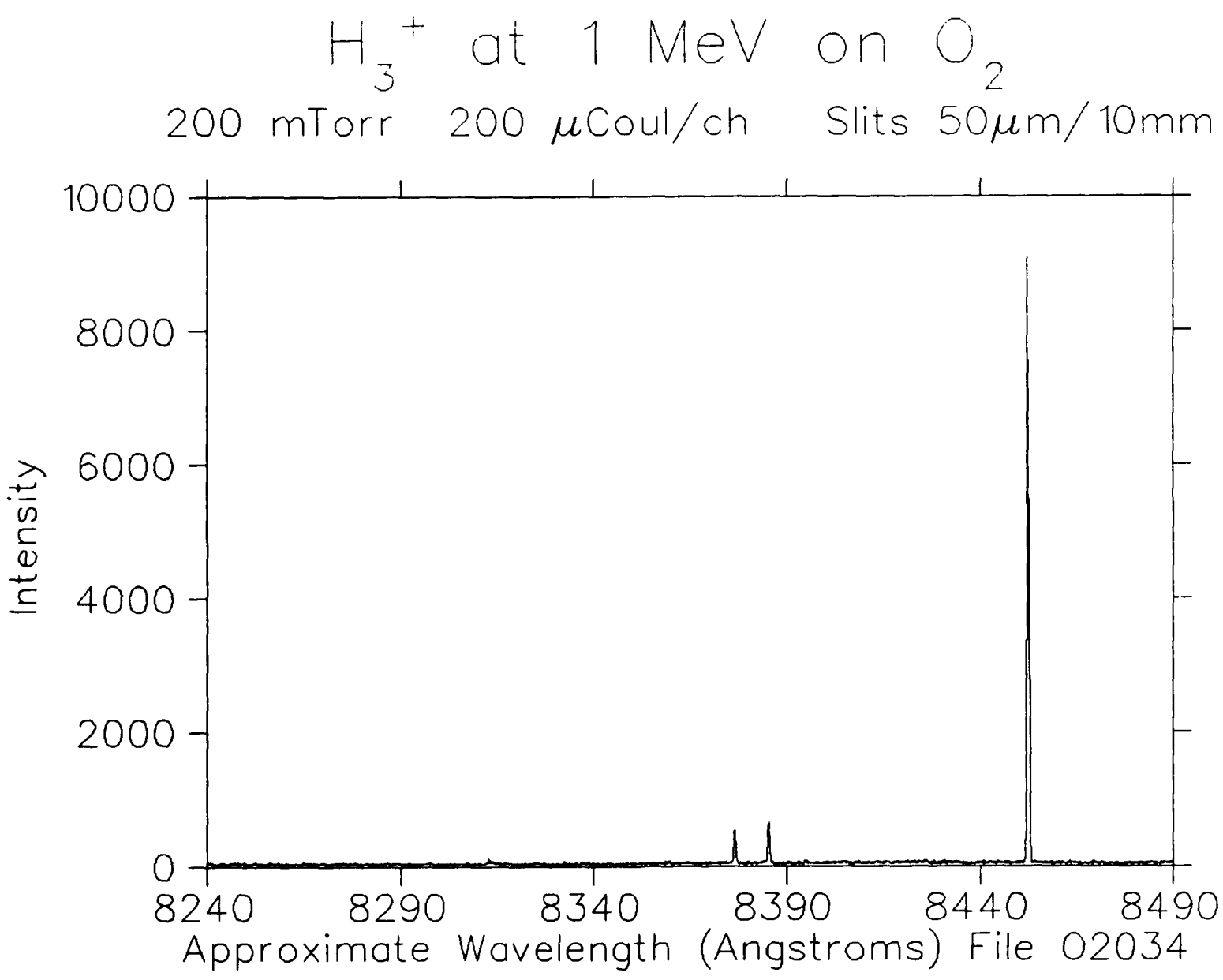
$H_3^+$ at 1 MeV on $O_2$
200 mTorr 200 μCoul/ch Slits 50μm/10mm
10000
8000
6000
4000
2000
0
Intensity
8240
8290
8340
8390
8440
8490
Approximate Wavelength (Angstroms) File 02034

Fig. 98

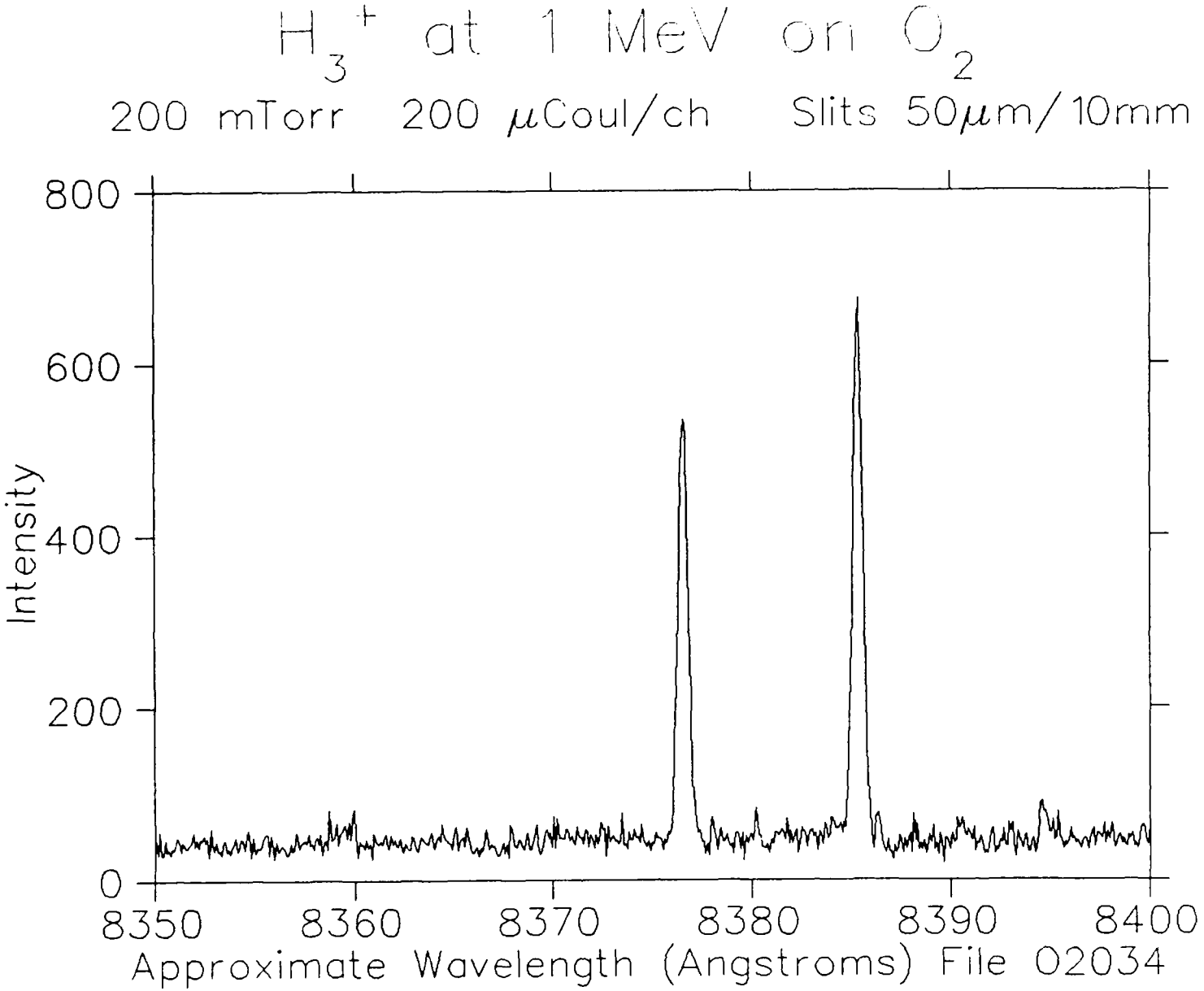
$H_3^+$ at 1 MeV on $O_2$
200 mTorr 200 μCoul/ch Slits 50μm/10mm
800
600
400
200
0
Intensity
8350
8360
8370
8380
8390
8400
Approximate Wavelength (Angstroms) File 02034

Fig. 99

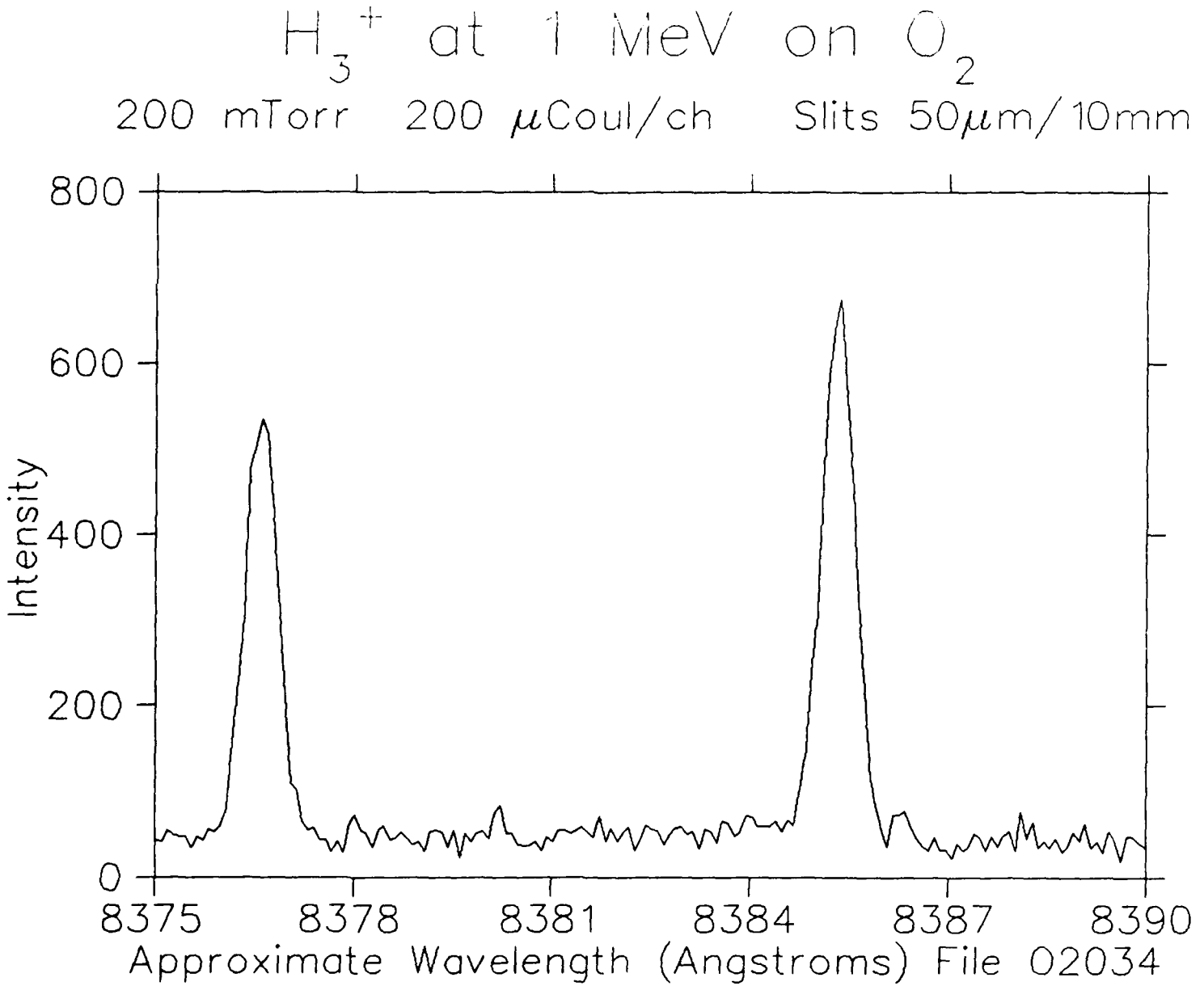
$H_3^+$ at 1 MeV on $O_2$
200 mTorr 200 μCoul/ch Slits 50μm/10mm
800
600
400
200
0
Intensity
8375
8378
8381
8384
8387
8390
Approximate Wavelength (Angstroms) File 02034

Fig. 100

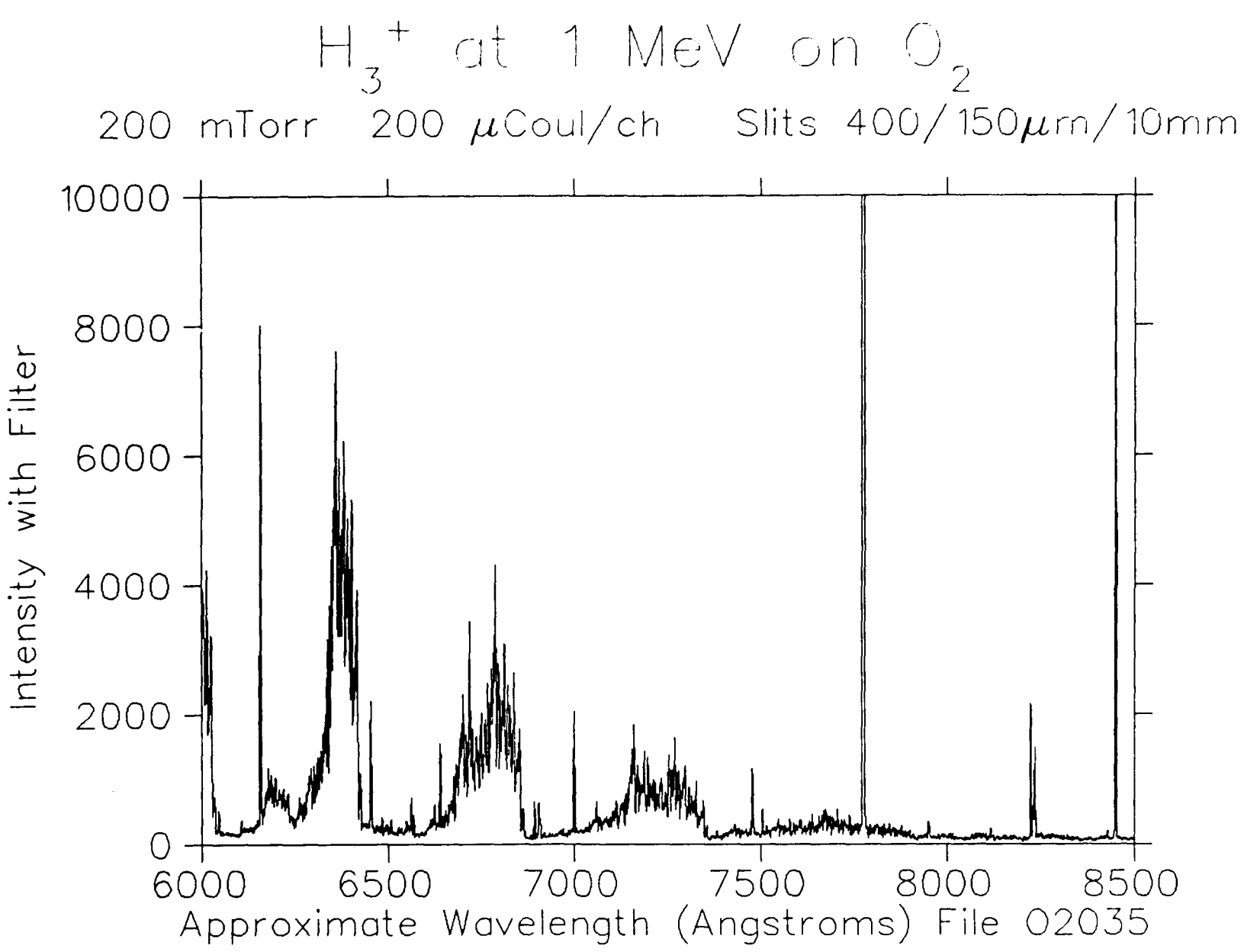
$H_3^+$ at 1 MeV on $O_2$
200 mTorr 200 μCoul/ch Slits 400/150μm/10mm
Intensity with Filter
10000
8000
6000
4000
2000
0
6000
6500
7000
7500
8000
8500
Approximate Wavelength (Angstroms) File 02035

Fig. 101

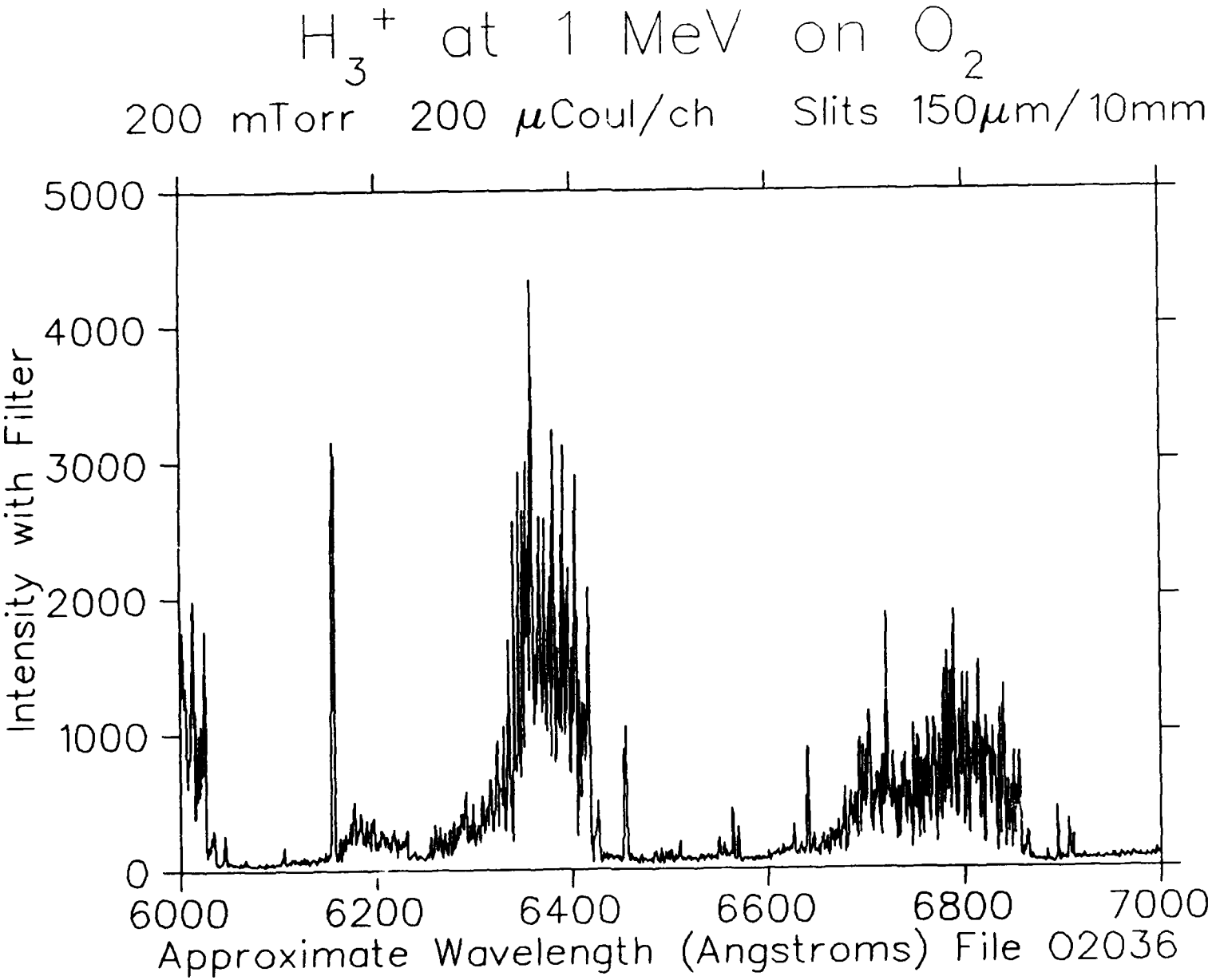
$H_3^+$ at 1 MeV on $O_2$
200 mTorr 200 μCoul/ch Slits 150μm/10mm
Intensity with Filter
5000
4000
3000
2000
1000
0
6000
6200
6400
6600
6800
7000
Approximate Wavelength (Angstroms) File 02036

Fig. 102

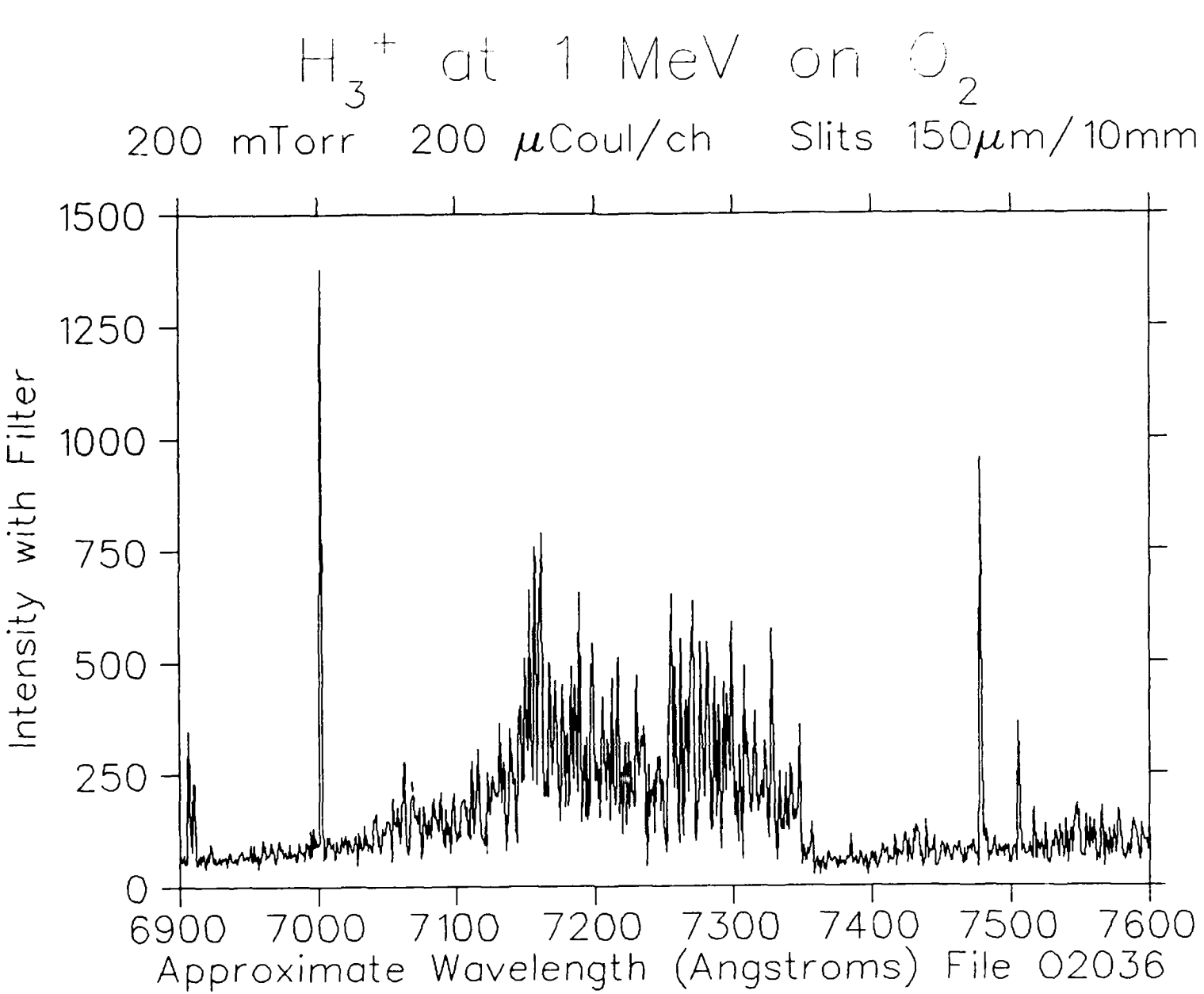
$H_3^+$ at 1 MeV on $O_2$
200 mTorr 200 μCoul/ch Slits 150μm/10mm
Intensity with Filter
1500
1250
1000
750
500
250
0
6900 7000 7100 7200 7300 7400 7500 7600
Approximate Wavelength (Angstroms) File 02036

Fig. 103

$H_3^+$ at 1 MeV on $O_2$
200 mTorr 200 μCoul/ch Slits 150μm/10mm
Intensity with Filter
60000
50000
40000
30000
20000
10000
0
7740 7750 7760 7770 7780 7790 7800
Approximate Wavelength (Angstroms) File 02036

Fig. 104

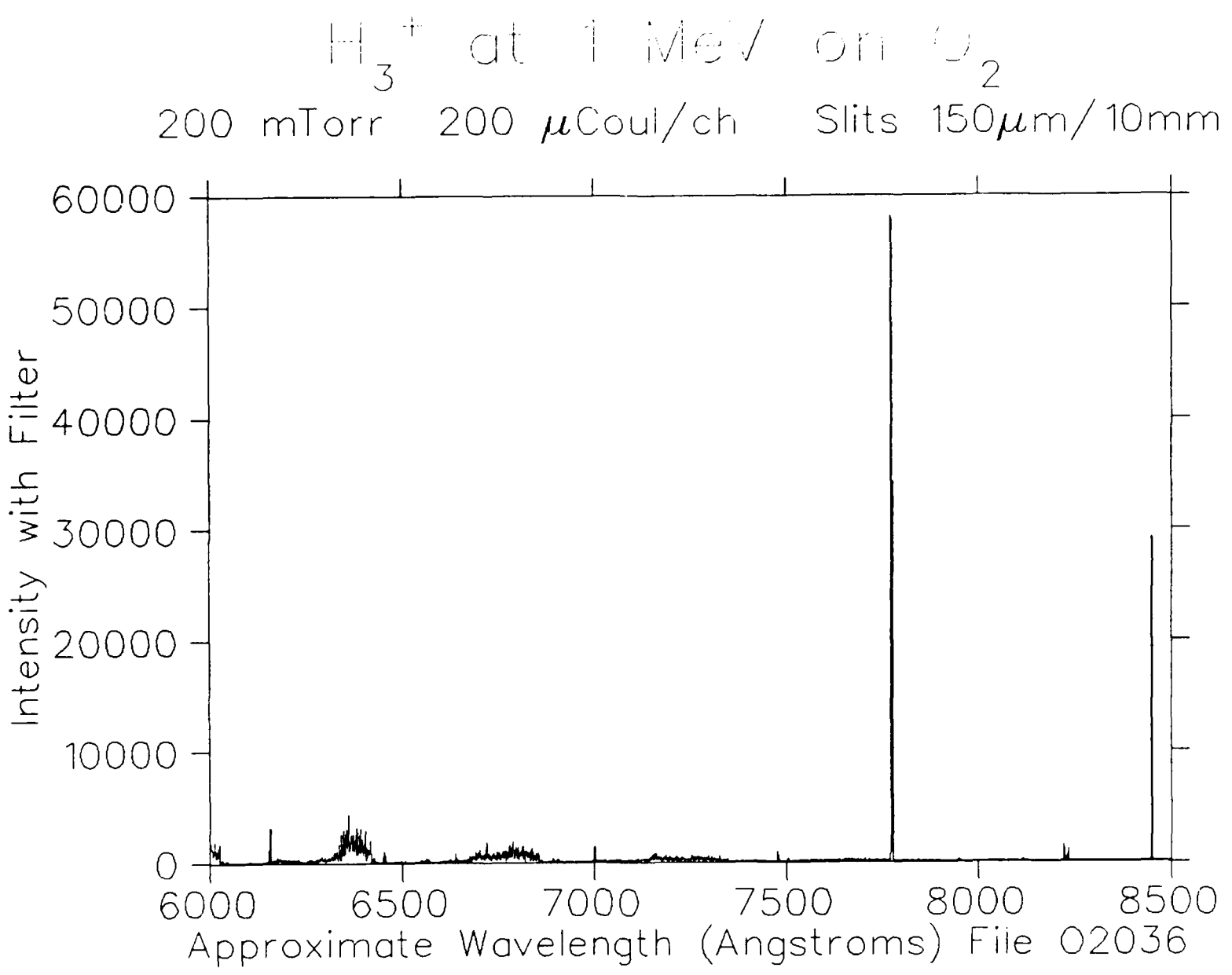
$H_3^+$ at 1 MeV on $O_2$
200 mTorr 200 μCoul/ch Slits 150μm/10mm
Intensity with Filter
60000
50000
40000
30000
20000
10000
0
6000
6500
7000
7500
8000
8500
Approximate Wavelength (Angstroms) File 02036

Fig. 105

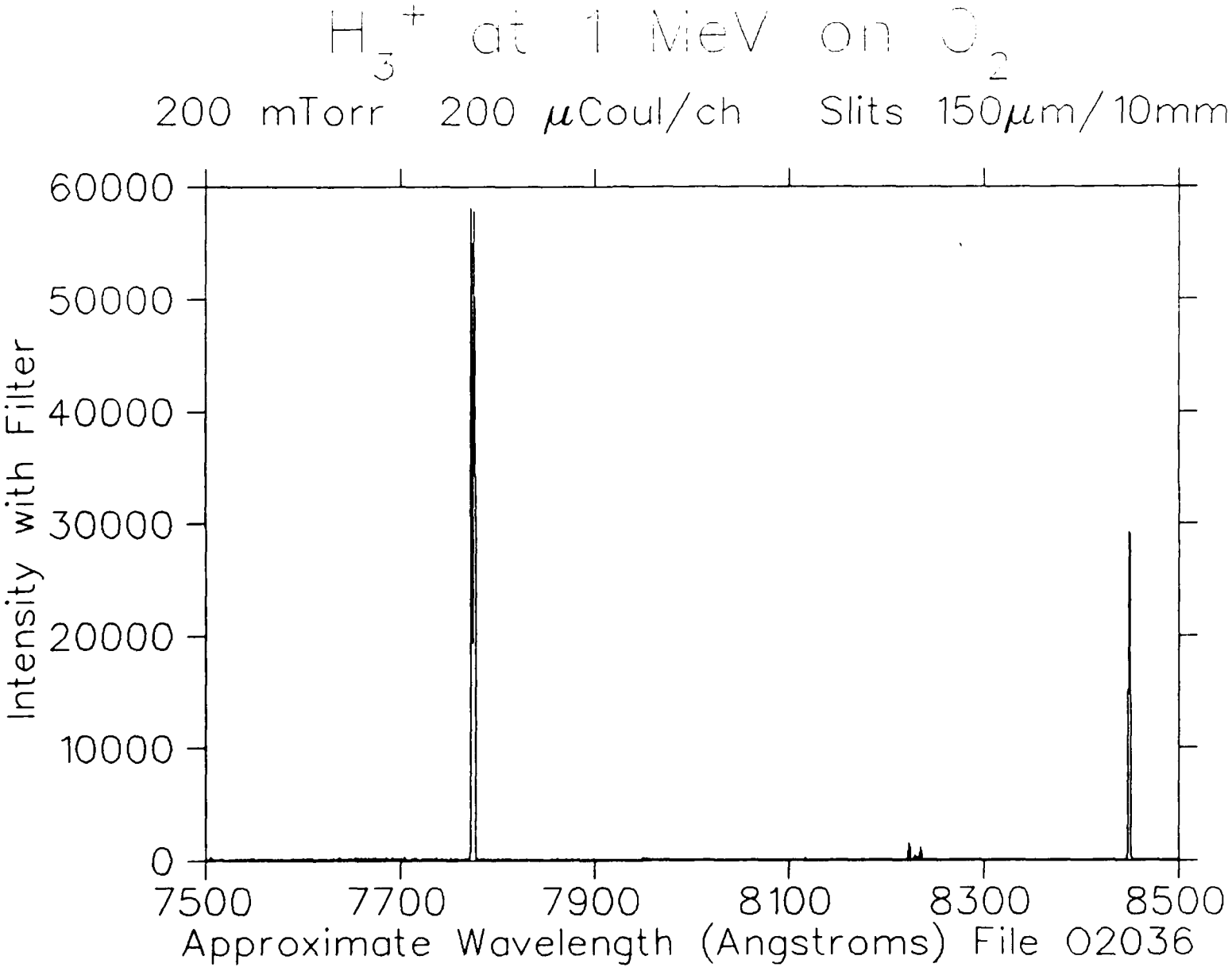
$H_3^+$ at 1 MeV on $O_2$
200 mTorr 200 μCoul/ch Slits 150μm/10mm
Intensity with Filter
60000
50000
40000
30000
20000
10000
0
7500
7700
7900
8100
8300
8500
Approximate Wavelength (Angstroms) File 02036

Fig. 106

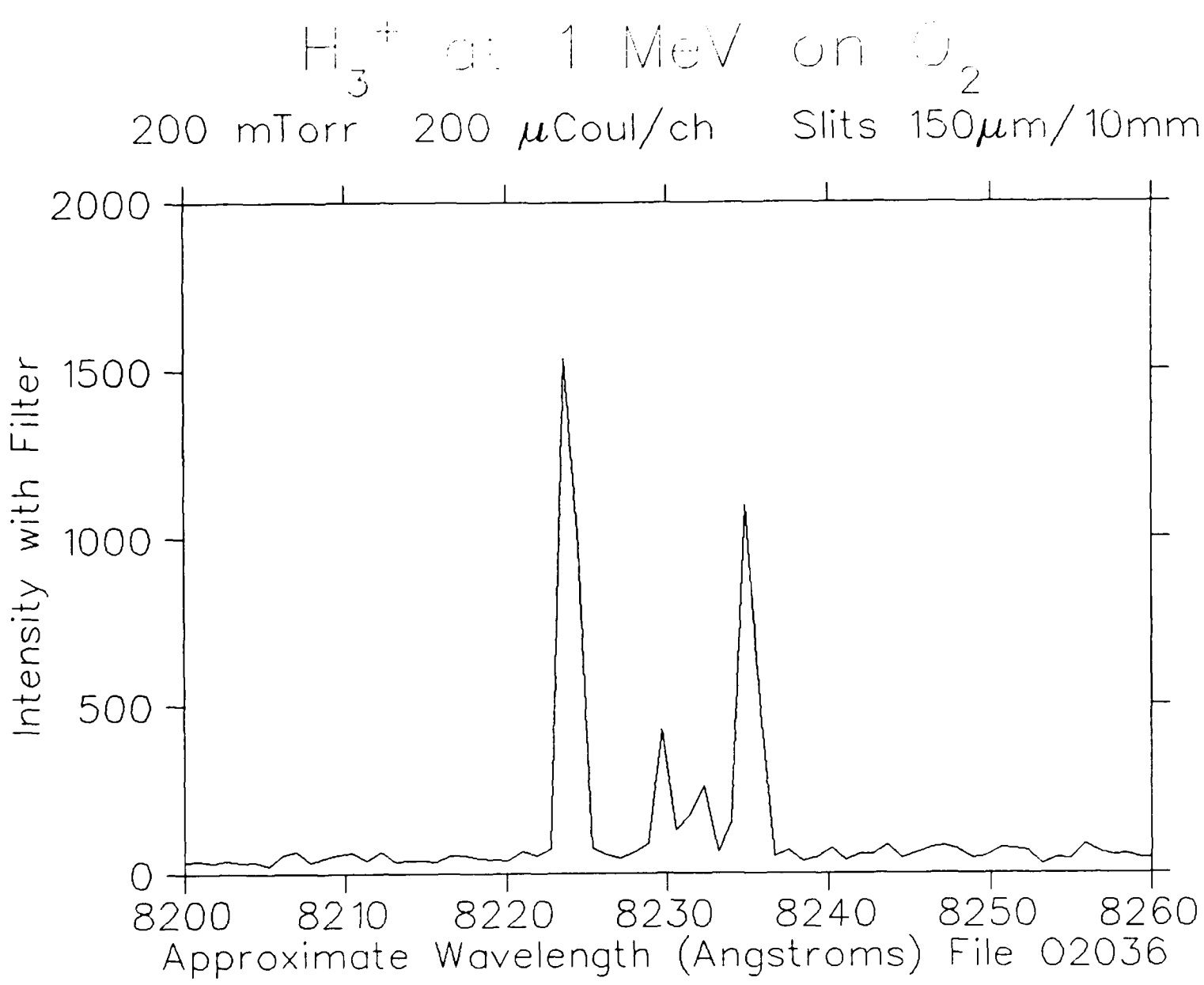
$H_3^+$ at 1 MeV on $O_2$
200 mTorr 200 μCoul/ch Slits 150μm/10mm
Intensity with Filter
2000
1500
1000
500
0
8200
8210
8220
8230
8240
8250
8260
Approximate Wavelength (Angstroms) File 02036

Fig. 107

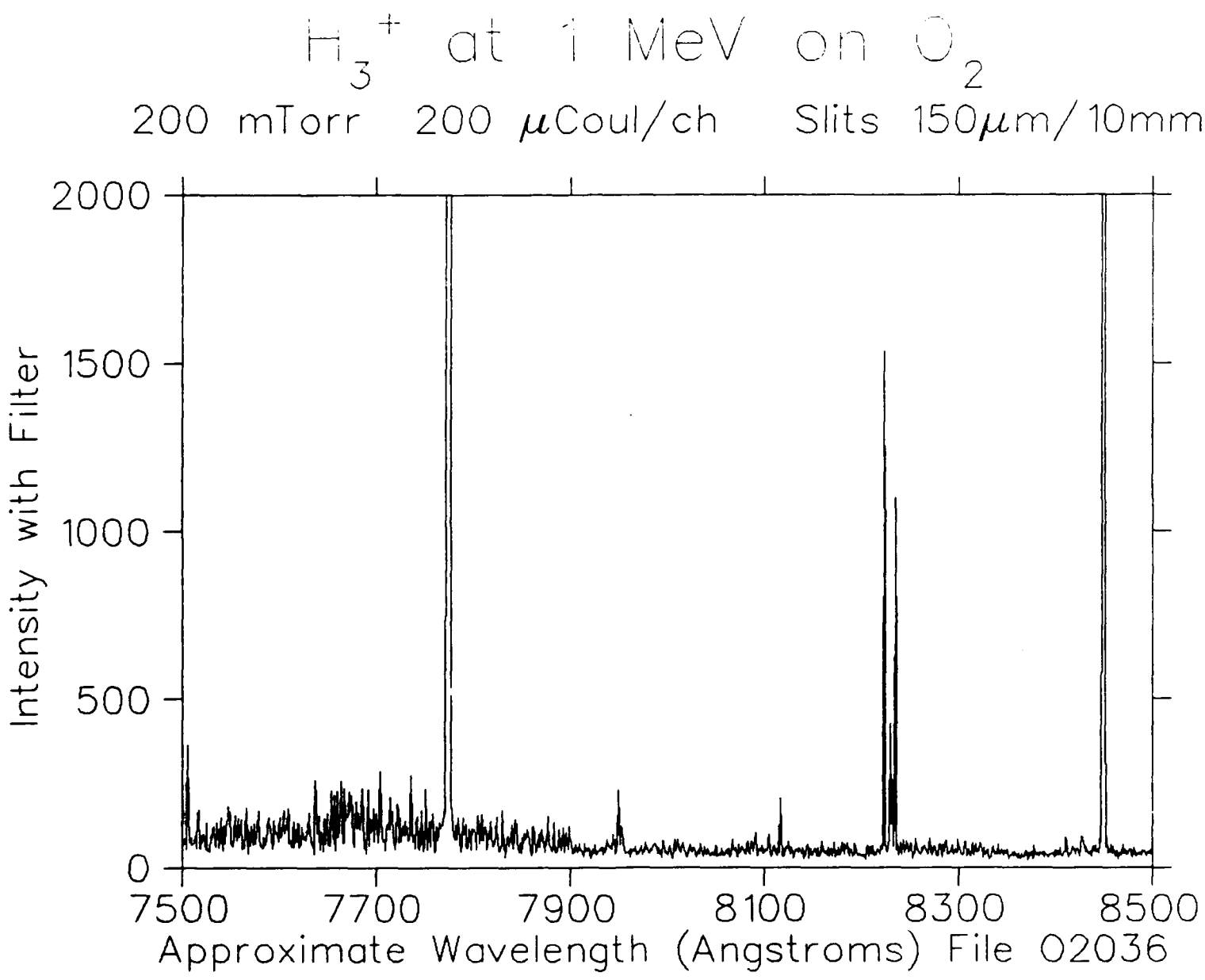
$H_3^+$ at 1 MeV on $O_2$
200 mTorr 200 μCoul/ch Slits 150μm/10mm
Intensity with Filter
2000
1500
1000
500
0
7500
7700
7900
8100
8300
8500
Approximate Wavelength (Angstroms) File 02036

Fig. 108

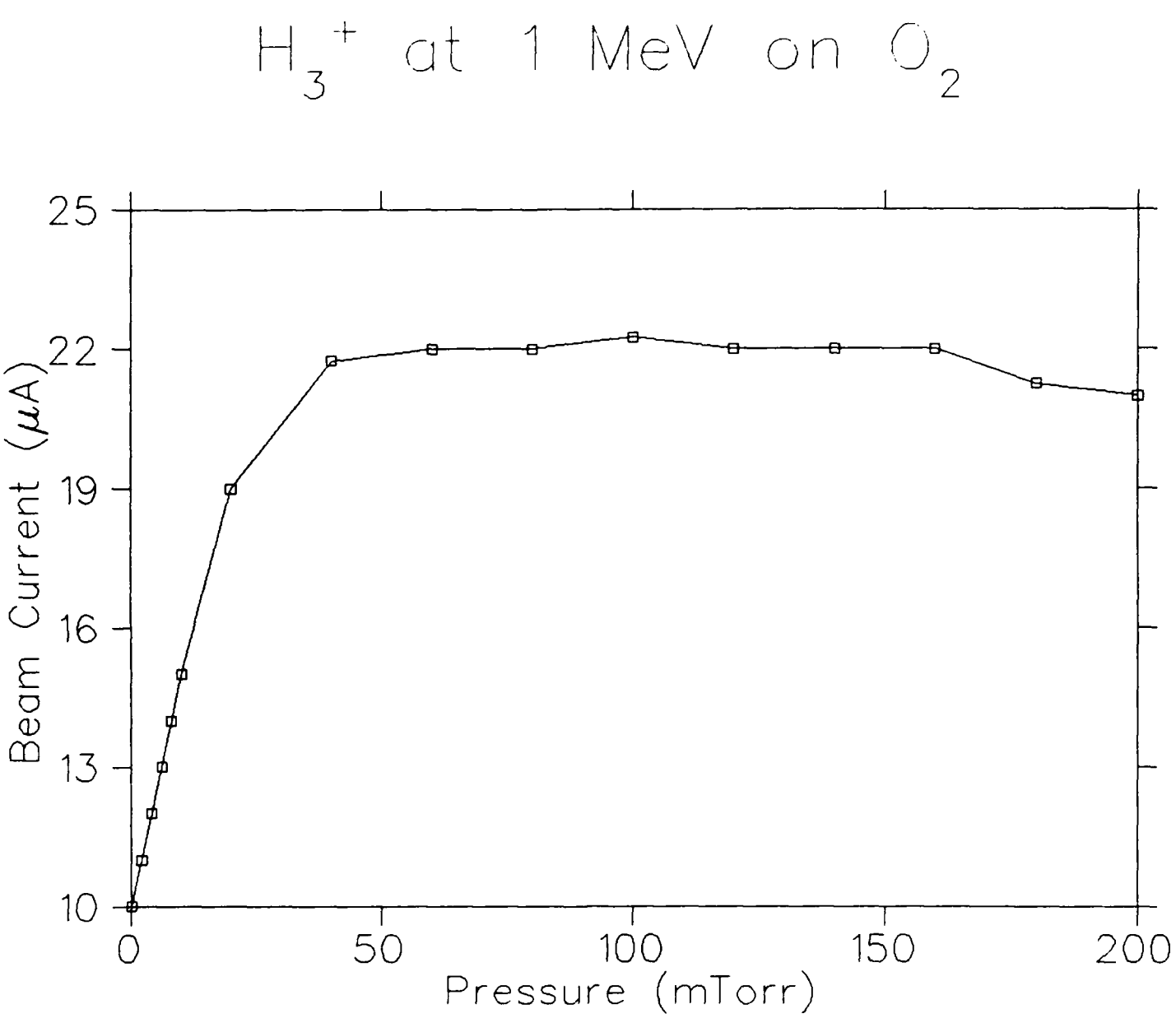
$H_3^+$ at 1 MeV on $O_2$
Beam Current ($\mu A$)
25
22
19
16
13
10
0
50
100
150
200
Pressure (mTorr)

Fig. 109

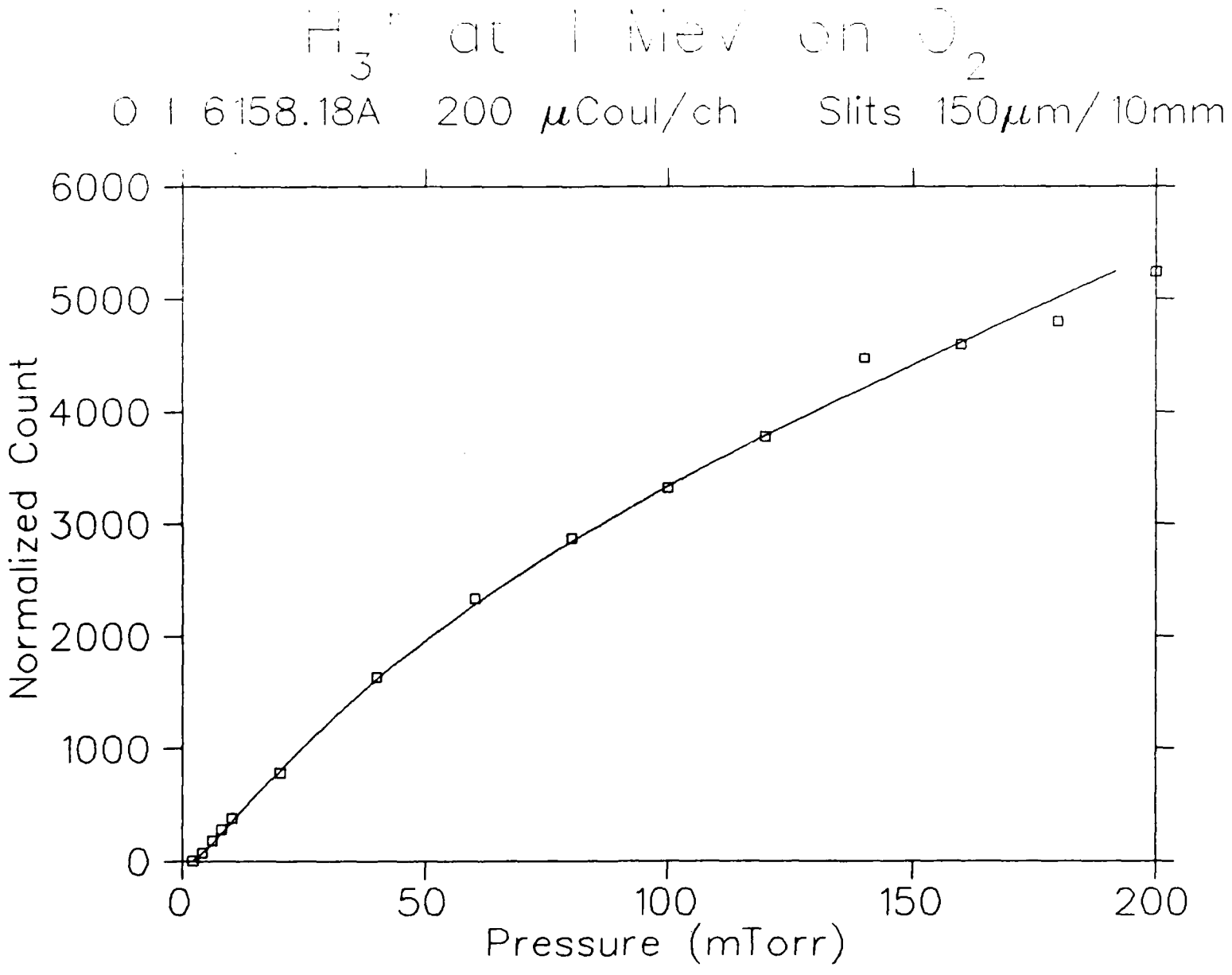
$H_3^+$ at 1 MeV on $O_2$
O I 6158.18A 200 μCoul/ch Slits 150μm/ 10mm
Normalized Count
6000
5000
4000
3000
2000
1000
0
0
50
100
150
200
Pressure (mTorr)

Fig. 110

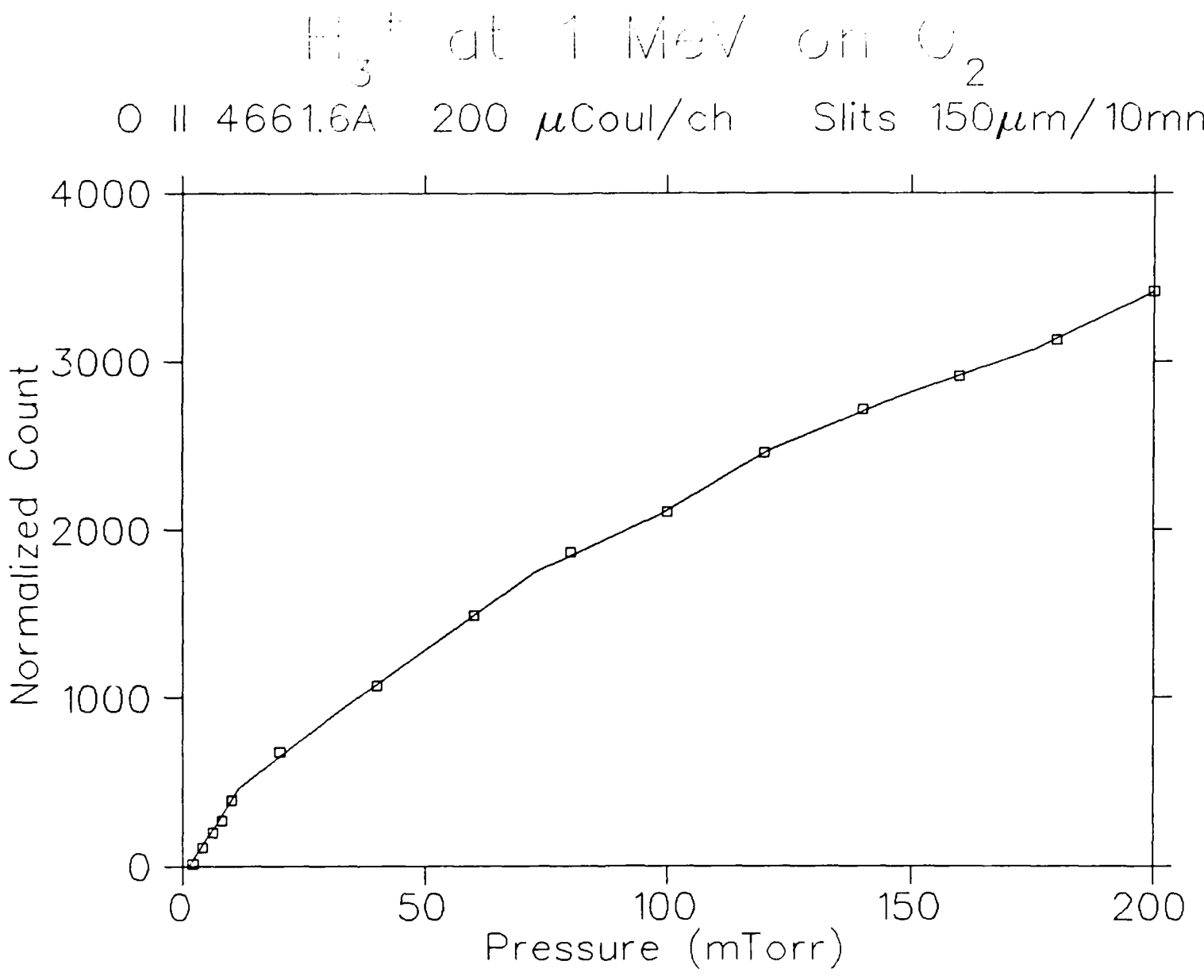
$H_3^+$ at 1 MeV on $O_2$
O II 4661.6A 200 μCoul/ch Slits 150μm/10mm
Normalized Count
4000
3000
2000
1000
0
0
50
100
150
200
Pressure (mTorr)

Fig. 111

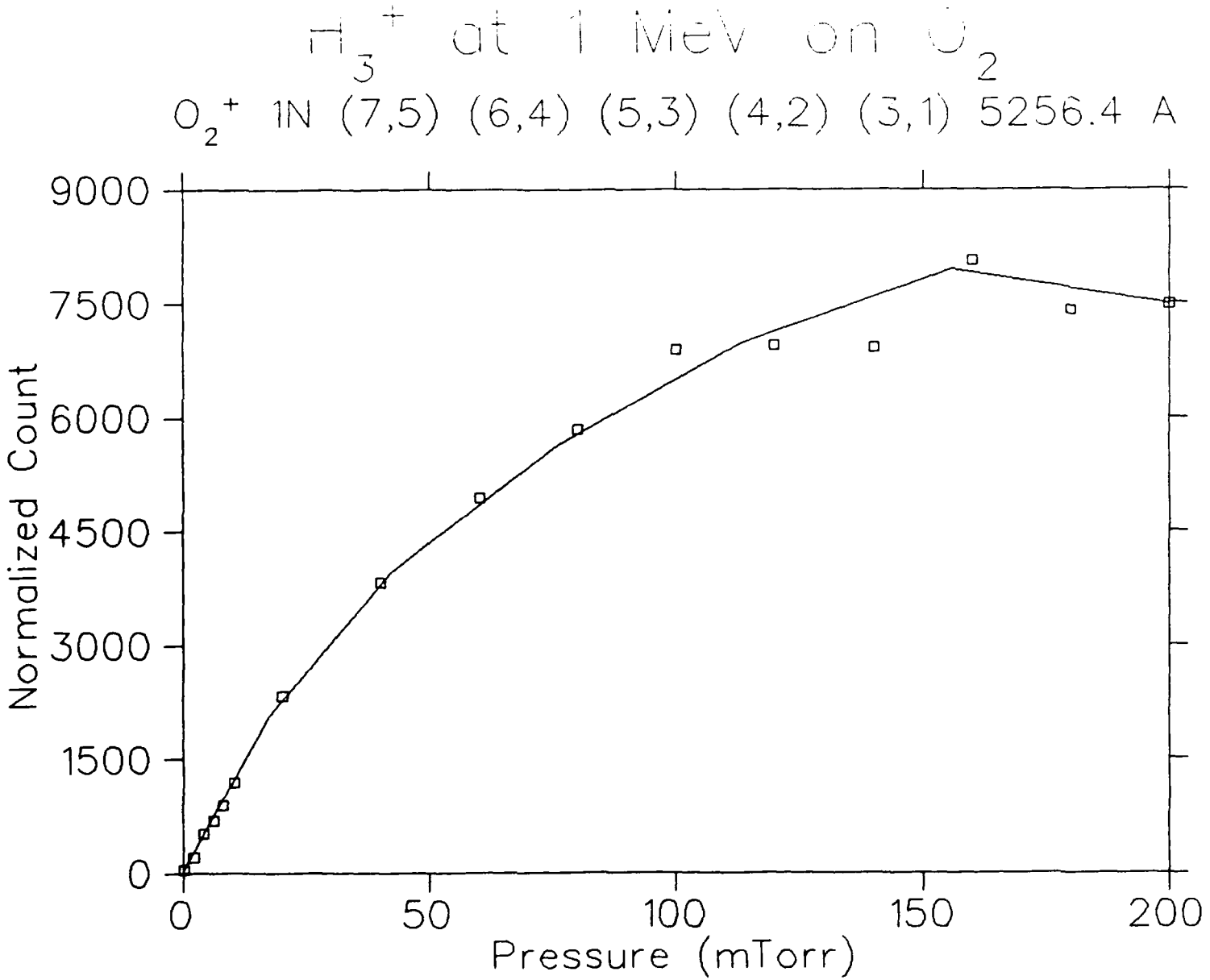
$H_3^+$ at 1 MeV on $O_2$
$O_2^+$ 1N (7,5) (6,4) (5,3) (4,2) (3,1) 5256.4 A
Normalized Count
9000
7500
6000
4500
3000
1500
0
0
50
100
150
200
Pressure (mTorr)

Fig. 112